

Wireless Networking Technologies for Smart Cities 2020

Lead Guest Editor: Jaime Lloret,

Guest Editors: Syed Hassan Ahmed, Danda B. Rawat, Waleed Ejaz, and Wei Yu





Wireless Networking Technologies for Smart Cities 2020

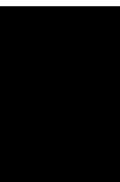
Wireless Communications and Mobile Computing

Wireless Networking Technologies for Smart Cities 2020

Lead Guest Editor: Jaime Lloret,

Guest Editors: Syed Hassan Ahmed, Danda B.

Rawat, Waleed Ejaz, and Wei Yu




Copyright © 2020 Hindawi Limited. All rights reserved.

This is a special issue published in “Wireless Communications and Mobile Computing.” All articles are open access articles distributed under the Creative Commons Attribution License, which permits unrestricted use, distribution, and reproduction in any medium, provided the original work is properly cited.

Chief Editor

Zhipeng Cai , USA

Associate Editors

Ke Guan , China
Jaime Lloret , Spain
Maode Ma , Singapore

Academic Editors

Muhammad Inam Abbasi, Malaysia
Ghufran Ahmed , Pakistan
Hamza Mohammed Ridha Al-Khafaji ,
Iraq
Abdullah Alamoodi , Malaysia
Marica Amadeo, Italy
Sandhya Aneja, USA
Mohd Dilshad Ansari, India
Eva Antonino-Daviu , Spain
Mehmet Emin Aydin, United Kingdom
Parameshchhari B. D. , India
Kalapaveen Bagadi , India
Ashish Bagwari , India
Dr. Abdul Basit , Pakistan
Alessandro Bazzi , Italy
Zdenek Becvar , Czech Republic
Nabil Benamar , Morocco
Olivier Berder, France
Petros S. Bithas, Greece
Dario Bruneo , Italy
Jun Cai, Canada
Xuesong Cai, Denmark
Gerardo Canfora , Italy
Rolando Carrasco, United Kingdom
Vicente Casares-Giner , Spain
Brijesh Chaurasia, India
Lin Chen , France
Xianfu Chen , Finland
Hui Cheng , United Kingdom
Hsin-Hung Cho, Taiwan
Ernestina Cianca , Italy
Marta Cimitile , Italy
Riccardo Colella , Italy
Mario Collotta , Italy
Massimo Condoluci , Sweden
Antonino Crivello , Italy
Antonio De Domenico , France
Floriano De Rango , Italy



Antonio De la Oliva , Spain
Margot Deruyck, Belgium
Liang Dong , USA
Praveen Kumar Donta, Austria
Zhuojun Duan, USA
Mohammed El-Hajjar , United Kingdom
Oscar Esparza , Spain
Maria Fazio , Italy
Mauro Femminella , Italy
Manuel Fernandez-Veiga , Spain
Gianluigi Ferrari , Italy
Luca Foschini , Italy
Alexandros G. Fragkiadakis , Greece
Ivan Ganchev , Bulgaria
Óscar García, Spain
Manuel García Sánchez , Spain
L. J. García Villalba , Spain
Miguel Garcia-Pineda , Spain
Piedad Garrido , Spain
Michele Girolami, Italy
Mariusz Glabowski , Poland
Carles Gomez , Spain
Antonio Guerrieri , Italy
Barbara Guidi , Italy
Rami Hamdi, Qatar
Tao Han, USA
Sherief Hashima , Egypt
Mahmoud Hassaballah , Egypt
Yejun He , China
Yixin He, China
Andrej Hrovat , Slovenia
Chunqiang Hu , China
Xuexian Hu , China
Zhenghua Huang , China
Xiaohong Jiang , Japan
Vicente Julian , Spain
Rajesh Kaluri , India
Dimitrios Katsaros, Greece
Muhammad Asghar Khan, Pakistan
Rahim Khan , Pakistan
Ahmed Khattab, Egypt
Hasan Ali Khattak, Pakistan
Mario Kolberg , United Kingdom
Meet Kumari, India
Wen-Cheng Lai , Taiwan

Jose M. Lanza-Gutierrez, Spain
Pavlos I. Lazaridis , United Kingdom
Kim-Hung Le , Vietnam
Tuan Anh Le , United Kingdom
Xianfu Lei, China
Jianfeng Li , China
Xiangxue Li , China
Yaguang Lin , China
Zhi Lin , China
Liu Liu , China
Mingqian Liu , China
Zhi Liu, Japan
Miguel López-Benítez , United Kingdom
Chuanwen Luo , China
Lu Lv, China
Basem M. ElHalawany , Egypt
Imadeldin Mahgoub , USA
Rajesh Manoharan , India
Davide Mattera , Italy
Michael McGuire , Canada
Weizhi Meng , Denmark
Klaus Moessner , United Kingdom
Simone Morosi , Italy
Amrit Mukherjee, Czech Republic
Shahid Mumtaz , Portugal
Giovanni Nardini , Italy
Tuan M. Nguyen , Vietnam
Petros Nicolitidis , Greece
Rajendran Parthiban , Malaysia
Giovanni Pau , Italy
Matteo Petracca , Italy
Marco Picone , Italy
Daniele Pinchera , Italy
Giuseppe Piro , Italy
Javier Prieto , Spain
Umair Rafique, Finland
Maheswar Rajagopal , India
Sujan Rajbhandari , United Kingdom
Rajib Rana, Australia
Luca Reggiani , Italy
Daniel G. Reina , Spain
Bo Rong , Canada
Mangal Sain , Republic of Korea
Praneet Saurabh , India





Hans Schotten, Germany
Patrick Seeling , USA
Muhammad Shafiq , China
Zaffar Ahmed Shaikh , Pakistan
Vishal Sharma , United Kingdom
Kaize Shi , Australia
Chakchai So-In, Thailand
Enrique Stevens-Navarro , Mexico
Sangeetha Subbaraj , India
Tien-Wen Sung, Taiwan
Suhua Tang , Japan
Pan Tang , China
Pierre-Martin Tardif , Canada
Sreenath Reddy Thummaluru, India
Tran Trung Duy , Vietnam
Fan-Hsun Tseng, Taiwan
S Velliangiri , India
Quoc-Tuan Vien , United Kingdom
Enrico M. Vitucci , Italy
Shaohua Wan , China
Dawei Wang, China
Huaqun Wang , China
Pengfei Wang , China
Dapeng Wu , China
Huaming Wu , China
Ding Xu , China
YAN YAO , China
Jie Yang, USA
Long Yang , China
Qiang Ye , Canada
Changyan Yi , China
Ya-Ju Yu , Taiwan
Marat V. Yuldashev , Finland
Sherali Zeadally, USA
Hong-Hai Zhang, USA
Jiliang Zhang, China
Lei Zhang, Spain
Wence Zhang , China
Yushu Zhang, China
Kechen Zheng, China
Fuhui Zhou , USA
Meiling Zhu, United Kingdom
Zhengyu Zhu , China

Contents




Analysis of WOFDM over LTE 1.25 MHz Band

Sandeep Sarowa , Naresh Kumar , and Ram Sewak Singh
Research Article (9 pages), Article ID 8835879, Volume 2020 (2020)


A Hybrid Spectrum Combinational Auction Mechanism Based on a Weighted Bipartite Graph for Energy Internet in Smart Cities

Huibin Feng , Zhaocai Yu , Jian Guan , and Geng Lin 
Research Article (13 pages), Article ID 8829602, Volume 2020 (2020)


Demand Response Management Research Based on Cognitive Radio for Smart Grid

Tingting Yang , Tiancong Huang , Haifeng Zhang , Peiyi Li , Canyon Xiong , and Yucheng Wu 
Research Article (10 pages), Article ID 8827777, Volume 2020 (2020)



Architecture and Protocol to Optimize Videoconference in Wireless Networks

Jose M. Jimenez, José Luis García-Navas, Jaime Lloret , and Oscar Romero
Research Article (22 pages), Article ID 4903420, Volume 2020 (2020)



Energy-Efficient Asynchronous QoS MAC Protocol for Wireless Sensor Networks

Sohail Sarang , Goran M. Stojanović, Stevan Stankovski, Željko Trpovski, and Micheal Drieberg
Research Article (13 pages), Article ID 8860371, Volume 2020 (2020)

Truthful Mechanism Design for Multiregion Mobile Crowdsensing

Yu Qiao , Jun Wu, Hao Cheng, Zilan Huang, Qiangqiang He, and Chongjun Wang 
Research Article (15 pages), Article ID 8834983, Volume 2020 (2020)

LoRa-Based Smart IoT Application for Smart City: An Example of Human Posture Detection

Jinkun Han , Wei Song , Amanda Gozho, Yunsick Sung, Sumi Ji, Liangliang Song, Long Wen, and Qi Zhang
Research Article (15 pages), Article ID 8822555, Volume 2020 (2020)

Research Article

Analysis of WOFDM over LTE 1.25 MHz Band

Sandeep Sarowa ¹, Naresh Kumar ², and Ram Sewak Singh³

¹CERT-In, MeitY, India

²UIET, PU, Chandigarh, India

³ASTU, Adama, Ethiopia

Correspondence should be addressed to Sandeep Sarowa; sasarowa@gmail.com

Received 2 June 2020; Revised 23 October 2020; Accepted 15 November 2020; Published 1 December 2020

Academic Editor: Jaime Lloret

Copyright © 2020 Sandeep Sarowa et al. This is an open access article distributed under the Creative Commons Attribution License, which permits unrestricted use, distribution, and reproduction in any medium, provided the original work is properly cited.

Orthogonal Frequency Division Multiplexing (OFDM) is the one of the most preferred multiplexing technique for realizing high-speed wireless communication, like Long Term Evolution (LTE) and LTE-Adv. In the era of digital wireless communication, applications of wavelet theory have been favorably applied in many areas of signal processing. Orthogonality, flexible time-frequency analysis, and the ability to characterize signals accurately have attracted the attention of the telecommunication community to use wavelet as a basis function for OFDM. In this paper, discrete wavelet transform (DWT) has been proposed as an alternative signal analysis with multiple merits such as support high-speed applications, immune to distortion, wavelet diversity, better error performance, and efficient bandwidth utilization. A simulative analysis of various wavelets, at different modulation techniques, over OFDM has been presented to demonstrate the improvement in BER performance. Further, in accordance with the LTE parameterization over 1.25 MHz band, the performance of wavelet-based OFDM (WOFDM) is found significantly higher in terms of maximum achievable data rate and system spectral efficiency.

1. Introduction

OFDM distributes the offered spectrum among multiple subcarriers where each subcarrier gets modulated by information signal stream to efficiently utilize available bandwidth [1, 2]. Apparently, whole information carrying data stream is fragmented into multiple subsets, separately modulated with orthogonal carriers. Each subcarrier is orthogonal to each other in time domain; however, frequency domain overlapping of multiple signals is well visible. However, information transmitted in the shape of closely packed symbols is expected to interfere each other to generate intersymbol interference (ISI) [3, 4]. To avoid ISI, cyclic prefix (CP) is used but at the cost of bandwidth consumption; this may even consume more than 25% of total available bandwidth. In order to save this precious bandwidth, discrete wavelet transform (DWT) provides a better solution as it does not use CP to sideline the ISI.

DWT is the multiresolution analysis (time-frequency), i.e., excellent time resolution properties at high frequencies

and poor frequency resolution properties at low frequencies. Wavelet is like a tiny waveform that exhibits useful properties to analyze edges of a signal to better represent local features. DWT can be the best alternative to the Discrete Fourier Transform (DFT) based signal analysis for OFDM system, with multiple advantages such as high energy consumption, compact support, multiresolution analysis in frequency-time domain, interference immunity, better phase linearity, no CP requirement, flexibility to choose suitable wavelet, and wavelet diversity [5]. There is a significant bandwidth advantage associated with wavelets, as it does not need cyclic prefix because in wavelet decomposition, symbols overlap in both time and frequency domain [6]. Wavelet offers a higher degree of suppression to the side lobes (thus wavelet-based OFDM ought to have longer basis functions). Also, the wavelet-based multicarrier communication system bears less complexity as compared to the DFT-based system [7–9]. Large spectrum efficiency, high-speed data transmission support, and MIMO compatibility make OFDM a preferred access

technique for advanced wireless mobile communication [10]. Wavelet-based OFDM systems are spectrum efficient as they do not seek CP to restrict ISI. Moreover, pilot tones are not necessary in wavelet transform, thus providing an additional 8% of bandwidth efficiency as compared to the conventional OFDM. For a conventional OFDM system, power amplifier's (PA) energy consumption can go as high as 60% of the energy consumption of BTS transmitter [4]. Wavelet implication improves PA efficiency, thereby restricting energy expenditure at mobile equipment (batteries that last longer) and at the base stations (energy savings) [11]. Many researchers have demonstrated the BER analysis for WOFDM [12, 13] and standard OFDM systems to highlight the benefits of different types of wavelets in an OFDM system, i.e., db2, db4, db6, db10, db8, db32, haar, symlet, biorthogonal, reverse biorthogonal [14–17] under AWGN, and Rayleigh fading channel over a wide SNR range.

In this paper, a quantitative analysis of maximum achievable data rate and spectral efficiency for WOFDM is performed with different modulation levels at 1.25 MHz LTE spectrum band. Simulative analysis of BER performance of WOFDM with respect to five different wavelets is also performed to attain the improvements against standard OFDM. Further, this paper is organized as follows: Section 2 describes the technological concept of LTE and its functions. Section 3 investigates the operational parameterization of LTE. Section 4 summarizes the related work and associated literature. Section 5 presents the proposed WOFDM using various wavelets. Section 6 presents the results and analysis. Finally, Section 7 summarizes and concludes the paper.

2. Long Term Evolution (LTE)

LTE is the technological upgradation and advancement of the Universal Mobile Telecommunications System (UMTS) through many evolutions. 3GPP (3rd Generation Partnership Project) worked over the decade (since 2004) to make LTE roll-out possible where high mobile data usage and advent of new applications have motivated it to touch extremities [18]. 3GPP working committee members organize to build up a framework keeping prime objectives aligned to evolve 3GPP radio-access technology for achieving high-data-rate, low-latency, and packet-optimized radio-access technology. LTE Radio Access delivers significant improvement in end to end user throughput, spectrum efficiency and offers a substantial improvement in mobility experience by exploiting OFDM and Multi-in Multi-Out (MIMO) antenna schemes [19].

The 3GPP working committee provides LTE specifications, the performance requirements pertaining to control plane, and user plane protocols for commercial deployments [20].

The following is the summary of the performance parameters:

- (i) *Peak data rate*: up to 300 Mbps in downlink and 100 Mbps in uplink.

- (ii) *Latency*: one-way transit time shall be less than 5 ms.
- (iii) *Spectrum efficiency (bit/sec/Hz/site)*: up to 5 bit/sec/Hz.
- (iv) *Mobility*: high performance up to 120 km/h and support maintained for 120-350 km/h.
- (v) *Coverage*: high performance up to 5 km and compromised performance till distance increases up to 100 km.
- (vi) *Spectrum allocation*: Frequency Division Duplex (FDD) and Time Division Duplex (TDD) support.
- (vii) *Capacity*: 200 users/cell to 400 users/cell support.
- (viii) *Spectrum flexibility*: support different spectrum sizes: 1.25 MHz, 2.5 MHz, 5 MHz, 10 MHz, and 20 MHz.
- (ix) *Interworking*: uninterrupted backward compatibility with legacy systems.
- (x) *Costs*: Reduced Capital Expenditure (CAPEX) and Operational Expenditure (OPEX).

Power consumption is a key attention to choose user equipment (UE), and therefore, LTE uplink requirements differ from downlink requirements. The high PAPR and related loss allied with OFDM leads to a search for an alternative low power consumption technique for LTE uplink transmission. Thus, LTE uplink transmission is designed with Single Carrier Frequency Division Multiple Access (SC-FDMA) scheme to save UE battery power. The potential merit of SC-FDMA over OFDM is low PAPR and which makes it accountable for a low cost implementation of power amplifiers [21]. Unlike the non-3GPP compliance, LTE deployed with OFDM for downlink and SC-FDMA for uplink, FDD/TDD duplex mode and have greater VoIP capacity (80 users/sector/MHz) [22]. The higher the performance of OFDM (either spectral efficiency or data rate), the more would be the attribution to achieve performance goals of 4G-5G systems. Where legacy cellular systems worked on circuit-switched model, 3GPP defined a new System Architecture Evolution (SAE) that operates with less network elements and works for both data and voice traffic through only IP-based protocol. Figure 1 shows a simplified LTE architecture, where LTE core network EPC (Evolved Packet Core) provides IP connectivity through Packet Data Network (PDN) Gateway for accessing the Internet.

LTE is provisioned to support packet-switching services between UE to Packet Data Network (PDN), without interfering consumer's applications during mobility. The LTE evolved base station (eNodeB), which is a part of E-UTRAN and gets connected to EPC through S1AP protocol. As shown in Figure 1, Mobility Management Entity (MME) is the heart of EPC, and it manages control plane signaling as well as user plane data S1U interface (handled by Serving Gateway). PDN gateway (PGW) acts as a mobility anchor for interworking, IP address allocation for the UE, and flow-based charging. In order to establish multiple bearers

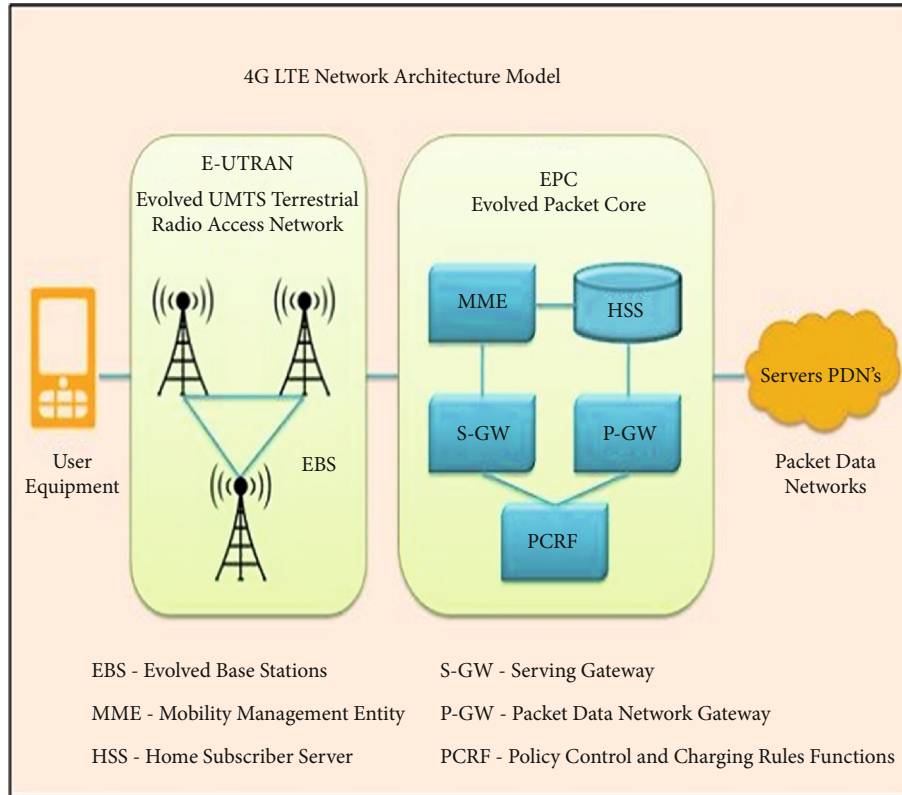


FIGURE 1: LTE network elements [18].

to a user, different connectivity to different PDNs is granted gracefully. For example, a user busy with web browsing or media streaming while simultaneously might be performing a voice over IP (VoIP) call. Serving gateway (SGW) acts as the mobility anchor for inter 3GPP eNodeB handovers. The Policy Control and Charging Rules Function (PCRF) administrates the policy control and decision-making, QoS authorization, and bit rate according to the subscription. The Home Subscriber Server (HSS) retains the user data and MME identification with which it is registered.

3. LTE Parameterization

LTE supports both TDD and FDD mode of operations in downlink and uplink transmission. Since LTE adopts two different access techniques, i.e., OFDMA for downlink and SC-FDMA for uplink transmissions, physical layer parameters and system requirements become different, and thus, that must be treated separately for uplink case and downlink case [20]. There are two radio frames, each one of 10 ms duration.

The following are the two types of radio frame structures:

- (i) *Type 1*: supports FDD mode.
- (ii) *Type 2*: supports TDD mode.

The type 1 FDD-based radio frame structure is shown in Figure 2. It consists of 20 equal-sized time slots. The

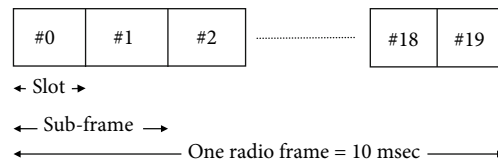


FIGURE 2: Frame structure type 1.

whole radio frame is also grouped into 10 equal-sized sub-frames where each one of the subframes consists of two equal-size radio time slots. In type1 structure (FDD mode), the whole frame is equally distributed for uplink and downlink transmission, i.e., 5 subframes are made available for downlink and 5 subframes for uplink. So each subframe is of 1 ms duration where each time slot occupies 0.5 ms time duration.

Type 2 TDD-based radio frame structure is shown in Figure 3. It consists also of 20 equal-sized time slots that are grouped into 10 subframes of 1 ms duration each. Now, one radio frame is divided into two equal portions of TDD frames (5 ms each) where each half portion of the frame is structured with 8 slots of duration 0.5 m, and one subframe consists of three special fields related to the guard period (GP), downlink pilot time slot (DwPTS), and uplink pilot time slot (UpPTS). The time duration of DwPTS and UpPTS is variable enough to satisfy the condition of 1 ms length of the subframe. In this frame structure, subframe number 1 and subframe number 6 with half-frame periodicity (5 ms switch-point) consist of DwPTS, GP, and UpPTS; however,

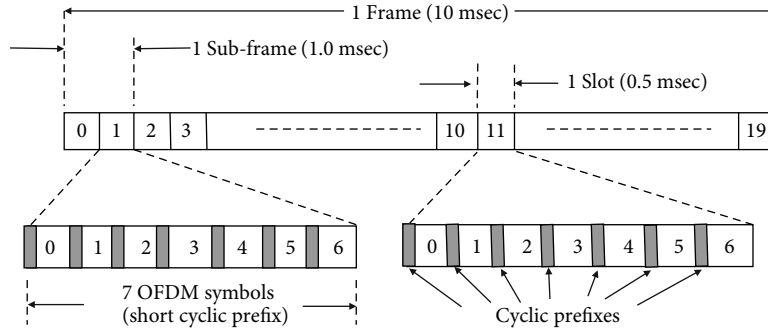


FIGURE 3: LTE frame structure type 2.

TABLE 1: LTE parameters for downlink [21].

Parameters	OFDM					
Bandwidth (MHz)	1.25	2.5	5	10	15	20
Subcarrier spacing	15 kHz					
Symbol time	66.7 μ s					
FFT size	128	256	512	1024	1536	2048
No. of subcarrier	76	151	301	601	901	1201
Error coding	Convolution coding					

the rest of the subframes contain two equally sized radio slots. In TDD mode, downlink and uplink operations are separated in the time domain.

OFDM technique with CP is used for downlink communication, maintaining the subcarrier spacing $\Delta f = 15$ kHz. Subcarrier spacing (Δf) is related to OFDM symbol duration (T_s) by $\Delta f = 1/T_s$. Therefore, it is essentially important to choose an appropriate size of T_s to enable Δf sufficient enough to sustain against Doppler offset and other sources of frequency offset. There are two variants of CP length (normal cyclic prefix and extended cyclic prefix) used for OFDM symbol (seven and six OFDM symbols per radio slot) having 15 kHz subcarrier spacing.

For a channel delay spread " T_d " and maximum Doppler frequency " $f_{D_{max}}$ ", the following is the design criteria for choosing the CP duration " T_{CP} ":

$$\begin{cases} T_{CP} \geq T_d & \text{to avoid ISI,} \\ \frac{f_{D_{max}}}{\Delta f} \ll 1 & \text{to maintain ICI sufficient low,} \\ T_{CP}\Delta f \ll 1 & \text{to maintain OFDM spectral efficient.} \end{cases} \quad (1)$$

In compliance with the LTE specifications defined by 3GPP, Table 1 presents the OFDM parameters to be adopted for downlink communication. According to LTE parameterization [21], for all available spectrum bands, there should be 15 kHz subcarrier spacing maintained for orthogonality, and thus, the symbol rate comes out to be $(1/15 \text{ kHz}) = 66.7 \mu\text{s}$.

Utilization of higher spectrum bands with dynamic carrier aggregation technique is still a matter of future

research and exploration to alleviate the spectrum scarcity and capacity limitations of current/future wireless communication systems [23]. Advanced technological developments like 5G, Internet of Things (IoT), and Machine to Machine (M2M) are aligned with many revolutionary ideas to explore the possible enhancements in energy efficiency, network latencies, and reliable interconnectivity [24].

4. Related Work

OFDM is used in LTE systems. OFDM provides higher data rates, but at the same time, it has two major drawbacks: (i) High Peak to Average Power Ratio (PAPR) and (ii) Intercarrier Interference (ICI). It is desirable to have low PAPR and null ICI for a better quality of service. Many researchers have worked on different algorithms to reduce PAPR like Signal Scrambling Techniques, Signal Distortion Techniques, and Hybrid Techniques; a brief overview of these techniques is given in [25]. Techniques to combat ICI are also proposed like ICI Self Cancellations; recently, an overview of different ICI self-cancellation techniques based on conventional OFDM based on simulink is presented in [26–28] and also reported in [29]. Now, all these techniques are based on conventional OFDM in which IFFT/IDFT is used at the transmitter side and FFT/DFT is used in the receiver side. Sarowa et al. and Kaur et al. [6, 30] have focused their research on wavelet-based OFDM, i.e., replacing the IFFT/DFT with IDWT and FFT/DFT with DWT to improve the system performance. A comparative analysis of conventional OFDM with wavelet-OFDM is also presented for PAPR reduction [31] and ICI cancellations [32]. As in conventional OFDM, orthogonality among subcarriers is lost, and thus, the problems of high PAPR and ICI arises; along with this, the cyclic prefix is also used. Cyclic prefix consumes almost 20% of bandwidth and hence makes the system less bandwidth efficient. In cases of wavelets, as they maintain orthogonality and at the same time subcarriers are not required, the PAPR and ICI problems can be handled in a better way. Recently, wavelet-based OFDM is used in many other applications in including 5G and underwater acoustic communications [33, 34]. It is desirable that if wavelet-based OFDM is used in LTE, it can enhance its performance. The present article is focused on the use of wavelet-based OFDM in LTE 1.25 MHz band to test its feasibility in LTE systems. Initially, the AWGN channel is considered for

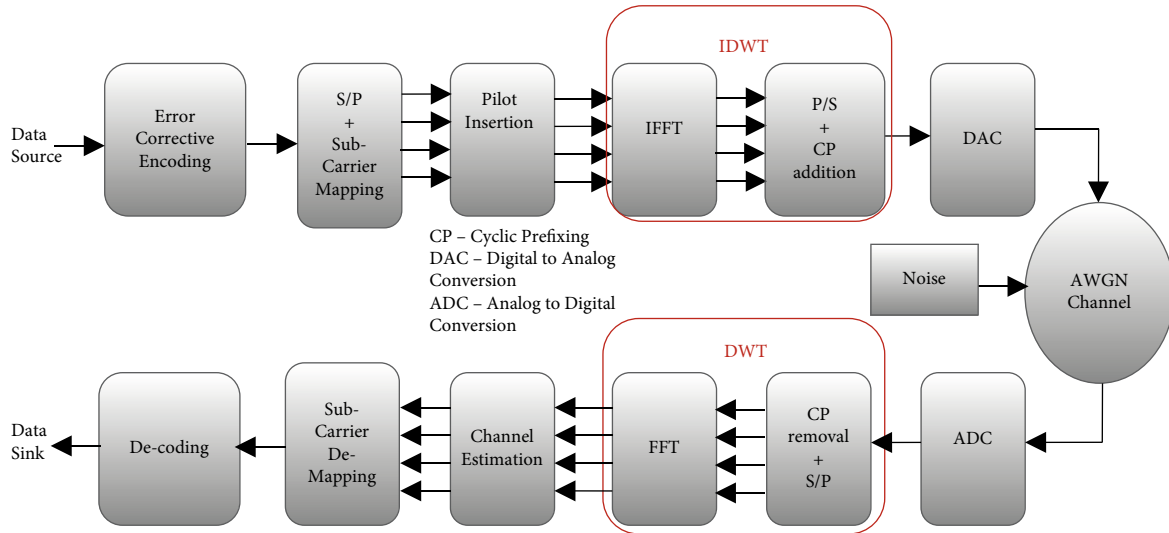


FIGURE 4: Building blocks of wavelet-based OFDM system.

simulation purposes; work can further be extended with Rayleigh fading and Rician fading channels also. As the AWGN channel is simple to implement and at the same time it is easy to analyse the system, simulations are carried using AWGN channels. Conventional OFDM and wavelet-OFDM are compared at different modulations and with different wavelet families.

5. WOFDM System

Discrete wavelet transform deals with the multiresolution analysis of signals under consideration in both frequency domain and time domain through wavelet coefficients. Wavelets are small waveforms having some set oscillations in the time domain, with some additional properties useful for analyzing edges and transient properties of a signal to better represent sharp changes and local features. Wavelet gives better orthogonality among subcarriers against multipath signal propagation and has localization in both time and frequency domain. Wavelets have higher energy compaction since side lobes are of very small magnitude. In wavelet-based OFDM, there is no requirement of cyclic prefix and pilot tones which are potential advantages of this scheme where bandwidth saving is achieved significantly.

The merits of the wavelet transform are summarized below:

- (i) Compact support (localization) both in time and frequency domain
- (ii) Better orthogonality to reduce ISI power and make the system less affected by Doppler shift
- (iii) No cyclic prefix requirements, which makes OFDM system 20% more bandwidth efficient
- (iv) No major requirements to use pilot tones, which may further save 8% of valuable bandwidth

- (v) High energy compaction, which makes side lobes to bear a small amount of energy
- (vi) The adverse effect of the channel can be further reduced by suitably choosing the appropriate type of wavelet with desired modulation technique as different wavelet produces different performance under the undesirable channel conditions
- (vii) Wavelet transform renders the flexibility of configurable transform size which eventually makes a number of subcarriers configurable in accordance with the different channel conditions

Keeping all the benefits of wavelet transform in view, we propose a wavelet-based OFDM system as shown in Figure 4. In this system, cyclic prefix block is missing which otherwise could have consumed more than 20% of precious bandwidth. In this WOFDM system, IFFT and CP blocks (transmitter side) are replaced with inverse discrete wavelet transform (IDWT) block. At the receiver side, FFT and CP removal blocks are replaced with the discrete wavelet transform (DWT) block.

Here, source data is encoded with a convolution coder (error corrective encoder as same as that used for FFT-based OFDM for simulative comparison). Pilots are inserted (for better tracking of the signal at the receiver side after modulation (QPSK/QAM both techniques give better performance) which is followed by subcarrier mapping. Subcarrier mapped symbols are then processed by inverse discrete wavelet transform. IDWT section consists of perfectly reconstructed quad mirror filter banks that employ half band low pass filter (LPF) having impulse response " g " and half band high pass filter (HPF) having impulse response " h ." For IDWT and DWT processing, one can choose any type of wavelet family-like Haar, db, symlet, bior wavelets, etc. At the receiver side, respective functions are suitably reversed to reconstruct the original information signal.

Haar wavelet and db wavelet are the most commonly used wavelets due to their simplicity and easy synthesis.

The descriptions of Haar wavelet $\psi(t)$ is:

$$\psi(t) = \begin{cases} \frac{1}{\sqrt{T_0}} & \text{if } 0 \leq t \leq \frac{T_0}{2} \\ -\frac{1}{\sqrt{T_0}} & \text{if } \frac{T_0}{2} \leq t \leq T_0 \\ 0 & \text{else} \end{cases}, \quad (2)$$

WOFDM output is:

$$X(t) = \left[\left(\sum_{n=0}^{N_s} C_k \psi(t - nT_s) \right) \right], \quad (3)$$

where C_k and T_s are complex representations of the sub-carrier symbols and symbol period. The Haar wavelet is the oldest and simplest wavelet and has a closed-form expression in the time and frequency domains.

6. Results and Analysis

BER performance of the standard OFDM system is evaluated against the WOFDM system to analyze the performance improvement. Performance improvement in BER at different SNR values for conventional FFT-based OFDM system and WOFDM system are analyzed with a set of five different wavelets, i.e., “haar,” “db2,” “sym2,” “coif1,” “bior1.1.” As BER is dependent on the signal to noise ratio, so the performance curve of BER is plotted with respect to SNR. However, the BER performance of the OFDM system is also dependent on coding schemes, modulation techniques, multipath propagation, fading environment, channel noise, etc. In the present simulation model, an error corrective encoding (convolution coding) is used to get better BER performance of the system. Pilots are inserted suitably with respect to the volume of data and modulation scheme (to track the signal at the receiver side). Different modulation techniques (4 QAM, 16 QAM, and 64 QAM) for FFT-based OFDM and WOFDM are simulated to compare the BER performance of the OFDM system. Available bandwidth plays a crucial role in deciding data rate, number of subcarriers used, and further separation between subcarriers in the frequency domain. The wireless communication channel is considered to be an AWGN channel under a flat fading environment. Data signals are transmitted through a large number of orthogonal subcarriers, and each subcarrier bears a limited bandwidth.

The simulative parameters used here in the analysis for FFT and wavelet-based OFDM configuration are in compliance with the LTE specifications defined by 3GPP, tabulated in Table 1. According to LTE parameterization [11], subcarrier spacing = 15 kHz, for keeping orthogonality;

TABLE 2: Spectral efficiency vs. max attainable data rate.

Modulation	Parameters	OFDM	WOFDM
4 QAM	Max data rate	0.95 Mbps	1.13 Mbps
	Spectral efficiency	0.76 bps/Hz	0.9 bps/Hz
16 QAM	Max data rate	1.9 Mbps	2.27 Mbps
	Spectral efficiency	1.52 bps/Hz	1.81 bps/Hz
64 QAM	Max data rate	2.85 Mbps	3.415 Mbps
	Spectral efficiency	2.28 bps/Hz	2.73 bps/Hz

symbol rate should be $(1/15\text{kHz}) = 66.7 \mu\text{s}$. If the CP used here is of 20% of the OFDM symbol time, then the overall symbol duration becomes $66.7 + 13.3 = 80 \mu\text{s}$. Also, wavelet-based OFDM does not use CP, and thus, the symbol duration will remain $66.7 \mu\text{s}$. As shown in Table 1, the number of subcarriers used is 76, and the symbol duration is $80/66.7 \mu\text{sec}$ for WOFDM/OFDM. Now the number of bits carried by modulation symbol is 6 for 64 QAM, and it will be different for different modulation techniques.

Number of bits/OFDM symbol

$$= \text{no of subcarriers} \times \text{no.of bits/QAM symbol} \quad (4)$$

$$= 76 \times 6 = 456 \text{ bits/OFDM symbol,}$$

(Max data rate)_{OFDM}

$$= \text{number of bits per OFDM symbol/OFDM symbol time}$$

$$= 456/80 = 5.7 \text{ Mbps,}$$

(5)

$$(\text{Max data rate})_{\text{WOFDM}} = 456/66.7 = 6.83 \text{ Mbps.} \quad (6)$$

For error-correcting codes where conventional coder 1/2 rate is used:

$$(\text{Max data rate})_{\text{OFDM}} = 5.7/2 = 2.85 \text{ Mbps,} \quad (7)$$

$$(\text{Max data rate})_{\text{WOFDM}} = 6.83/2 = 3.415 \text{ Mbps.} \quad (8)$$

Now, (Spectral efficiency)_{OFDM} = max.data rate/allocated bandwidth = $2.85 \text{ Mbps}/1.25 \text{ Mbps} = 2.28 \text{ bps/Hz}$.

$$(\text{Spectral efficiency})_{\text{WOFDM}} = 3.415/1.25 = 2.73 \text{ bps/Hz.} \quad (9)$$

In a similar manner, spectral efficiency and max data rate are calculated for other modulation techniques, i.e., 4 QAM and 16 QAM are tabulated in Table 2.

A comparative analysis is separately plotted for spectral efficiency and maximum attainable data rate for each 4 QAM, 16 QAM, and 64 QAM to highlight the significant improvements. Figure 5 depicts the comparative improvements in spectral efficiency where WOFDM can be able to achieve 16.5% higher spectral efficiency to standard OFDM.

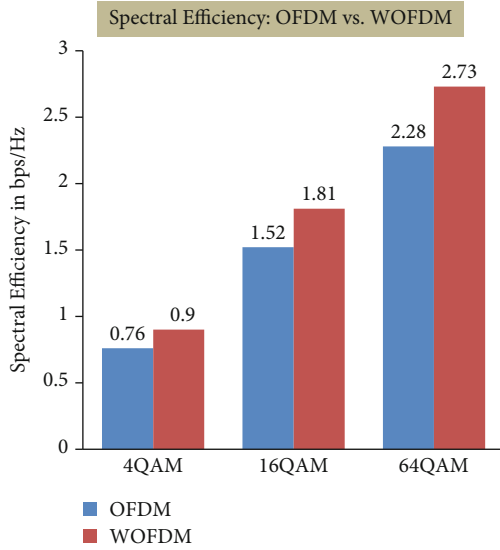


FIGURE 5: Spectral efficiency improvement in WOFDM.

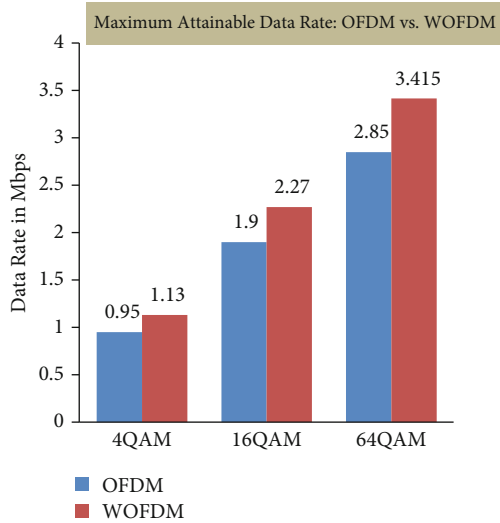


FIGURE 6: Data rate improvements in WOFDM.

Similarly, Figure 6 depicts the comparative improvements in maximum attainable data rate where WOFDM can be able to achieve a 16.6% higher data rate than the standard OFDM.

The simulation parameters for BER vs. SNR analysis of different wavelet-based OFDM are tabulated in Table 3 for 1.25 MHz spectrum band over AWGN channel condition.

Simulative analysis is shown in Figures 7, 8, 9, where different wavelet-based OFDM (five wavelets) are evaluated against the BER performance. Spectral efficiency and max data rate of M-ary PSK comes out similar to M-ary QAM; however, its BER performance deteriorates significantly, and therefore, M-ary PSK is not an advisable configuration for LTE deployment.

In Figure 7, BER vs. SNR for WOFDM and FFT-based OFDM with 4 QAM modulation scheme is plotted to dem-

TABLE 3: Simulation parameters.

Specification	FFT-based OFDM	Wavelet-based OFDM
Bandwidth	1.25 MHz	1.25 MHz
FFT size	128	NA
No. of subcarriers	76	76
No. of bits	19200	19200
Number of symbols	100	100
Max data rate	2.85 Mbps	3.41 Mbps
Spectral efficiency	2.28 bps/Hz	2.73 bps/Hz
Cyclic prefixing	20%	Nil
Channel	AWGN	AWGN
Modulation	64 QAM	64 QAM
Convolution coding	1/2	1/2

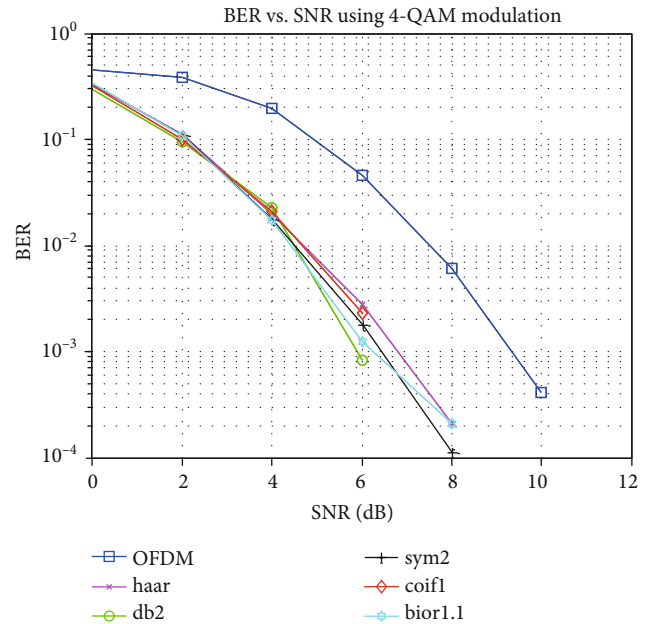


FIGURE 7: BER vs. SNR for different wavelet-based OFDM at 4 QAM.

onstrate the 3 dB gain. In this plot, db2 wavelet outperforms other under-considered wavelet variants.

In Figure 8, BER vs. SNR for 16 QAM modulation scheme is plotted to demonstrate nearly 4 dB gain over standard FFT-based OFDM. In this plot, coif1 wavelet seems to be performing better than other under-considered wavelets.

However, there is almost a 4 dB difference observed in BER performance when 4 QAM and 16 QAM configurations are compared.

In Figure 9, the BER performance of conventional OFDM and WOFDM is compared where it is investigated that Haar wavelet (outperforms other wavelet variants by more than 1 dB) delivers more than 4 dB better performance to OFDM.

Also, it is almost a 6 dB difference observed in SNR to achieve the same BER performance when 16 QAM and 64 QAM configurations are compared.

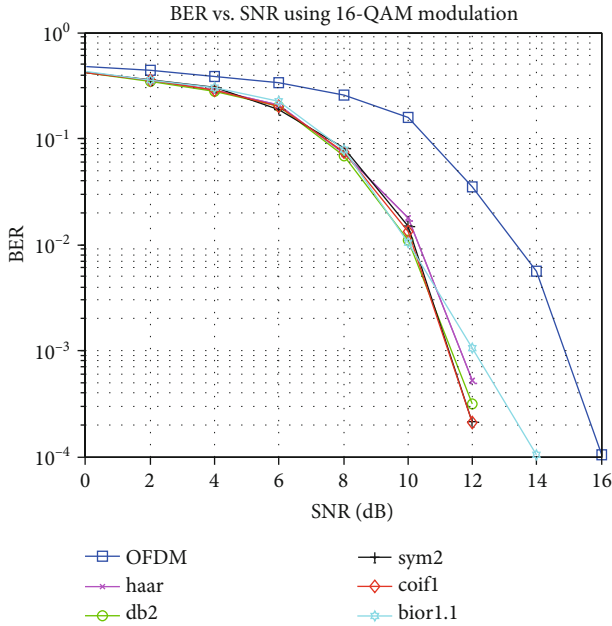


FIGURE 8: BER vs. SNR for different wavelet-based OFDM having 16 QAM.

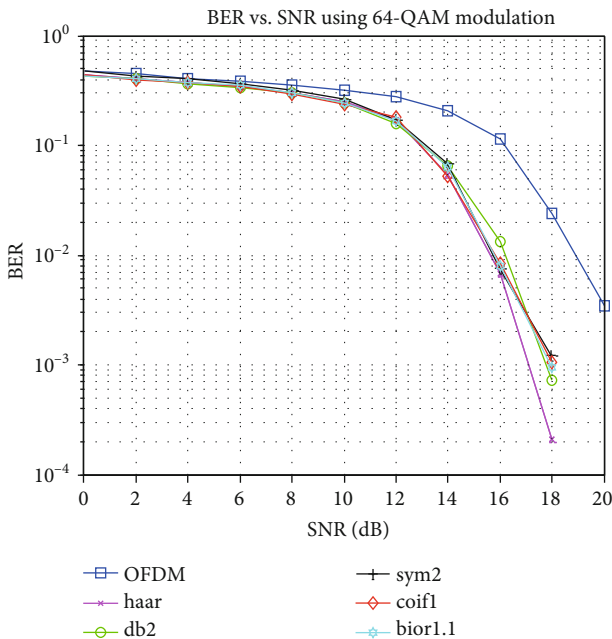


FIGURE 9: BER vs. SNR for different wavelet-based OFDM having 64 QAM.

7. Conclusion and Future Scope

A quantitative analysis of maximum attainable data rate and spectral efficiency for WOFDM demonstrates more than 16% improvement as compared to conventional OFDM. Simulative analysis of standard OFDM against five different wavelet-based OFDM, i.e., “haar,” “db2,” “sym2,” “coif1,” “bior1.1,” is performed to investigate the BER performance. For all different modulation levels, i.e., 4 QAM,

16 QAM, and 64 QAM, it is found that WOFDM significantly outperforms conventional OFDM in terms of BER performance. However, the BER performance of one wavelet type OFDM over other wavelet type OFDM (under-considered five wavelets) relies on the modulation level. Apparently, the BER performance is a tradeoff between spectral efficiency and maximum data rate. As the modulation level increases (more number of bits per modulated signal), spectral efficiency and data rate improve but BER performance degrades. As observed in the above plots, the BER performance gets degraded (up to 10 dB) as the modulation level increases from 4 QAM to 64 QAM; however, spectrum efficiency and data rate increases by 1.83 bps/Hz and 2.285 Mbps, respectively. In the view of future scope and depth of research, potential can be further exploited through the exploration of wavelet diversity and the impact of different fading channels, viz., Rayleigh and Rician, over the WOFDM system. In the future, the proposed solution can be further evolved to explore the performance deliverables at the upper spectrum band (20 MHz) with higher offset errors.

Data Availability

No standard database was used.

Conflicts of Interest

The authors declare that they have no conflicts of interest.

References

- [1] Y. G. Li and G. L. Stuber, *Orthogonal Frequency Division Multiplexing for Wireless Communications*, Springer Science & Business Media, 2006.
- [2] Y. G. Li, *Orthogonal Frequency Division Multiplexing for Wireless Communications*, Springer-Verlag, New York, 2009.
- [3] T. Hwang, C. Yang, G. Wu, G. Y. Li, and G. Ye Li, “OFDM and its wireless applications: A survey,” *IEEE Transactions on Vehicular Technology*, vol. 58, no. 4, pp. 1673–1694, 2009.
- [4] C. Shahriar, M. la Pan, M. Lichtman et al., “PHY-layer resiliency in OFDM communications: A tutorial,” *IEEE Communications Surveys & Tutorials*, vol. 17, no. 1, pp. 292–314, 2015.
- [5] K. O. O. Anoh, J. M. Noras, R. A. Abd-Alhameed, S. M. Jones, and K. N. Voudouris, “A new approach for designing orthogonal wavelets for multicarrier applications,” *AEU - International Journal of Electronics and Communications*, vol. 68, no. 7, pp. 616–622, 2014.
- [6] S. Sarowa, H. Singh, S. Agrawal, and B. S. Sohi, “Design of a novel hybrid intercarrier interference mitigation technique through wavelet implication in an OFDM system,” *Digital Communications and Networks*, vol. 4, no. 4, pp. 258–263, 2018.
- [7] M. K. Lakshmanan and H. Nikookar, “A review of wavelets for digital wireless communication,” *Journal of Wireless Personal Communications*, vol. 37, no. 3-4, pp. 387–420, 2006.
- [8] A. N. Akansu, W. A. Serdijn, and I. W. Selesnick, “Emerging applications of wavelets: A review,” *Physical Communication*, vol. 3, no. 1, pp. 1–18, 2010.

- [9] W. Gregory, "Emerging applications of multirate signal processing and wavelets in digital communications," *Proceedings of the IEEE*, vol. 84, no. 4, pp. 586–603, 1996.
- [10] A. E. Stanciu, L.-M. Nemtoi, and I. M. Moise, "Considerations regarding the spectral efficiency of orthogonal frequency division multiplexing," in *11th International conference on development and application systems*, pp. 128–134, Suceava (Romania), 2012.
- [11] M. Chafii, J. Palicot, and R. Gribonval, "Wavelet modulation: An alternative modulation with low energy consumption," *Comptes Rendus Physique*, vol. 18, no. 2, pp. 156–167, 2017.
- [12] J. Chunkath, S. S. Arjun, V. S. Sheeba, and S. A. Raj, "Performance improvement of multicarrier systems using wavelet filter banks," *Procedia Technology*, vol. 24, pp. 775–781, 2016.
- [13] Anuradha and N. Kumar, "BER analysis of conventional and wavelet based OFDM in LTE using different modulation techniques," in *2014 Recent Advances in Engineering and Computational Sciences (RAECS)*, pp. 1–4, Chandigarh, India, March 2014.
- [14] A. H. Kattoush, W. A. Mahmoud, and S. Nihad, "The performance of multiwavelets based OFDM system under different channel conditions," *Digital signal processing*, vol. 20, no. 2, pp. 472–482, 2010.
- [15] V. Kumbasar and O. Kucur, "Performance comparison of wavelet based and conventional OFDM systems in multipath Rayleigh fading channels," *Digital Signal Processing*, vol. 22, no. 5, pp. 841–846, 2012.
- [16] B. G. Negash and H. Nikookar, "Wavelet-based multicarrier transmission over multipath wireless channels," *Electronic Letters*, vol. 36, no. 21, article 1787, 2000.
- [17] M. K. Gupta and S. Tiwari, "Performance evaluation of conventional and wavelet based OFDM system," *International Journal on Electronics and Communication*, vol. 67, no. 4, pp. 348–354, 2013.
- [18] 3GPP, "UTRA-UTRAN long term evolution (LTE) and 3GPP system architecture evolution," 2008, http://www.3gpp.org/ftp/Inbox/2008_web_files/LTA_Paper.pdf.
- [19] S. Schwarz, J. C. Ikuno, M. Simko, M. Taranetz, Qi Wang, and M. Rupp, "Pushing the limits of LTE: A survey on research enhancing the standard," *IEEE Access*, vol. 1, pp. 51–62, 2013.
- [20] 3GPP Technical Specification 36.300, "Evolved universal terrestrial radio access (E-UTRA) and evolved universal terrestrial radio access network (E-UTRAN), overall description, stage2 (Release 8)," <http://www.3gpp.org>.
- [21] S. Sesia, I. Toufik, and M. Baker, *LTE-The UMTS Long Term Evolution: From Theory to Practice*, Wiley, West Sussex, UK, 2nd edition, 2011.
- [22] I. F. Akyildiz, D. M. Gutierrez-Estevez, and E. C. Reyes, "The evolution to 4G cellular systems: LTE-Advanced," *Physical Communication*, vol. 3, no. 4, pp. 217–244, 2010.
- [23] H. Narman and M. Atiquzzaman, "Joint and partial carrier components assignment techniques based on user profile in LTE systems," in *2015 IEEE Wireless Communications and Networking Conference (WCNC)*, New Orleans, LA, 2015.
- [24] V. Sharma, F. Song, I. You, and M. Atiquzzaman, "Energy efficient device discovery for reliable communication in 5G-based IoT and BSNs using unmanned aerial vehicles," *Journal of Network and Computer Applications*, vol. 97, pp. 79–95, 2017.
- [25] S. Sarowa, N. Kumar, S. Agrawal, and B. S. Sohi, "Evolution of PAPR reduction techniques: a wavelet based OFDM approach," *Wireless Pers Commun*, vol. 115, no. 2, pp. 1565–1588, 2020.
- [26] N. Kaur and N. Kumar, "Comparative analysis of ICI self cancellation techniques for wavelet OFDM under different channels in simulink," *Wireless Personal Communications*, vol. 105, no. 4, pp. 1513–1525, 2019.
- [27] N. Kaur and N. Kumar, "Review and analysis of simulink based OFDM," in *2017 3rd International Conference on Advances in Computing, Communication & Automation (ICACCA) (Fall)*, pp. 1–5, Dehradun, 2017.
- [28] N. Kaur and N. Kumar, "On effects of frequency offset on simulink model of OFDM," *Wireless Personal Communications*, vol. 115, no. 3, pp. 2349–2361, 2020.
- [29] P. Singh and O. P. Sahu, "An overview of ICI self cancellation techniques in OFDM systems," in *2015 IEEE International Conference on Computational Intelligence & Communication Technology*, pp. 299–302, Ghaziabad, 2015.
- [30] G. Kaur, N. Kumar, and B. S. Sohi, "PAPR reduction technique on wavelet based OFDM system by employing multi-level wavelet transform," in *2015 International Conference on Signal Processing, Computing and Control (ISPCC)*, pp. 215–219, Wanknaghat, 2015.
- [31] A. Joshi, A. Manas, S. Garg, and R. Wason, "Photonic crystal fiber (PCF) Raman amplifier," in *Advances in Signal Processing and Communication*, B. Rawat, A. Trivedi, S. Manhas, and V. Karwal, Eds., vol. 526 of Lecture Notes in Electrical Engineering, pp. 107–115, 2019.
- [32] N. Kumar and B. S. Sohi, "Evaluation of conventional and wavelet based OFDM system for ICI cancellation," *Wireless Personal Communication*, vol. 91, no. 3, pp. 1435–1446, 2016.
- [33] M. F. Raji, J. P. Li, A. U. Haq, E. Raji, and M. Happy, "Performance evaluation of orthogonal wavelet division multiplex for 5G and beyond," in *2019 16th International Computer Conference on Wavelet Active Media Technology and Information Processing*, pp. 1–5, Chengdu, China, 2019.
- [34] N. Kumar and B. S. Sohi, "Wavelet based OFDM with ICI self-cancellation in underwater acoustic communications," *International Journal of Computer Science and Information Security*, vol. 14, no. 4, pp. 347–352, 2016.

Research Article

A Hybrid Spectrum Combinational Auction Mechanism Based on a Weighted Bipartite Graph for Energy Internet in Smart Cities

Huibin Feng ^{1,2,3}, Zhaocai Yu ¹, Jian Guan ⁴, and Geng Lin ⁵

¹College of Computer and Control Engineering, Minjiang University, Fuzhou 350108, China

²Fujian Provincial Key Laboratory of Information Processing and Intelligent Control, Fuzhou 350108, China

³Digital Fujian Internet of Thing Laboratory of Intelligent Production, Minjiang University, Fuzhou 350108, China

⁴Modern Educational Technology Center, Minjiang University, Fuzhou 350108, China

⁵College of Mathematics and Data Science, Minjiang University, Fuzhou 350108, China

Correspondence should be addressed to Geng Lin; lingeng413@163.com

Received 21 March 2020; Revised 30 September 2020; Accepted 19 October 2020; Published 5 November 2020

Academic Editor: Wei Yu

Copyright © 2020 Huibin Feng et al. This is an open access article distributed under the Creative Commons Attribution License, which permits unrestricted use, distribution, and reproduction in any medium, provided the original work is properly cited.

Energy Internet (EI) is aimed at sustainable computing by integrating various energy forms into a highly flexible grid similar to the Internet. The network subsystems of EI connect different components to enable real-time monitoring, controlling, and management. In this paper, the spectrum allocation problem of the cognitive radio network for EI in a smart city is investigated. The network spectrum allocation with both heterogeneous primary operators and secondary users is formulated as the combinatorial auction problem and then is converted to a subset selection problem on a weighted bipartite graph. We propose a hybrid algorithm to solve the problem. Firstly, the proposed algorithm uses a constructive procedure based on the Kuhn-Munkres algorithm to obtain an initial solution. Then, a local search is used to improve the solution quality. In addition, the truthfulness of the auction is guaranteed by adopting a “Vickrey-like” mechanism. Simulation results show that the performance of the proposed algorithm is better than existing greedy algorithms in terms of the social welfare, seller revenue, buyer satisfaction ratio, and winning buyer ratio.

1. Introduction

The smart city is an innovation of the physical city with high integration of advanced monitoring, sensing, communication, and control technologies aimed at providing real-time, interactive, and intelligent urbanization services to end users [1]. To realize the smart city, Energy Internet is one of the key technologies. Energy Internet (EI) is aimed at sustainable computing by integrating various energy forms into a highly flexible grid similar to the Internet in the smart city [2]. A typical EI system for a smart city consists of three subsystems: energy subsystem, information subsystem, and network subsystem [3]. The network subsystems connect different devices of EI to enable real-time monitoring, controlling, and management [4, 5]. The devices in the network subsystem use wired or wireless technologies to establish direct transmission links between devices, such as D2D communication, WiMAX, cognitive radio (CR) network, and cel-

lular network [6, 7]. These communication technologies are combined in EI to implement real-time monitoring of devices in a smart city [8, 9]. To improve the reliability and efficiency of device information communications in a smart city, the cognitive radio network spectrum allocation technology is required. Cognitive radio [10] technology has been introduced to increase transmission availability and efficiency. In a cognitive radio network, the secondary user can dynamically access the spectrum bands when the licensed primary users are not occupied according to the dynamic spectrum access technology. The dynamic spectrum access technology makes the primary wireless service providers not only satisfy their own spectrum requirement but also obtain additional profit by offering a free spectrum to the other secondary users. So it is vital to design a mechanism to encourage the primary spectrum operators to permit the secondary users to access the idle primary operators' spectrum band and to enhance the spectrum availability

and efficiency. While dynamic spectrum access is attractive, how to allocate the spectrum across multiple primary operators and secondary users is still an important open issue. The fact of the matter is to construct a mechanism that can effectively allocate the spectrum. There are many works that had been done about the dynamic spectrum allocation for the cognitive radio network with many tools such as game theory [11, 12] and contract theory [13]. Different from [12, 13], the dynamic spectrum access on auction is more suitable because of its economic incentive and joint consideration about the quality of service and statistical reference in the network. To achieve the economic incentive for the spectrum auction, the truthfulness, revenue, and utilization must be guaranteed. The truthfulness can make the bidders in the auction not benefit from their untrue valuation for the spectrum opportunity, the revenue can make the total amount of payment from all winning buyers in the auction maximized, and the utilization can make as many buyers as possible to reuse the spectrum. So the auction has been widely applied to the spectrum market.

In general, the spectrum auction mechanism includes online auction and periodical auction. The online auction is developed based on short intervals in the time domain and small areas in the space domain, while in the periodical auction, the spectrum is sold periodically by the primary operator and the intervals are relatively long. For the periodical auction, in [14], Gandhi et al. proposed a general centralized periodical auction framework for spectrum allocation in the cognitive radio network. In [15], the spectrum opportunity in a time-frequency division manner and the spectrum allocation mechanism on combinatorial auction are proposed. As for the online auction, Tehrani and Uysal proposed an auction-based spectrum trading method to maximize the total satisfaction of the secondary users and revenue of the wireless service provider in [16]. In [17], Yi et al. proposed an online spectrum auction framework for the cognitive radio network which considered the uncertain activities of primary users. To further improve the spatial reusability of the spectrum, Wang et al. proposed an online auction framework using a mixed graph for licensed shared access systems in [18]. Different from [18], group buying strategy is used to design the spectrum auctions to increase the buying power of small network providers in [19]. Considering the channels are heterogeneous, Khairulla and Chatterjee proposed an auction-based allocation algorithm in a distributed multichannel cognitive radio network in [20]. To satisfy the quality of service of user equipment in the specific network, Shen et al. proposed a spectrum sharing framework for the hybrid access in the two-tier macro-femtocell networks in [21]. Secondary spectrum auction taking communication constraints into account is studied in [22]. Yi and Cai introduced another spectrum auction framework among heterogeneous secondary users with various quality of service requirements for recall-based cognitive radio networks in [23].

To improve the fairness and efficiency of the online auction, another research topic for spectrum sharing is the double auction. Compared with the single auction on spectrum allocation, the double auction is more fair and effective because both buyers and sellers can submit bids to the central

auctioneer. In [24], a truthful multichannel spectrum double auction framework is proposed. Considering the shared spectrum consists of a wide range of frequencies, a truthful double auction framework for a heterogeneous spectrum named TAMES is proposed in [25]. Assuming without the valuation distribution knowledge, a framework for spectrum double auction which jointly considers spectrum reusability, truthfulness, and profit maximization is designed in [26]. To ensure strategy-proof auction, Sun et al. proposed a multiunit double auction approach that guarantees the competitive fairness among buyers while remaining strategy-proof for spectrum allocation in [27]. Another spectrum allocation on double auction for explicitly decoupling the buyer-side and seller-side auction while achieving truthfulness, individual rationality, and budget balance is investigated in [28].

For both online auctions mentioned above, none of them takes both multiple multichannel primary operators and secondary users existing in the cognitive radio network into account. In [29], Zhou et al. firstly proposed a spectrum allocation framework on combinatorial auction and an approximation algorithm is presented. Another spectrum combinatorial auction framework for the scenario that each primary user has multiple channels to sell and each secondary user demands multiple channels is proposed in [30]. Assuming primary users possess heterogeneity and secondary users may request different types of spectrum bands, a spectrum combinatorial double auction and corresponding greedy allocation algorithm are proposed in [31].

Spectrum allocation for the cognitive radio network on both multiple multichannel primary users and secondary users is mostly based on combinatorial auction, because the combinatorial auction problem is NP-hard; most studies in the literature model the combinatorial auction as a multiple multidimensional knapsack problem or integer program problem, then use greedy algorithms to solve the problem and derive an approximate solution, but the quality of the solution is not good enough. In this paper, we focus on the spectrum auction problem with multiple heterogeneous primary operators and multiple secondary users in a smart city. Each primary operator in a smart city has multiple channels, and the channels have different widths (e.g., the channel width for a TV broadcast network is 6 MHz, and the channel width of a global system for mobile communications is 200 kHz). The secondary user in a smart city can dynamically access the different primary operators according to cognitive radio technology [32]. We also assume that each secondary user in a smart city has a different spectrum requirement, and it must request different channel numbers from multiple primary operators. So the spectrum allocation in a smart city can be formulated as a combinatorial auction problem because the secondary user bids a bundle of channels. To make the auction mechanism work efficiently, we firstly model the spectrum combinatorial auction problem in a smart city as a subset selection problem on the weighted bipartite graph; then, we design a hybrid algorithm which can run in a hybrid manner with high efficiency. Simulation results and comparison show that the efficiency of the proposed auction mechanism can be enhanced.

The key contributions of this paper can be summarized as follows:

- (i) We consider the spectrum allocation problem of the cognitive radio network for EI in a smart city. The spectrum combinational auction problem of the cognitive radio network with multiple heterogeneous primary operators and multiple secondary users is converted to a subset selection problem on a weighted bipartite graph
- (ii) We design a constructive procedure, which iteratively uses the Kuhn-Munkres (KM) algorithm [33, 34], to generate an initial solution. Then, a swap procedure and an interchange procedure are applied to improve the solution quality
- (iii) We design extensive experiments to verify the performance of the proposed auction mechanism. Social welfare, seller revenue, buyer satisfaction ratio, and winning buyer ratio have been carefully investigated. Simulation results show that the proposed algorithm can obtain higher allocation performance and efficiency for the cognitive radio network of EI in a smart city

The remainder of this paper is organized as follows. Section 2 formulates the spectrum allocation model and describes the framework with multiple heterogeneous primary operators and multiple secondary users in a smart city. Section 3 presents a hybrid spectrum allocation algorithm on a weighted bipartite graph model to obtain a good-quality allocation scheme. Section 4 gives the simulation results and comparisons. The concluding remarks are made in Section 5.

2. System Model

2.1. System Model. In this section, the spectrum allocation model and framework for the cognitive radio network for EI in a smart city are described in Figure 1. We consider a cognitive radio network of EI in a smart city [35] with n secondary users (such as the neighborhood area network gateway) and m primary operators. We also assume that the primary operators have a different number of channels, and the channel width of the primary operators is different. To share the spectrum between the primary operators and the secondary users, we assume that there exists a centralized control center that acts as the spectrum auctioneer which manages the spectrum allocation. In the auction, the primary operators act as the seller and the secondary users act as buyers; we also assume that the auctioneer is a nonprofit body which runs the auction, determines the winners, and allocates the spectrum to the secondary user.

Each primary operator owns a spectrum which serves its licensed users. When the spectrum is idle at a time, the primary operator would like to allow the secondary user to access the idle spectrum to earn extra profits. We assume that the auction is an online auction-based short interval in the time domain. Because the auctioned spectrum bandwidth

of the primary operator is different, without loss of generality, we further assume that each primary operator's ideal spectrum band is divided into a series of channels with identical channel bandwidth; thus, the number of channels may be different for each primary operator in terms of the different channel bandwidths, for example, 6 MHz for a TV band and 200 kHz for a global system band for mobile communication.

Assume that the secondary users in the system can request and obtain multiple channels from different primary users to satisfy their own bandwidth demand, but it is difficult for the secondary users to use multiple discontinuous spectrum bands from different primary operators; we assume that each secondary user can only access the spectrum band for the same primary operator. All secondary users in the system are not interfere-free because within the same communication range, one channel can only be accessed by secondary users at some specific time.

In order to describe the formulation and our spectrum combinational auction mechanism clearly, some notations are introduced. Let $M = \{1, 2, \dots, m\}$ be the set of the primary operators and $c_i \in \mathbb{Z}^+$ denote the number of channels owned by the i th primary operator, where $i = 1, 2, \dots, m$. Then, the set of primary operators in the auction channel in terms of quantity can be denoted as $C = (c_1, c_2, \dots, c_i, \dots, c_m)$. Let $b_i \in \mathbb{Z}^+$ be the channel's bandwidth of the i th primary operator. The vector $B = (b_1, b_2, \dots, b_i, \dots, b_m)$ represents the set of primary operators of the channel bandwidth.

Let $N = \{1, 2, \dots, n\}$ be the set of secondary users; each secondary user has a spectrum bandwidth demand to satisfy its own quality of service. Let $d_j > 0$ be the specific spectrum demand of the j th secondary user. The secondary user's valuation of its own spectrum demand is denoted as v_j ; we also denote the $v_j = d_j \times \log(1 + \gamma_j)$, where the γ_j denotes the signal-to-noise ratio of the j th secondary user, and we also assume that it is a constant during the auction interval. Let $p_j > 0$ be the bid price the secondary user is willing to pay for using the spectrum demand d_j ; thus, the bid price vector of the secondary user can be denoted as $P = (p_1, p_2, \dots, p_j, \dots, p_n)$. We assume that the auction is the truthful auction; then, the bidding price is equal to the valuation price of the secondary user, i.e., $p_j = v_j$.

For the reason that each secondary user can bid a bundle of channels for different primary operators, we can formulate the spectrum allocation as a combinational auction model. For each round of the auction, the auctioneer collects each primary operator channel number and channel bandwidth; it also collects each secondary user's private spectrum bandwidth demand and bid price. Then, the auctioneer determines the optimal spectrum allocation according to these sealed bid information.

2.2. Problem Formulation. We assume that the primary operators and secondary users in the network subsystem can exchange the information with the auctioneer. After receiving the primary operator-submitted information, the auctioneer generates the channel bandwidth vector B , the channel quantity C of the primary operators, the specific

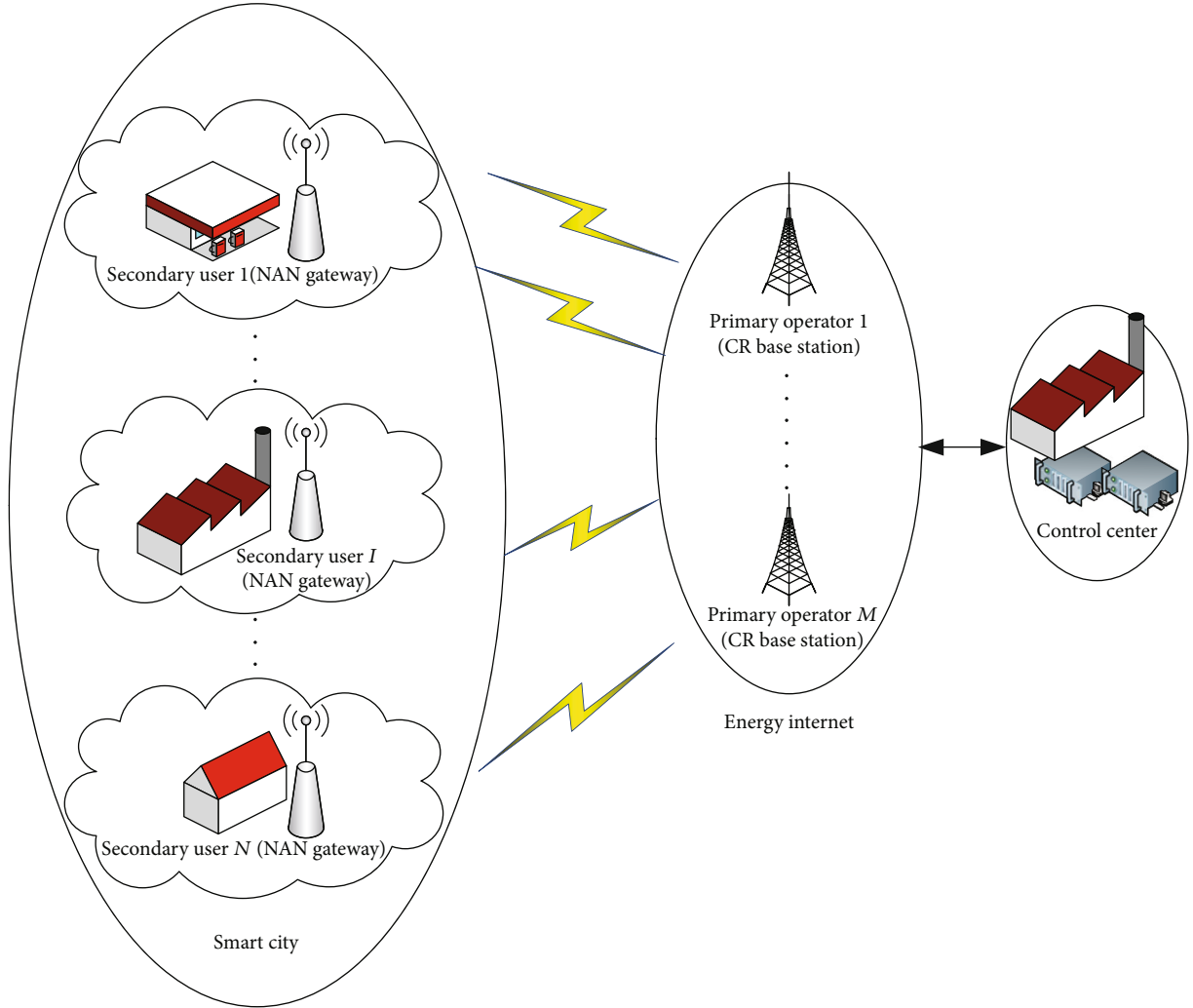


FIGURE 1: Cognitive radio network of EI in a smart city.

spectrum demand vector $D = (d_1, \dots, d_m)$, and the bid price vector P .

Basing on the above bid information, the auctioneer executes the winner determination algorithm to maximize the

utility of the seller, and thus, the allocation matrix can be achieved. The allocation matrix can be denoted by X_{nm} .

The element in the allocation matrix can be denoted by x_{ij} and can be defined as follows:

$$x_{ij} = \begin{cases} 1, & \text{if primary operator } i \text{ allocates the spectrum chunk to secondary user } j, \\ 0, & \text{otherwise.} \end{cases} \quad (1)$$

Since each secondary user can only acquire the specific spectrum demand from no more than one primary operator, the spectrum allocation constrained equation of the j th secondary user can be written as follows:

$$\sum_{i=1}^m x_{ij} \leq 1. \quad (2)$$

Similarly, the primary operator spectrum is limited; thus, the requested spectrum chunk of all the secondary users cannot exceed the bandwidth the primary operator owns. So the spectrum bandwidth constraint of the i th primary operator can be written as follows:

$$\sum_{j=1}^n x_{ij} d_j \leq c_i b_i. \quad (3)$$

The objective of the spectrum combinational auction is to determine an optimal allocation matrix so that the social welfare is maximized. We can model the above problem as an optimization problem as follows:

$$\max z = \sum_{i=1}^m \sum_{j=1}^n x_{ij} p_j. \quad (4)$$

The optimization problem with spectrum constrain condition must satisfy equations (1)–(3), and the optimization problem is known to be NP-hard [36].

2.3. Spectrum Auction Model on a Weighted Bipartite Graph. Due to the high complexity of solving the optimization problem, we propose a heuristic method to find good-quality allocation schemes. Existing greedy algorithms used the individual information to allocate the spectrum. In order to consider all information simultaneously, we use the

$$w_{ij} = \begin{cases} p_j, & \text{if primary operator } i \text{ connects to secondary user } j \text{ with one edge,} \\ 0, & \text{otherwise.} \end{cases} \quad (6)$$

Based on the above definition, we convert the spectrum combinatorial auction model to a weighted bipartite graph. The vertices of the graph are the primary operator and secondary user in the network. The edges between the primary operators and the secondary users exist only if the primary operators, which can satisfy the corresponding secondary user's spectrum requirement, and the edges are constructed according to equation (5). The weights of the edges are set according to equation (6).

In fact, an edge subset $T \in E$ represents a spectrum allocation scheme. If an edge e_{ij} is selected in T , it means that primary operator i allocates the spectrum chunk to secondary user j . Otherwise, primary operator i does not allocate the spectrum chunk to secondary user j . An edge set T is called feasible if its corresponding spectrum allocation scheme satisfies equations (2) and (3).

The objective of the spectrum allocation is to maximize the social welfare for allocating the spectrum to the secondary user. Maximizing the social welfare of the auction can be converted to finding a feasible edge set, such that the sum of the weights of the selected edges is maximized.

3. Spectrum Allocation Mechanism on a Weighted Bipartite Graph

In this section, we propose a hybrid spectrum auction mechanism by finding a feasible edge set of the weighted bipartite graph. The hybrid spectrum auction mechanism consists of two phases. In the first phase, a constructive procedure based on the well-known Kuhn-Munkres (KM) algorithm [33, 34] is used to generate a feasible edge set (i.e., an initial spectrum

weighted bipartite graph to model the considered spectrum combinational auction problem in a smart city.

Let $G = (V, E)$ be an undirected weighted bipartite graph, where V is the vertex set and E is the edge set. The vertex set consists of two disjoint subsets N and M . Each vertex in the set N represents a secondary user, and each vertex in the set M represents a primary operator. Each edge in the edge set is denoted by e_{ij} , where $i \in N$ and $j \in M$; the edge e_{ij} exists only if the vertex $i \in N$ and the vertex $j \in M$ satisfy the following equation:

$$d_j \leq c_i b_i. \quad (5)$$

If there exists an edge e_{ij} between the primary operator i and the secondary user j , the weight of e_{ij} is set as the secondary user's bid price p_j . So we have

allocation scheme). Then, the initial spectrum allocation scheme is further improved by the local search procedure in the second phase. In the following subsection, we will give the detailed descriptions of the constructive procedure based on KM and the local search procedure and analyze the computational complexity and the auction properties of the mechanism.

3.1. The Constructive Procedure Based on KM. The existing greedy algorithm [30] used the individual information to generate a spectrum allocation scheme. In each iteration, only one secondary user obtained the spectrum. In this work, our proposed constructive procedure applies the KM to achieve global optimization efficiently and generate an initial spectrum auction scheme. Different from existing greedy algorithms, in each iteration of our constructive procedure, several secondary users are simultaneously allocated by global consideration. It enhances the efficiency of the allocation.

The pseudocode of the constructive procedure is given in Algorithm 1. After receiving all channel information and bid information, the constructive procedure firstly constructs the weighted bipartite graph $G = (V, E)$, where $V = M \cup N$. Note that the number of primary operators is usually smaller than the number of secondary users (i.e., $m < n$). In order to apply the KM, we add $n - m$ virtual vertices to M for ensuring $n = m$. Meanwhile, we add edges between each virtual vertex and each vertex in N , and the weights of these adding edges are set to zero. The obtained graph is also denoted by G . Let T and SumW be the selected edge set and the weight sum of the selected edges in T , respectively.

Require: input n, m, b, c, d, p .
Ensure: T , and SumW.
1: Construct the initial weighted bipartite graph $G = (V, E)$, where $V = M \cup N$.
2: Add virtual vertices and edges.
3: Initialize $T = \emptyset$, SumW = 0.
4: **repeat**
5: Find the maximum perfect matching MT by using the KM.
6: Let $T = T \cup \text{MT}$, SumW = SumW + $\sum_{e_{ij} \in \text{MT}} w_{ij}$, and for each $e_{ij} \in \text{MT}$, update $c_i = c_i - \lfloor d_j/b_i \rfloor$.
7: Update graph G .
8: **until** activepn = 0
9: RETURN T , and SumW

ALGORITHM 1: Constructive procedure

Then, the proposed constructive procedure employs the KM to find a maximum perfect matching MT of G . The obtained maximum perfect matching MT is an edge set which indicates a spectrum auction scheme. Add the obtained maximum perfect matching MT into T . After adding the obtained maximum perfect matching, for each $e_{ij} \in \text{MT}$, the primary operator i allocates the spectrum to the secondary users j , and its surplus spectrum is calculated by $c_i = c_i - \lfloor d_j/b_i \rfloor$. There may exist primary operators whose surplus spectrum exceeds the requested spectrum chunk of unallocated secondary users. In other words, after the above auction allocation, some primary operators may still have enough spectrum to provide to secondary users. A primary operator is called active if it can allocate the surplus spectrum chunk to at least one unallocated secondary user in the system. We update the graph G as follows. First, we delete all edges with $w_{ij} \neq 0$. Second, for each $i \in M$ and $j \in N$, if equation (5) is satisfied, we add an edge e_{ij} into E , and the weight of e_{ij} is set to p_j . Finally, we remove all edges between the allocated secondary user and primary operator, which indicates that the allocated secondary user is not allowed to receive the spectrum again. Let activepn be the number of active primary users. If activepn $\neq 0$, the constructive procedure executes the above process. Otherwise, if there is no active primary operator in the system, we stop the algorithm and return the selected edge set T , which indicates an initial spectrum allocation scheme and its social welfare SumW.

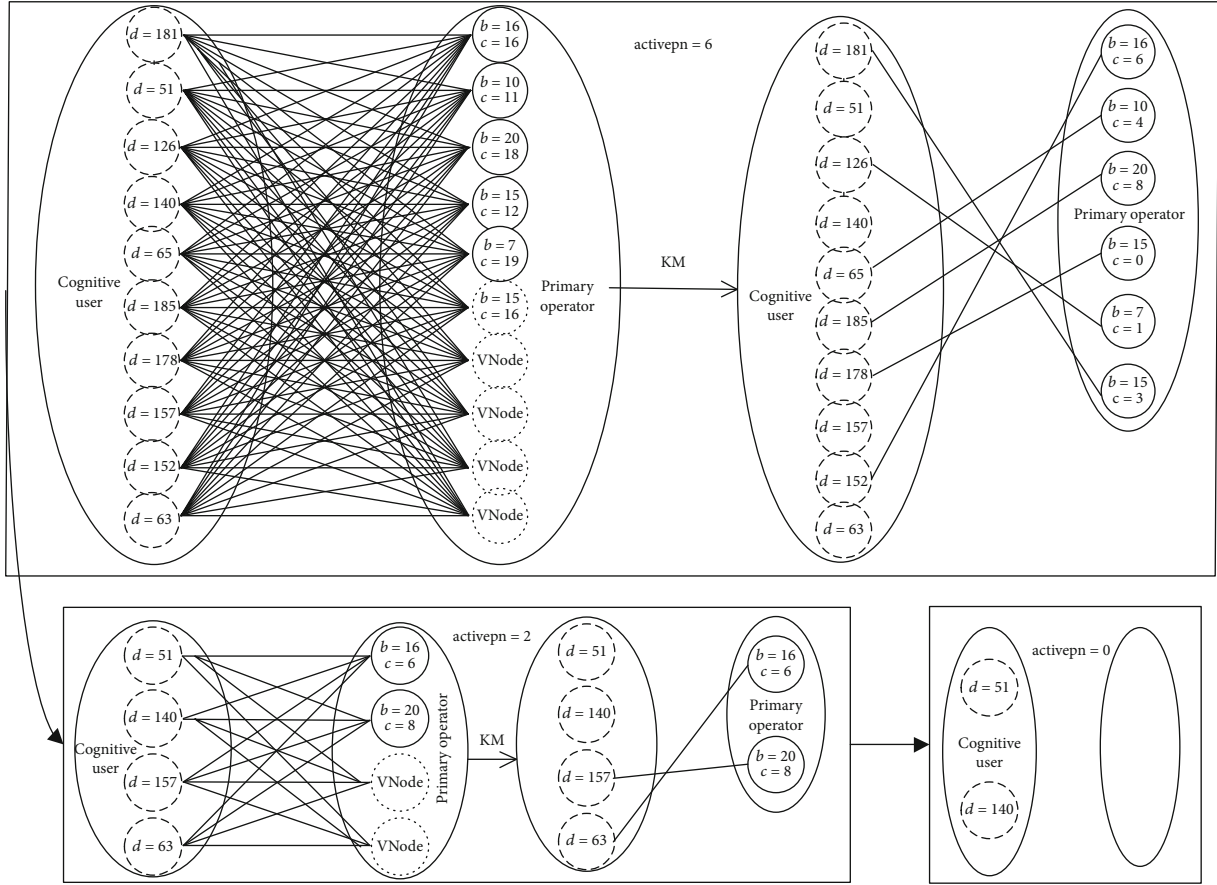
Figure 2 shows an example of the constructive procedure based on KM with $n = 10$ and $m = 6$. The spectrum demand and the signal-to-noise ratio of secondary users (cognitive users) N are set to [181,51,126,140,65,185,178,157,152,63] and [112,117,117,200,139,108,185,117,186,144], respectively. The number of channels and the channel's bandwidth of primary operators M are set to [16,10,20,15,7,15] and [16,11,18,12,19,16], respectively. The weighted bipartite graph G is constructed by adding four virtual vertices in M . The weights of the edges between the primary operator and the secondary user are set as $d_j \times \log(1 + \gamma_j)$. The weights of the edges between the virtual vertices and the secondary user are set to zero.

There are six active primary operators in the weighted bipartite graph, i.e., activepn = 6; the KM algorithm is applied to find the maximum perfect matching. The secondary users with spectrum demand $D = [181,126,65,185,178]$ are allocated with a spectrum by primary operators with the channel's bandwidth $B = [16,10,20,15,7,15]$. After the first match, the primary operator with the channel's bandwidth of sixteen has four channels remaining, and the primary operator with the channel's bandwidth of twenty has eight channels remaining also. Therefore, the new weighted bipartite graph can be constructed. The number of active primary operators is activepn = 2, the KM algorithm is applied to find the maximum perfect matching, and finally the secondary users with spectrum demand $D = [157,63]$ are allocated with a spectrum by primary operators with the channel's bandwidth $B = [20,16]$. After the second match, the secondary users with spectrum demand $D = [51,140]$ are still not allocated. Because all the primary operators are not active, the constructive procedure on KM stops and we get the initial spectrum allocation.

3.2. Local Search Procedure. According to the execution of Algorithm 1, an initial spectrum allocation scheme is obtained. Although there are no primary operators that can directly allocate the spectrum to any secondary users in the system, the allocation is not the optimal allocation for the system because some of the primary operators also have some idle spectrum chunk. We propose a local search procedure, which integrates a swap procedure and an interchange procedure, to improve the solution quality.

The basic idea of the swap procedure is to swap the allocated spectrum chunk between the primary operators and make some primary operators get a bigger idle spectrum chunk. So it is possible for the primary operators with a bigger idle spectrum chunk to assign spectrum chunk to some unallocated secondary users.

Let $Asnum_i$ be the number of secondary users which the primary operator i has been allocated to and s_i^k be the quantity of the spectrum chunk of the k th secondary user in the array the primary user i has been assigned to. To swap the allocated spectrum chunk, we also define the value of the swap flag as F_{swap} , where $F_{\text{swap}} = \text{true}$ denotes that there exist


 FIGURE 2: An example with $n = 10$ and $m = 6$.

primary operators swapping allocated secondary users. Variable Sf_j records the status of the secondary user j , where Sf_j can be defined as follows:

$$Sf_j = \begin{cases} i, & \text{if primary operator } i \text{ allocates the spectrum to secondary user } j, \\ 0, & \text{otherwise.} \end{cases} \quad (7)$$

At the beginning of the swap procedure, we first sort all the primary operators according to the surplus spectrum chunk quantity value c_i in descending order; then, we swap the idle spectrum chunk between the sorted primary operators to make one of the primary operator idle spectrum chunk bigger. During the swap procedure, if the primary operator with a bigger idle spectrum chunk can be allocated to an unallocated secondary user, the primary operator allocates the spectrum to this unallocated secondary user to improve the social welfare. We iteratively implement the swap process until all primary operators have been checked. The swap procedure is presented in Algorithm 2.

After the swap procedure, we use an interchange procedure to further improve the social welfare. The proposed interchange procedure uses the interchange of the allocated secondary user by some unallocated users set with higher

bid price, so as to promote the total social welfare of the auction.

In order to describe the interchange procedure clearly, we introduce some notations. Let $Sump$ be the total value of some given secondary user set bid price, TS be the value of the temporary secondary user set, and $counter$ be the number of the vector TS , respectively. cp represents the value of the spectrum quantity. The step of the interchange algorithm on local search can be presented as Algorithm 3.

3.3. The Computational Complexity. We now analyze the computational complexity of the proposed spectrum auction mechanism. The proposed mechanism contains three main procedures: the constructive procedure, the swap procedure, and the interchange procedure. The computational complexity of the constructive procedure (Algorithm 1) is decided by

```

1: Generate primary operator array according to the assigned secondary user.
2: Sort primary operator array on the surplus spectrum chunk in descending order.
3: set  $F_{\text{swap}} = \text{false}$ ;  $q = 0$ .
4: for ( $i = m - 1$ ;  $i > 0$ ;  $i--$ ) do
5:   for ( $j = i + 1$ ;  $j < = m$ ;  $j++$ ) do
6:     for ( $k = 0$ ;  $k < \text{Asnum}_j$ ;  $k++$ ) do
7:       if  $\lfloor s_i^k / b_j \rfloor b_j \leq b_j c'_j$  then
8:         Move secondary user  $k$  in primary operator  $i$  to the idle surplus spectrum of primary operator  $j$ ;  $k--$ .
9:       else
10:        for ( $l = \text{Asnum}_j - 1$ ;  $l > = 0$ ;  $l--$ ) do
11:          if ( $s_j^l > = s_i^k$ ) then
12:            break.
13:          else
14:            if ( $c'_j b_j + \lfloor s_j^l / b_j \rfloor b_j > = s_i^k$ ) then
15:              Swap allocated spectrum between  $k$  secondary user in primary operator  $i$  and  $l$  secondary user in primary operator
16:               $j$ .
17:            end if
18:          end if
19:        end for
20:      end if
21:    end for
22:  Finding an unassigned secondary user  $q$  with maximal bid price.
23:  if  $q \neq 0$  then
24:     $\text{Sf}_q = i$ ,  $\text{Asnum}_i = \text{Asnum} + 1$ ,  $c'_i = c'_i - \lfloor d_q / b_i \rfloor$ .
25:  end if
26:  Sort the primary operator  $i$  on the assigned spectrum chunk in descending order.
27: end for
28: if ( $F_{\text{swap}} == \text{true}$ )
29:    $i++$ .

```

ALGORITHM 2: Swap procedure

```

1: Inherit the parameter value obtained from Algorithm 1 and Algorithm 2.
2: for ( $i = 1$ ;  $i < n$ ;  $i++$ ) do
3:   if  $\text{Sf}_i > 0$  then
4:     Set  $k = \text{Sf}_i$ ;  $\text{cp} = s_i^k + c_k$ .
5:     Set  $\text{Sump} = 0$ ;  $\text{counter} = 0$ .
6:     Set  $\text{TS} = \emptyset$ .
7:     for ( $j = 1$ ;  $j < n$ ;  $j++$ ) do
8:       if ( $\text{Sf}_j == 0$ ) and ( $\text{cp} > = s_j^k$ ) then
9:          $\text{counter} = \text{counter} + 1$ ;  $T_{\text{counter}} = j$ .
10:         $\text{cp} = \text{cp} - s_j^k$ ;  $l = \text{Sf}_j$ .
11:         $\text{Sump} = \text{Sump} + p_l$ .
12:      end if
13:    end for
14:    if  $\text{Sump} > p_k$  then
15:      for ( $y = 0$ ;  $y < \text{counter}$ ;  $y++$ ) do
16:         $\text{Sf}_y = k$ .
17:      end for
18:       $c_k = \text{cp}$ ;  $\text{Sf}_i = 0$ .
19:       $\text{SumW} = \text{SumW} + \text{Sump} - p_k$ .
20:    end if
21:  end if
22: end for
23: Return  $\text{SumW}$ .

```

ALGORITHM 3: Interchange procedure

the application of the KM. The computational complexity of the KM is $O(n^3)$. Since the KM is executed at most m iterations in the constructive procedure, the computational complexity of the constructive procedure is bounded by $O(mn^3)$. To find a bigger spectrum chunk for secondary users, the swap procedure (Algorithm 2) searches the idle spectrum chunk between all the primary operators. This operator takes $O(m^2)$ time. If a bigger idle spectrum chunk is found, the swap procedure needs $O(n)$ to find a secondary user for allocation. Hence, the swap procedure is bounded by $O(nm^2)$. The interchange procedure (Algorithm 3) takes $O(n^2)$ to further improve the social welfare. Therefore, the computational complexity of the proposed spectrum auction mechanism is bounded by $O(mn^3 + nm^2 + n^2)$.

3.4. The Payment Rule and Economic Properties. We propose the payment rule and the economic properties for the auction model. After executing the proposed algorithm, we adopt the payment of each winning secondary user; if secondary user j was denied in the auction or $B_{-j} = \emptyset$, then its payment is zero. Otherwise, secondary user j wins, and its payment is $\sqrt{d_j} \times (p_k / \sqrt{d_k})$, where $k \in B_{-j}$, B_{-j} represents the bid set of the secondary user j that was denied in the auction, and B_j denotes the bid bundle of the secondary user j that won in the auction, and the B_{-j} and B_j can be calculated according to the following: bid B_j blocks B_{-j} or not. We say the bid B_j blocks B_{-j} if removing secondary user j from the bidders' set, all bids in B_{-j} can be granted.

[30] analyzed the economic properties of their auction model. Although our proposed spectrum auction mechanism is different from the mechanism in [30], we use the same payment rule. The results in [30] indicate that our auction model has incentive compatibility and individual rationality. Therefore, it guarantees that no secondary user can get a higher utility by bidding untruthfully and all true bidding for the secondary user can get nonnegative utilities in the proposed auction model.

4. Experiment

In this section, we evaluate the performance of the proposed spectrum auction mechanism of the cognitive radio network for EI in a smart city. We run the implementation in a Windows 7 system with Intel Core i5-3210M 2.5GHZ and 4GB memory. The program was written in C language and run in software C-Free 5. We also generate the scenario with heterogeneous primary operators (the channel bandwidth and the number of channels are different) and multiple secondary users with different spectrum demands in the cognitive radio network of EI in a smart city. For comparison purposes, the specific simulation parameters in this paper are similar to those in [30]. We also coded the spectrum allocation algorithm in [30] in C language and made comparisons between this spectrum allocation algorithm [30] and our proposed algorithm.

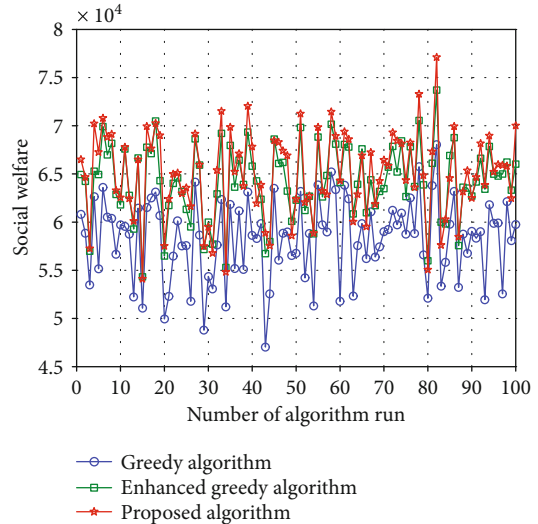


FIGURE 3: Comparison of the social welfare under different algorithms with a fixed secondary user.

4.1. Experimental Setup. We assume that there are 100 secondary users randomly distributed in the network. All the primary operators are independent, and the number of channels of each primary operator is randomly selected in $[10, 20]$; the channel bandwidth of each primary operator is also randomly selected in $[5, 20]$ MHz. In the same way, we also assume that the spectrum demand of each secondary user in the network is randomly chosen in $[50, 20]$ MHz, and the corresponding secondary users' SNR γ_j for secondary user j is randomly selected in $[100, 200]$; the bid price of the secondary user is defined as $d_j \times \log(1 + \gamma_j)$, where d_j is the spectrum demand of secondary users j . We use the following performance metrics to evaluate the proposed auction model:

- (i) *Social Welfare.* The sum bid price of the secondary user in the auction.
- (ii) *Seller Revenue.* The sum of charged payments of all the winning secondary users in the auction.
- (iii) *Buyer Satisfaction Ratio.* The percentage of winning secondary user bids to the total demands.
- (iv) *Winning Buyer Ratio.* The percentage of the number of winning secondary users to the total number of secondary users.

4.2. Experimental Results

4.2.1. Fixed Network Size. Firstly, we evaluate the proposed algorithm performance with the number of primary operators is fixed to 50. The other network parameter is randomly generated as described in Section 4.1. The result generated under the greedy algorithm and the enhanced greedy algorithm in [30] is, respectively, denoted as the Greedy algorithm and Enhanced Greedy algorithm; the results of the social welfare, seller revenue, buyer satisfaction ratio, and winning buyer ratio for the different algorithms are compared on the value over 100 runs.

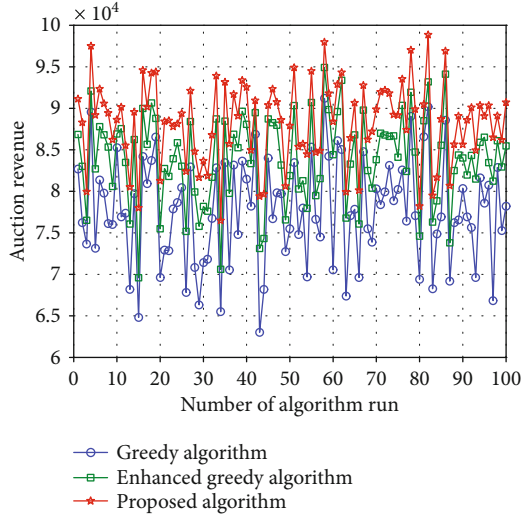


FIGURE 4: Comparison of the auction revenue under different algorithms with a fixed network size.

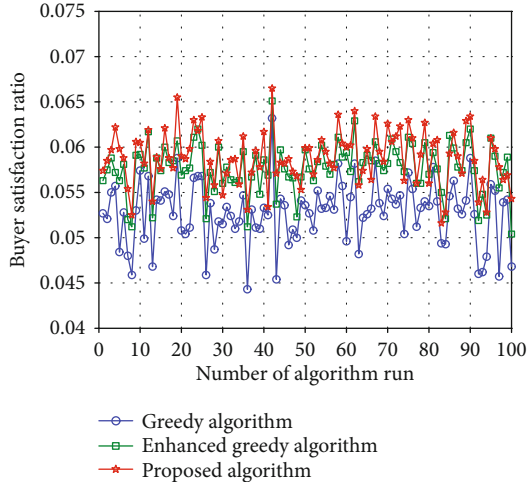


FIGURE 5: Comparison of the buyer satisfaction ratio under different algorithms with a fixed network size.

Figure 3 shows the computational results with respect to the social welfare when the number of different algorithm run indexes varies from 1 to 100. It can be clearly seen that the proposed algorithm is higher (average of 11.48% times) than the Greedy algorithm on the social welfare with different algorithm run indexes. The proposed algorithm is also higher (average of 1.23% times) than the Enhanced Greedy algorithm. The simulation result shows that the proposed algorithm is more efficient than the benchmark algorithms in terms of the social welfare.

Figure 4 shows the computational results with respect to the auction revenue when the number of different algorithm run indexes varies from 1 to 100. It can be clearly seen that the proposed algorithm is higher (average of 13.7% times) than the Greedy algorithm on the auction revenue with different algorithm run indexes. The proposed algorithm is also higher (average of 5.19% times) than the Enhanced Greedy algorithm. The simulation result shows that the proposed

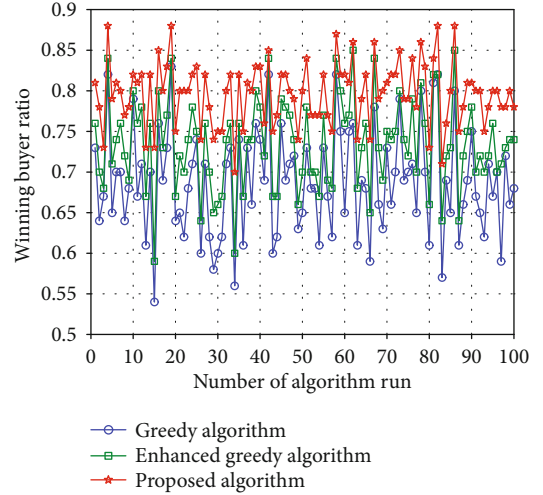


FIGURE 6: Comparison of the winning buyer ratio under different algorithms with a fixed network size.

algorithm is more efficient than the benchmark algorithms in terms of the auction revenue.

Figure 5 shows the computational results with respect to the buyer satisfaction ratio when the number of different algorithm run indexes varies from 1 to 100. It can be clearly seen that the proposed algorithm is higher (average of 11.3% times) than the Greedy algorithm on the buyer satisfaction ratio with different algorithm run indexes. The proposed algorithm is also higher (average of 1.9% times) than the Enhanced Greedy algorithm. The simulation result shows that the proposed algorithm is more efficient than the benchmark algorithms in terms of the buyer satisfaction ratio.

Figure 6 shows the computational results with respect to the winning buyer ratio when the number of different algorithm run indexes varies from 1 to 100. It can be clearly seen that the proposed algorithm is higher (average of 15.99% times) than the Greedy algorithm on the winning buyer ratio with different algorithm run indexes. The proposed algorithm is also higher (average of 8.47% times) than the Enhanced Greedy algorithm. The simulation result shows that the proposed algorithm is more efficient than the benchmark algorithms in terms of the winning buyer ratio.

4.2.2. Varied Network Size. Secondly, we varied the number of primary operators from 5 to 50 to evaluate the proposed algorithm performance with different network sizes. The result also generated under the greedy algorithm and the enhanced greedy algorithm in [30] is, respectively, denoted as Greedy algorithm and Enhanced Greedy algorithm; the results of the social welfare, seller revenue, buyer satisfaction ratio, and winning buyer ratio for the different algorithms are compared on the average value over 1000 runs.

In Figure 7, the social welfare of different algorithms increases when the number of primary operators varies from 5 to 50. That is because more primary operators in the network can allocate more spectrum requirements for higher bid secondary users. When the number of primary operators varies from 5 to 50, the gap between the proposed algorithm and the Greedy algorithm increases, and the social welfare is

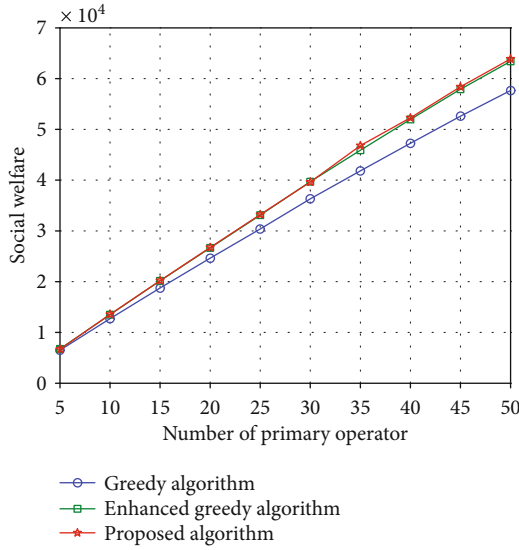


FIGURE 7: Comparison of the social welfare under different algorithms.

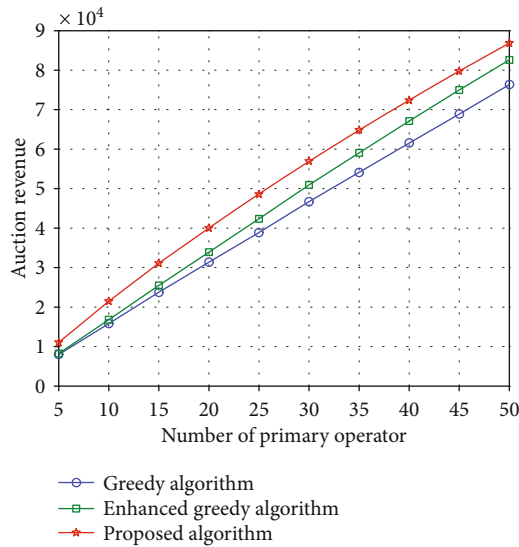


FIGURE 8: Comparison of the auction revenue under different algorithms.

varied from 2.96% to 11.03% times higher than the Greedy algorithm. Compared with the Enhanced Greedy algorithm, the proposed algorithm can achieve larger social welfare. Moreover, the social welfare of the proposed algorithm is about averagely 0.42% times higher than that of the Enhanced Greedy algorithm. From the simulation result, we can see that when the network size is small, the social welfare of the proposed algorithm is slightly larger than that of the two benchmark algorithms. When the number of the primary operator and secondary users is large, the social welfare of the proposed algorithm is more efficient than that of the benchmark algorithms.

Figure 8 shows the computational results with respect to the auction revenue. We can see clearly from Figure 8 that the auction revenue increases when the number of primary oper-

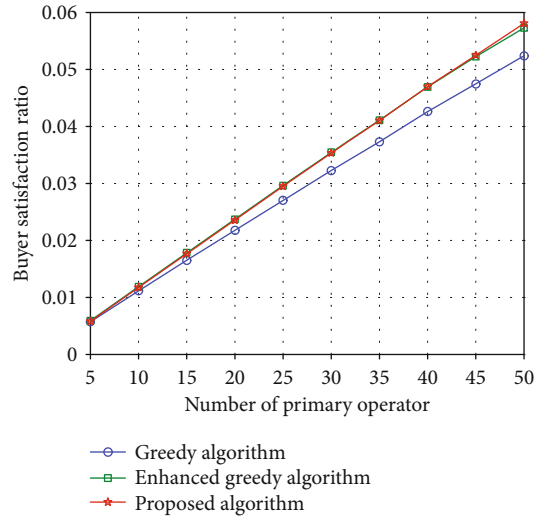


FIGURE 9: Comparison of the buyer satisfaction ratio under different algorithms.

ators varies from 5 to 50. That is because the more primary operators in the network, the more spectrum requirements of secondary users can be satisfied. The proposed algorithm is 13.75% to 38.6% times higher than the Greedy algorithm on the auction revenue (average of 24.67%). The proposed algorithm is 4.89% to 25.31% times higher than the Enhanced Greedy algorithm (average of 13.08%). The simulation result shows that the proposed algorithm is more efficient than the benchmark algorithms in terms of the auction revenue.

Figure 9 lists the buyer satisfaction ratio obtained by three algorithms. In Figure 9, we can see that with the increase of primary operators, the buyer satisfaction ratio goes up. The buyer satisfaction ratio of the proposed algorithm is averagely 8.3% and 0.12% times higher than that of the Greedy algorithm and the Enhanced Greedy algorithm, respectively.

In Figure 10, we compare the winning buyer ratio achieved by our proposed algorithm with the two benchmark algorithms. We can see that with the increase of primary operators, the winning buyer ratio increases because more secondary users' spectrum demands are satisfied. The proposed algorithm is averagely 47.79% times and 23.78% times higher than the Greedy algorithm and Enhanced Greedy algorithm on the winning buyer ratio, respectively. The proposed algorithm can allocate more secondary users because the demand and the bid price are globally considered.

Figure 11 shows the time of each run (the average value over 1000 runs) achieved by our proposed algorithm with the two benchmark algorithms. We can see the running time increases with primary operators increasing. That is because more primary operators in the network increase the computational complexity. Though the running time of the proposed algorithm is a few milliseconds than the two benchmark algorithms, the proposed algorithm achieves obviously higher social welfare, auction revenue, buyer satisfaction ratio, and winning buyer ratio than the two benchmark algorithms. The proposed algorithm can obtain

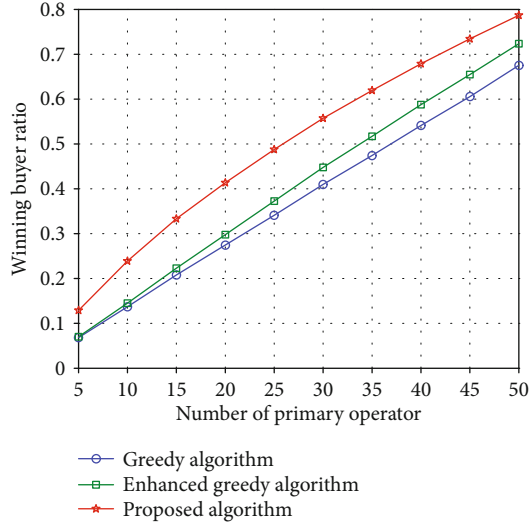


FIGURE 10: Comparison of the winning buyer ratio under different algorithms.

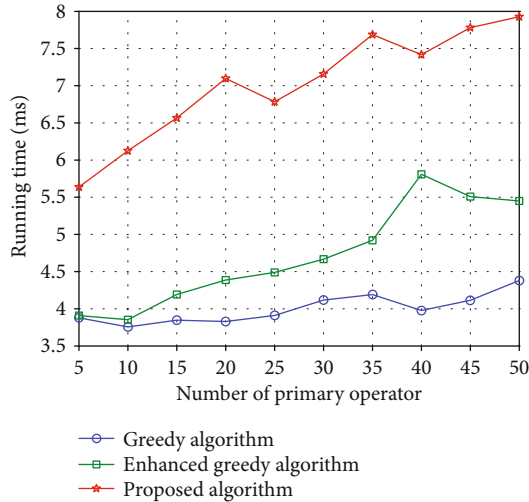


FIGURE 11: Comparison of the time of each run under different algorithms.

higher allocation performance and efficiency for the cognitive radio network of EI in a smart city.

From the above observations, we can conclude that our proposed algorithm outperforms the two greedy algorithms in terms of the above four performance metrics. The proposed algorithm provides an efficient method to allocate the allocation spectrum resource in the cognitive radio system of EI for a smart city.

5. Conclusions

In this paper, we have proposed a novel spectrum combinatorial auction mechanism for the cognitive radio network of EI in a smart city with multiple heterogeneous primary spectrum operators and multiple secondary users. The proposed mechanism iteratively used the well-known KM to generate an initial allocation scheme. Then, a swap procedure and an interchange procedure were applied to further promote the

spectrum allocation efficiency. The truthfulness was guaranteed by adopting a “Vickrey-like” mechanism. Simulation results show that the proposed auction mechanism can enhance the spectrum allocation efficiency of the cognitive radio network in a smart city in terms of the social welfare, seller revenue, buyer satisfaction ratio, and winning buyer ratio by comparing with the existing mechanism. As a future work, our hybrid spectrum auction mechanism can be extended to resource allocation problems in other networks of EI in a smart city.

Data Availability

No data were used to support this study.

Conflicts of Interest

The authors declare no conflict of interest.

Authors’ Contributions

The contributions of the authors involved in this study are as follows: conceptualization, H.F. and G.L.; methodology, G.L.; software, Z.Y.; validation, H.F., J.G., and Z.Y.; formal analysis, H.F.; investigation, H.F.; resources, J.G.; data curation, Z.Y.; writing—original draft preparation, H.F.; and writing—review and editing, G.L. All authors have read and agreed to the published version of the manuscript.

Acknowledgments

This research was supported partially by the National Natural Science Foundation of China (61163055), Fujian Natural Science Fund of China (No. 2016J05160), Technology Project of Fujian Province (JK2015040), and Technology Project of Minjiang University (MYK14008).

References

- [1] X. He, K. Wang, H. Huang, and B. Liu, “QoE-driven big data architecture for smart city,” *IEEE Communications Magazine*, vol. 56, no. 2, pp. 88–93, 2018.
- [2] K. Wang, X. Hu, H. Li, P. Li, D. Zeng, and S. Guo, “A survey on energy internet communications for sustainability,” *IEEE Transactions on Sustainable Computing*, vol. 2, no. 3, pp. 231–254, 2017.
- [3] M. Gao, K. Wang, and L. He, “Probabilistic model checking and scheduling implementation of an energy router system in energy Internet for green cities,” *IEEE Transactions on Industrial Informatics*, vol. 14, no. 4, pp. 1501–1510, 2018.
- [4] H. Jiang, K. Wang, Y. Wang, M. Gao, and Y. Zhang, “Energy big data: a survey,” *IEEE Access*, vol. 4, pp. 3844–3861, 2016.
- [5] C. Xu, K. Wang, P. Li, R. Xia, S. Guo, and M. Guo, “Renewable energy-aware big data analytics in geo-distributed data centers with reinforcement learning,” *IEEE Transactions on Network Science and Engineering*, vol. 7, no. 1, pp. 205–215, 2020.
- [6] L. Jiang, H. Tian, Z. Xing et al., “Social-aware energy harvesting device-to-device communications in 5G networks,” *IEEE Wireless Communications*, vol. 23, no. 4, pp. 20–27, 2016.

- [7] K. Wang, L. Gu, X. He et al., "Distributed energy management for vehicle-to-grid networks," *IEEE Network*, vol. 31, no. 2, pp. 22–28, 2017.
- [8] X. Hu, K. Wang, X. Liu, Y. Sun, P. Li, and S. Guo, "Energy management for EV charging in software-defined green vehicle-to-grid network," *IEEE Communications Magazine*, vol. 56, no. 5, pp. 156–163, 2018.
- [9] K. Wang, Y. Wang, Y. Sun, S. Guo, and J. Wu, "Green industrial Internet of Things architecture: an energy-efficient perspective," *IEEE Communications Magazine*, vol. 54, no. 12, pp. 48–54, 2016.
- [10] S. Haykin, "Cognitive radio: brain-empowered wireless communications," *IEEE Journal on Selected Areas in Communications*, vol. 23, no. 2, pp. 201–220, 2005.
- [11] K. Wang, Z. Ouyang, R. Krishnan, L. Shu, and L. He, Eds., "A game theory-based energy management system using price elasticity for smart grids," *IEEE Transactions on Industrial Informatics*, vol. 11, no. 6, pp. 1607–1616, 2015.
- [12] Q. Zhao and B. M. Sadler, "A survey of dynamic spectrum access," *IEEE Signal Processing Magazine*, vol. 24, no. 3, pp. 79–89, 2007.
- [13] L. Gao, X. Wang, Y. Xu, and Q. Zhang, "Spectrum trading in cognitive radio networks: a contract-theoretic modeling approach," *IEEE Journal on Selected Areas in Communications*, vol. 29, no. 4, pp. 843–855, 2011.
- [14] S. Gandhi, C. Buragohain, L. Cao, H. Zheng, and S. Suri, "A general framework for wireless spectrum auctions," in *2007 2nd IEEE International Symposium on New Frontiers in Dynamic Spectrum Access Networks*, pp. 22–33, Dublin, Ireland, 2007.
- [15] C. Li, Z. Liu, X. Geng et al., "Two dimension spectrum allocation for cognitive radio networks," *IEEE Transactions on Wireless Communications*, vol. 13, no. 3, pp. 1410–1423, 2014.
- [16] M. N. Tehrani and M. Uysal, "Auction based spectrum trading for cognitive radio networks," *IEEE Communications Letters*, vol. 17, no. 6, pp. 1168–1171, 2013.
- [17] C. Yi, J. Cai, and G. Zhang, "Online spectrum auction in cognitive radio networks with uncertain activities of primary users," in *2015 IEEE International Conference on Communication*, pp. 7576–7581, London, UK, 2015.
- [18] H. Wang, E. Dutkiewicz, G. Fang, and M. D. Mueck, "Framework of joint auction and mixed graph for Licensed Shared Access systems," in *2015 IEEE International Symposium on Dynamic Spectrum Access Networks (DySPAN)*, pp. 154–163, 2005.
- [19] D. Yang, G. Xue, and X. Zhang, "Group buying spectrum auctions in cognitive radio networks," *IEEE Transactions on Vehicular Technology*, vol. 66, pp. 1–817, 2016.
- [20] E. F. Khairulla and M. Chatterjee, "Multi-bid auctions for channel allocation in multi-channel dynamic spectrum access networks," in *2016 European Conference on Networks and Communications (EuCNC)*, pp. 282–287, Athens, Greece, 2016.
- [21] F. Shen, D. Li, P. H. Lin, and E. Jorswieck, "Auction based spectrum sharing for hybrid access in macro-femtocell networks under QoS requirements," in *2015 IEEE International Conference on Communication*, pp. 3335–3340, London, UK, 2015.
- [22] D. S. Palguna, D. J. Love, and I. Pollak, "Secondary spectrum auctions for markets with communication constraints," *IEEE Transactions on Wireless Communications*, vol. 15, no. 1, pp. 116–130, 2016.
- [23] C. Yi and J. Cai, "Multi-item spectrum auction for recall-based cognitive radio networks with multiple heterogeneous secondary users," *IEEE Transactions on Vehicular Technology*, vol. 64, no. 2, pp. 781–792, 2015.
- [24] Z. Chen, H. Huang, Y.-e. Sun, and L. Huang, "True-MCSA: a framework for truthful double multi-channel spectrum auctions," *IEEE Transactions on Wireless Communications*, vol. 12, no. 8, pp. 3838–3850, 2013.
- [25] Y. Chen, J. Zhang, K. Wu, and Q. Zhang, "TAMES: a truthful double auction for multi-demand heterogeneous spectrums," *IEEE Transactions on Parallel and Distributed Systems*, vol. 25, no. 11, pp. 3012–3024, 2014.
- [26] D. Yang, X. Zhang, and G. Xue, "PROMISE: a framework for truthful and profit maximizing spectrum double auctions," in *2014 IEEE Conference on Computer Communications*, pp. 109–117, Toronto, ON, Canada, 2014.
- [27] Y.-e. Sun, H. Huang, K. Xing et al., "SPRITE: a novel strategy-proof multi-unit double auction scheme for spectrum allocation in ubiquitous communications," *Personal and Ubiquitous Computing*, vol. 18, no. 4, pp. 939–950, 2014.
- [28] W. Dong, S. Rallapalli, L. Qiu, K. K. Ramakrishnan, and Y. Zhang, "Double auctions for dynamic spectrum allocation," *IEEE/ACM Transactions on Networking*, vol. 24, no. 4, pp. 2485–2497, 2016.
- [29] W. Zhou, T. Jing, W. Cheng, T. Chen, and Y. Huo, "Combinatorial auction based channel allocation in cognitive radio networks," in *8th International Conference on Cognitive Radio Oriented Wireless Networks*, pp. 135–140, Washington, DC, USA, 2013.
- [30] C. Yi and J. Cai, "Combinatorial spectrum auction with multiple heterogeneous sellers in cognitive radio networks," in *2014 IEEE International Conference on Communications*, pp. 1626–1631, Sydney, Australia, 2014.
- [31] L. Huang, Z. Sun, H. Guo, L. Chen, and H. Xu, "Spectrum combinatorial double auction for cognitive radio network with ubiquitous network resource providers," *IET Communications*, vol. 9, no. 17, pp. 2085–2094, 2015.
- [32] K. Wang, Y. Wang, X. Hu et al., "Wireless big data computing in smart grid," *IEEE Wireless Communications*, vol. 24, no. 2, pp. 58–64, 2017.
- [33] H. W. Kuhn, "The Hungarian method for the assignment problem," *Naval Research Logistics Quarterly*, vol. 2, no. 1-2, pp. 83–97, 1955.
- [34] J. Munkres, "Algorithms for the assignment and transportation problems," *Journal of the Society for Industrial and Applied Mathematics*, vol. 5, no. 1, pp. 32–38, 1957.
- [35] K. Wang, J. Yu, Y. Yu et al., "A survey on energy internet: architecture, approach, and emerging technologies," *IEEE Systems Journal*, vol. 12, no. 3, pp. 2403–2416, 2018.
- [36] S. K. Shil, M. Mouhoub, and S. Sadaoui, "Winner determination in combinatorial reverse auctions," *Studies in Computational Intelligence*, vol. 489, no. 1, pp. 35–40, 2013.

Research Article

Demand Response Management Research Based on Cognitive Radio for Smart Grid

Tingting Yang ¹, Tiancong Huang ¹, Haifeng Zhang ², Peiyi Li ¹, Canyun Xiong ¹,
and Yucheng Wu ¹

¹School of Microelectronics and Communication Engineering, Chongqing University, Chongqing, China

²Beijing Smartchip Microelectronics Technology Company Limited, Beijing, China

Correspondence should be addressed to Tiancong Huang; htc@cqu.edu.cn

Received 11 June 2020; Revised 19 September 2020; Accepted 23 September 2020; Published 12 October 2020

Academic Editor: Jaime Lloret

Copyright © 2020 Tingting Yang et al. This is an open access article distributed under the Creative Commons Attribution License, which permits unrestricted use, distribution, and reproduction in any medium, provided the original work is properly cited.

Cognitive radio is introduced into the demand response management (DRM) of smart grid with the hope of alleviating the shortage of spectrum resources and improving communication quality. In this paper, we adopt an energy detection algorithm based on generalized stochastic resonance (GSRED) to improve the spectrum sensing accuracy under the circumstances of low signal-to-noise ratio without increasing system overhead. Specifically, a DRM scheme based on real-time pricing is investigated, and the social welfare is taken as the main index to measure system control performance. Furthermore, considering the adverse effects incurred by incorrect spectrum sensing, we incorporate the probability of the DRM system causing interference to primary user and spectrum loss rate into the evaluation index of the system control performance and give the final expression of the global optimization problem. The influence of sensing time on system communication outage probability and spectrum loss rate is elaborated in detail through theoretical derivation and simulation analysis. Simulation results show that the GSRED algorithm has higher detection probability under the same conditions compared with the traditional energy detection algorithm, thus guaranteeing lower communication outage probability and spectrum loss rate.

1. Introduction

With the rapid growth in various electrical equipment, electric power plays an increasingly important role in social life and has become an indispensable necessity in human society. However, the dramatic increase of power demand has brought about the increase of the complexity of the power grid and the rapid growth of load, which makes the issue of safe and stable operation of the power grid attract widespread attention [1–3]. The smart grid, which is the intellectualization of the power grid, is considered to be the next generation of power grid in which the security and stability can be improved. The smart grid is an integrated network based on high-speed bidirectional communication and physical grid, which enables it to operate safely and steadily under the increasingly severe demand for electricity. It is actually a new type of power grid formed by the advanced sensor measurement technique, communication technology, infor-

mation technology, computer technology, control technology, and physical power grid [4, 5]. The rapid development of the smart grid and the wide application of smart meters require more frequency bands to achieve the transmission of power data, which makes the shortage of spectrum resources in wireless communication more prominent.

Cognitive radio (CR) is applied to the smart grid, which realizes efficient usage of the wireless spectrum with the opportunistic spectrum access [6–8]. Spectrum sensing in CR can monitor the occupied state of the spectrum in real-time. When the available idle spectrum is detected, cognitive user can complete the data transmission on the idle channel through channel switching to realize the sharing of spectrum resources [9, 10]. The commonly used spectrum sensing technologies include matched filter detection, cyclostationary feature detection, and energy detection (ED) [11–13]. Matched filter detection is optimum when prior information is known. However, it is not easy to obtain prior information

in practice, which is also the reason why the matched filter is not widely used. Cyclostationary feature detection has high detection accuracy and can also identify the types of signals, but the computational complexity is high. ED is widely used in practical engineering because of its low computational complexity and no prior information required.

On the other hand, as a key technology to realize intelligent operation and maintenance of power system, demand response management (DRM) in the smart grid has attracted the attention of various institutions and scholars around the world [14, 15]. DRM is aimed at improving the interactivity of the power system, thereby stabilizing the power market and optimizing power resource allocation [16, 17]. The core of DRM is to control the electricity consumption on the demand side according to the different demand response patterns of consumers when the price of the power supply market is high and the reliability of the power system is low. In the smart grid, it can be divided into price-based and incentive-based DRM [18]. Direct load control and interruptible load control are the main modes of DRM based on incentive, while the DRM based on price mainly includes time-of-use price, real-time pricing (RTP), and critical peak pricing [19–22]. RTP is regarded as a crucial method to realize instantaneous power supply and demand balance and improve power utilization.

There are large bodies of research regarding DRM based on RTP, with the attempt to reduce and shift the peak-hour load [23–27]. The authors in [23] proposed a new pricing scheme to minimize the peak-to-average ratio in aggregate load demand with the uncertainty about the impact of power price on consumers' load profiles. However, the impact of communication unreliability on the control performance of DRM has not been considered [23]. An improved RTP approach to address the problems of bad convergence and applicable conditions of this existing optimal RTP model based on utility maximization has been proposed in [24]. This algorithm can obtain the optimal price to maximize the total utility of all consumers and power suppliers. The authors of [25] introduced CR into the smart grid to improve the communication quality between power suppliers and consumers. Besides, they formulated a sensing-performance tradeoff problem between better control performance and lower system overhead. A wideband hybrid access strategy based on the two-stage power pricing model has been proposed and analyzed in [26] which is aimed at minimizing the system power price by jointly optimizing the sensing time and transmission time. In [27], a multiobjective scheme for spectrum sensing control in a CR-based smart grid has been investigated. An aggregator that serves power suppliers and power consumers has two objectives: maximizing the aggregated benefit of power suppliers and consumers and minimizing the CR system overhead. However, the sensing performance tradeoff problem at low signal-to-noise ratio (SNR) is not revealed in these literatures. In addition, these literatures do not fully consider that CR brings some negative impact while improving communication performance, such as interference to primary user (PU) communication caused by unreliable detection and loss of spectrum resources caused by false alarm detection.

In this paper, we study the DRM control problem in CR enabled smart grid. We focus on improving the control performance of DRM while considering the effect of spectrum sensing time and spectrum sensing accuracy. The main contributions of this paper are as follows.

- (i) To improve spectrum utilization and communication reliability, we introduce spectrum sensing and channel switching techniques of CR into the smart grid
- (ii) We adopt an energy detection algorithm based on generalized stochastic resonance (GSRED) to complete the reliable spectrum sensing at low SNR
- (iii) We consider the impact of communication performance on power system and assess the impact of communication outage probability on the control performance of DRM
- (iv) We incorporate the interference of inaccurate spectrum sensing to PU into the system performance evaluation index and consider the influence of spectrum loss caused by false alarm probability
- (v) We propose a DRM algorithm based on RTP to maximize social welfare and present the global optimal problem of the DRM system with considering the negative impact incurred by unreliable spectrum sensing. In addition, we provide both theoretical analysis and simulation to verify the effectiveness of the proposed algorithm

The rest of the paper is organized as follows. The system model is described in Section 2. In Section 3, we briefly review the traditional ED algorithm and analyze how GSRED ensures the spectrum detection accuracy under low SNR. Besides, it is also devoted to detailing how CR improves the communication quality and how to realize DRM based on RTP. In addition, we also derive the expressions of communication outage probability and social welfare in DRM. The corresponding simulation results are given in Section 4, while the conclusions follow in Section 5.

For the sake of convenience, we present a list of the major symbols of this paper in Table 1 with their definitions.

2. System Model

As shown in Figure 1, we consider a smart grid consisting of a power supplier and power market, K power consumers, and one control unit. All power consumers are assumed to be equipped with smart meters which can transmit power demand d_k (where $k = 1, 2, \dots, K$) to and receive pricing information from the control unit. Similar to [25], for the same power supplier, we assume power price p is the same for all power consumers. The power supplier adjusts the power supply s according to the pricing information provided by the control unit to achieve the optimal distribution of power resources. Without loss of generality, the cost function of the power supplier indicating the expense of supplying power s by the supplier is denoted by $C(s)$, and let

TABLE 1: List of major symbols.

Symbol	Description
K	Number of power consumers
d_k	Power demand of power consumers
d	Total power demand of all consumers
p	Power price
s	Power supply of the supplier
$C(s)$	Cost function of the power supplier
$G_k(d_k)$	Gain function of power consumers
$\phi(s)$	Profit of the power supplier
$\varphi_k(d_k)$	Benefits of power consumers
ψ	Social benefits
m	Number of iterations
$Ch_{1,l}$	Original channel
$Ch_{2,l}$	Cognitive channel
H_0	State that $Ch_{2,l}$ is busy
H_1	State that $Ch_{2,l}$ is idle
P_0	Probability of H_0
P_1	Probability of H_1
σ_n^2	Variance of AWGN noise
σ_s^2	Variance of PU's signal
d	Intensity of the DC noise
τ	Spectrum sensing time
λ	Preset decision threshold
P_d	Detection probability
P_f	False alarm probability
ζ_1	Communication outage probability of $Ch_{1,l}$
ζ_2	Communication outage probability of $Ch_{2,l}$
ζ	Average DRM communication outage probability
P_{sw}	Channel switching probability
P_I	Interference probability to PU
P_L	Spectrum loss rate
ϕ	System utility

$G_k(d_k)$ denote the utility function of power consumer k representing the obtained satisfaction with power demand d_k . In fact, $C(s)$ is increasing and convex, and $G_k(d_k)$ is non-decreasing and concave [28], and

$$C(s) = as^2 + bs + c, \quad (1)$$

$$G_k(d_k) = \begin{cases} wd_k - \frac{\alpha}{2}d_k, & 0 \leq d_k \leq \frac{w}{\alpha}, \\ \frac{w^2}{2\alpha} & d_k > \frac{w}{\alpha}, \end{cases} \quad (2)$$

where a , b , and c are constants, w is a system parameter related to power consumer's behavior, and α is a default

parameter which is related to the quantity of power demand to reach the saturation point.

For the power supplier, under power price p , the profit function is defined as $\phi(s) = ps - C(s)$. Obviously, its goal is to regulate the power supply to maximize its own profit. For each power consumer k , the benefit function can be expressed as $\varphi_k(d_k) = G_k(d_k) - pd_k$. Similarly, the aim of power consumers is to maximize their own benefits by adjusting power demand. Considering the level of society, the basic purpose of the proposed scheme is to maximize the benefits of consumers while minimizing the cost of power suppliers. Therefore, the social welfare can be defined as $\psi = \sum_{k=1}^K G_k(d_k) - C(s)$ with $s \geq \sum_{k=1}^K d_k$ [25]. Under the constraint that the power supply should meet the total power demand, the social welfare is taken as the evaluation index of DRM control performance, and the global optimization problem can be formulated as

$$\begin{aligned} \psi &= \max_{s, \{d_k\}} \sum_{k=1}^K G_k(d_k) - C(s) \\ \text{s.t.} \quad & s \geq \sum_{k=1}^K d_k. \end{aligned} \quad (3)$$

In real application, both the cost function of power supplier and the utility function of power consumers are private [29]. Therefore, we adopt a distributed and iterative approach to obtain the optimal solution of (3). The detailed steps can be given as follows

- (i) The initial power price $p_1 \geq 0$ is broadcasted to the power supplier and each power consumer by the control unit
- (ii) The power supplier updates the power supply s_m^* according to the power price p_m ($m \in \mathbb{N}^+$ denotes the number of iterations) in order to maximize its own profit $\phi(s)$. At the same time, each power consumer updates its power demand $d_{k,m}^*$ to maximize its own benefit $\varphi_k(d_k)$
- (iii) The control unit collects local power supply and power demand information and adopts a gradient approach to obtain the next iteration power price p_{m+1} , i.e.,

$$p_{m+1} = \left[p_m - \theta \left(s_m^* - \sum_{k=1}^K d_{k,m}^* \right) \right]^+, \quad (4)$$

where $\theta > 0$ is the step size which adjusts the convergence rate, and $[x]^+ \Delta = \max \{0, x\}$.

- (i) Repeat the second and third steps until the power price converges

In fact, the above process is based on ideal and perfect two-way communication, that is, communication outage is

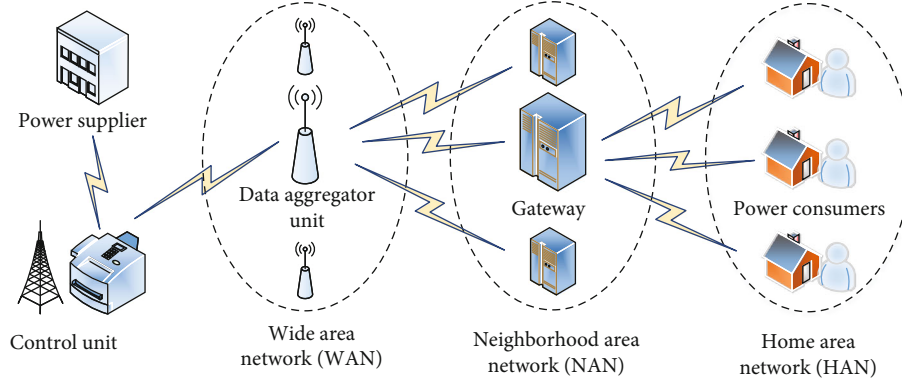


FIGURE 1: System model.

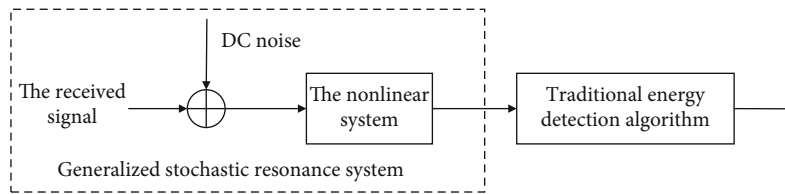


FIGURE 2: The implementation block diagram of the GSRED algorithm.

not considered. Usually, the control unit is installed on the power supplier side, and we suppose that reliable communication between the control unit and the power supplier can be guaranteed. However, the control unit is far away from the power consumers, and when wireless communication technology is used to transmit power data, packet loss and delay will inevitably occur. We introduce the average communication outage probability ζ to describe the communication performance between the power consumer and the control unit, and ζ is considered to be the same for all power consumers. With considering the impact of communication outage, the next iteration power price can be modified as follows

$$p_{m+1} = \left[p_m - \theta \left(s_m^* - (1 - \zeta) \sum_{k=1}^K d_{k,m}^* \right) \right]^+. \quad (5)$$

3. DRM Based on Cognitive Radio Enabled Smart Grid

In this section, CR is applied to the smart grid to cope with the shortage of spectrum resources and improve communication performance. The spectrum sensing of CR is used to detect the idle channel, and the channel switching is to select the appropriate channel to transfer information. An algorithm is proposed to maximize social welfare under the constraint of spectrum sensing performance. The interference of inaccurate spectrum sensing to PU and the spectrum loss caused by false alarm probability are incorporated into the system performance evaluation index. Besides, the detailed theoretical analysis and formula derivation of our proposed algorithm are presented.

3.1. Spectrum Sensing in DRM. Among all the spectrum sensing algorithms, ED is a blind detection algorithm, which is widely used in spectrum sensing due to its low computational complexity and easy implementation. The principle of energy detector is actually to measure the energy of the received signals and to draw a conclusion by comparing it with a preset decision threshold [30]. However, the traditional ED algorithm is particularly sensitive to noise, and it is difficult to ensure the reliability and stability of spectrum sensing at low SNR. Thus, we adopt the GSRED algorithm to improve the detection performance and detection efficiency at low SNR [31].

In this paper, we assume that the data of smart meter can be transmitted through two different channels: one is from the unlicensed spectrum, noted as the original channel Ch1; the other one belongs to the licensed spectrum, denoted as the cognitive channel Ch2, which is randomly occupied by the PU. This means that the smart meters can opportunistically access the licensed channel which is not occupied by PU. Let H_0 indicate the absence of PU (Ch2 is idle), and H_1 denote the presence of PU (Ch2 is busy), respectively. Let P_0 denote the probability of H_0 , and P_1 be that of H_1 , where $P_0 + P_1 = 1$.

The GSRED algorithm is to add a certain intensity of DC noise to the received signal to make the noise, useful signal, and interference resonate in the nonlinear system and then use the traditional energy detection algorithm to complete the spectrum sensing, so as to improve the SNR and the detection performance [31]. The implementation block diagram of the GSRED algorithm is shown in Figure 2. It can be seen from Figure 2 that compared with the traditional energy detection algorithm, the GSRED algorithm only adds one processing, that is, adding DC noise to the received

TABLE 2: Basic parameters of system simulation.

Parameters	Values
SNR	-18 dB
Signal bandwidth W	1 MHz
Power cost function parameters a, b, c	0.2, 0.5, 0
User behavior w	3
Default parameter α	0.5
Convergence parameter θ	0.1
Preset minimum detection probability \tilde{P}_d	0.95
Noise variance σ_n^2	1
Mean of PU's transmission signal μ	0.05
Probability for Ch2 is idle P_0	0.7
Outage probability of Ch1 ζ_1	0.5
Outage probability of Ch2 ζ_2	0.2
Parameter ρ	2
Parameter ε_1	5
Parameter ε_2	0.4

signal, so the GSRED algorithm does not greatly increase the algorithm complexity.

With the generalized stochastic resonance energy detector, by integrating the output signal (bandwidth is W) of the stochastic resonance module over sensing time τ , the smart meter compares the detection statistic with a decision threshold λ to determine whether Ch2 is occupied by PU. The detection probability P_d indicates that the PU exists and the spectrum detection result is H_1 , while the false alarm probability P_f indicates that the spectrum is idle but the detection result is H_0 . The detection accuracy is usually described by P_f and P_d , then according to [31], we have

$$P_f = Q\left(\frac{\lambda - \sqrt{W\tau}(\sigma_n^2 + d^2)}{\sqrt{\sigma_n^4 + 2\sigma_n^2 d^2}}\right), \quad (6)$$

$$P_d = Q\left(\frac{\lambda - \sqrt{W\tau}(\sigma_n^2 + \sigma_s^2 + (\mu + d)^2)}{\sqrt{(\sigma_n^2 + \sigma_s^2)^2 + 2(\sigma_n^2 + \sigma_s^2)(\mu + d)^2}}\right), \quad (7)$$

where $Q(x) = 1/\sqrt{2\pi} \int_x^\infty e^{-t^2/2} dt$, σ_n^2 is the variance of additive white Gaussian noise (AWGN), and d is the intensity of the stochastic resonance DC noise. It is assumed that the mean of PU's transmission signal is μ , and the variance is σ_s^2 . Spectrum sensing always expects to improve the detection probability and reduce the false alarm probability as much as possible, even at the cost of system overhead, such as increasing sampling points and sensing time to improve the detection accuracy [32].

3.2. Cognitive Radio Improves Communication Quality. Before each smart meter transmits power data, it is necessary

to select the transmission channel. In the CR framework of bidirectional communication, spectrum sensing is used to determine whether Ch2 is occupied. If the result of spectrum sensing shows that Ch2 is idle, that is, it is not occupied by the PU, the system uses channel switching technology to switch the transmission channel to Ch2. Otherwise, the transmission of power information is still completed on Ch1. In fact, spectrum perception also has unreliability, which will directly affect the choice of the transmission channel. For example, when the channel is not occupied but the spectrum perception results in busy channel, the system will not switch to Ch2. Similarly, when the channel is occupied but the result of spectrum perception is that the channel is free, the system will choose Ch2 as the transmission channel. Thus, the global channel switching probability can be expressed as

$$P_{sw} = 1 - P_0 P_f - P_1 P_d. \quad (8)$$

Let ζ_1 and ζ_2 denote the communication outage probability of Ch1 and Ch2 ($\zeta_1 > \zeta_2$), respectively. And the average outage probability of DRM system is

$$\bar{\zeta} = (1 - P_{sw})\zeta_1 + P_{sw}\zeta_2 < \zeta_1, \quad (9)$$

where $\bar{\zeta} - \zeta_1 = (1 - P_{sw})\zeta_1 + P_{sw}\zeta_2 - \zeta_1 = P_{sw}(\zeta_2 - \zeta_1)$, and $P_{sw} \geq 0$, obviously we have $\bar{\zeta} \leq \zeta_1$. This proves that the application of CR technology can effectively reduce the communication outage probability of the DRM system and improve the communication reliability and stability.

3.3. DRM Based on Spectrum Sensing and Channel Switching. Introducing CR technology into the smart grid can realize spectrum-sharing and dynamic spectrum access. Generally, the detection probability of spectrum sensing should not be lower than a certain preset value to restrict the interference to the PU. The false alarm probability should be lower enough to reduce the spectrum sensing and improve the utilization of spectrum resources. In practical application, a minimum detection probability \tilde{P}_d is preset, and it can be known from (7) that the decision threshold satisfies [33].

$$\lambda = A Q^{-1}(\tilde{P}_d) + \sqrt{W\tau}(\sigma_n^2 + \sigma_s^2 + (\mu + d)^2), \quad (10)$$

where $A = \sqrt{(\sigma_n^2 + \sigma_s^2)^2 + 2(\sigma_n^2 + \sigma_s^2)(\mu + d)^2}$. Substituting (10) into (6), we have

$$P_f = Q\left(\frac{A Q^{-1}(\tilde{P}_d) + \sqrt{W\tau}(\sigma_s^2 + 2\mu d + \mu^2)}{\sqrt{\sigma_n^4 + 2\sigma_n^2 d^2}}\right), \quad (11)$$

When the Ch2 is occupied while the spectrum decision result is H_0 , the access to Ch2 will bring interference to the PU, thus the probability of the DRM system causing interference to PU is

$$P_I = P_1(1 - \tilde{P}_d). \quad (12)$$

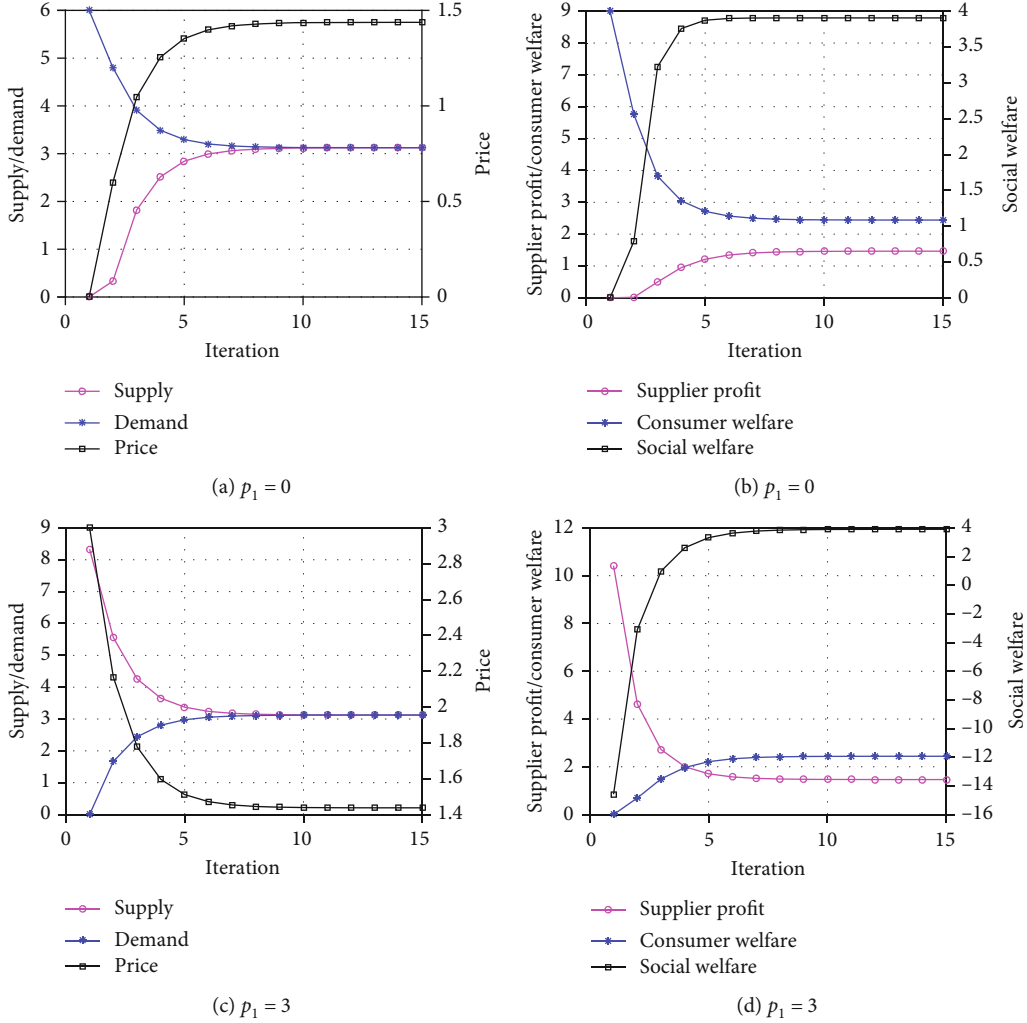


FIGURE 3: The control performance of DRM with different initial price.

When the Ch2 is idle while the spectrum decision result is H_1 , the smart meters mistakenly consider that the Ch2 is busy and still transmit data on Ch1 resulting in the idle of Ch2. Hence, the spectrum loss rate is calculated by

$$P_L = P_0 Q \left(\frac{A Q^{-1} (\tilde{P}_d) + \sqrt{W \tau} (\sigma_s^2 + 2 \mu d + \mu^2)}{\sqrt{\sigma_n^4 + 2 \sigma_n^2 d^2}} \right). \quad (13)$$

From (12) and (13), it is not hard to conclude that increasing the sensing time can reduce the interference to PU and reduce the spectrum loss, but also increase the system overhead and delay. Therefore, setting reasonable sensing time to avoid excessive system cost is the main issue of DRM under the condition of meeting the system performance requirements.

Considering that the power supply cannot meet the demand of all power consumers in the smart grid, i.e., $s < \sum_{k=1}^K d_k$, so it is necessary to purchase part of the electricity in the power market. We assume that the electricity

cost function in the power market is $C_m(s)$, and $C_m(s) = \rho C(s)$. Then the original optimization problem (3) can be modified to

$$\psi = \begin{cases} \max_{s, \{d_k\}} \sum_{k=1}^K G_k(d_k) - C(s), & s \geq \sum_{k=1}^K d_k, \\ \max_{s, \{d_k\}} \sum_{k=1}^K G_k(d_k) - C(s) - \beta C_m, & s < \sum_{k=1}^K d_k, \end{cases}$$

$$\text{s.t. } P_d \geq \tilde{P}_d,$$

(14)

where $\beta = \sum_{k=1}^K d_k - s$. Obviously, the goal of the DRM system is to maximize the social welfare of the smart grid while minimizing the interference to PU and spectrum loss rate. In order to evaluate the overall performance of the DRM system more comprehensively, the interference and spectrum loss rate to the primary user are included in the system performance evaluation index. The system

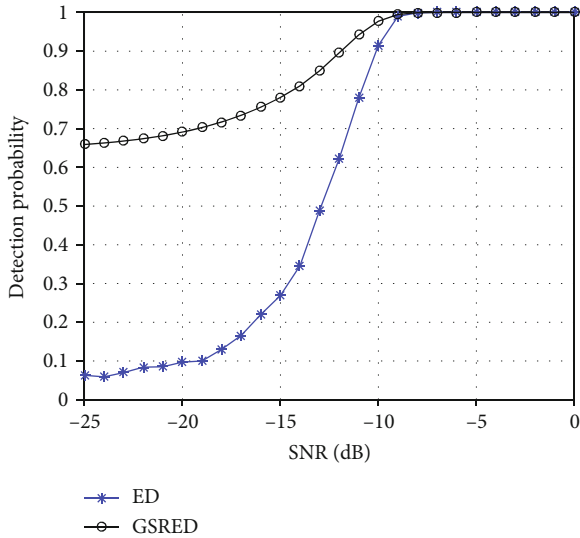


FIGURE 4: Comparison of detection probability among ED algorithm and GSRED algorithm.

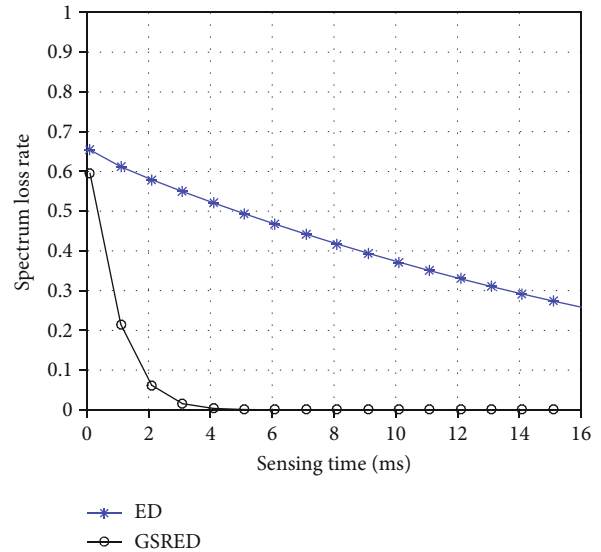


FIGURE 6: Comparison of spectrum loss rate among ED algorithm and GSRED algorithm.

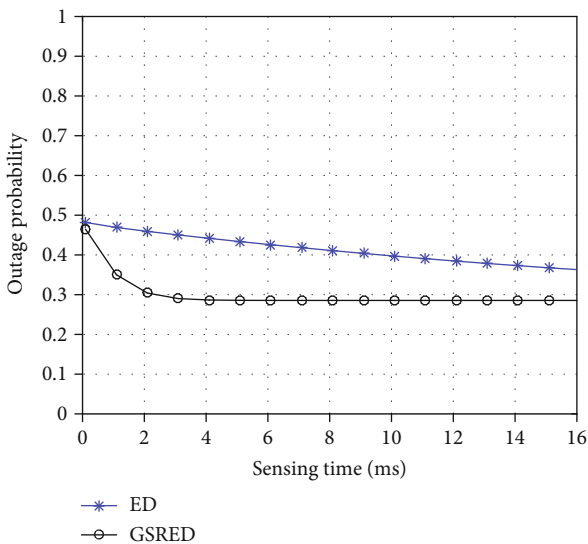


FIGURE 5: Comparison of outage probability among ED algorithm and GSRED algorithm.

utility related to the overall performance of DRM can be defined as

$$\phi = \psi - \varepsilon_1 P_I - \varepsilon_2 P_L, \quad (15)$$

where ε_1 and ε_2 are system parameters to measure the adverse effects of inaccurate spectrum sensing.

4. Simulation Results and Analysis

To evaluate the distributed and iterative approach of DRM, a simple one-supplier and one-consumer system is considered. In fact, the simulation results can be extended to one-supplier and multiple-consumers scenarios. We use

MATLAB® to realize the simulation, and the system parameters are summarized in Table 2 [6, 25].

To demonstrate the efficiency of the distributed and iterative algorithm for realizing the tradeoff between power supply and demand, the control performance of DRM under ideal communication is simulated, i.e., $\zeta = 0$. In Figure 3, we set the initial price $p_1 = 0$ and $p_1 = 3$, respectively. The results show that even under different initial power price, the power price will converge to a certain value with the increase of iteration times, and the DRM system can achieve the balance of supply and demand. In addition, as the number of iterations increases, the social welfare will gradually increase until it reaches a maximum, at which time the profit of the power supplier and the consumers' benefits do not change.

In order to demonstrate the superiority of the GSRED algorithm at low SNR, we chose the ED algorithm as the comparison algorithm to complete the simulation [34]. In Figure 4, it is evident that the GSRED algorithm has a higher detection probability than the ED under the same conditions, that is, the GSRED algorithm is significantly better than the ED algorithm. In addition, the lower the SNR is, the greater the performance difference between the two. As the SNR increases, the difference in performance between the two will gradually decrease. When the SNR is greater than -8 dB, there is no difference between these two.

Figure 5 plots the communication outage probability of these two schemes when the sensing time increases. It is evident that as the sensing time increases, the system outage probability of the two declines continuously. In contrast, the outage probability of the proposed scheme drops rapidly at first and then becomes relatively stable. This observation shows that the GSRED algorithm has lower outage probability than the traditional ED algorithm and can effectively guarantee better communication performance.

Figure 6 demonstrates the spectrum loss rate when the sensing time increases. According to the result described by

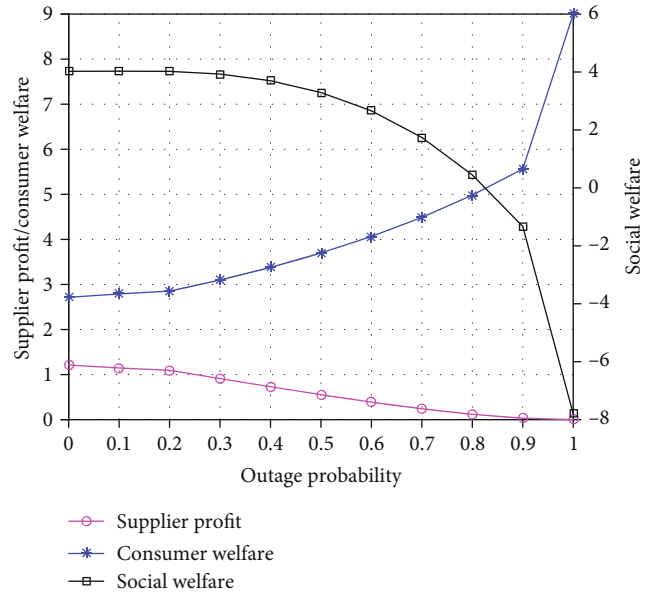
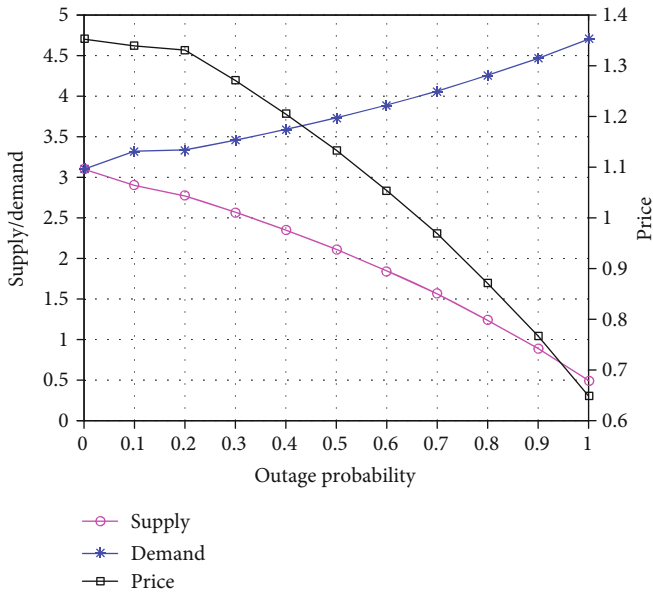


FIGURE 7: The control performance of DRM versus outage probability.

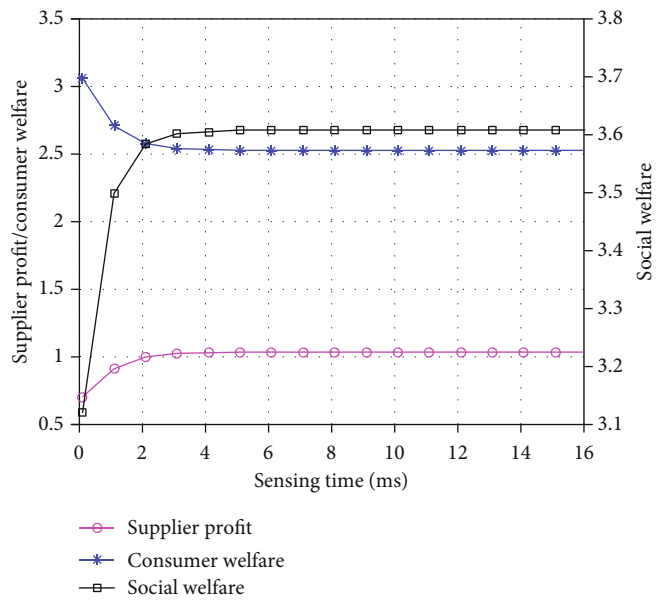
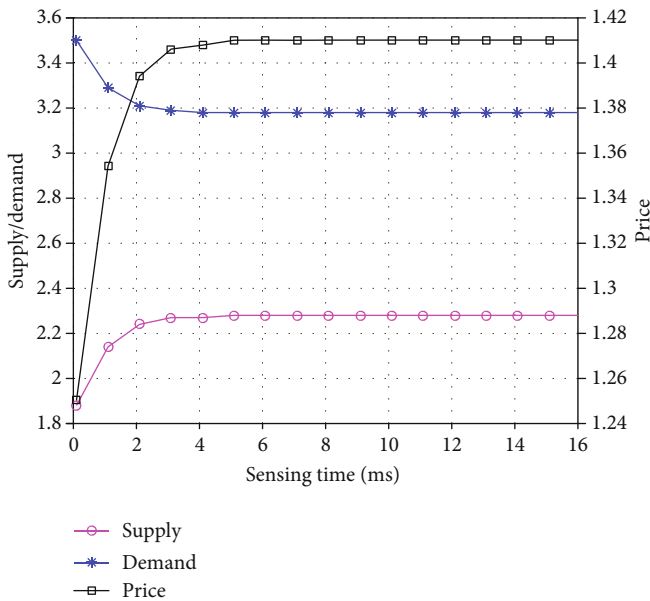


FIGURE 8: The control performance of DRM versus sensing time with GSRED algorithm.

Figure 6, we can find that the GSRED algorithm can obtain a lower spectrum loss rate and outperforms the ED. When the sensing time is larger than 4 ms, the spectrum loss rate of the GSRED algorithm becomes zero. It is evident that the shortage of spectrum resources problem is reduced effectively by the GSRED algorithm through reducing the spectrum loss rate.

Figure 7 shows the relationship between the control performance of DRM and different outage probability. The simulation shows that when the probability of system communication outage is zero, the power supply and demand are balanced and the social welfare is the largest. That is to

say, under the ideal communication condition, DRM can realize the balance of power supply and demand and optimize the allocation of power resources. With the increase of outage probability, the gap between power demand and power supply becomes wider, and the relationship between power supply and demand becomes more unbalanced. The increase of outage probability leads to the decline of profit and social welfare of the power supplier and also reduces the welfare of power users. The communication outage probability directly affects the control performance of DRM. Therefore, on the premise of guaranteeing system overhead and delay, it is a core issue to improve communication

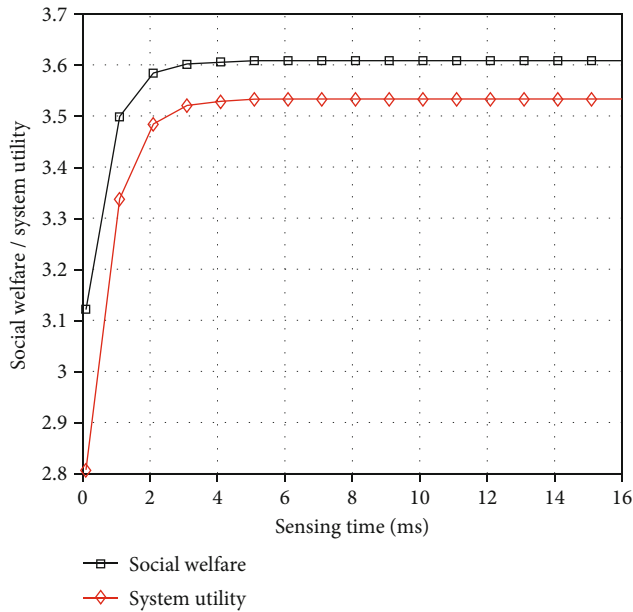


FIGURE 9: The system utility of DRM.

performance and optimize power resource allocation as much as possible.

Figure 8 shows the variation of DRM control performance with sensing time using the GSRED algorithm. With the increase of sensing time, the price of electricity continues to rise, and the gap between supply and demand is shrinking, which can alleviate the imbalance of power supply and demand. At the same time, as the sensing time increases, the social welfare increases to a specific value, which means that the performance of DRM is improved. However, when the sensing time increases from 6 ms to 8 ms, the gain of the performance of the algorithm is not obvious, which means that the sensing time is no longer the main factor limiting the performance improvement of DRM. Therefore, the sensing time is not always as long as possible. Reasonable setting of sensing time can reduce system delay while avoiding the loss of performance.

Figure 9 illustrates the curve of the social welfare and system utility versus sensing time. Obviously, as the sensing time increases, the social welfare and system utility are generally on the rise. When the sensing time is less than 2 ms, the social welfare and system utility grow rapidly with the increase of the sensing time. Conversely, when the sensing time is greater than 2 ms, the growth rate of social welfare and system utility slows down until it reaches a maximum value. Besides, a reasonable set of sensing time can minimize system overhead and delay while ensuring maximum social welfare and system utility.

5. Conclusion

DRM in the smart grid can promote the balance of power supply and demand and optimize the allocation of power resources. In DRM, a large number of power data transmission requirements lead to a sharp increase in the demand for spectrum resources, while communication quality will

affect the system control performance. Therefore, CR is introduced into DRM, and the GSRED algorithm is used to realize spectrum sensing under low SNR to improve communication performance. The influence of sensing time on communication outage probability and the influence of sensing time and outage probability on DRM control performance are analyzed analytically and numerically. Considering the interference to PU and spectrum loss caused by unreliable spectrum sensing, the system utility is used as the final index to measure the system performance. The simulation results show that compared with the ED algorithm, the GSRED algorithm can guarantee lower communication outage probability and spectrum loss rate under the same conditions and can guarantee better system performance of DRM.

Data Availability

The data used to support the findings of this study are included within the article.

Disclosure

This work was presented in part at the 2019 IEEE International Conference on Communication Technology Workshops (ICCT Workshops).

Conflicts of Interest

The authors declare that there is no conflict of interest regarding the publication of this paper.

Acknowledgments

This research was supported by the Core Electronic Devices, High-end General Chips and Basic Software Products Projects of China (2017ZX01030204).

References

- [1] W. Tushar, C. Yuen, B. Chai et al., "Smart grid testbed for demand focused energy management in end user environments," *IEEE Wireless Communications*, vol. 23, no. 6, pp. 70–80, 2016.
- [2] J. Su, Z. Sheng, V. C. M. Leung, and Y. Chen, "Energy efficient tag identification algorithms for rfid: survey, motivation and new design," *IEEE Wireless Communications*, vol. 26, no. 3, pp. 118–124, 2019.
- [3] N. U. Hassan, W. Tushar, C. Yuen, S. G. Kerk, and S. W. Oh, "Guaranteeing qos using unlicensed tv white spaces for smart grid applications," *IEEE Wireless Communications*, vol. 24, no. 2, pp. 18–25, 2017.
- [4] P. de Araújo, R. H. Filho, J. J. P. C. Rodrigues, J. P. C. M. Oliveira, and S. A. Braga, "Infrastructure for integration of legacy electrical equipment into a smart-grid using wireless sensor networks," *Sensors*, vol. 18, no. 5, p. 1312, 2018.
- [5] J. Su, Y. Chen, Z. Sheng, Z. Huang, and A. X. Liu, "From m-ary query to bit query: a new strategy for efficient large-scale rfid identification," *IEEE Transactions on Communications*, vol. 68, no. 4, pp. 2381–2393, 2020.
- [6] K. Zhang, Y. Mao, S. Leng, H. Bogucka, S. Gjessing, and Y. Zhang, "Cooperation for optimal demand response in

- cognitive radio enabled smart grid,” in *2016 IEEE International Conference on Communications (ICC)*, pp. 1–6, Kuala Lumpur, Malaysia, May 2016.
- [7] J. Su, Z. Sheng, A. X. Liu, Y. Han, and Y. Chen, “A group-based binary splitting algorithm for uhf rfid anti-collision systems,” *IEEE Transactions on Communications*, vol. 68, no. 2, pp. 998–1012, 2020.
- [8] R. Yu, Y. Zhang, S. Gjessing, C. Yuen, S. Xie, and M. Guizani, “Cognitive radio based hierarchical communications infrastructure for smart grid,” *IEEE Network*, vol. 25, no. 5, pp. 6–14, 2011.
- [9] J. Mitola and G. Q. Maguire, “Cognitive radio: making software radios more personal,” *IEEE Personal Communications*, vol. 6, no. 4, pp. 13–18, 1999.
- [10] S. Haykin, “Cognitive radio: brain-empowered wireless communications,” *IEEE Journal on Selected Areas in Communications*, vol. 23, no. 2, pp. 201–220, 2005.
- [11] F. Salahdine, H. El Ghazi, N. Kaabouch, and W. F. Fihri, “Matched filter detection with dynamic threshold for cognitive radio networks,” in *2015 International Conference on Wireless Networks and Mobile Communications (WINCOM)*, pp. 1–6, Marrakech, Morocco, October 2015.
- [12] Y. Yang, Y. L. Ji, H. H. Li, D. Lei, and M. Rui, “Adaptive two-stage sensing based on energy detection and cyclostationary feature detection for cognitive radio systems,” *Applied Mechanics and Materials*, vol. 411-414, pp. 1521–1528, 2013.
- [13] A. Singh, M. R. Bhatnagar, and R. K. Mallik, “Threshold optimization of a finite sample-based cognitive radio network using energy detector,” *Eurasip Journal on Wireless Communications and Networking*, vol. 2013, no. 1, 2013.
- [14] V. Chau, S. Feng, and N. K. Thang, “Competitive algorithms for demand response management in smart grid,” *LATIN 2018: Theoretical Informatics*, pp. 303–316, 2018.
- [15] F. Meng and X. Zeng, “A profit maximization approach to demand response management with customers behavior learning in smart grid,” *IEEE Transactions on Smart Grid*, vol. 7, no. 3, pp. 1516–1529, 2016.
- [16] P. Faria, Z. Vale, J. Soares, and J. Ferreira, “Demand response management in power systems using particle swarm optimization,” *IEEE Intelligent Systems*, vol. 28, no. 4, pp. 43–51, 2013.
- [17] S. Maharjan, Y. Zhang, S. Gjessing, and D. H. K. Tsang, “User-centric demand response management in the smart grid with multiple providers,” *IEEE Transactions on Emerging Topics in Computing*, vol. 5, no. 4, pp. 494–505, 2017.
- [18] W. Li, C. Yuen, N. U. Hassan et al., “Demand response management for residential smart grid: from theory to practice,” *IEEE Access*, vol. 3, pp. 2431–2440, 2015.
- [19] Z. Chen, L. Wu, and Y. Fu, “Real-time price-based demand response management for residential appliances via stochastic optimization and robust optimization,” *IEEE Transactions on Smart Grid*, vol. 3, no. 4, pp. 1822–1831, 2012.
- [20] Q. Tang, K. Yang, D. Zhou, Y. Luo, and F. Yu, “A real-time dynamic pricing algorithm for smart grid with unstable energy providers and malicious users,” *IEEE Internet of Things Journal*, vol. 3, no. 4, pp. 554–562, 2016.
- [21] B. Li, Q. Wu, B. Qi, J. Zhang, and S. Chen, “Plan of power utilization of time-of-use power price through smart grid user interface,” in *2015 4th International Conference on Computer Science and Network Technology (ICCSNT)*, vol. 1, pp. 203–206, Harbin, China, Dec 2015.
- [22] Z. Amjad, S. Batool, H. Arshad, K. Parvez, M. Farooqi, and N. Javaid, “Pigeon inspired optimization and enhanced differential evolution in smart grid using critical peak pricing,” *Advances in Intelligent Networking and Collaborative Systems*, pp. 505–514, 2018.
- [23] P. Samadi, H. Mohsenian-Rad, V. W. S. Wong, and R. Schober, “Real-time pricing for demand response based on stochastic approximation,” *IEEE Transactions on Smart Grid*, vol. 5, no. 2, pp. 789–798, 2014.
- [24] X. Song and Q. Jiayu, “An improved real-time pricing algorithm based on utility maximization for smart grid,” in *Proceeding of the 11th World Congress on Intelligent Control and Automation*, pp. 2509–2513, Shenyang, China, June 2014.
- [25] R. Deng, J. Chen, X. Cao, Y. Zhang, S. Maharjan, and S. Gjessing, “Sensing-performance tradeoff in cognitive radio enabled smart grid,” *IEEE Transactions on Smart Grid*, vol. 4, no. 1, pp. 302–310, 2013.
- [26] C. Yang, Y. Fu, and J. Yang, “Optimisation of sensing time and transmission time in cognitive radio-based smart grid networks,” *International Journal of Electronics*, vol. 103, no. 7, pp. 1098–1111, 2015.
- [27] W. Hsiao and W. Chiu, “Spectrum sensing control for enabling cognitive radio based smart grid,” in *2016 2nd International Conference on Intelligent Green Building and Smart Grid (IGBSG)*, pp. 1–6, Prague, Czech Republic, June 2016.
- [28] T. Yang, T. Huang, Y. Gu, H. Gan, Y. Wu, and H. Zhang, “Spectrum sensing for demand response management in smart grid,” in *2019 IEEE 19th International Conference on Communication Technology (ICCT)*, pp. 745–750, Xi’an, China, China, October 2019.
- [29] P. Samadi, A. Mohsenian-Rad, R. Schober, V. W. S. Wong, and J. Jatskevich, “Optimal real-time pricing algorithm based on utility maximization for smart grid,” in *2010 First IEEE International Conference on Smart Grid Communications*, pp. 415–420, Gaithersburg, MD, USA, October 2010.
- [30] H. Urkowitz, “Energy detection of unknown deterministic signals,” *Proceedings of the IEEE*, vol. 55, no. 4, pp. 523–531, 1967.
- [31] T. Yang, Y. Wu, L. Li, W. Xu, and W. Tan, “A two-step cooperative energy detection algorithm robust to noise uncertainty,” *Wireless Communications and Mobile Computing*, vol. 2019, 10 pages, 2019.
- [32] T. Yang, Y. Wu, L. Li, W. Xu, and W. Tan, “Fusion rule based on dynamic grouping for cooperative spectrum sensing in cognitive radio,” *IEEE Access*, vol. 7, pp. 51630–51639, 2019.
- [33] S. Atapattu, C. Tellambura, and H. Jiang, “Energy detection based cooperative spectrum sensing in cognitive radio networks,” *IEEE Transactions on Wireless Communications*, vol. 10, no. 4, pp. 1232–1241, 2011.
- [34] C. Charan and R. Pandey, “Eigenvalue based double threshold spectrum sensing under noise uncertainty for cognitive radio,” *Optik*, vol. 127, no. 15, pp. 5968–5975, 2016.

Research Article

Architecture and Protocol to Optimize Videoconference in Wireless Networks

Jose M. Jimenez, José Luis García-Navas, Jaime Lloret , and Oscar Romero

Instituto de Investigación para la Gestión Integrada de Zonas Costeras, Universitat Politècnica de València, Spain

Correspondence should be addressed to Jaime Lloret; jlloret@dcom.upv.es

Received 23 February 2020; Revised 27 August 2020; Accepted 13 September 2020; Published 6 October 2020

Academic Editor: Tuan M. Nguyen

Copyright © 2020 Jose M. Jimenez et al. This is an open access article distributed under the Creative Commons Attribution License, which permits unrestricted use, distribution, and reproduction in any medium, provided the original work is properly cited.

In the past years, videoconferencing (VC) has become an essential means of communications. VC allows people to communicate face to face regardless of their location, and it can be used for different purposes such as business meetings, medical assistance, commercial meetings, and military operations. There are a lot of factors in real-time video transmission that can affect to the quality of service (QoS) and the quality of experience (QoE). The application that is used (Adobe Connect, Cisco Webex, and Skype), the internet connection, or the network used for the communication can affect to the QoE. Users want communication to be as good as possible in terms of QoE. In this paper, we propose an architecture for videoconferencing that provides better quality of experience than other existing applications such as Adobe Connect, Cisco Webex, and Skype. We will test how these three applications work in terms of bandwidth, packets per second, and delay using WiFi and 3G/4G connections. Finally, these applications are compared to our prototype in the same scenarios as they were tested, and also in an SDN, in order to improve the advantages of the prototype.

1. Introduction

Video conferencing is a widespread means of communication in an era where technologies are constantly evolving. It allows people to communicate all over the world using only an electronic device connected to the Internet. Video conferencing allows not only video and voice transmission but also data transmission, allowing collaborative working. Video conferencing has always been characterized by the necessity of synchronization, low delay, low jitter, low loss ratio of packets, etc., and it has to confront the user's requirements, according to the quality of the communication, that are constantly increasing.

The audio and video contents that are transmitted over the Internet are constantly growing. One of these contents that is transmitted over the Internet is television. It is known as IPTV (Internet Protocol Television), and it consists of the distribution of high-quality television content [1]. It can be real-time video or Video on Demand (VoD). IPTV provides traditional TV services to the home through the Internet Service Providers (ISP). IPTV has become a key product for

Internet Service Providers (ISP). IPTV offers benefits to both ISP and end users [2]. The Internet was not designed to transmit real-time video/audio information, so Quality of Service (QoS) is one of the most important tasks to deal with when generating IPTV services. QoS directly affects the Quality of Experience (QoE). Users demand the best QoE as possible. In order to evaluate QoE, there are both objective and subjective approaches, such as objective metrics and subjective users' evaluation [2]. Huang et al. [3] propose data-driven QoE prediction for IPTV services. They firstly evaluate user experience of IPTV in a data-driven approach, and then they analyze the user's interest and experience.

Real-time video services, such as IPTV, and especially videoconferencing, require rigorous QoS requirements in terms of bandwidth, delay, and jitter. Video transcoding is a challenging task, and meeting QoS requirements could be critical to transmit information in a reliable and secure manner [4]. QoS needs to be analyzed not only from a metric perspective but also from a customer satisfaction perspective. Quantitative metrics must be correlated with qualitative metrics from the customers [5]. QoE in video

streaming is a task that can be improved in both wired and wireless networks.

QoE prediction consists of studying the relationship between the user experience and features from the video. Some authors have investigated ways of improving QoE over wired networks by different ways. Mao et al. [6] propose an IPTV user QoE prediction algorithm based on the Long Short-Term Memory (LSTM) network. They select subjective and objective features and use the LSTM network to perform QoE modeling. Their proposal shows a higher performance in QoE prediction than other conventional neural networks. Other authors such as Jiménez et al. [7] analyze QoE from the point of view of the number of devices connected and the use of bandwidth. They study a basic topology on which a video is broadcasted and propose an algorithm to improve quality of experience when network parameters can vary.

Quality of experience can also be studied over wireless networks. Su et al. [8] conducted a survey on existing literatures about video streaming QoE. They started from the point of view of the resource allocation problem and managed to bring together separated QoE metrics into seven categories. This allowed them to analyze their importance and complexity in video source coding and wireless networks. All these measurements can be used to carry out some other investigations. QoE management systems can be developed to guarantee enough QoE in IPTV services [9]. Delay, jitter, bandwidth, and zapping time measurements are used to calculate QoE over wireless networks, using a formula.

Video streaming, including videoconferencing, consumes a substantial portion of network resources. Video transmission requires high-bandwidth and strong latency requirements. Software-Defined Networking (SDN) gives the possibility of changing the network dynamically. SDN, joined to other techniques oriented to improve video streaming, can optimize video transmission through flexible controls [10]. Jimenez et al. [11] carried out a performance comparison between Mininet and a real network when multimedia streams were being delivered. Bandwidth, delay, and jitter were studied.

Taking into account these issues, this paper proposes an architecture for videoconferencing to provide better quality of experience than other existing solutions. First of all, the system used in our prototype is defined. This system consists of an E2E QoE management scheme for real-time video communication structured in different layers. The system will have three basic processes, which correspond to the basic actions to establish a videoconference: register, connection, and transmission process. Later, a finite-state machine is proposed, and also the different states are presented and defined. In addition, three different existing VC applications (Adobe Connect, Cisco Webex, and Skype) are tested in terms of bandwidth, packets per second, and delay, using WiFi and 3G/4G connections. Finally, these applications are compared to our prototype in the same scenarios as they were tested and in another scenario where SDN is applied in order to improve the advantages of the prototype.

The remainder of this paper is organized as follows. Section 2 presents some related work. The architecture pro-

posal for videoconferencing is explained in Section 3. Section 4 describes the proposal of the protocol of communication. The performance test in videoconference applications is carried out in Section 5. Section 6 presents the performance test of the developed application. And finally, Section 7 draws the main conclusions and future works.

2. Related Works

This section presents some works where video streaming, in particular videoconferencing, is studied from different points of view.

Chakraborti et al. [12] propose an audio/videoconferencing architecture based on the Virtualized Service Edge Router (VSER) platform. Their solution uses the VSER platform for notifications and the ICN framework for data exchange. This design provides good scalability and reliability, and it also allows discovering of new participants, dynamic synchronization, and multicasting for data exchange.

In [13], Hajiesmaili et al. discuss about the multiparty cloud videoconferencing architecture. They study the advantages of using cloud resources to effectively improve videoconferencing performance. The proposed architecture consists of using multiple agents that perform transcoding tasks. Each user is assigned to the best agent in terms of bandwidth and processing availabilities for each one. Their solution decreases the operational cost and reduces conferencing delays.

There are many papers that present improvements and solutions for videoconferencing using WebRTC for different purposes. Jang-Jaccard et al. [14] propose a design and implementation of a practical videoconferencing system for telehealth using WebRTC technology. Their goal is to evaluate the possibility of improving healthcare outcomes by high-bandwidth-enabled telehealth services. Their solution seeks to be standard-based, interoperable, simple, and inexpensive. They show the limitations of using WebRTC, describe various insights into the prototype implementation, and provide code snippets.

Bestak and Hlavacek [15] discuss a videoconferencing platform based on WebRTC technology. They test the impact on the multiplexing server's CPU load and RAM requirements for different numbers of users, using different hardware and software configurations at end-point devices. The results show a strong relation between the video resolution and bit rate, and the importance of dimensioning the server according to the number of users.

Pasha et al. [16] show the shortcomings and challenges faced by videoconferencing through WebRTC and propose a Multipoint Control Unit (MCU) as a solution. They propose the best centralized architecture to support WebRTC by using MCU. Their aim is to expose how WebRTC works and how it can be improved.

Many other authors propose other different solutions for carrying out videoconferencing. Gusev and Burke [17] present a discussion about the design and implementation in C++ of Real-Time Videoconferencing over Named Data Networking (NDN-RTC) on an NDN testbed. They build the solution in C++ using the WebRTC library due to the

necessity of reasonable CPU and bandwidth efficiency. They generate a functional low latency streaming tool that can be used as a platform for studying design challenges in real-time media over NDN.

Sambath et al. [18] face the task of improving the QoS scheme in an IP multimedia subsystem (IMS) for videoconferencing. They implement IntServ and DiffServ with MPLS and study parameters such as end-to-end delay, packet loss, and jitter. Their investigation shows that proper adaptation of QoS and appropriate resource allocation provide qualitative transmission of videoconferencing in a wireline.

Hossain and Khan [19] investigate a novel Multipoint Videoconferencing (MVC) architecture potentially suitable for a Peer-to-Peer (P2P) platform, such as Gnutella. Their proposal is based on the idea that autonomous peer nodes can dynamically assume the role of the MCU. This idea improves the architecture by minimizing total traffic, individual node hotness, and video composition delay.

Video conferencing is widely used for medical purposes, and many papers are focused on how technologies can improve videoconferencing for health. Khalifeh et al. [20] describe an e-health videoconferencing platform to facilitate patients' follow-up and communication with their healthcare professionals from a distance and at low cost. This system is developed for its potential usage in the Jordanian healthcare system and, in particular, medical centers and hospitals located in the rural areas. The main challenge is its high cost, so the proposed platform seeks to provide similar service at a lower cost.

In [21], Taylor et al. study which technical factors influence the quality of videoconferencing in the home setting and evaluate the impact of these factors on the clinical perceptions and acceptance of videoconferencing for health care. They conclude that the quality of videoconferencing when using 3G instead of broadband fiber-based services was less due to failed calls, jitter, and video pixilation.

Mat Kiah et al. [22] propose a secure framework for health videoconferencing systems and a complete management solution for secure videoconferencing groups. They use Real-Time Transport Protocol over UDP to transmit information, and they also use RSA and AES algorithms to provide security services. Their study shows that an encryption algorithm insignificantly increases the videoconferencing computation time.

Furthermore, the correct operation of videoconferencing depends on secure and reliable communication such as good QoS and QoE. Many papers are focused on these aspects. Mishra et al. [23] study how cryptographic techniques are used to achieve security protection to videoconferencing. The authors propose a novel, computationally efficient and secure video encryption algorithm. Security and performance analysis are carried out over their algorithm and show that it is well secured, computation efficient, and applicable for real-life operations.

Pattaranantakul et al. [24] present an achievable secure videoconferencing system based on quantum key encryption. They propose a secure key management methodology to ensure a trusted quantum network and a secure videoconferencing system. Their proposal includes secure communica-

tion channels to exchange secret keys and management. The authors point out that encryption can produce some initial delay.

Zhao et al. [25] present an overview of selected issues about QoE and its application in video transmission. The authors study QoE modeling, assessment, and management of video transmission over different types of networks.

Gunkel et al. [26] study different video stream configurations and layouts for multiparty conferencing in respect to individual network limitations. This study explores the relationship between QoE and three different factors: layout, video quality (resolution), and network limitations (packet loss).

In [27], García et al. show the procedure to set up a server to support the MPEG DASH protocol in the Polimedia e-learning System. They use this server to present a subjective QoE study to evaluate the performance of MPEG DASH. The authors determine the aspects that are most annoying to users of Polimedia. They carry out this study in order to improve the QoE of the user. They conclude that an 8-second video is the most stable segment size for videos of Polimedia.

Finally, all the solutions, ideas, and improvements presented before can be improved by using SDN, due to the possibility of changing the network dynamically and adapting it to the necessities. Henni et al. [28] focus on an improvement of the traditional OpenFlow Controllers. They propose a dynamical QoS routing implemented by a new controller. This new way of routing supports video conferencing flow delivery over OpenFlow networks. Dynamical routing focuses on protecting such traffic over nonconstrained flows. Their proposal simulated under Mininet shows the effectiveness of the proposed approach.

Yang et al. [29] propose a videoconferencing architecture based on SDN-enabled Scalable Video Coding (SVC) multicasting. The architecture discards the traditional Internet Group Management Protocol (IGMP) and MCU to obtain a better performance. Their results show that their system can provide flexible and controllable video delivery, can reduce the network bandwidth usage, and can guarantee the quality of a videoconference.

Al Hasrouty et al. [30] investigate the impact of using SVC and SDN techniques on videoconferencing. Their aim is to reduce the bandwidth consumed by videoconferencing (using SDN) and take advantage of SVC by sacrificing video quality for usability purposes. Their algorithm defines where and how many video layers should be dropped in order to adapt the streams to the bandwidth capacities of the network.

Our proposal improves the methods previously described. We ensure better End-to-End (E2E) QoE in videoconferencing by using the Network-adaptive Control Protocol, adjusting the transmission to the optimal values based on the characteristics of the devices and network. In addition, our proposal includes the use of SDN to get an optimal network transmission.

3. Architecture Proposal for Video Conference

3.1. System Definition. We must define an E2E QoE management scheme for real-time video communication systems, including those operating in resource varying environments.

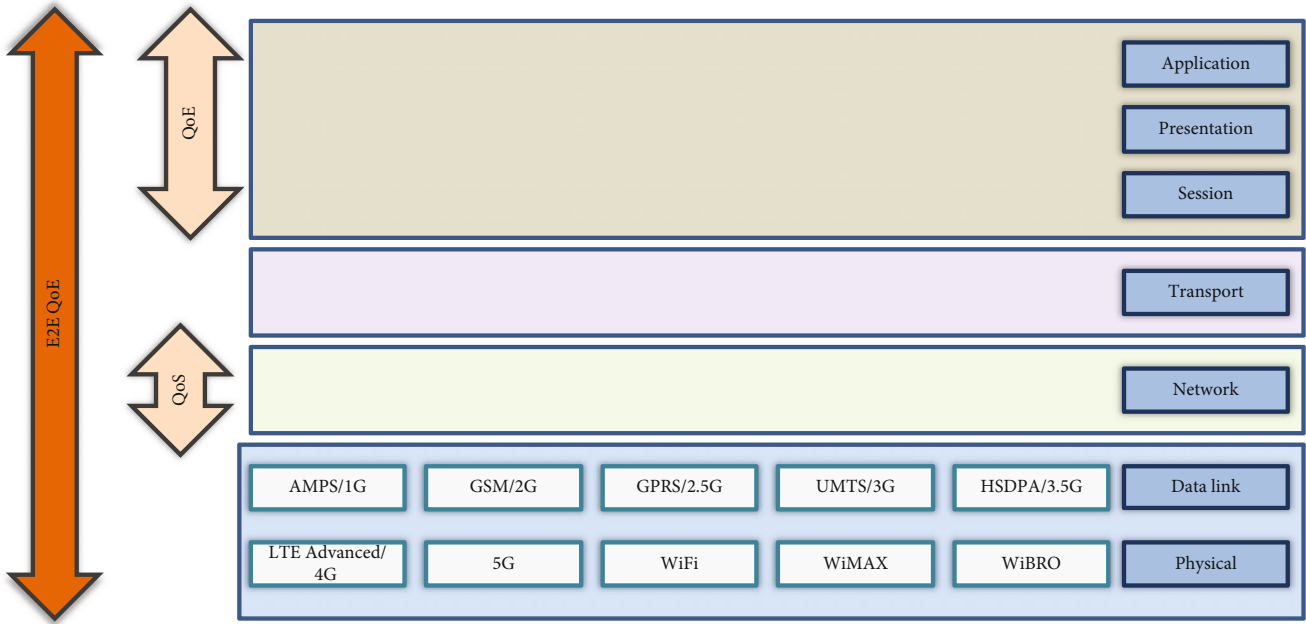


FIGURE 1: Proposed layer architecture, according to the type of QoS and QoE parameters.

In our proposal, we define a human visual perception-based E2E QoE metric and the methodology for correlating this metric to real-time video data, application/network-level QoS measurements, the capabilities of user devices, and subjective user factors.

Initially, to use it in our work, different groups of users observed the transmission of multiple videoconferences. The subjective quality of each videoconference was defined by the user's perception. This is measured in mean opinion score (MOS), from 1 to 5, where 1 is perceived as very bad quality, and 5 is considered very good quality. In this way, we obtained a subjective QoE classification to apply to the different transmissions. In addition, we vary the network parameters and the characteristics of the streams used in the communication equipment in each one of them, so that in the proposal of our system, what we do is adjust the maximum QoE selected by our users, based on to the parameters that are obtained from the computers that are communicating and the network.

We also define network-adaptive video-encoding and decoding algorithms utilizing device-based E2E QoE-driven feedback and, where available, network-based E2E QoE-driven feedback to achieve real-time adaptation according to the available device and/or network resources.

Besides, we define real-time device-based and network-based feedback control mechanisms that can be used to regulate E2E QoE by one or more of the following methods: application-level objective measurement and reporting of the actual received real-time video signal quality; network-level objective measurement and reporting of the in-transit real-time video signal quality; application-level measurement and reporting of device and/or network resources and QoS performance; and network-level measurement and reporting of device and/or network resources and QoS performance.

To carry out these objectives, we will consider which parameters affect the QoE, which algorithm is the most appropriate for the network, which algorithms are the most appropriate to provide the best QoE for end-user devices, how to make the network "adaptive" for this case, and what is the best system decision procedure to provide an "adaptive" network.

The proposed layer architecture, according to the type of QoS and QoE parameters that are considered, is shown in Figure 1.

An architecture that includes all the previously established objectives is shown in Figure 2.

As can be seen in Figure 2, our architecture is based on a Network-adaptive Control Protocol. Through this protocol, we manage to adapt the transmission between the end users to the maximum possible QoE. To achieve the goal, we must take into account how to handle a large amount of information, at least during the initial process of the connection.

Information can be classified depending on where the information is obtained from: obtained from the source devices, obtained from the network between end users, or obtained from the destination device. The information obtained from the source devices can be about available features of the devices (type of camera, CPU, RAM, and iOS), characteristics of device-based network analysis (bandwidth, delay, jitter, and packet loss), characteristics relative to video compression that can be achieved (codecs supported by software), and data calculated from monitoring video-encoded targets (bits/frame, frames/sec, and achievable QoE). Information that can be obtained from the network between end users includes available features of the devices in all the networks where the communication between end users pass through (bandwidth, delay, jitter, packet loss, and achievable QoE). Information that can be obtained from the destination device includes available features of the devices (type of

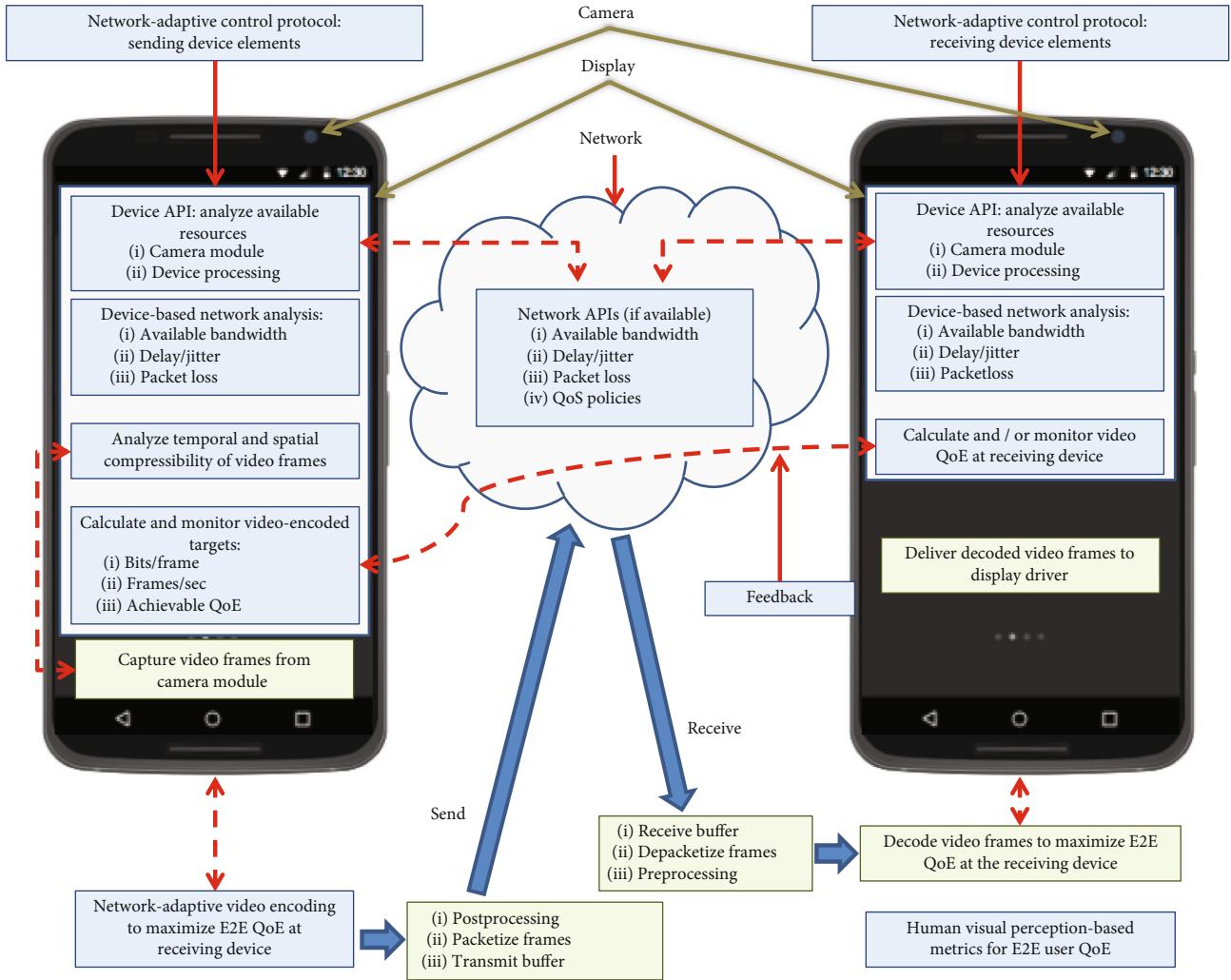


FIGURE 2: Architecture that includes all the established objectives.

camera, CPU, RAM, and iOS), characteristics of device-based network analysis (bandwidth, delay, jitter, and packet loss), and data calculated from monitoring video-encoded targets (bits/frame, frames/sec, and achievable QoE).

Figure 3 shows a generic communication protocol between two users connected to two different service providers, for the establishment of the call. Later, in Section 4, we will detail the proposed protocol for our architecture.

3.2. System Process. In order to design the architecture, we propose three basic processes. They correspond to the basic actions to establish a video communication. Each process is associated to a set of states and transitions that will be detailed later when the system state machine is explained. Figure 4 shows the relationship between the processes of the system. The register process is the start and end process of the system. It is the only process that requires the user’s intervention for executing it.

System processes, with the states of each process, are next described in detail.

3.2.1. Register Process. This process includes three states: Idle state, Registered state, and Failed state. The user, when start-

ing or ending the videoconference, is in the Idle state. From the Idle state, the user enters the Registered state where the final user with whom it will establish the communication will be identified and selected. The Failed status will be reached whenever video communication is interrupted for any reason. From the Failed state, the user passes to the Idle state where they can try again to start a new videoconference.

3.2.2. Connection Process. This process includes two states: the Active state and the Established state. The Active state is accessed after the registration phase, that is, when the connection is requested through the application used to connect to the end user. In this state, the initial information exchange of the adjustment parameters occurs, which are used by the connected users. The Active state is also reached, from the Forwarding state, in the case of a small failure during the transmission, trying to recover the transmission again before reaching the Failed state. From the Active state, users can arrive to the Failed state when it is impossible establish the connection with the final user. The Established state is accessed only from the Active state. In this state, videoconference begins. From the Established state, only the Forwarding state can be reached.

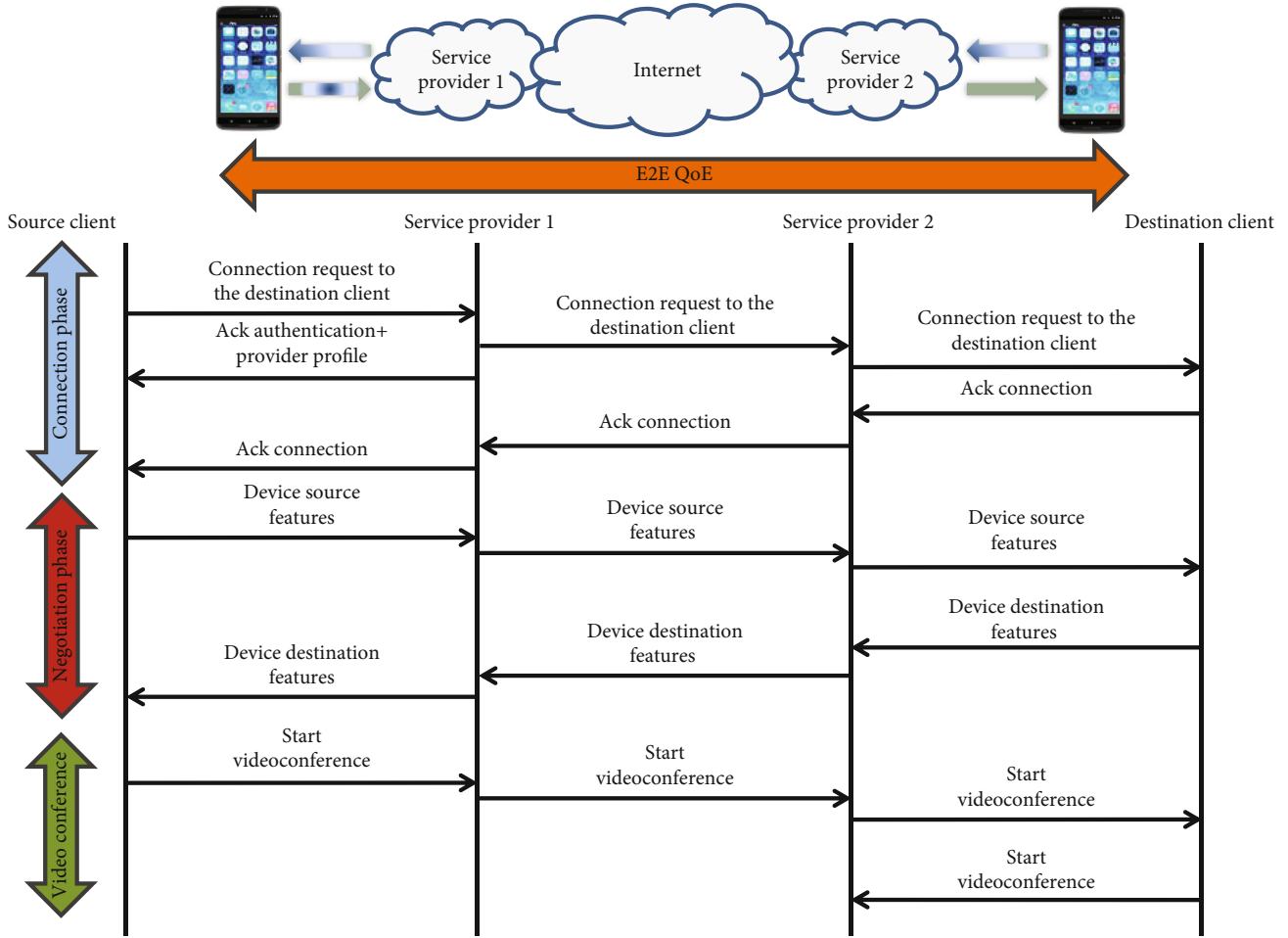


FIGURE 3: Communication protocol between two users connected to two different service providers.

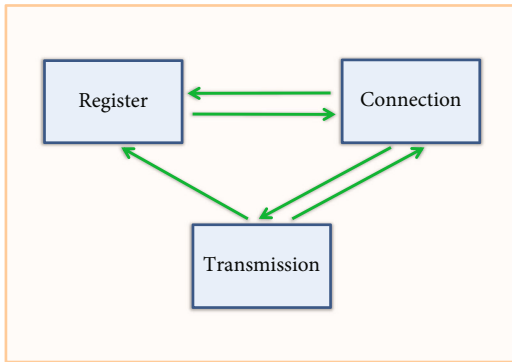


FIGURE 4: System processes of videoconference architecture.

3.2.3. *Transmission Process.* This process includes only one state: Transmission state. Users arrive at the Forwarding state from the Established state, when users have already begun the video communication. In this state, the instantaneous parameters of the devices and the network are controlled periodically. In case of need, the characteristics of the video communication are varied. In the event of a small communication failure, we can try to reenter at the Active state, and if the transmission is terminated or it is impossible to

establish communication with the end user, it is passed to the Failed state.

3.3. *Finite-State Machine.* Figure 5 shows the System Finite-State machine. We can see its different states and the transitions between states. In this section, we describe each state of the system and the conditions and events that will make the node change from one state to another inside a process.

The processes included in Figure 5 are as follows.

3.3.1. *Idle State.* At first, this is the state where the user is, before initiating access to the application to establish the videoconference, or once the videoconference is finished. Then, after the application is selected to make a videoconference, the user will go from this state to the Registered state.

3.3.2. *Registered States.* This state is accessed only from the Idle state. The user initiating the videoconference, depending on the employed software, must initiate the authentication process in the server. Once authenticated, it will search for the remote user that it wants to connect to, in its own database or in the server database. Once the end user is found, it will demand the connection with the selected end user to the server. The server tries to make contact between the users to

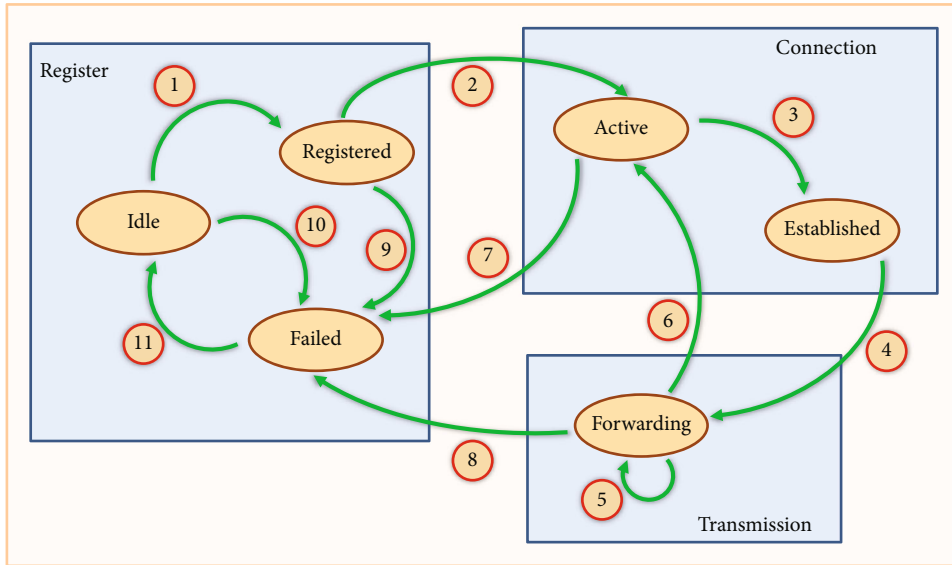


FIGURE 5: Finite-State machine.

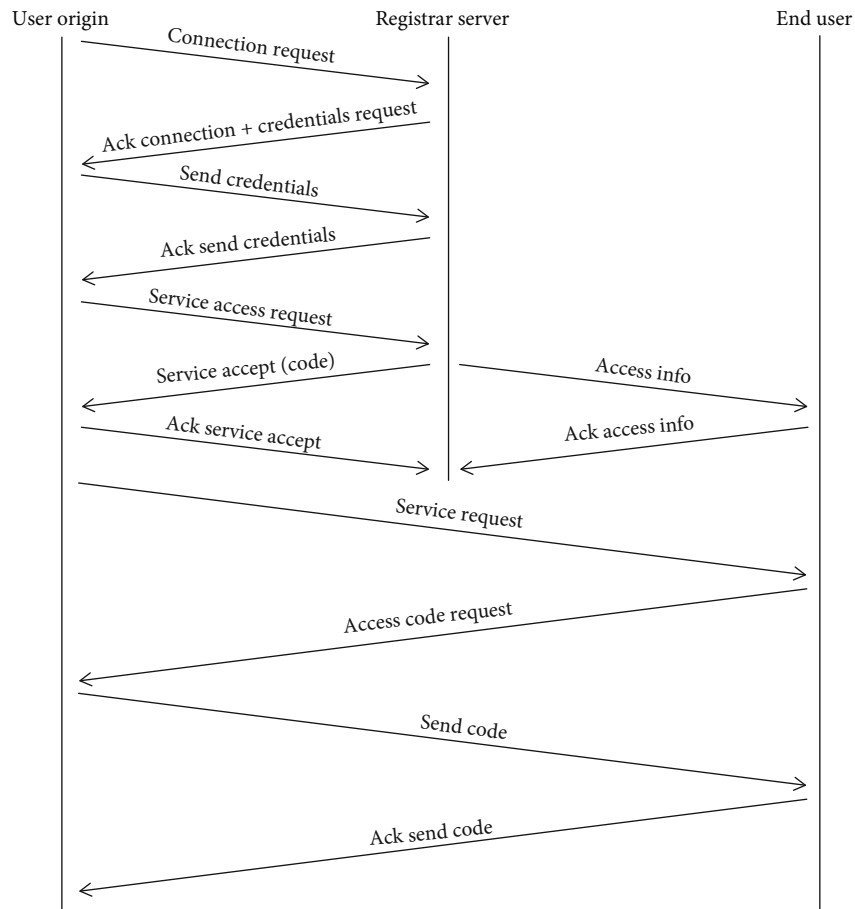


FIGURE 6: Protocol proposed for the Idle and Registered states.

establish an initial connection, and they will go to the Active state. In case the user that is initiating the call does not want to connect with any of the available users or cannot establish a connection with the end user, it will go to the Failed state.

3.3.3. *Active State.* This state can be reached from the Registered or Forwarding states. From the Active state, we can move to the Established or Failed states. Once the initial contact between the users participating in the videoconference

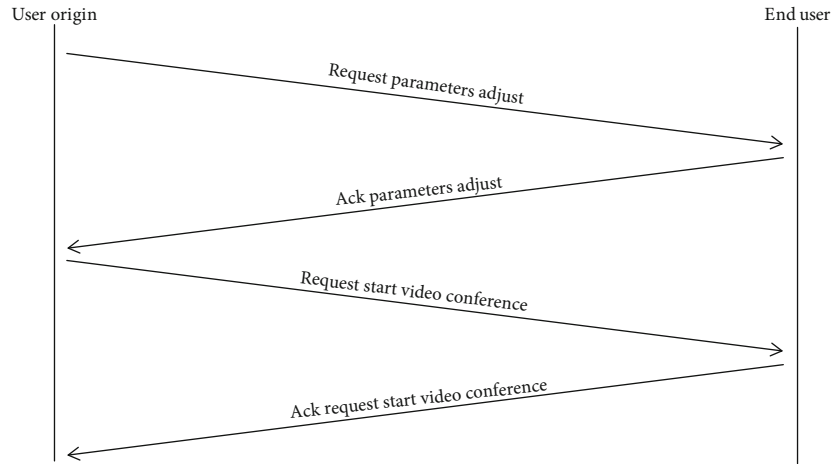


FIGURE 7: Protocol proposed for the Active state.

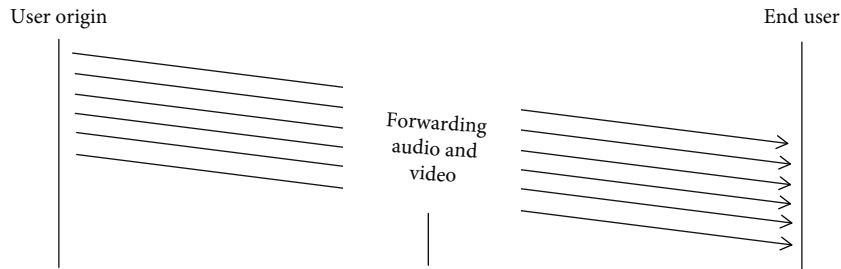


FIGURE 8: Protocol proposed for the Established state.

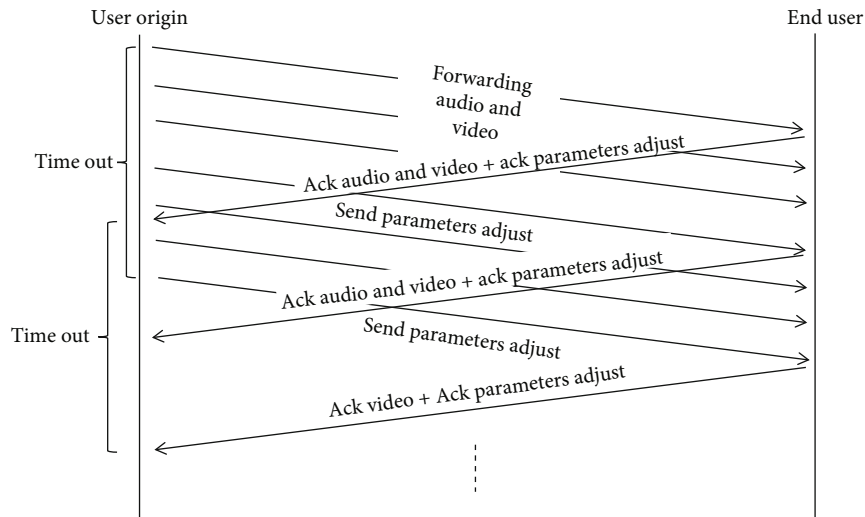


FIGURE 9: Protocol proposed for the Forwarding state when the videoconference is running correctly.

has been established, in the Active state, an exchange of parameters between the end devices of the users will be initiated, at the same time that the information of the network parameters is obtained. Using the information obtained, an algorithm to get an agreement to reach the maximum E2E QoE among the users at that moment will be applied. From this moment on, it will go to Established status. In case that one of the two users rejects or terminates the connection, or a connection agreement cannot be reached due to the

parameters of any of the user devices or of the network, it will go to the Failed state.

3.3.4. Established State. Established status can only be reached from the Active state. From the Established state, you can only move to the Forwarding state. Once the Established state is reached, the video starts from the devices of the connected users, moving to the Forwarding state.

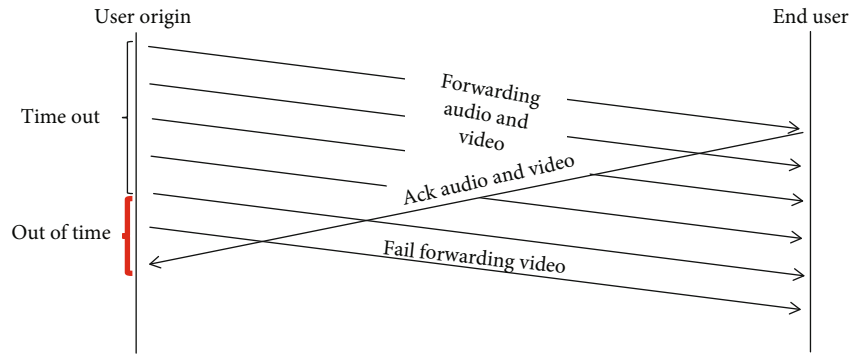


FIGURE 10: Protocol proposed for the Forwarding state when there is a problem.

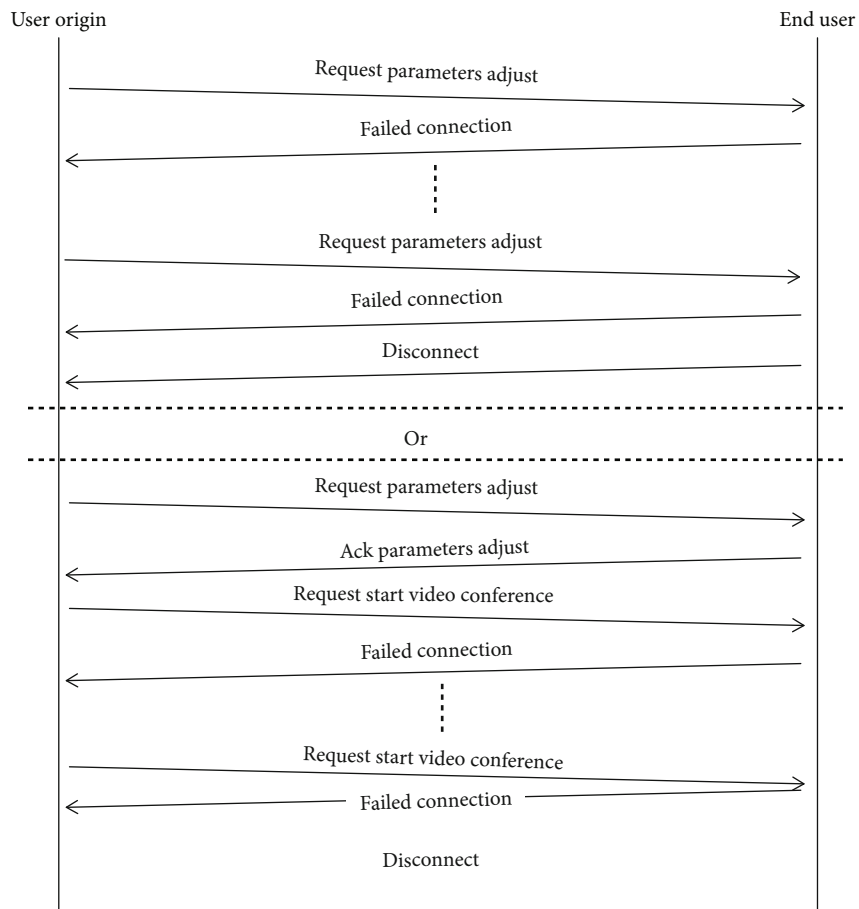


FIGURE 11: Protocol proposed for the transition from the Active state to the Failed state.

3.3.5. *Forwarding State.* The Forwarding state can be reached from the Established state and from the Forwarding state itself. Once the videoconference starts, we will remain in the Forwarding state while everything is working correctly. In this state, the final devices will continuously control the characteristics of the devices themselves and the network, so that when any variation appears, the appropriate measures are taken and the maximum E2E QoE is still maintained. We can vary the codec that was used until then, in case of a need for more compression. Periodically, an acknowledgment

message (Ack) will be exchanged (both for an appropriate videoconference reception and for the adjustment of parameters) between the devices of the users participating in the videoconference. It will establish a maximum period of time (time out) that, if exceeded, the corresponding Ack will not be received. Thus, it will be considered that the videoconference is failing. If a failure occurs, it will go back to the Active state to try to renegotiate the parameters of the devices and the network parameters and go on to relaunch the transmission. In case of not being able to establish the connection

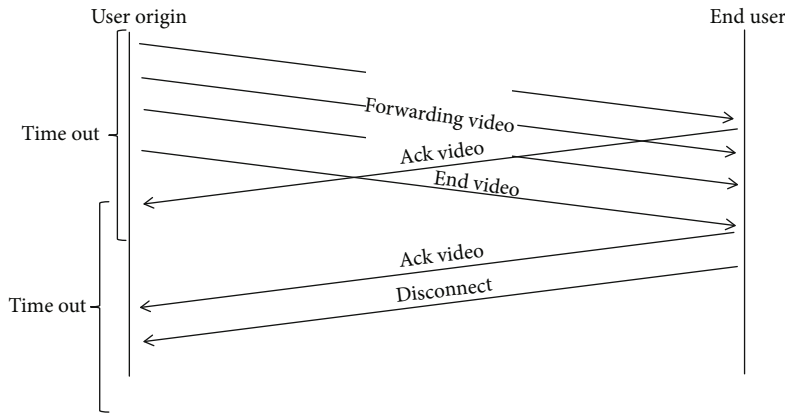


FIGURE 12: Protocol proposed for the transition from the Forwarding state to the Failed state.

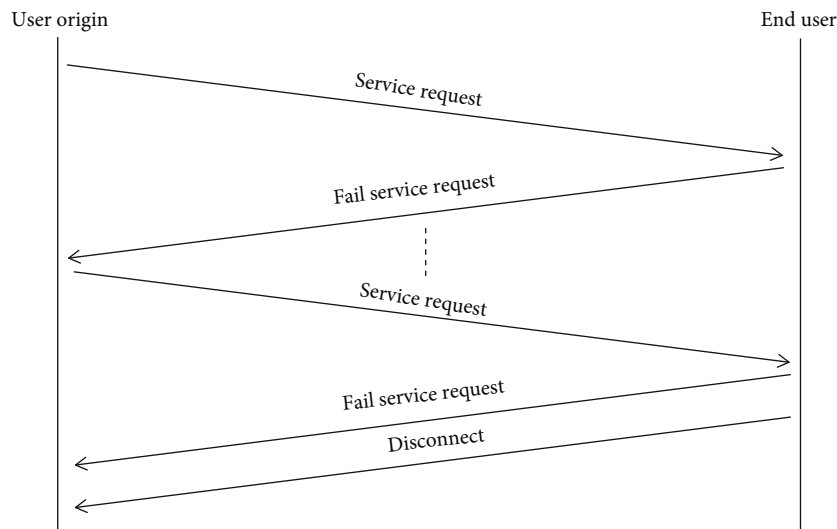


FIGURE 13: Protocol proposed for the transition from the Registered state to the Failed state.

again, it will go to the Failed state. In the event that any of the users ends the videoconference, it will go to the Failed state.

3.3.6. *Failed State.* The Failed status is reached if the videoconference did not work correctly or if one of the users decided to disconnect. The Failed state is reached from the Idle, Registered, Active, and Forwarding states. From the Failed state, it passes to the Idle state to start the whole process again.

4. Protocol Proposal

Figure 6 shows the protocol proposed for the start of the establishment of the connection. It includes the generic actions that will be carried out during the Idle and Registered states.

Figure 7 shows the proposed protocol for the Active state. In this state, users exchange characteristic parameters of their devices and also of the network, in order to achieve the transmission of the videoconference with the maximum E2E QoE.

Figure 8 shows the proposed protocol for the Established state. In this state, the video and audio transmission of the videoconference between the interlocutors begins. The transmission of audio and video will be done in both directions simultaneously, although in Figure 8, the delivery can be observed in only one direction.

Figure 9 shows the proposed protocol for the Forwarding state, but only during the correct operation of the videoconference. It can be seen that the transmission initiated during the Established state continues. Its correct operation is being controlled by the exchange of Acks. They are received before the time out expires. The transmission of audio, video, and Acks will be done in both directions simultaneously, although Figure 9 shows the transmission in only one direction.

Figure 10 shows the proposed protocol for the Forwarding state, when the videoconference stops working correctly, since the Ack is not received from the remote user within the time out. When this situation occurs, it will go back to the Active state to try to recover the transmission. The transmission of audio and video will be done in both directions

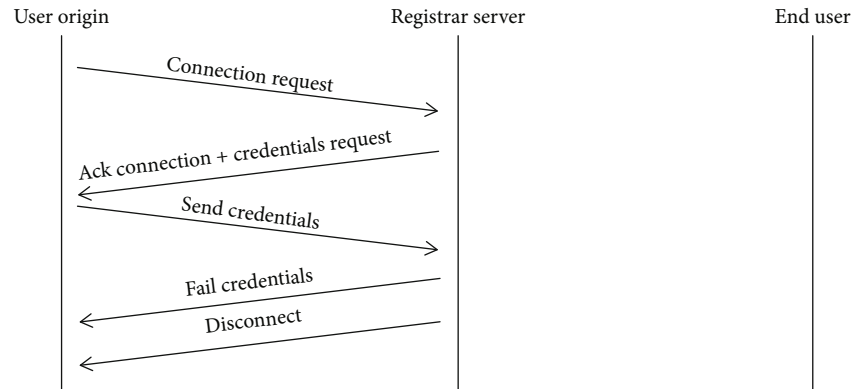


FIGURE 14: Protocol proposed for the transition from the Idle state to the Failed state.

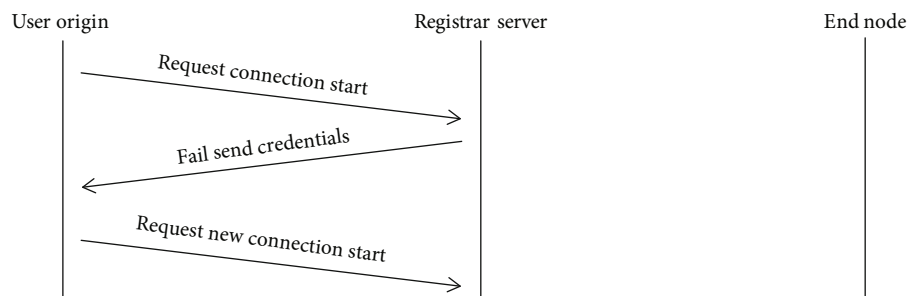


FIGURE 15: Protocol proposed for the transition from the Failed state to the Idle state.

simultaneously, although in Figure 10, the transmission can be observed in only one direction.

Figure 11 shows the proposed protocol for the transition from the Active state to the Failed state. As seen in Figure 11, the transition can occur for two reasons, after several requests for adjustment parameters that have not been answered or after several failures in the attempt to start the videoconference. The transmission of audio and video will be done in both directions simultaneously, although in Figure 11, the transmission can be observed in only one direction.

Figure 12 shows the proposed protocol for the transition from the Forwarding state to the Failed state. As shown in Figure 12, the transition occurs when one of the users involved in the videoconference decides to end it, without any transmission error. The transmission of audio and video will be done in both directions simultaneously, although in Figure 12, the transmission can be observed in only one direction.

Figure 13 shows the proposed protocol for the transition from the Registered state to the Failed state. As shown in Figure 13, the transition occurs when, once the user origin is authenticated, the connection to the end user cannot be established. When this connection attempt fails, it passes to the Failed state in which it will be disconnected.

Figure 14 shows the proposed protocol for the transition from the Idle state to the Failed state. As seen in the image, the transition occurs when, once the videoconferencing software application starts, the user origin cannot be authenticated in the server. When this authentication attempt fails, it passes to the Failed state in which it will be disconnected.

Finally, Figure 15 shows the proposed protocol for the transition from the Failed state to the Idle state. As shown in Figure 15, the transition occurs when the credentials sent by the user origin failed and when it cannot be authenticated in the server. It sends it to the Idle state, where it can try to start a new connection.

5. Performance Test in Videoconference Applications

We have made several performance tests using some of the best-known videoconference applications used in business, academic, and even personal areas. We have made multiple videoconferencing sessions with Adobe Connect, Webex, and Skype.

The topology used during the test is shown in Figure 16. We have used two PCs with the following features: Intel Core i7-7700 3.6 Ghz, 16 GB RAM DDR4 2400 MHz, integrated network card 10/100/1000, integrated wireless network card, and Windows 10 64-bit OS. The network devices we have used were a router for accessing the Internet with a connection of 300 Mbps and two Linksys RE6500-EJ access points that support the 802.11 a, b, g, and n standards. We have also used two JIAYU smartphones model JY-S3 with an eight-core MT6752 processor at 1.7 Ghz, with 2 GB of RAM and 16 GB of internal memory and an Android 5.1 operating system.

In all the equipment, PCs, and smartphones, we installed the software to make the videoconference, which can be downloaded from web pages and as apps provided by the

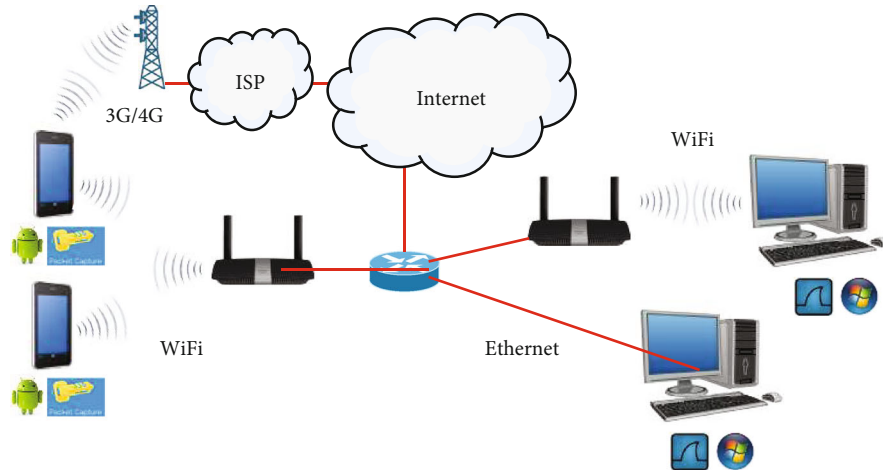


FIGURE 16: Topology used in the videoconference performance test.

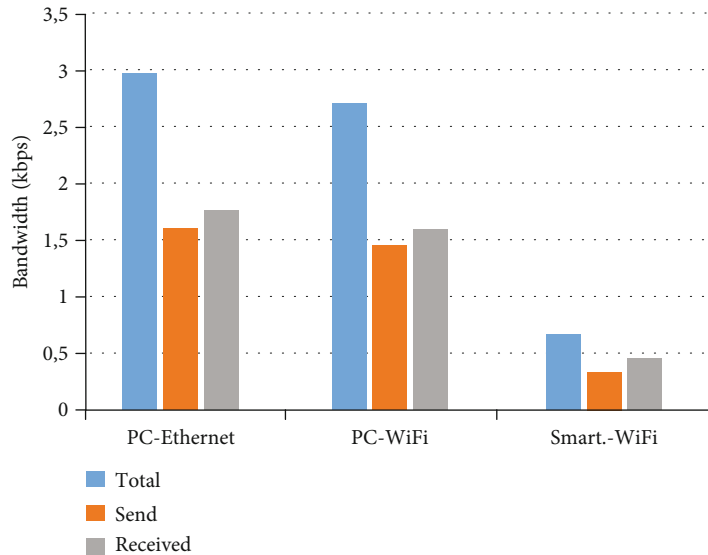


FIGURE 17: Results obtained when using Adobe Connect and smartphone destination with WiFi.

manufacturers (Adobe Connect, Cisco Webex, and Skype). We have also installed the software that allows us to capture the traffic sent. In the case of PCs, we have installed Wireshark, while in smartphones, we have used an app called tcpdump.

In our performance tests, we made different captures to observe the characteristics of the sent traffic with each application and with a duration of 3 minutes.

The data has been captured when the origin of the videoconference was made from different devices, PCs, or smartphones (connected by cable or wireless), and the destination was a smartphone that was connected via WiFi, 3G, or 4G.

5.1. Results Obtained When Using Adobe Connect (WiFi). In Figure 17, it can be seen that when the transmission is made from a PC, both through its Ethernet and wireless interfaces, the traffic increases (approximately 300%) with respect to the

transmission made from the smartphone. Due to these results, we consider that Adobe Connect takes into consideration the type of device from which the transmission is made, PC or smartphone, above the technology used, wired or wireless.

5.2. Results Obtained When Using Adobe Connect (3G/4G). In Figure 18, it is observed that the significant differences are more related to the type of device being used in the test, PC or smartphone, regardless of the connection technology (3G/4G) used in the target device as it happens in Figure 17. When 3G or 4G is used, unlike when both ends employ WiFi technology, the bandwidth consumption is very asymmetric. The bandwidth used by a PC multiplies approximately by 4 the bandwidth used by the mobile.

5.3. Results Obtained When Using Cisco Webex (WiFi). Figure 19 shows the bandwidth consumption when the target device is a smartphone connected via WiFi. In general, there

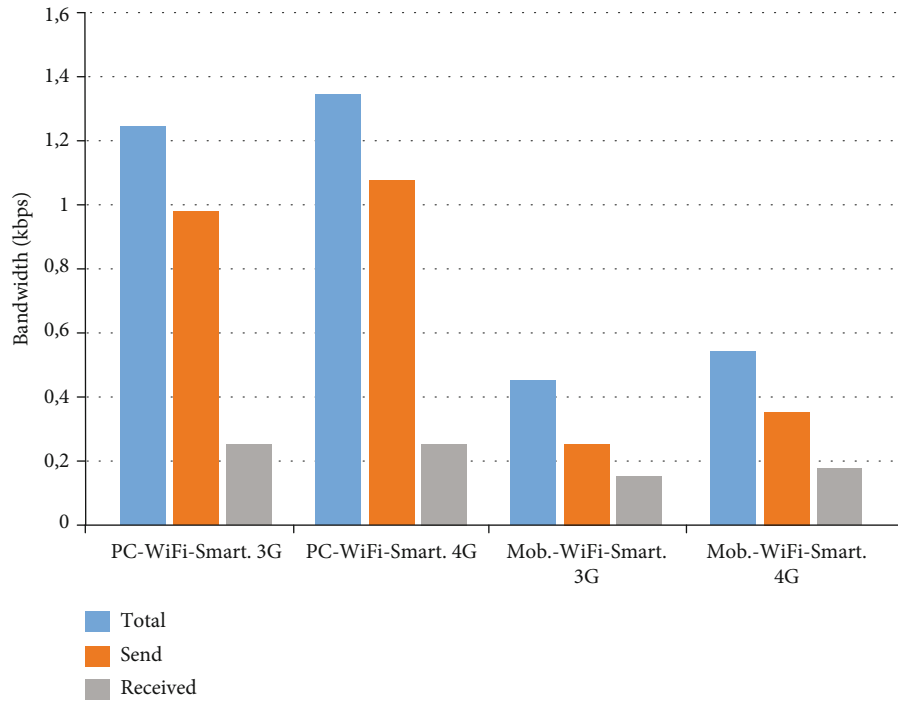


FIGURE 18: Results obtained when using Adobe Connect and smartphone destination with 3G/4G.

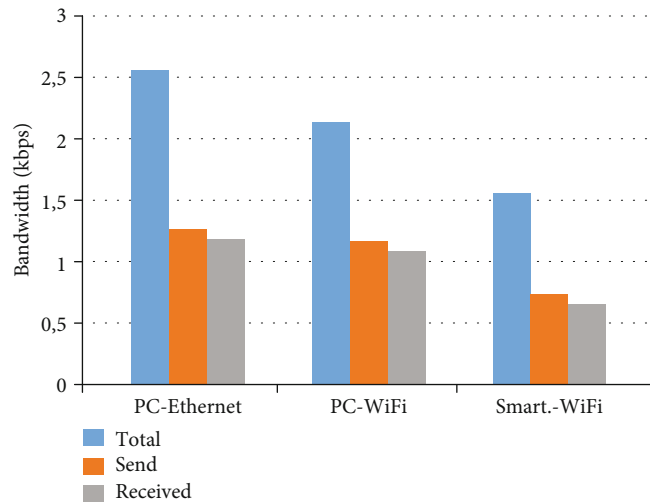


FIGURE 19: Results obtained when using Cisco WebEx and smartphone destination with WiFi.

are no significant differences when changing the device or technology. In the experimental data presented, it was observed that we obtained lower bandwidth consumption results when we use WiFi technology compared to when we use the Ethernet interface.

5.4. Results Obtained When Using Cisco Webex (3G/4G).

Figure 20 shows the results when the target device is connected using 3G/4G technologies. As can be seen in Figure 20, it does not show great differences. The consumption of bandwidth is slightly asymmetric when the transmission is made from a mobile phone connected by WiFi to a

mobile phone connected by 3G or 4G; the smartphone connected via WiFi tends to consume less.

5.5. *Results Obtained When Using Skype (WiFi)*. Figure 21 shows the results obtained when we used the Skype application. The results are very similar to those obtained when we used Adobe for the transmission. Significant differences can be observed when using a PC or a smartphone. In the case of establishing the videoconference between a PC and a smartphone or between a smartphone and another smartphone, the transmission is very asymmetric. When the transmission is made between two smartphones, there is a greater bandwidth saving, reaching a reduction of 80%.

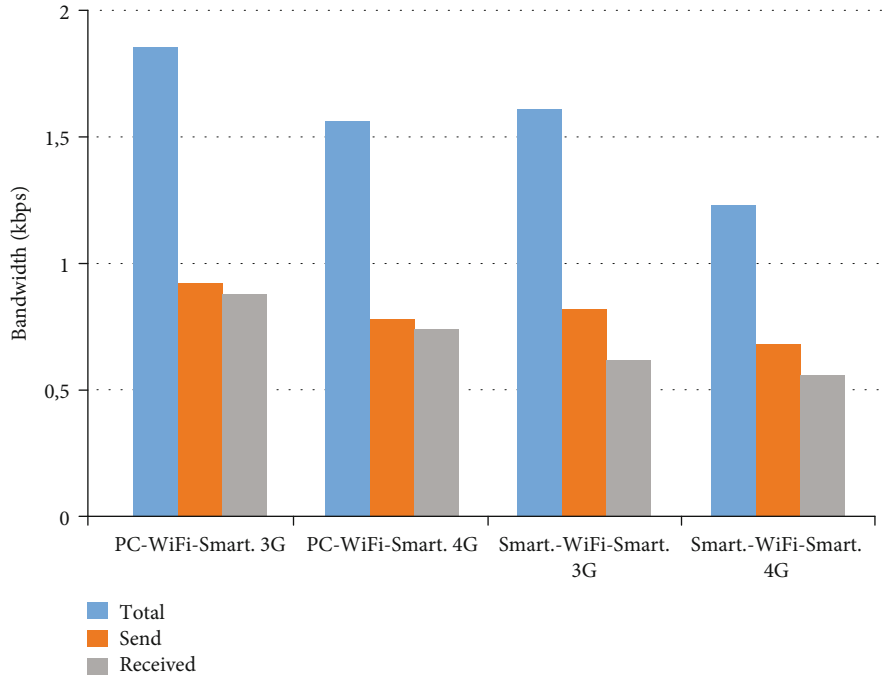


FIGURE 20: Results obtained when using Cisco WebEx and smartphone destination with 3G/4G.

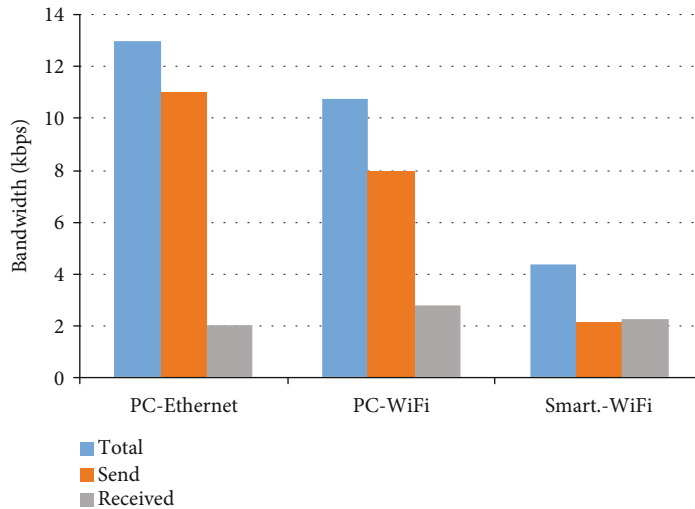


FIGURE 21: Results obtained when using Skype and smartphone destination with WiFi.

5.6. *Results Obtained When Using Skype (3G/4G).* In Figure 22, it can be seen that bandwidth consumption is greater when a PC is used than when a smartphone is used. It is also observed that bandwidth consumption when using 4G technology is slightly higher than when using 3G.

5.7. *Comparison of Cisco Webex vs. Adobe Connect in Terms of Sent Packets.* In Figure 23, we observed the number of transmitted packets in both Cisco Webex and Adobe Connect. A correlation can be seen between the bandwidth consumption and the number of transmitted packets in each of the experimental assumptions. In the case of using the fragmentation of packages, depending on the technology or type

of device, several differences have been observed. An improvement could be achieved by modifying the fragmentation of the packets depending on the technologies or devices.

6. Performance Test of the Developed Application

6.1. *Developed Application.* The operation mode of the application used for testing the prototype proposed in this paper is shown in Figure 24. When starting the application, the login page is shown first. In case the user has no account, the application will enter into a sign up login activity. In order to be

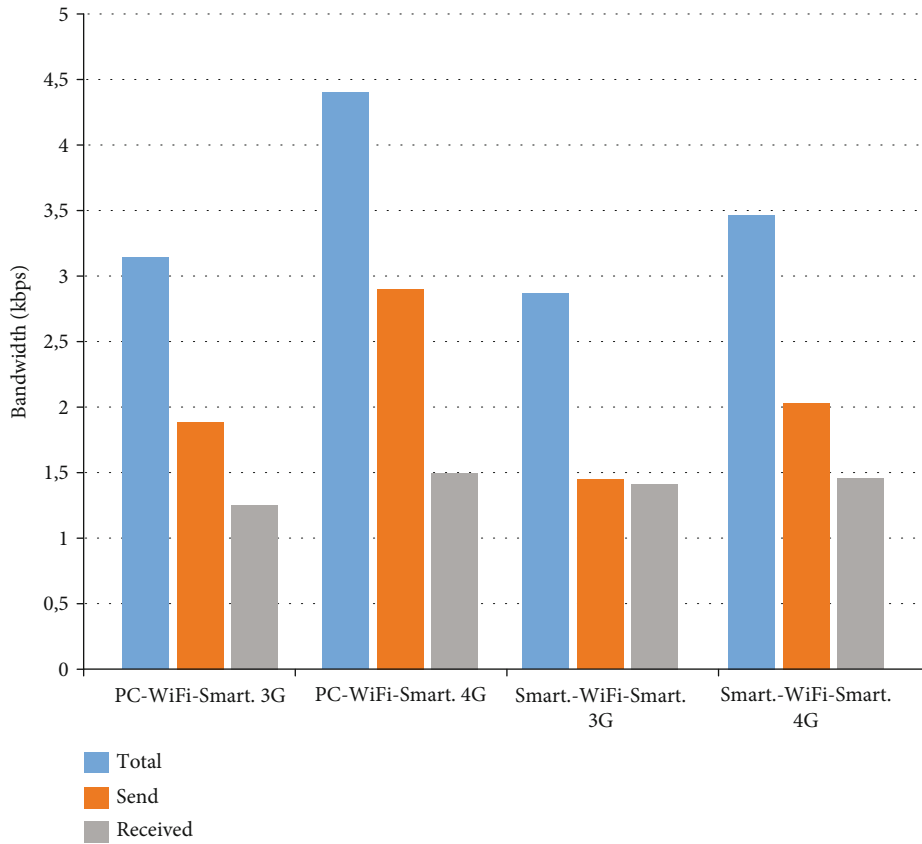


FIGURE 22: Results obtained when using Skype and smartphone destination with 3G/4G.

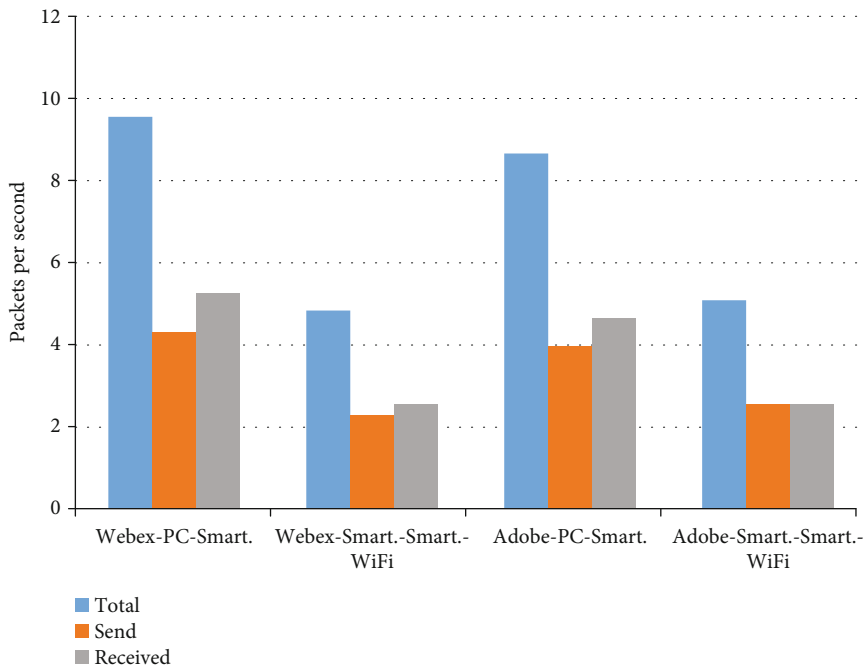


FIGURE 23: Comparison of Cisco WebEx vs. Adobe Connect in terms of sent packets.

registered on the application, it is necessary for the application to have permission to read the Phone_state. When the user already has an account, the user can login. Once the user

is logged in, the main screen is shown and it contains the About button, Contacts button, and field to enter a user and call him. The Contacts button will show the contacts of

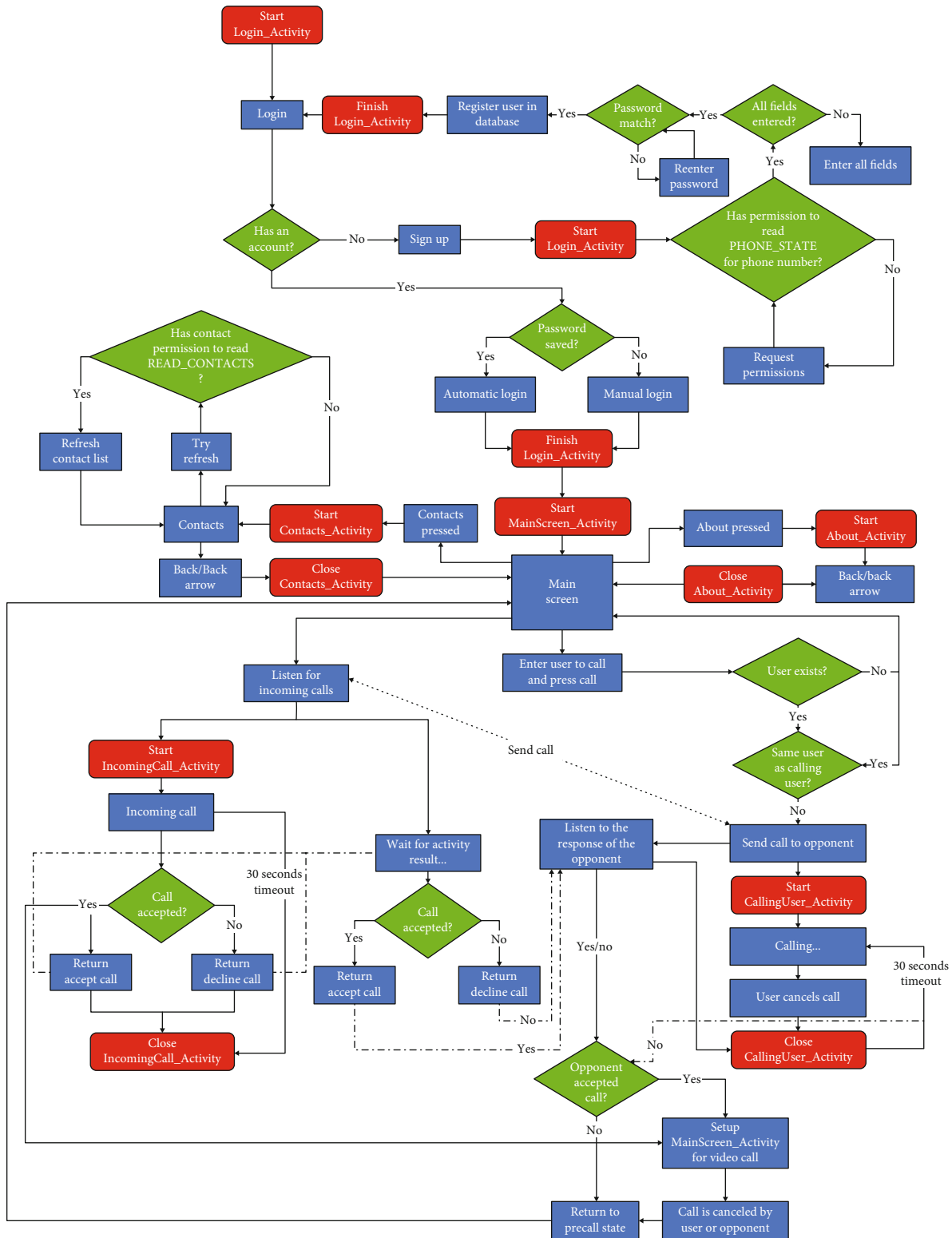


FIGURE 24: Block diagram of application operation.

the mobile phone, so the application needs permission to read them from the mobile phone. When the field of user to be called is filled up and then the call button is pressed, the application will check if the user requested is correct and available.

When a user tries to initiate a call, the application will initiate the activity Start_Calling_User, which will be cancelled in case the user cancels it manually or in the case of running out of time after 30 seconds. The user that receives the call will have the option to accept or reject the call. If the

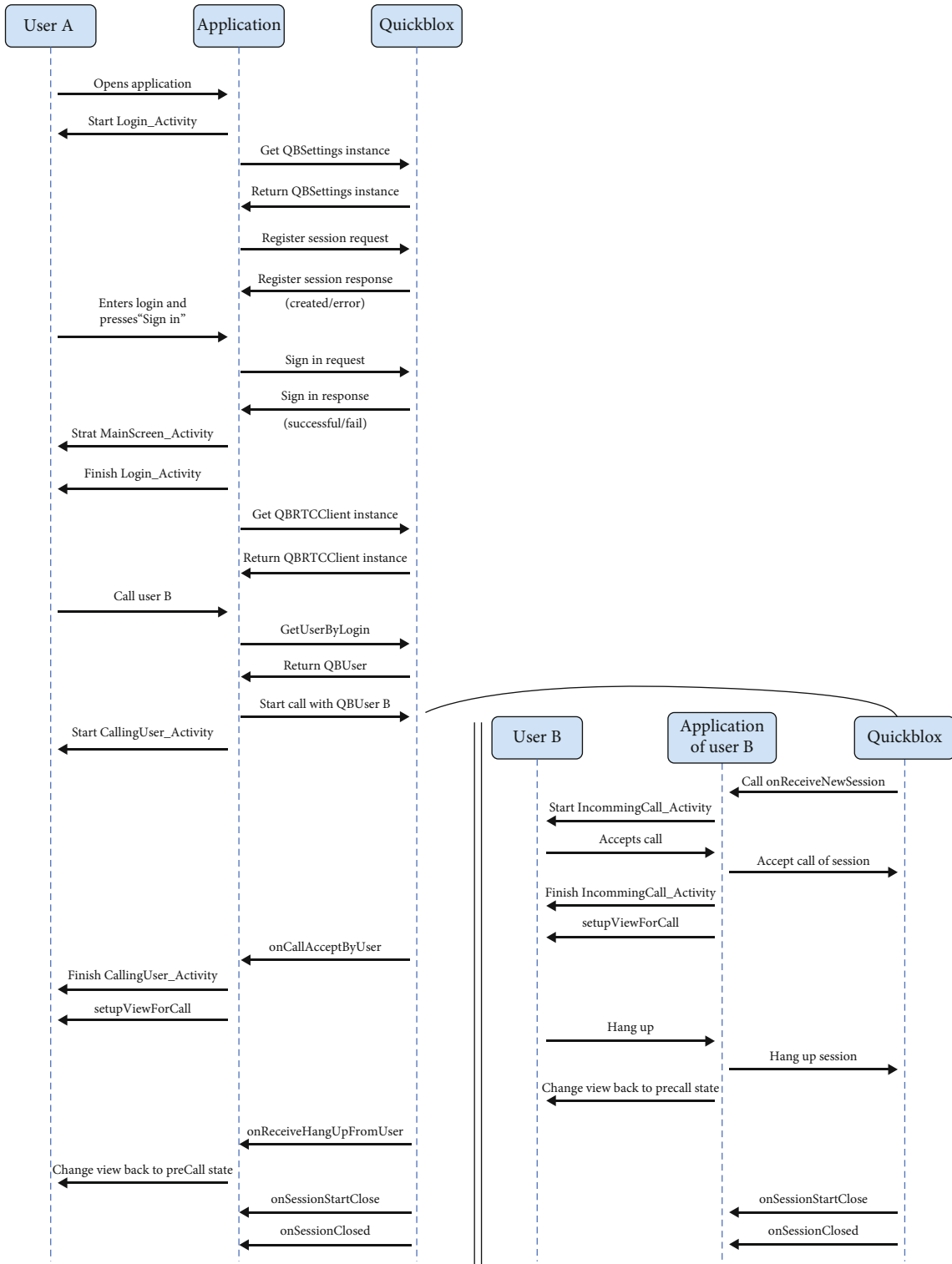


FIGURE 25: Application protocol flow diagram.

communication is established, a MainScreen_Activity will be initiated. Finally, when the call ends, the application will return to precall state.

Figure 25 shows how the application protocol works since a user (user A) opens the application until a conversation is started (with user B), maintained, and finalized. When

user A opens the application, the app will respond with the StartLogin_Activity and will communicate with the Quickblox to get a QBSettings instance and get information about whether the user is registered or not. After that, the user is able to login. When the user presses the login button, the application will send to the Quickblox a sign-in request and

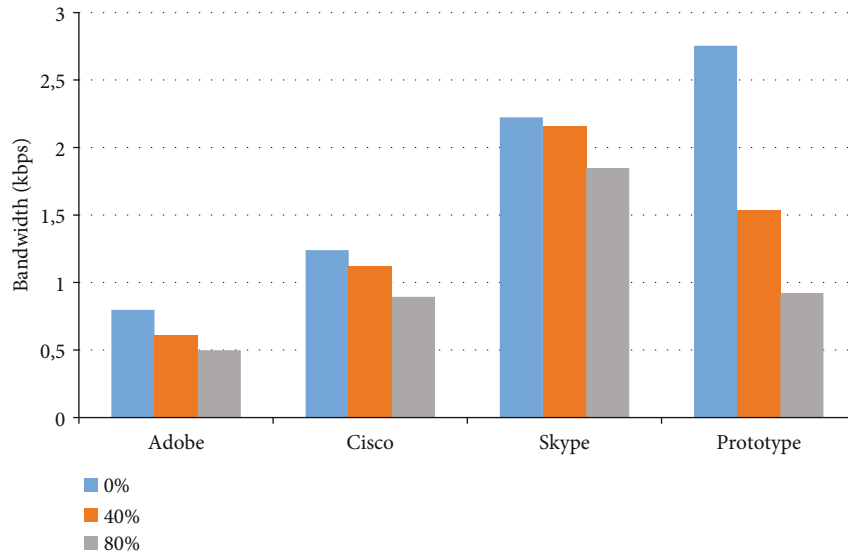


FIGURE 26: Results of scenario 1.

it will respond with a successful/failed state. If the user's login is successful, the application will show the Main Screen and will finish the login activity. The application will get a QBRTCCClient instance from the Quickblox. Now the calls are available.

If user A wants to call user B, the user will ask for the application for calling user B, and the application will ask Quickblox for the QBUser of user B. With that information, the application of user A is able to call user B, passing through the Quickblox. The Quickblox communicates to the application of user B that is receiving a call. User B accepts the call and will Setup View for call. User A will receive an onCallAcceptByUser B and will also Setup View for call.

In case one of the users hangs up the call, the application of the user that is hanging up will communicate this to the Quickblox which sends it to the other application. Both applications change view back to the precall state and close the session.

6.2. Test. In this section, the tests performed with the developed application are presented. We have developed a basic application for videoconferencing which implements the features and characteristics of the algorithm and protocol that have been defined and explained in Section 3 and 4. This application allows us to show the validity of our proposal compared to other commercial applications. The main goal is to show that this work improves the QoE of the videoconference users.

The comparison has been performed on three different scenarios:

- (1) *Scenario 1.* It focuses on the analysis of the resources of the local device, such as the CPU and the RAM combined with the smartphone characteristics (resolution available, camera features, etc.). Following this information, the implementation of our algorithm

adapts the videoconference transmission to guarantee the best conditions for the user

- (2) *Scenario 2.* It focuses on the analysis of the network status from the point of view of the local device. QoS parameters (loss packet, delay, jitter, and bandwidth availability) are observed. When changes in the network conditions happen, the algorithm acts to achieve the best possible QoE
- (3) *Scenario 3.* Finally, in this last scenario, the whole network is analyzed through the capabilities of SDN. The developed protocol links the mobile device with a network managed by SDN, in order to optimize the path of the video transmission used in the videoconference and to minimize the end-to-end delay, jitter, and packet loss

In the next subsections, the measurements from our developed application will be referenced as prototype.

6.2.1. Scenario 1. The experimental set used in this scenario is the same as the one presented in Figure 16, described in Section 5. Each test has been repeated 10 times, and the average has been calculated. The obtained values are presented in Figure 26. Figure 26, we can see how the developed prototype has been able to adapt the bandwidth when the available resources of the CPU and RAM have changed.

In order to perform the measurements in this scenario, in addition to the prototype videoconference application, another experimental app has been developed. The goal of this last application is to spend the resources of the device. The application runs an infinite loop making some random mathematical calculations and can be adjusted to manage the amount of resources of the device.

The first column of each application shows the bandwidth used for the videoconference when there are no other applications running in the same device. For the second

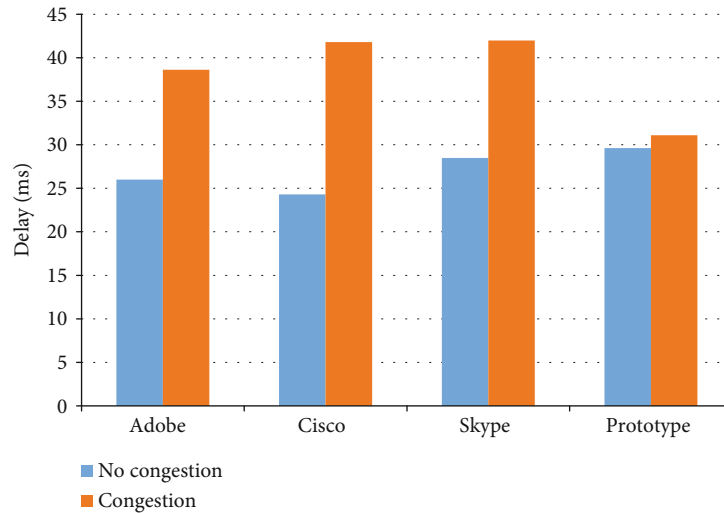


FIGURE 27: Results of scenario 2.

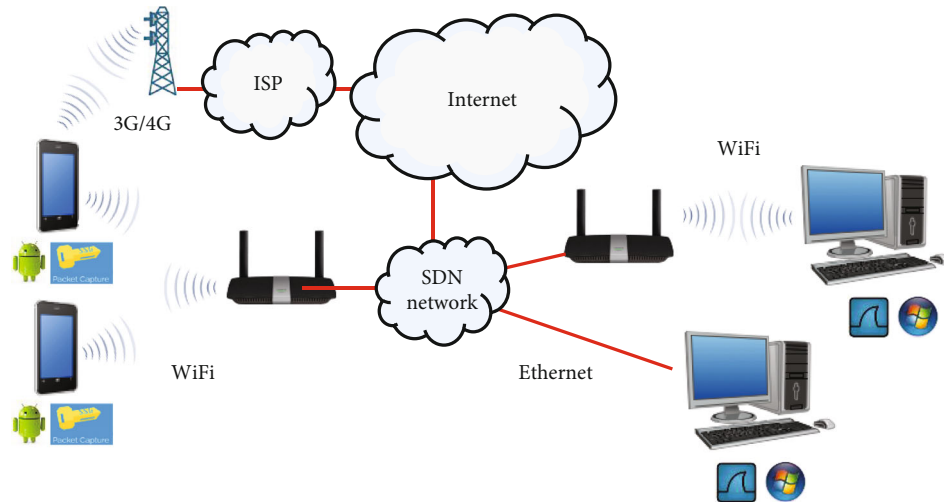


FIGURE 28: Topology used in scenario 3.

and third experimental conditions, shown at the second and third columns, the resources consumed by the application described above were 40% and 80%, respectively.

From the results, we can see how our prototype application gets worse results when the resources of the device are free (0%). But, when the resources decrease, the algorithm used for the prototype is able to adapt in order to reduce the bandwidth consumption, while the commercial solutions show similar results in the three experimental conditions.

6.2.2. Scenario 2. In this scenario, we use the same topology as in scenario 1, which was presented in Figure 16. As in the previous scenario, we have repeated the tests 10 times for this scenario. Now, our goal is to observe the behavior of our application when the local network parameters (loss packet, delay, jitter, and bandwidth availability) change. Basically, we increase the traffic that is sent to the network.

In order to increase network traffic, to achieve congestion, we have developed an application that generates traffic.

In addition, the application, which runs on both ends of the network, allows measuring the latency, based on the exchange of standard ICMP packets, between the final devices that perform the videoconference.

As can be seen in Figure 27, commercial applications have worse latency when congestion appears in the network, because they do not make any type of adaptation in the new situation generated, while our prototype adapts and maintains low levels of latency.

6.2.3. Scenario 3. Figure 28 shows the topology used to perform the tests in scenario 3. In this scenario, we have replaced the router used in previous scenarios by an SDN network.

The SDN network is made up of different devices, including an SDN controller and several layer 3 switches (model HP ProCurve 3500yl-24G-PWR Intelligent Edge). These switches support the OpenFlow protocol and allow us to work with SDN.

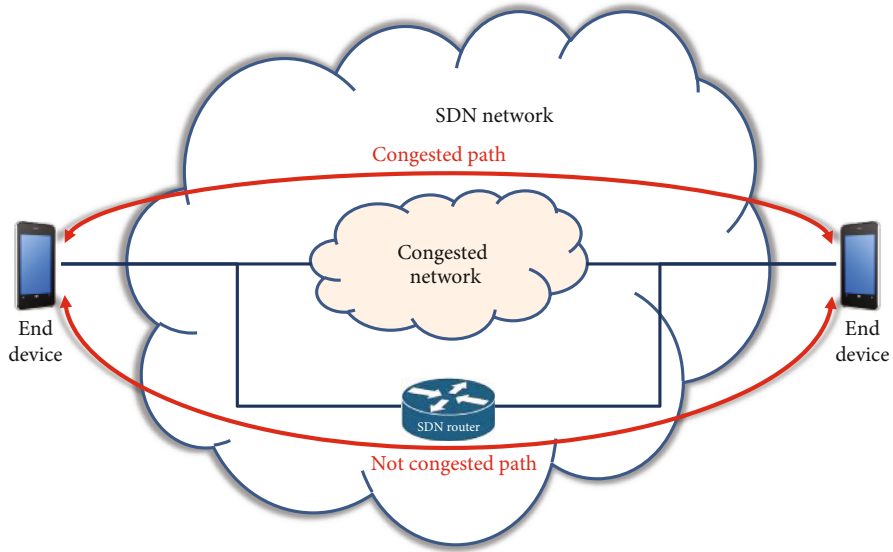


FIGURE 29: SDN network.

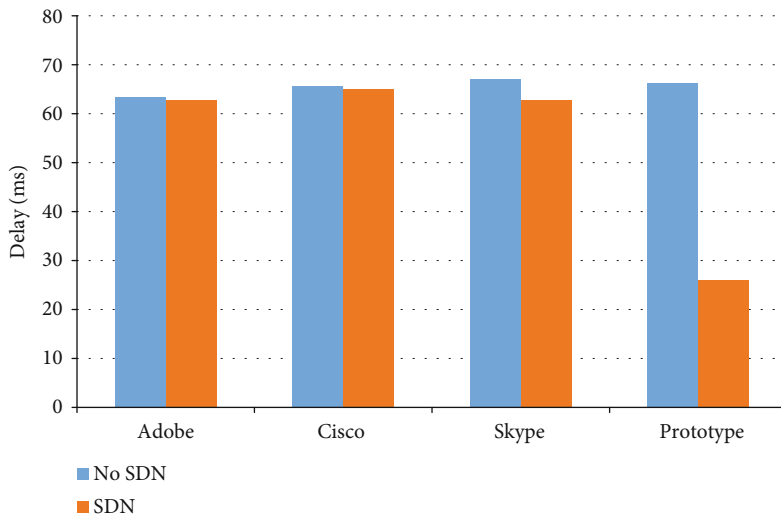


FIGURE 30: Results of scenario 3.

Our target in this scenario is to observe the correct functioning of our proposal when there is congestion in the transport network. As can be seen in Figure 29, we have created an SDN network using two basic routes. One of the routes uses a path that crosses a congested network, and the path of the other route avoids the congestion (Congested path and Not congested path).

The SDN controller has been programmed to communicate to mobile devices with the SDN network. For this purpose, an extension of the OpenFlow protocol has been developed. From our prototype, which we have installed on mobile devices, we launched an SDN activation request to the controller. From that moment, the SDN controller manages the traffic by transmitting the packets through the noncongested links.

As can be seen in Figure 30, commercial solutions, since they do not support SDN technology, do not change their behavior in an SDN network.

However, when using our prototype together with SDN, it can be clearly seen how the latency decreases in a very significant way. The SDN controller sends the traffic through an alternative path, completely free of congestion.

All the tests that are presented in our work have been carried out on a network that meets special requirements. Only the videoconference traffic stream was being sent. By using SDN, we added a new stream, which was sent at the same time as the videoconference stream. This new stream was always controlled for us. The newly added stream was sent to saturate the available bandwidth in the network and to automatically readjust the transmission parameters of the videoconference to the optimal ones to achieve the highest QoE under those conditions. If instead of controlling the traffic sent, the network is transmitting multiple streams, you can use FluidRAN [31] or LayBack [32] architectures, which have been shown to present substantial gains in handling streams by statistical multiplexing.

7. Conclusion

In this paper, we have presented a new architecture and a new protocol to optimize videoconferencing. First, we have defined an E2E QoE Management Scheme. This scheme utilizes correlation of both subjective and objective E2E QoE with received real-time video data (stream header and/or video signal), application-level QoS measurements, and network-level QoS measurements. We define real-time device-based and network-based feedback control mechanisms that can be used to adjust E2E QoE, and we present our proposal of architecture for videoconference. We propose three basic processes, which correspond to the basic actions to establish a videoconference (register, connection, and transmission). Later, we propose a Finite-State Machine, and we present and define the different states. After defining the system, we present our new protocol for videoconferencing.

Various videoconferencing applications, such as Adobe Connect, Cisco Webex, and Skype, have been tested. Data about bandwidth, packets/s, and delay have been collected and compared with the results of our prototype. Results show that when the resources of the device to be used for the application decrease, the algorithm used for the prototype is able to adapt in order to reduce the bandwidth consumption, while the commercial solutions are not able to do this. Regarding delay, commercial applications have worse latency when congestion appears in the network, while our prototype adapts and maintains low levels of latency.

Finally, commercial solutions do not change their behavior regardless of whether or not they use SDN technology. However, our prototype with SDN shows that latency decreases in a very significant way.

This paper is part of the dissertation of Jose M. Jimenez [33]. In future work, we will add more functionality in terms of codec selection, video conversion formats, and the selection of type of device among others.

Data Availability

There is no database of measurements in this research work.

Conflicts of Interest

The authors declare that they have no conflict of interest.

Acknowledgments

This work has been supported by the “Ministerio de Economía y Competitividad” in the “Programa Estatal de Fomento de la Investigación Científica y Técnica de Excelencia, Subprograma Estatal de Generación de Conocimiento” within the project under Grant TIN2017-84802-C2-1-P.


References

- [1] J. Lloret, M. García, and F. Boronat, *IPTV: la televisión por Internet*, vol. 230, Editorial Vértice, Málaga, España, 2008.
- [2] J. Frnda, J. Nedoma, J. Vanus, and R. Martinek, “A hybrid QoS-QoE estimation system for IPTV service,” *Electronics*, vol. 8, no. 5, p. 585, 2019.
- [3] R. Huang, X. Wei, Y. Gao, C. Lv, J. Mao, and Q. Bao, “Data-driven QoE prediction for IPTV service,” *Computer Communications*, vol. 118, pp. 195–204, 2018.
- [4] A. D. Tesfamicael, V. Liu, E. Foo, and B. Caelli, “Modeling for a QoS-efficient real-time video conferencing system in the cloud,” in *2018 26th International Conference on Software, Telecommunications and Computer Networks (SoftCOM)*, pp. 1–6, Split, Croatia, 2018.
- [5] N. Rao, A. Maleki, F. Chen et al., “Analysis of the effect of QoS on video conferencing QoE,” in *2019 15th International Wireless Communications & Mobile Computing Conference (IWCMC)*, pp. 1267–1272, Tangier, Morocco, 2019.
- [6] J. Mao, R. Huang, X. Wei, Q. Bao, Z. Dong, and Y. Qian, “IPTV user QoE prediction based on the LSTM network,” in *2017 9th International Conference on Wireless Communications and Signal Processing (WCSP)*, pp. 1–6, Nanjing, China, 2017.
- [7] J. M. Jiménez, A. Canovas, A. López, and J. Lloret, “A new algorithm to improve the QoE of IPTV service customers,” in *2015 IEEE International Conference on Communications (ICC)*, pp. 6990–6995, London, UK, 2015.
- [8] G. M. Su, X. Su, Y. Bai, M. Wang, A. V. Vasilakos, and H. Wang, “QoE in video streaming over wireless networks: perspectives and research challenges,” *Wireless Networks*, vol. 22, no. 5, pp. 1571–1593, 2016.
- [9] M. Garcia, A. Canovas, M. Edo, and J. Lloret, “A QoE management system for ubiquitous IPTV devices,” in *2009 Third International Conference on Mobile Ubiquitous Computing, Systems, Services and Technologies*, pp. 147–152, Sliema, Malta, 2009.
- [10] S. Shen, “Efficient SVC multicast streaming for video conferencing with SDN control,” *IEEE Transactions on Network and Service Management*, vol. 16, no. 2, pp. 403–416, 2019.
- [11] J. M. Jimenez, O. Romero, A. Rego, A. Dilendra, and J. Lloret, “Study of multimedia delivery over software defined networks,” *Network Protocols and Algorithms*, vol. 7, no. 4, 2016.
- [12] A. Chakraborti, S. O. Amin, B. Zhao, A. Azgin, R. Ravindran, and G. Wang, “ICN based scalable audio-video conferencing on virtualized service edge router (VSER) platform,” *Proceedings of the 2nd International Conference on Information-Centric Networking - ICN '15*, 2015, pp. 217–218, New York, NY, USA, 2015.
- [13] M. H. Hajiesmaili, L. T. Mak, Z. Wang, C. Wu, M. Chen, and A. Khonsari, “Cost-effective low-delay design for multiparty cloud video conferencing,” *IEEE Transactions on Multimedia*, vol. 19, no. 12, pp. 2760–2774, 2017.
- [14] J. Jang-Jaccard, S. Nepal, B. Celler, and B. Yan, “WebRTC-based video conferencing service for telehealth,” *Computing*, vol. 98, no. 1-2, pp. 169–193, 2016.
- [15] R. Bestak and J. Hlavacek, “A Videoconferencing System Based on WebRTC Technology,” in *Computer Networks*, P. Gaj, A. Kwiecień, and M. Sawicki, Eds., vol. 718 of CN 2017. Communications in Computer and Information Science, Springer, 2017.
- [16] M. Pasha, F. Shahzad, and A. Ahmad, “Analysis of challenges faced by WebRTC videoconferencing and a remedial architecture,” in *2016 International Journal of Computer Science and Information Security*, vol. 14, 2016no. 10.

- [17] P. Gusev and J. Burke, "NDN-RTC: real-time videoconferencing over named data networking," in *Proceedings of the 2nd International Conference on Information-Centric Networking - ICN '15*, pp. 117–126, New York, NY, USA, 2015.
- [18] School of Computing, Telkom University, Bandung, Indonesia, K. Sambath, M. Abdurahman, and V. Suryani, "High quality of service video conferencing over IMS," *International Journal of Information and Education Technology*, vol. 6, no. 6, pp. 470–476, 2016.
- [19] M. A. Hossain and J. I. Khan, "Dynamic MCU placement for video conferencing on peer-to-peer network," in *2015 IEEE International Symposium on Multimedia (ISM)*, pp. 144–147, Miami, FL, USA, 2015.
- [20] A. Khalifeh, M. A. Al-Tae, F. AlAbsi, S. Alrawi, and A. Murshed, "A videoconferencing platform for eHealth services in Jordan," in *2016 3rd Middle East Conference on Biomedical Engineering (MECBME)*, pp. 98–101, Beirut, Lebanon, 2016.
- [21] A. Taylor, G. Morris, J. Pech, S. Rechter, C. Carati, and M. R. Kidd, "Home telehealth video conferencing: perceptions and performance," *JMIR mHealth uHealth*, vol. 3, no. 3, article e90, 2015.
- [22] M. L. Mat Kiah, S. H. al-Bakri, A. A. Zaidan, B. B. Zaidan, and M. Hussain, "Design and develop a video conferencing framework for real-time telemedicine applications using secure group-based communication architecture," *Journal of Medical Systems*, vol. 38, no. 10, p. 133, 2014.
- [23] M. K. Mishra, S. Mukhopadhyay, and G. P. Biswas, "Architecture and secure implementation for video conferencing technique," in *Proceedings of the 2015 Third International Conference on Computer, Communication, Control and Information Technology (C3IT)*, pp. 1–6, Hooghly, 2015.
- [24] M. Pattaranantakul, K. Sanguannam, P. Sangwongngam, and C. Vorakulpipat, "Efficient key management protocol for secure RTMP video streaming toward trusted quantum network," *ETRI Journal*, vol. 37, no. 4, pp. 696–706, 2015.
- [25] T. Zhao, Q. Liu, and C. W. Chen, "QoE in video transmission: a user experience-driven strategy," *IEEE Communications Surveys & Tutorials*, vol. 19, no. 1, pp. 285–302, 2017.
- [26] S. N. B. Gunkel, M. Schmitt, and P. Cesar, "A QoE study of different stream and layout configurations in video conferencing under limited network conditions," in *2015 Seventh International Workshop on Quality of Multimedia Experience (QoMEX)*, pp. 1–6, Pylos-Nestoras, Greece, 2015.
- [27] L. García, J. Lloret, C. Turro, and M. Taha, "QoE assesment of MPEG-DASH in polimedia e-learning system," in *2016 International Conference on Advances in Computing, Communications and Informatics (ICACCI)*, pp. 1117–1123, Jaipur, India, 2016.
- [28] D. Henni, A. Ghomari, and Y. Hadjadj-Aoul, "Videoconferencing over OpenFlow Networks: an optimization framework for QoS routing," in *2015 IEEE International Conference on Computer and Information Technology; Ubiquitous Computing and Communications; Dependable, Autonomous and Secure Computing; Pervasive Intelligence and Computing*, pp. 491–496, Liverpool, UK, 2015.
- [29] E. Yang, L. Zhang, Z. Yao, and J. Yang, "A video conferencing system based on SDN-enabled SVC multicast," *Frontiers of Information Technology & Electronic Engineering*, vol. 17, no. 7, pp. 672–681, 2016.
- [30] C. Al Hasrouty, C. Olariu, V. Autefage, D. Magoni, and J. Murphy, "SVC videoconferencing call adaptation and bandwidth usage in SDN networks," in *GLOBECOM 2017-2017 IEEE Global Communications Conference*, pp. 1–7, Singapore, Singapore, 2017.
- [31] A. Garcia-Saavedra, X. Costa-Perez, D. J. Leith, and G. Iosifidis, "Fluid RAN: optimized vRAN/MEC orchestration," in *IEEE INFOCOM 2018—IEEE Conference on Computer Communications*, pp. 2366–2374, Honolulu, HI, USA, 2018.
- [32] P. Shantharama, A. Thyagaturu, N. Karakoc, L. Ferrari, M. Reisslein, and A. Scaglione, "LayBack: SDN management of multi-access edge computing (MEC) for network access services and radio resource sharing," *IEEE Access*, vol. 6, pp. 57545–57561, 2018.
- [33] J. Herranz, "Design of an architecture and communication protocol for video transmission and videoconference, [Ph.D Thesis]," Universitat Politècnica de València, 2018.

Research Article

Energy-Efficient Asynchronous QoS MAC Protocol for Wireless Sensor Networks

Sohail Sarang ¹, Goran M. Stojanović,¹ Stevan Stankovski,¹ Željko Trpovski,¹
and Micheal Drieberg²

¹Faculty of Technical Sciences, University of Novi Sad, Trg Dositeja Obradovića 6, 21000 Novi Sad 21000, Serbia

²Department of Electrical and Electronic Engineering, Universiti Teknologi PETRONAS, 32610 Seri Iskandar, Perak, Malaysia

Correspondence should be addressed to Sohail Sarang; sohailsarang109@gmail.com

Received 23 May 2020; Revised 1 September 2020; Accepted 4 September 2020; Published 24 September 2020

Academic Editor: Jaime Lloret

Copyright © 2020 Sohail Sarang et al. This is an open access article distributed under the Creative Commons Attribution License, which permits unrestricted use, distribution, and reproduction in any medium, provided the original work is properly cited.

In recent years, wireless sensor networks (WSNs) have gained significant attention in both industry and academia. In WSNs, each sensor node is normally equipped with a small-size battery with finite capacity. Hence, energy-efficient communication is considered a key factor for the extension of network lifetime. Formerly, a large number of medium access control (MAC) protocols have been proposed to improve energy efficiency to prolong the network lifetime. There are applications that generate different types of data packets and require quality of service (QoS) without any disruption in network operation. Therefore, these applications need an energy-efficient QoS MAC protocol that can support QoS by considering energy efficiency as the primary goal to avoid any failure in the network. This article proposes an energy-efficient asynchronous QoS (AQSen) MAC protocol, called AQSen-MAC. The AQSen-MAC considers different types of data packets and uses two novel techniques: self-adaptation and scheduling to enhance energy efficiency, packet delivery ratio, and network throughput. Furthermore, in the protocol, the receiver adjusts its duty cycle according to the remaining energy to prolong the network operation. Finally, the performance of the AQSen-MAC protocol has been evaluated through detailed simulation using Castalia and compared with MPQ-MAC, PMME-MAC, and QAEE-MAC protocols. The simulation results indicate that the AQSen-MAC protocol significantly reduces the energy consumption at the receiver of up to 13.4%, consumption per bit of up to 3% and improves the packet delivery ratio and network throughput of up to 12% in the network.

1. Introduction

Internet of things (IoT) is a fast-growing technology and is playing a vital role in many applications such as smart home infrastructure [1], wearable devices [2], and building automation [3]. The wireless sensor network (WSN) is a key component for the IoT [4–7]. A WSN consists of low-power, low-cost, and small-in-size sensor nodes, which have the ability to sense, measure, gather, and process information (i.e., conductivity, temperature, and pressure) gathered from the sensor coverage area [8, 9]. The sensor nodes can communicate wirelessly with each other. WSNs have a wide range of advantages in terms of scalability, deployment, simplicity, self-organizing capabilities, and others [10] and have many applications including smart cities, food quality, and environment monitoring, industrial process monitoring, and health-care [11–13].

In WSNs, sensor nodes are traditionally powered by small batteries with limited capacity [14–17]. Hence, energy efficiency plays an essential role in the lifetime extension [18–20]. This is due to some scenarios, for instance, volcano monitoring [21], where it is difficult to replace the battery; hence, it requires a longer operational time [22]. This has motivated the researchers to introduce energy-efficient schemes to prolong the network lifetime [7, 17]. The network lifetime is defined as the time elapsed until the failure of the first node due to energy depletion in the network [23]. For example, the wake-up radio approach helps the node to save energy by putting its main radio in the deep sleep mode [7, 24, 25]. The packet aggregation routing scheme proposed that reduces the transmission delay, amount of redundant data, and energy consumption by adjusting the forwarder nodes and duty cycle in body sensor networks [22]. Recently,

energy harvesting technology allows nodes to harvest energy from the surrounding environment and use the harvested energy to improve network performance [26–29]. For instance, QPPD-MAC [28], CEH-MAC [30], and PEH-QoS [31] schemes optimize the use of available energy to achieve better QoS in the network. Furthermore, QPPD-MAC [28] is developed for solar-based EH-WSNs, where each node harvests energy from the surrounding using a solar cell. The duty cycle management mechanism proposed in QPPD-MAC uses the harvest-store-consume design alternative and adjusts the receiver duty cycle based on three different ranges of the available energy. For example, if the node's energy is above 85%, the highest duty cycle of 1 is assigned to the node to improve the performance. However, when employed in battery-powered WSNs, it can lead to power outage rapidly due to the limited capacity, resulting in overall degradation in the network performance. In some applications such as battlefield [7] and mine monitoring [32], it is difficult to replace the battery; hence, energy efficiency is still the prime consideration. In the past, considerable research work has been conducted to conserve energy, which mainly focused on medium control access (MAC) optimization [33], routing algorithms [7, 20, 34], cross-layer optimization methods [35], and data fusion [36]. However, the major sources of energy consumption occur at the MAC layer in channel sensing, packet reception, and transmission, packet overhearing, idle listening, and collision [37].

The MAC protocol regulates the access of a common medium between sensor nodes [38]. In the literature, a large number of MAC protocols have been developed that focus on different applications and scenarios. TCH-MAC [39] and CTh-MAC [40] achieve better energy efficiency and throughput in the network. The protocol in [41] uses intracluster communication to save energy; RI-MAC [42] maintains energy efficiency while achieving good packet delivery ratio and packet delay. In [43], QTSAC is proposed to achieve better energy efficiency. However, many existing MAC protocols for battery-powered WSNs have limited support for QoS while considering energy efficiency and network lifetime as primary goals. The QoS is a set of services required by the application [28, 44]. For example, forest surveillance application generates different types of packets such as fire detection (high priority) vs wildlife monitoring (low priority). Thus, a fire detection data packet cannot tolerate a higher delay and needs to be delivered with 1 second [45, 46]. Moreover, the application also requires a longer network lifetime. Hence, such applications need QoS MAC protocol with the prime requirement of energy efficiency to avoid any disruption in the network. Furthermore, the protocol performance evaluation should also consider other QoS parameters such as the packet delivery ratio, network throughput, and delay in the network [47].

Hence, significant improvements were made to the MPQ-MAC protocol [48] to improve energy efficiency while supporting the priority of packets in the network. Therefore, this paper proposes an energy-efficient QoS MAC protocol for WSNs (AQSen-MAC), where the receiver node shares its wake-up time information with senders that helps in finding a rendezvous point for data transmission. The protocol

uses the self-adaptation technique and considers the remaining energy of the receiver node to improve performance and avoid any network failure due to energy depletion, respectively. The results show that the AQSen-MAC protocol achieves better performance than other protocols.

The contributions of this work are as follows:

- (i) An energy-efficient QoS MAC protocol is proposed to support the priority of packets in the network
- (ii) The protocol uses the self-adaptation technique by which the sender node holding a data packet avoids transmitting the packet when its remaining listening time is less than the minimum listening time required for successful packet transmission. It reduces packet loss and energy consumption of both the sender and receiver nodes
- (iii) The receiver in the AQSen-MAC protocol shares its next wake-up time with sender nodes to improve coordination between nodes for priority data transmission
- (iv) The mechanism by which the receiver node adjusts its duty cycle according to the remaining energy helps to extend the network operation
- (v) The performance of the protocol is evaluated in the Castalia simulator for 10 hours of simulation time using the CC2420 radio module and TelosB sensor node. A comprehensive performance evaluation is conducted by considering all QoS parameters in terms of the average energy consumption at the receiver, energy consumption per bit, energy consumption per sender node, packet delivery ratio, network throughput, and the average delay for a priority data packet and all packets
- (vi) Performance comparison is conducted with MPQ-MAC, PMME-MAC, and QAEE-MAC, which are well-known receiver-initiated QoS protocols for WSNs. The simulation results show that the proposed AQSen-MAC achieves better performance in terms of energy consumption at the receiver, energy consumption per bit, packet delivery ratio, and network throughput

The remainder of the paper is organized as follows: in Section 2, the related works are reviewed. The development of the AQSen-MAC protocol is discussed in Section 3. In Section 4, the performance evaluation of AQSen-MAC protocol is described, and the results are presented and explained in detail. Finally, the conclusion and future work are discussed in Section 5.

2. Related Work

In WSNs, MAC protocols can be categorized into three classes, namely, contention-free, contention-based, and hybrid protocols as in Figure 1 [49–51]. The contention-free protocols assign variable or fixed time slots to each sensor node for

data transmission [52]. This allows nodes to access the channel in the allocated time slots, and as a result, collisions in the network are reduced. ETPS-MAC [53] uses a scheduling algorithm that considers energy and traffic load factors while assigning priority to the node. However, nodes are required to exchange their time slots information frequently with each other which incurs additional packet overhead. Furthermore, nodes waste the channel bandwidth when they do not have any packet to transmit in their time slots.

The contention-based protocols avoid time slot overhead for packet transmission among nodes and allow them to access the medium randomly. Thus, the risk of collision may increase, which can be avoided by employing different mechanisms, i.e., carrier sense multiple access (CSMA). The contention-based protocols can be further classified into synchronous and asynchronous [54]. In synchronous such as S-MAC [55], T-MAC [56], DW-MAC [57], DSMAC [58], SMACS [59], and PQMAC [60], nodes are required to follow a common listening time in a virtual cluster, where nodes can exchange the data packets. EEQ-MAC [61] and DQTSM [62] support QoS and also achieve better energy efficiency in the network. However, the tight synchronization requires additional overhead that leads to limitations in terms of adaptability, scalability, robustness, and others.

In the asynchronous approach, nodes do not require synchronization and consequently, each node can wake up and sleep independently [42]. Thus, nodes require a rendezvous point for data communication. Comparisons suggest that asynchronous schemes are more energy-efficient than synchronous [63, 64]. The asynchronous protocols are further divided as either sender-initiated or receiver-initiated protocols [65]. In the sender-initiated protocols such as B-MAC [63], X-MAC [66] uses preamble sampling or low power listening (LPL) technique to establish a communication link between the receiver and sender nodes. These protocols shift the burden at the sender side to initiate the communication, where the node with a data packet transmits a preamble before sending its actual data packet.

The receiver upon waking up detects the preamble and waits for the data packet. In this scheme, the preamble transmission requires a longer time and thus, the sender node holding a data packet is required to wait until the channel becomes free which causes an increase in packet delay and a decrease in network throughput [42]. On the other hand, in receiver-initiated schemes such as RI-MAC [42], RICER [67] and AW-RB-PS-MAC [68], the receiver starts communication by broadcasting a wake-up beacon to inform all senders that it is available to receive the data packets. The sender node with a data packet turns on its radio and listens for the wake-up beacon. Upon receiving the beacon, the sender sends the packet and then, it waits for the acknowledgment packet. The receiver-initiated protocols perform better in terms of energy efficiency than sender-initiated protocols [42, 69].

Formerly, several receiver-initiated QoS MAC protocols have been proposed that consider the priority of data packets such as QAEE-MAC [70], MPQ-MAC, [48] and PMME-MAC [71]. QAEE-MAC proposed to support the priority of packets by reducing the delay for the higher priority packets.

The receiver initiates communication by broadcasting a wake beacon that is defined by its duty cycle and then initiates a waiting timer T_w , to receive Tx beacons from senders. On the other side, the sender node with a data packet waits for the receiver wake-up beacon. After receiving the beacon, it transmits the Tx beacon that contains the packet priority and source address. The receiver collects Tx beacons from sender nodes and waits for the completion of the waiting timer. Then, it selects the highest packet priority node and sends the Rx beacon to all senders that include the address of the selected node. After receiving the Rx beacon, the selected node sends the packet to the receiver and waits for the acknowledgment packet while other nodes go to sleep. However, it supports only two priority levels and the receiver needs to wait until the waiting timer expires. As a result, the node with the highest priority packet experiences a higher delay and it also consumes extra energy in idle listening.

Hence, MPQ-MAC [48] and PMME-MAC [71] have been developed to support the multipriority of packets. MPQ-MAC is aimed at reducing the delay for the highest priority packet and improving energy efficiency in the network. The protocol follows the receiver-initiated approach and assigns four types of priority levels based on a number (R) generated between 0 and 1. It uses a novel technique by which the receiver controls the waiting timer T_w , according to the packet priority. Hence, the receiver after receiving the highest priority Tx beacon cancels the waiting timer to reduce the delay for the highest priority packet. Similarly, PMME-MAC proposed to support the multipriority of the packets and assigns the channel access probability according to the packet priority level. It provides a higher value of access probability to the highest priority packet and vice versa. As a result, the sender node with the highest priority packet gets to access the medium earlier when compared to other priority packets. Moreover, it cancels the waiting time when it receives the first Tx beacon from the sender node to reduce the packet delay.

However, these QoS protocols have the following limitations. First, sender nodes holding data packets do not have any information related to the wake-up schedule of the receiver. Thus, nodes wait for a longer time for the wake-up beacon, which increases delay and energy consumption. Second, once wake-up beacon is received, the node with data packet goes directly for channel sensing without checking its remaining listening time, which can lead to packet loss and energy consumption at both receiver and sender sides. Third, the receiver operates on a fixed duty cycle that uses a significant amount of energy, so, this may cause a failure in the network operation. Finally, their performance evaluations have not included all QoS metrics such as energy efficiency, packet delivery ratio, network throughput, and packet delay. For instance, the performance of QAEE-MAC has not been evaluated in terms of the packet delivery ratio and network throughput and also has not been compared with any other protocol. Similarly, energy efficiency and network throughput parameters have not been included in the performance evaluation of PMME-MAC. Table 1 shows some prominent QoS MAC protocols for WSNs.

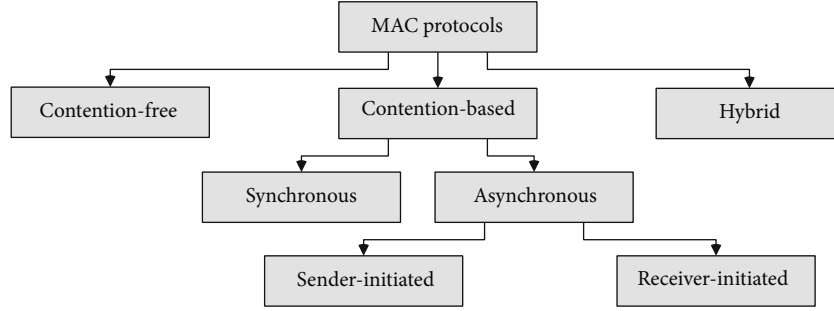


FIGURE 1: Categorization of MAC protocols [49–51].

The hybrid protocols [39, 40, 72] use the features of both contention-free and contention-based protocols for better network performance. For example, TCH-MAC [39] combines TDMA and CSMA schemes to provide better energy efficiency in a network. However, the use of TDMA structure increases protocol overhead and complexity, which limits the scalability of the protocol [73].

Thus, there is a requirement to propose an energy-efficient MAC protocol for WSNs that can use techniques to find a rendezvous point for priority data transmission between nodes and improve energy efficiency to prolong the network lifetime.

3. Development of AQSen-MAC Protocol

This section focuses on the design of the AQSen-MAC protocol. The main goal is to improve energy efficiency while considering the priority of data packets. To achieve the goal, the protocol design consists of three major components; basic communication overview, data transmission, and energy-aware duty cycle management.

3.1. Basic Communication Overview. The AQSen-MAC protocol follows the receiver-initiated approach as given in Figure 2. The receiver node wakes up and broadcasts a beacon, named wake-up beacon (WB). Then, it starts the waiting timer (T_w) to collect the incoming Tx beacon (TxB) from senders. The receiver node includes the source address (SA) and its next duty cycle (d_c) in the wake-up beacon, as shown in Figure 3(a). The sender nodes holding different types of data packets, urgent (emergency alarm), most important (real time), on-demand (important), and periodic (normal), wait for the receiver beacon to start the communication. The highest P_4 priority is assigned to the urgent data as it cannot tolerate much delay as shown in Table 2.

After receiving the wake-up beacon, the sender checks if the remaining listening time (T_{RL}) is greater than the minimum listening time required for successful packet transmission (T_{Tx}). Then, it performs a clear channel assessment (CCA) to check the channel. If the channel is free, it transmits the Tx beacon using the p -persistent CSMA scheme. The Tx beacon has four fields: priority (P), SA, destination address (DA), and NAV (network allocation), as shown in Figure 3(b). Otherwise, it goes to sleep and saves energy. The time required to switch the radio state and process a data packet is called short interframe space (SIFS).

On the other side, the receiver node collects Tx beacon from the sender and checks its priority field. If P_4 priority appears, then it cancels the T_w timer to reduce the delay for the highest priority packet and it transmits the Rx beacon to all senders which contains the address of the selected sender (SS), as given in Figure 3(c). Once Rx beacon is received, the selected sender transmits the packet and waits for the acknowledgment (ACK packet), which indicates successful packet transmission. Meanwhile, the nonselected senders go to sleep and will wait for the next cycle.

3.2. Data Transmission. The receiver and sender nodes wake up and sleep independently. Therefore, the node holding a data packet spends a significant amount of energy in the idle listening for the wake-up beacon. To address the challenge, the protocol uses self-adaptation and scheduling techniques.

In the former, after receiving the wake-up beacon, sender nodes check their remaining listening time, T_{RL} . If $T_{RL} > T_{Tx}$, they sense the medium for Tx beacon transmission using the p -persistent CSMA mechanism. Else, the sender node avoids channel sensing and goes to sleep to minimize energy consumption and packet retransmission. Consider a scenario for data transmission as shown in Figure 2, where Sender 1 (S_1) and Sender 2 (S_2) transmit Tx beacons with P_1 and P_4 , respectively. However, Sender 3 goes to sleep and waits for the next cycle. The receiver after receiving both Tx beacons from S_1 and S_2 checks the priority. It selects the sender node that has P_4 priority and cancels the T_w timer to reduce the delay. Then, it broadcasts Rx beacon which includes the address of S_2 . After receiving the Rx beacon, S_2 sends the actual data packet while other nonselected nodes go to sleep and wait for wake-up beacon in the next cycle. In case when more than one Tx beacons are received with the same priority, then the receiver selects the node based on the first received Tx beacon. In case when P_4 does not appear, then the receiver waits until T_w timer expires. Once T_w expires, it selects the sender node that has the highest priority among all received Tx beacons. In the worst scenario, a sender node with P_1 priority may contend with several new nodes that have P_4 priority. In this case, unfortunately, it will only get the opportunity to send its data packet after all the nodes with P_4 priority. However, this occurs rarely and its occurrence probability decreases with the number of nodes with P_4 priority. This is a tradeoff in the AQSen-MAC protocol as it ensures that the P_4 priority node is able to send its packet faster than normal packets.

TABLE 1: Comparative analysis of different priority MAC protocols.

Protocol	Clock synchronization	Packet priority	Adaptive duty cycle	Idle listening
MPQ-MAC [48]	No	Yes	No	High
PQMAC [61]	Yes	Yes	No	Low
EEQ-MAC [62]	Yes	Yes	Yes	Low
QAEE-MAC [70]	No	Yes	No	High
PMME-MAC [71]	No	Yes	No	High

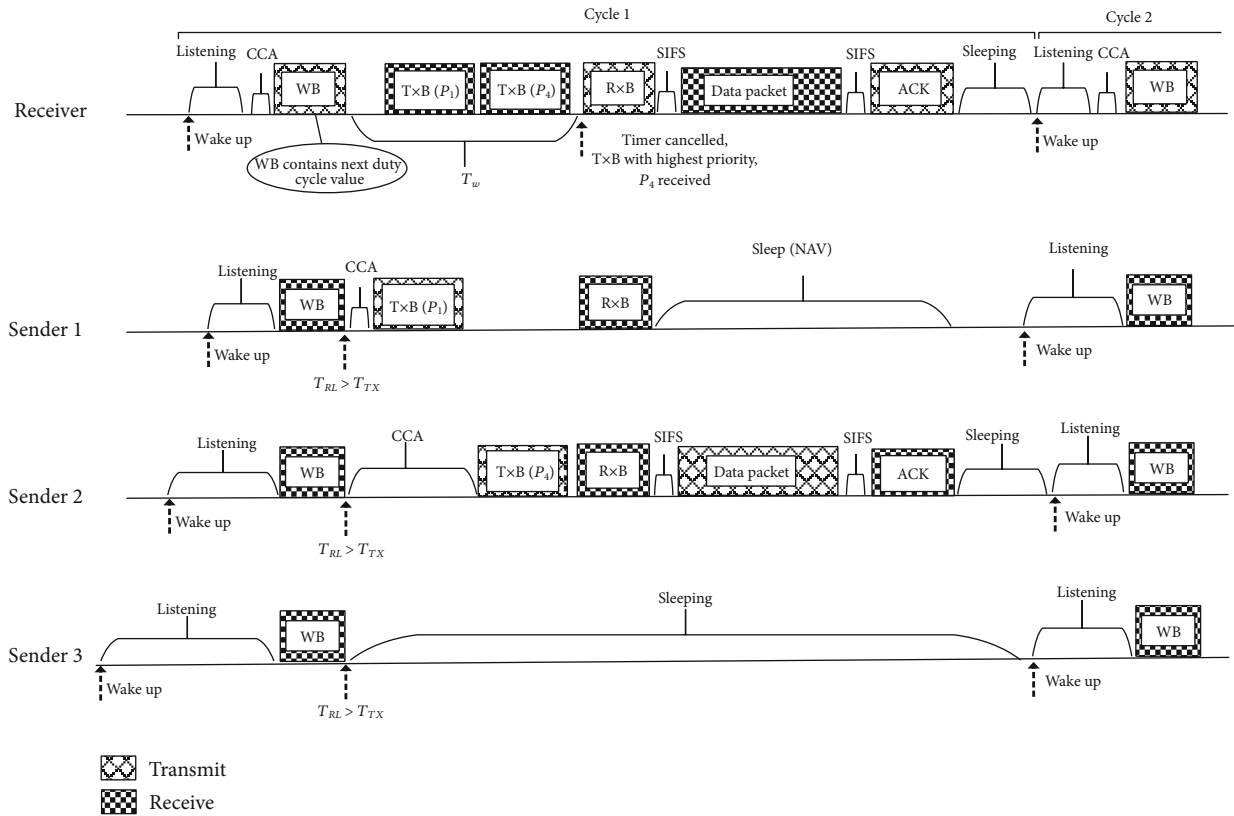


FIGURE 2: Communication overview of AQSen-MAC protocol.

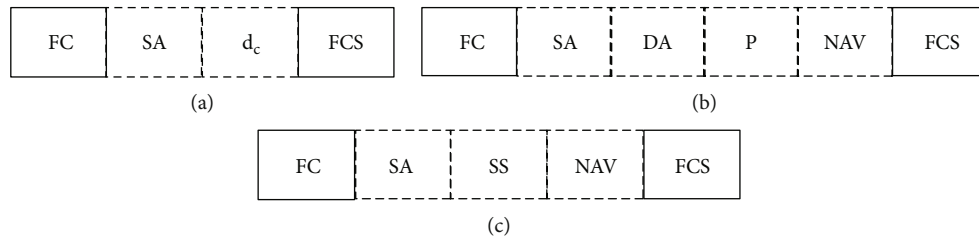


FIGURE 3: (a) Wake-up beacon (WB). FC and FCS represent frame control and frame check sequence fields, respectively. (b) Tx beacon (TxB). (c) Rx beacon (RxB).

In the latter, the receiver node includes its next duty cycle in the wake-up beacon which allows the sender nodes to adjust their sleeping time accordingly and wake up slightly before the receiver for data transmission. This technique helps in coordination between the receiver and sender nodes for successful data transmission and also reduces energy consumption in idle listening.

3.3. *Energy-Aware Duty Cycle Management.* The receiver node is equipped with a small-size battery with limited capacity, and its energy level decreases with time. Thus, the node can only operate for a longer period of time if it uses its energy more effectively. Therefore, the receiver in the AQSen-MAC protocol wakes up periodically to receive data packets and adjusts its duty cycle, d_c , according to the

TABLE 2: Priority levels.

Data type	Priority	Max. Delay limit	Example
Urgent	P_4	1	Emergency alarm
Most important	P_3	2	Real time
Important	P_2	3	On-demand
Normal	P_1	4	Periodic

remaining energy in order to extend the network lifetime. The sleep duration is related to d_c ; thus, the receiver node in AQSen-MAC decreases the duty cycle by increasing its sleep duration (T_{sleep}) in order to conserve energy. As a result, it sustains its operation for a longer period of time. d_c can be calculated using the following formula:

$$d_c = \frac{(E_L - E_{th})}{100\% - E_{th}} \quad (1)$$

where E_L represents the remaining energy in percentage (%) and E_{th} (10%) is the threshold energy level, which is used to ensure that the node does not exhaust completely. When the receiver has a lower remaining energy level, it reduces its d_c to save energy. The remaining energy E_L is shown as follows:

$$E_L = \frac{E_r}{E_{\max}} \times 100\%, \quad (2)$$

where E_r and E_{\max} denote the remaining energy and maximum battery capacity in joules, respectively. The calculated d_c value can be used to determine the sleep duration (T_{sleep}) as shown in the following equation:

$$T_{\text{sleep}} = \frac{T_{\text{listen}} \times (1 - d_c)}{d_c}, \quad (3)$$

where T_{listen} denotes the listening time when the radio is turned On. Both T_{sleep} and T_{listen} parameters, and their relationship through d_c represents radio deactivation (OFF) and activation (ON), respectively. When the d_c is low, Equation (3) ensures that the T_{sleep} will be high in order to save energy.

4. Performance Evaluation of AQSen-MAC

4.1. Simulation Setup. The performance of the AQSen-MAC protocol is evaluated through Castalia 3.3 [74] simulator. Castalia simulates sensor applications using CC2420 radio module parameters [23], including sensor node TelosB [75]. The CC2420 radio is extensively used in sensor applications and has four operational states: sleep, reception, transmission, and idle listening. Table 3 shows the power consumption of CC2420 in each state. It can be noticed that both receive and idle states consume the same power [49]. In the AQSen-MAC protocol, when the number of sending nodes is higher per receiver, then the waiting time T_w will also increase, resulting in higher energy consumption.

TABLE 3: Power consumption in CC2420 [23].

Radio state	Power consumption (mW)
Transmission	57.42
Reception	62.04
Idle listening	62.04
Sleep	1.4

Hence, it is resolved by considering a network that consists of several smaller sized clusters where the number of sender nodes per receiver is small. Therefore, a star network is implemented to demonstrate the features of the AQSen-MAC protocols as shown in Figure 4. The clustering in a large network helps to improve energy efficiency and scalability [17, 76]. In addition, it is also widely used in modelling of effective solutions to minimize the suppression of malware actions in WSNs [77, 78]. In the network topology, the receiver node is located at the center while other nodes are randomly positioned in a square area of 30 m × 30 m. Each sender node generates a total of 36,000 packets with a rate of 1 packet per second, where the size of the data packet is 28 bytes. The performance of the AQSen-MAC is evaluated for all QoS parameters in terms of average energy consumption at receiver, energy consumption per bit, energy consumption per sender node, packet delivery ratio, average network throughput, and delay for priority and all data packets. Moreover, the protocol performance is also compared with MPQ-MAC, PMME-MAC, and QAEE-MAC, which are well-known receiver-initiated QoS protocols. The receiver's initial energy is set to a fixed value of 75% in all protocols and the receiver adjusts its duty cycle according to the remaining energy level. The receiver in MPQ-MAC, PMME-MAC, and QAEE-MAC operates on a fixed duty cycle of 0.72. All protocols use the p -persistent CSMA mechanism for the Tx beacon transmission, and the p value is set as $1/n_s$, where n_s represents the total number senders. In addition, they assign the packet priority randomly based on a number (R) generated between 0 and 1. In PMME-MAC, the p value is set according to the packet priority level, as given in Table 4. The simulation parameters are given in Table 5. For comparison, the linear priority assignment type of PMME-MAC is implemented.

4.2. Results and Discussion. The receiver energy consumption (E_T) in all protocols with the varying number of senders is shown in Figure 5. The formula to calculate the energy consumption of a node is as follows:

$$E_T = \sum_{i=0}^n P_i \times t_i, \quad (4)$$

where n , i , P , and t represent the number of states, radio state, power consumption rate, and the time spent in state i , respectively. The CC2420 radio is used which has four operational states: sleep, transmission, reception, and idle listening, consuming power of 1.4 mW, 57.42 mW, 62.04 mW, and 62.04 mW, respectively.

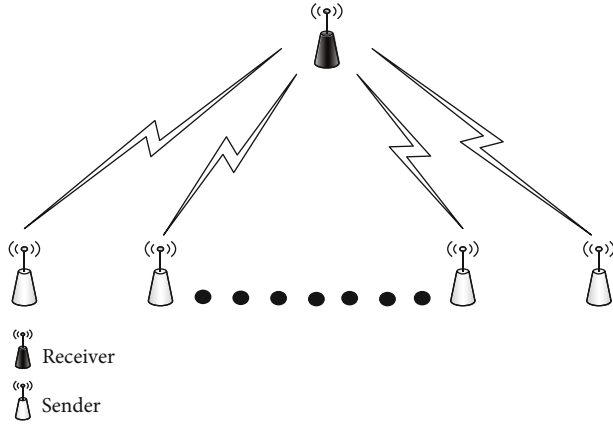


FIGURE 4: Studied network topology.

TABLE 4: Packet priority assignment.

Priority	R	P (linear type)
P_4	$0 < R \leq 0.25$	0.4
P_3	$0.25 < R \leq 0.5$	0.3
P_2	$0.5 < R \leq 0.75$	0.2
P_1	$0.75 < R \leq 1$	0.1

TABLE 5: Parameters used for the performance analysis of AQSen-MAC protocol.

Parameter	Value
Simulation time	10 h
Sender nodes	1 to 10
Area	$30 m \times 30 m$
Sensor node	Telos Rev B
Operating voltage	2.1 V
Size of data packet	28 bytes
Size of Tx beacon	14 bytes
Size of Rx beacon	13 bytes
ACK packet size	11 bytes
Wake-up beacon size	9 bytes
Data rate	250 kbps
Slot time	0.32 ms
CCA check delay	0.128 ms
SIFS	0.192 ms
T_w	5 ms
Packet rate	1 packet/s
Listen time	17 ms
Retransmission limit	10
Buffer size	32
Frequency	2.4 GHz
E_{\max}	810 Joules
E_{th}	10%

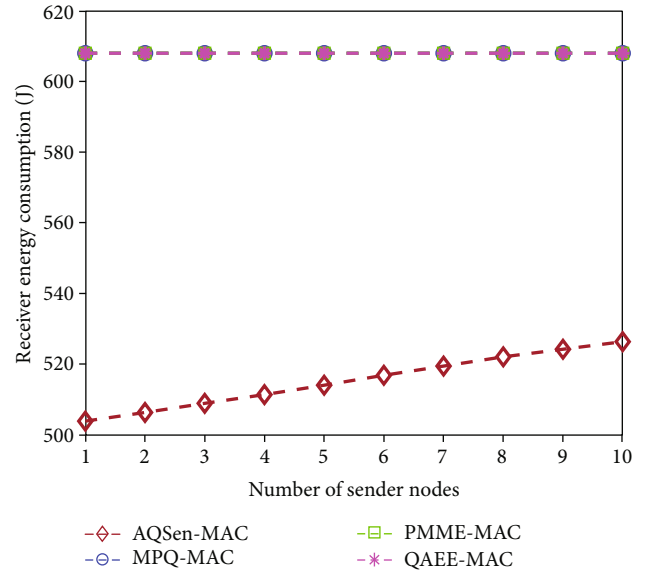


FIGURE 5: Average receiver energy as a function of the number of sender nodes (from 1 to 10).

It is observed that the AQSen-MAC provides a significant reduction in energy consumption of up to 13.4% than other protocols, which helps the receiver to operate for a longer period of time. This is due to the fact that the receiver node adjusts the duty cycle according to its remaining energy. The remaining energy decreases with time, and therefore, it also reduces the duty cycle by increasing the sleep duration to save energy. In MPQ-MAC, PMME-MAC, and QAEE-MAC, the receiver operates with a fixed duty cycle of 0.72 and therefore, its remaining energy declines rapidly. Hence, it becomes nonoperational after a few hours ($\approx 5h$), when its remaining energy goes below the threshold level E_{th} (10%), which caused an operational disruption in the network. It can also be seen that the receiver consumes more energy for the higher number of sender nodes. This is because the receiver receives more data packets when the number of sender nodes increases, which consumes more energy.

Figure 6 shows the remaining energy of the receiver when the number of sender nodes is 10. The receiver's initial energy is set to 75% of total capacity in all protocols. In AQSen-MAC, the remaining energy decreases to 10.09% after 10 h, while MPQ-MAC, PMME-MAC, and QAEE-MAC used all of their energy and became nonoperational after 5.5 h, 7 h, and 5.1 h, respectively. This is because the AQSen-MAC uses its remaining energy to adjust the duty cycle. Hence, it conserves energy by increasing its sleep time and as a result, its remaining energy does not drop below the E_{th} level. It can also be seen that the PMME-MAC operates for a longer period of time when compared to both MPQ-MAC and QAEE-MAC. The reason is that the receiver cancels the T_w timer when it received the first Tx beacon, which helps to conserve energy and increases its operation time.

The duty cycle of the receiver corresponding to the remaining energy is shown in Figure 7. It can be seen that the AQSen-MAC adjusts its duty cycle based on its

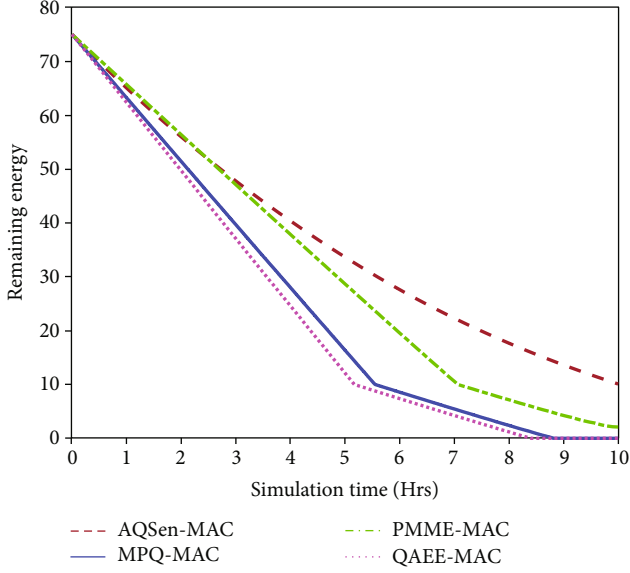


FIGURE 6: Receiver remaining energy when the number of sender nodes is 10.

remaining energy. It decreases its duty cycle when it has the lower remaining energy, and therefore, it does not suffer any disruption in the network. In MPQ-MAC, PMME-MAC, and QAEE-MAC, the receiver operates with a fixed duty cycle. When its remaining energy reaches the E_{th} level, it turns off the radio and goes to sleep, which causes a significant impact on network performance.

The packet delivery ratio (PDR) is defined as the total number of packets received by the receiver divided by the total number of packets transmitted by the sender nodes. The equation to calculate PDR is as follows:

$$PDR = \frac{NP_{pktR}}{NP_{pktT}} \times 100\%, \quad (5)$$

where NP_{pktR} and NP_{pktT} represent the total number of data packets received and transmitted, respectively.

Figure 8 presents the PDR of all protocols. It is seen that the AQSen-MAC outperforms other protocols by up to 12%. The first reason is that the AQSen-MAC does not face any disruption in the network and the receiver is available to receive the packets from senders. However, in other protocols, the receiver becomes nonoperational for more than 3 h and as a result, the sender nodes drop the incoming data packets when the buffer limit is exceeded. The second reason is that the receiver broadcasts its next duty cycle which helps the sender nodes with packets to synchronize with the receiver for packet transmission. The third reason is that the sender node, after receiving the wake-up beacon, checks its remaining listening time. If it has enough time for a successful packet transmission then transmits the Tx beacon else, it goes to sleep, which also avoids the packet loss. It can also be noticed that the PDR decreases marginally for the higher number of senders, which is due to the fact that the retransmission limit is exceeded.

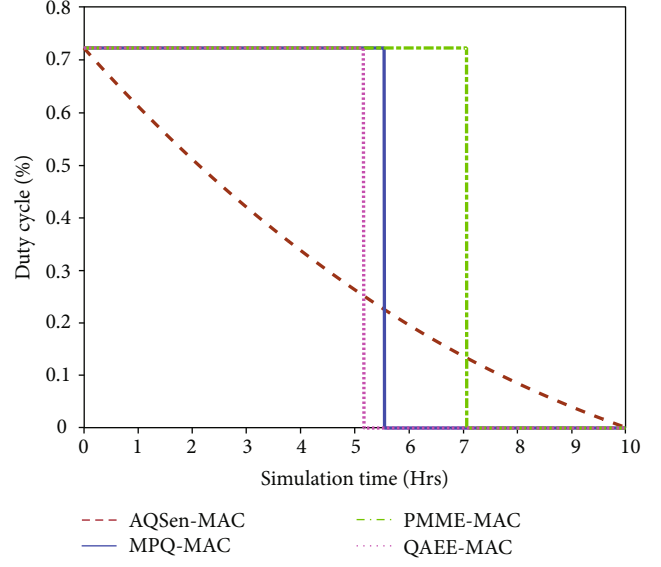


FIGURE 7: Receiver duty cycle when the number of sender nodes is 10.

The average network throughput (S) is defined as the number of data packets received at the receiver divided by the simulation time as shown below:

$$S = \frac{NP_{pktR} \times L_{pkt}}{T_s}, \quad (6)$$

where L_{pkt} and T_s denote the size of the packet in bits and simulation time in seconds, respectively.

Figure 9 shows the average network throughput performance comparison between the AQSen-MAC, MPQ-MAC, PMME-MAC, and QAEE-MAC. In all protocols, the network throughput increases linearly across the various number of sender nodes. It can be noticed that AQSen-MAC shows an improvement of up to 12% when compared to others. The reason is that the receiver in AQSen-MAC is able to maintain its operation whereas in other protocols, it became nonoperational for more than 3 h. As a result, the sender nodes are unable to transmit a large number of data packets to the receiver, which causes the lower network throughput.

The average energy consumption per bit (E) is shown in Figure 10, which is defined as the total energy consumed divided by the total number of data packets received, as shown below:

$$E = \frac{E_T}{NP_{pktR} \times L_{pkt}} \quad (7)$$

and for the calculation of E_T , (4) can be used.

The AQSen-MAC gives an improved performance of up to 30.29%, 3%, and 42%, when compared to MPQ-MAC, PMME-MAC, and QAEE-MAC, respectively. The first reason is that the AQSen-MAC receives more packets than other protocols as shown in Figure 8. The second reason is that sender nodes after receiving the wake-up beacon extend

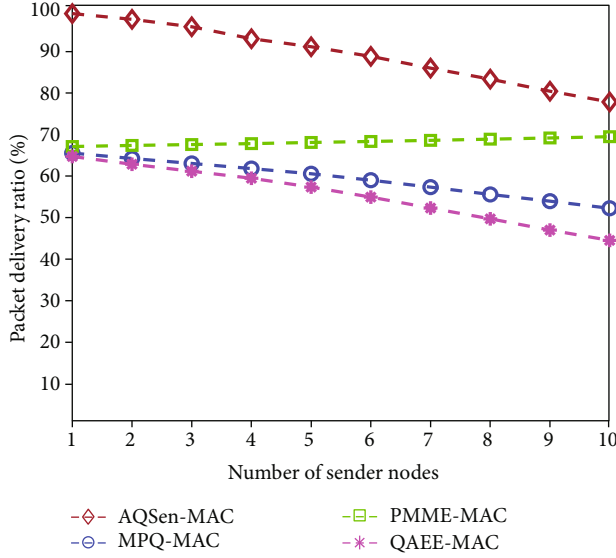


FIGURE 8: Average packet delivery ratio as a function of the number of sender nodes.

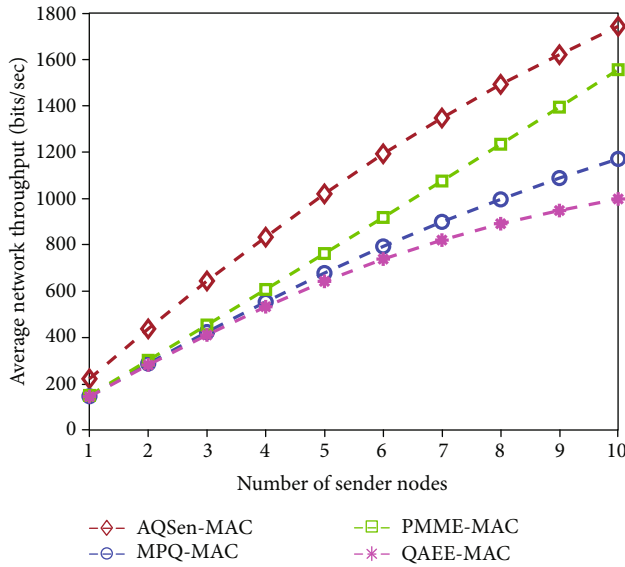


FIGURE 9: Average network throughput as a function of the number of sender nodes.

their sleep time for synchronization with the receiver, which also has influence on reducing energy at the sender side. It is observed that MPQ-MAC, PMME-MAC, and QAEE-MAC consume almost the same amount of energy; however, PMME-MAC transmits slightly more packets. Therefore, it shows better performance when compared to MPQ-MAC and QAEE-MAC.

The energy consumption per node is shown in Figure 11. It can be seen that the sender node in AQSen-MAC consumes slightly higher energy of up to 3.7%, 9%, and 1.8% when compared to MPQ-MAC, PMME-MAC, and QAEE-MAC protocols, respectively. This is because sender nodes in AQSen-MAC transmit more packets than other protocols, which consume more energy, whereas in other protocols, the

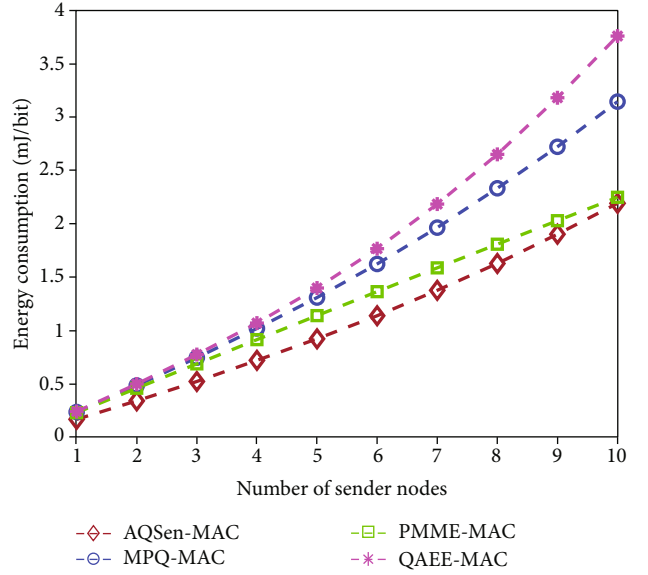


FIGURE 10: Average energy consumption per bit as a function of the number of sender nodes.

receiver node became nonoperational for more than 3 h and as a result, sender nodes are unable to send a large number of packets to the receiver. It can also be noticed that the PMME-MAC consumes less energy when compared to all other protocols. The reason is that the receiver in PMME-MAC does not wait for a specific Tx beacon and it cancels the waiting timer when it receives the first Tx beacon from the sender node, which conserves energy at the sender side. However, it significantly reduces the PDR and network throughput when its receiver became nonoperational for several hours.

The average packet delay (d_{ETE}) in all protocols is given in Figure 12. It is the time period between the generation of the packet until its reception at the receiver. The equation to calculate the average packet delay is as follows:

$$d_{ETE} = d_{queue} + d_{trans} + d_{prop} + d_{proc}, \quad (8)$$

where d_{queue} , d_{trans} , d_{prop} , and d_{proc} denote queuing, transmission, propagation, and processing delays, respectively.

It can be seen that the data packet experiences delay of around 52% in AQSen-MAC when compared to other protocols; however, the delay is still within an acceptable range (less than 0.36 s). This is because of the duty cycle mechanism, where the receiver increases its sleep time to save energy. Hence, the sender node with the data packet waits longer for the receiver beacon, which increases delay. It can also be seen that the PMME-MAC achieves better delay performance than other protocols. The reason is that the receiver after receiving the first Tx beacon cancels the T_w timer, which reduces the packet delay.

Figure 13 shows the average packet delay for the priority data packet in AQSen-MAC to that of MPQ-MAC, PMME-MAC, and QAEE-MAC. Only delays for the highest and lowest priority packets are shown for all protocols. It can be noticed that the AQSen-MAC protocol suffers up to 70%

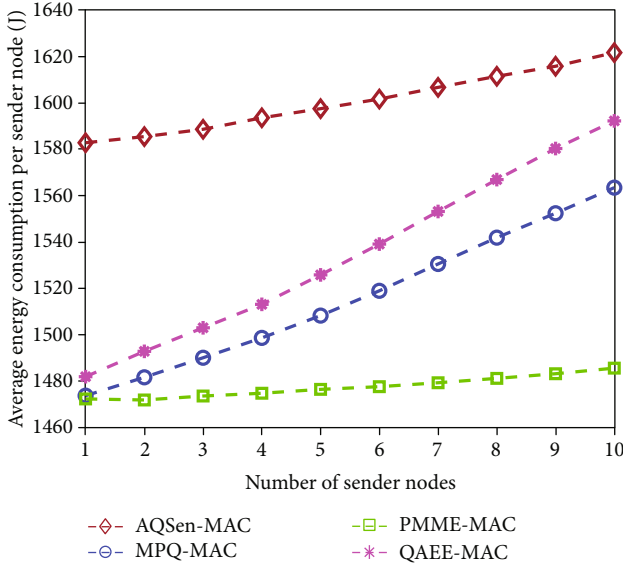


FIGURE 11: Average energy consumption per node as a function of the number of sender nodes.

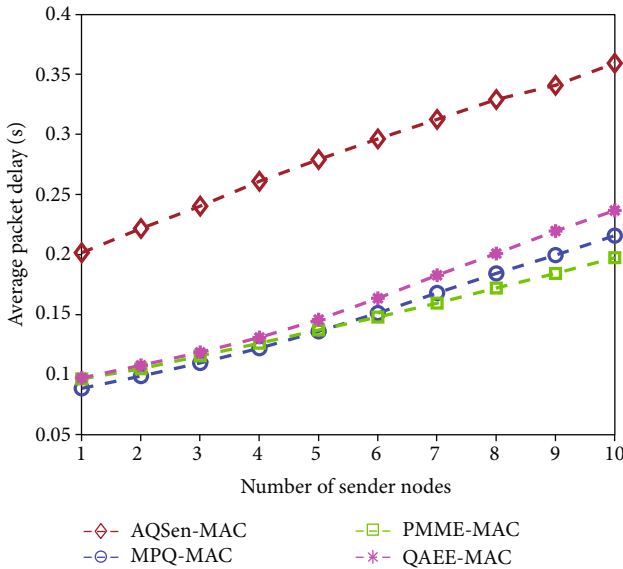


FIGURE 12: Average packet delay for data packet as a function of the number of sender nodes.

higher delay for the P_4 priority packet when it is compared with other analysed protocols, as expected. The fact is that the AQSen-MAC tries to preserve energy using duty cycle adjustment, at a price of increased delay in order to avoid any failure in the network operation. Nevertheless, the AQSen-MAC still supports the highest priority packet and also provides packet delays that are within acceptable limits (less than 1 s).

5. Conclusion and Future Work

In this paper, an energy-efficient QoS MAC protocol has been proposed for achieving better energy efficiency while consider-

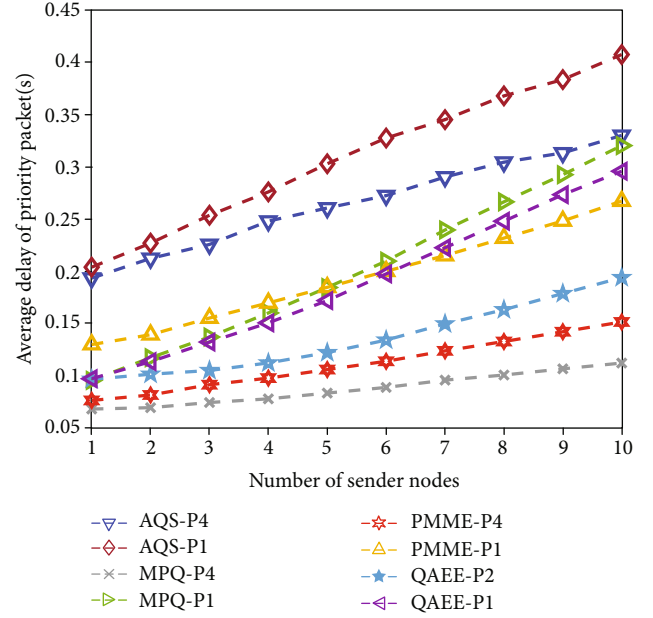


FIGURE 13: Average packet delay for priority data packet as a function of the number of sender nodes.

ing the priority of data packets. The AQSen-MAC protocol has used self-adaptation and scheduling techniques to improve energy efficiency and packet transmission in the network. The former helps to improve coordination between the receiver and sender nodes for packet transmission. In the latter, sender nodes avoid channel sensing to improve energy efficiency and packet delivery ratio. Furthermore, the protocol employs the energy-aware duty cycle management mechanism to prolong the network lifetime. The results show that the AQSen-MAC protocol provides a reduction in energy consumption at the receiver of up to 13.4%, consumption per bit of up to 3%, and improves the packet delivery ratio and network throughput by up to 12% in the network while maintaining its operation in the network. However, MPQ-MAC, PMME-MAC, and QAEE-MAC protocols were unable to sustain their operations and they became nonoperational after 5.5 h, 7 h, and 5.1 h, respectively. Finally, the AQSen-MAC MAC protocol can be used in applications that can tolerate a maximum delay of 1 s for the highest priority data packet and also require higher energy efficiency in the network.

The future work includes the extension of the AQSen-MAC protocol for solar-based energy harvesting WSNs. The performance will be evaluated on tests beds using a mesh network under realistic energy harvesting scenarios.

Data Availability

The simulation parameters used in the performance analysis of AQSen-MAC are given in the article.

Conflicts of Interest

The authors declare that there is no conflict of interest regarding the publication of this paper.

Acknowledgments

This research is a result of the AQUASENSE project which has received funding from the European Union's Horizon 2020 research and innovation programme under the Marie Skłodowska-Curie grant agreement No. 813680.

References

- [1] B. L. R. Stojkoska and K. V. Trivodaliev, "A review of internet of things for smart home: challenges and solutions," *Journal of Cleaner Production*, vol. 140, pp. 1454–1464, 2017.
- [2] J. L. Bayo-Monton, A. Martinez Millana, W. Han, C. Fernandez Llatas, Y. Sun, and V. Traver, "Wearable sensors integrated with Internet of Things for advancing eHealth care," *Sensors*, vol. 18, no. 6, p. 1851, 2018.
- [3] G. Bode, M. Baranski, M. Schraven et al., "Cloud, wireless technology, internet of things: the next generation of building automation systems," *Journal of Physics: Conference Series*, vol. 1343, no. 1, article 012059, 2019.
- [4] I. Khan, F. Belqasmi, R. Glitho, N. Crespi, M. Morrow, and P. Polakos, "Wireless sensor network virtualization: a survey," *IEEE Communications Surveys & Tutorials*, vol. 18, no. 1, pp. 553–576, 2015.
- [5] M. Sohail, S. Khan, R. Ahmad, D. Singh, and J. Lloret, "Game theoretic solution for power management in IoT-based wireless sensor networks," *Sensors*, vol. 19, no. 18, p. 3835, 2019.
- [6] W. Qi, W. Liu, X. Liu et al., "Minimizing delay and transmission times with long lifetime in code dissemination scheme for high loss ratio and low duty cycle wireless sensor networks," *Sensors*, vol. 18, no. 10, p. 3516, 2018.
- [7] M. Peng, W. Liu, T. Wang, and Z. Zeng, "Relay selection joint consecutive packet routing scheme to improve performance for wake-up radio-enabled WSNs," *Wireless Communications and Mobile Computing*, vol. 2020, 32 pages, 2020.
- [8] Q. Yu, G. Li, X. Hang, and K. Fu, "An energy efficient MAC protocol for wireless passive sensor networks," *Future Internet*, vol. 9, no. 2, pp. 1–12, 2017.
- [9] M. K. Khan, M. Shiraz, K. Zrar Ghafoor, S. Khan, A. Safaa Sadiq, and G. Ahmed, "EE-MRP: energy-efficient multistage routing protocol for wireless sensor networks," *Wireless Communications and Mobile Computing*, vol. 2018, 13 pages, 2018.
- [10] S. Li, J. G. Kim, D. H. Han, and K. S. Lee, "A survey of energy-efficient communication protocols with QoS guarantees in wireless multimedia sensor networks," *Sensors*, vol. 19, no. 1, p. 199, 2019.
- [11] T. Ruan, Z. J. Chew, and M. Zhu, "Energy-aware approaches for energy harvesting powered wireless sensor nodes," *IEEE Sensors Journal*, vol. 17, no. 7, pp. 2165–2173, 2017.
- [12] M. Ndiaye, G. P. Hancke, and A. M. Abu-Mahfouz, "Software defined networking for improved wireless sensor network management: a survey," *Sensors*, vol. 17, no. 5, p. 1031, 2017.
- [13] M. Hasan, A. Karmaker, M. S. Alam, and A. Craig, "Minimizing the adverse effects of asymmetric links: a novel cooperative asynchronous MAC protocol for wireless sensor networks," *Sensors*, vol. 19, no. 10, p. 2402, 2019.
- [14] K. A. Memon, M. A. Memon, M. M. Shaikh et al., "Optimal transmit power for channel access based WSN MAC protocols," *International Journal of Computer Science and Network Security*, vol. 18, pp. 51–60, 2018.
- [15] M. Malik and M. Sharma, "A novel approach for comparative analysis on energy effectiveness of H-MAC and S-MAC protocols for wireless sensor networks," *Advanced Science, Engineering and Medicine*, vol. 11, no. 1, pp. 29–35, 2019.
- [16] M. Kim, S. Park, and W. Lee, "Energy and distance-aware hopping sensor relocation for wireless sensor networks," *Sensors*, vol. 19, no. 7, p. 1567, 2019.
- [17] Z. Pooranian, A. Barati, and A. Movaghar, "Queen-bee algorithm for energy efficient clusters in wireless sensor networks," *World Academy of Science, Engineering and Technology*, vol. 73, pp. 1080–1083, 2011.
- [18] Y. Liu, Q. Wu, T. Zhao, Y. Tie, F. Bai, and M. Jin, "An improved energy-efficient routing protocol for wireless sensor networks," *Sensors*, vol. 19, no. 20, p. 4579, 2019.
- [19] P. G. V. Naranjo, M. Shojafar, H. Mostafaei, Z. Pooranian, and E. Baccarelli, "P-SEP: a prolong stable election routing algorithm for energy-limited heterogeneous fog-supported wireless sensor networks," *The Journal of Supercomputing*, vol. 73, no. 2, pp. 733–755, 2017.
- [20] Q. Li, A. Liu, T. Wang, M. Xie, and N. N. Xiong, "Pipeline slot based fast rerouting scheme for delay optimization in duty cycle based M2M communications," *Peer-to-Peer Networking and Applications*, vol. 12, no. 6, pp. 1673–1704, 2019.
- [21] R. Lara, D. Benitez, A. Caamano, M. Zennaro, and J. L. Rojo-Alvarez, "On real-time performance evaluation of volcano-monitoring systems with wireless sensor networks," *IEEE Sensors Journal*, vol. 15, no. 6, pp. 3514–3523, 2015.
- [22] X. Liu, M. Zhao, A. Liu, and K. K. L. Wong, "Adjusting forwarder nodes and duty cycle using packet aggregation routing for body sensor networks," *Information Fusion*, vol. 53, pp. 183–195, 2020.
- [23] A. Pathak, "A proficient bee colony-clustering protocol to prolong lifetime of wireless sensor networks," *Journal of Computer Networks and Communications*, vol. 2020, 9 pages, 2020.
- [24] L. Guntupalli, D. Ghose, F. Y. Li, and M. Gidlund, "Energy efficient consecutive packet transmissions in receiver-initiated wake-up radio enabled wsn," *IEEE Sensors Journal*, vol. 18, no. 11, pp. 4733–4745, 2018.
- [25] D. Ghose, F. Y. Li, and V. Pla, "MAC protocols for wake-up radio: principles, modeling and performance analysis," *IEEE Transactions on Industrial Informatics*, vol. 14, no. 5, pp. 2294–2306, 2018.
- [26] E. Ibarra, A. Antonopoulos, E. Kartsakli, J. J. Rodrigues, and C. Verikoukis, "Joint power-QoS control scheme for energy harvesting body sensor nodes," in *2014 IEEE International Conference on Communications (ICC)*, pp. 3511–3516, Sydney, NSW, Australia, June 2014.
- [27] H. H. R. Sherazi, L. A. Grieco, and G. Boggia, "A comprehensive review on energy harvesting MAC protocols in WSNs: challenges and tradeoffs," *Ad Hoc Networks*, vol. 71, pp. 117–134, 2018.
- [28] S. Sarang, M. Driberg, A. Awang, and R. Ahmad, "A QoS MAC protocol for prioritized data in energy harvesting wireless sensor networks," *Computer Networks*, vol. 144, pp. 141–153, 2018.
- [29] T. Kim, J. Park, J. Kim, J. Noh, and S. Cho, "REACH: an efficient MAC protocol for RF energy harvesting in wireless sensor network," *Wireless Communications and Mobile Computing*, vol. 2017, 8 pages, 2017.
- [30] V. Esteves, A. Antonopoulos, E. Kartsakli, M. Puig-Vidal, P. Miribel-Català, and C. Verikoukis, "Cooperative energy

- harvesting-adaptive MAC protocol for WBANs,” *Sensors*, vol. 15, no. 6, pp. 12635–12650, 2015.
- [31] E. Ibarra, A. Antonopoulos, E. Kartsakli, J. J. Rodrigues, and C. Verikoukis, “QoS-aware energy management in body sensor nodes powered by human energy harvesting,” *IEEE Sensors Journal*, vol. 16, no. 2, pp. 542–549, 2015.
- [32] P. Rawat, K. D. Singh, H. Chaouchi, and J. M. Bonnin, “Wireless sensor networks: a survey on recent developments and potential synergies,” *The Journal of Supercomputing*, vol. 68, no. 1, pp. 1–48, 2014.
- [33] X. Liu, A. Liu, Z. Li et al., “Distributed cooperative communication nodes control and optimization reliability for resource-constrained WSNs,” *Neurocomputing*, vol. 270, pp. 122–136, 2017.
- [34] M. Dong, K. Ota, A. Liu, and M. Guo, “Joint optimization of lifetime and transport delay under reliability constraint wireless sensor networks,” *IEEE Transactions on Parallel and Distributed Systems*, vol. 27, no. 1, pp. 225–236, 2015.
- [35] S. Lai, B. Ravindran, and H. Cho, “Heterogenous quorum-based wake-up scheduling in wireless sensor networks,” *IEEE Transactions on Computers*, vol. 59, no. 11, pp. 1562–1575, 2010.
- [36] J. Xu, A. Liu, N. Xiong, T. Wang, and Z. Zuo, “Integrated collaborative filtering recommendation in social cyber-physical systems,” *International Journal of Distributed Sensor Networks*, vol. 13, no. 12, pp. 1–17, 2017.
- [37] S. Galmés and S. Escolar, “Analytical model for the duty cycle in solar-based EH-WSN for environmental monitoring,” *Sensors*, vol. 18, no. 8, p. 2499, 2018.
- [38] Y. Su, X. Fu, G. Han, N. Xu, and Z. Jin, “Implementation of a cross-layer sensing medium-access control scheme,” *Sensors*, vol. 17, no. 4, pp. 1–12, 2017.
- [39] X. Yang, L. Wang, J. Xie, and Z. Zhang, “Energy efficiency TDMA/CSMA hybrid protocol with power control for WSN,” *Wireless Communications and Mobile Computing*, vol. 2018, 7 pages, 2018.
- [40] X. Yang, L. Wang, J. Su, and Y. Gong, “Hybrid MAC protocol design for mobile wireless sensors networks,” *IEEE Sensors Letters*, vol. 2, no. 2, pp. 1–4, 2018.
- [41] S. Prakasam and S. Lavanya, “Mac protocols for reduced power consumption in intra-cluster design for wireless sensor networks,” in *2017 Innovations in Power and Advanced Computing Technologies (i-PACT)*, pp. 1–5, Vellore, India, April 2017.
- [42] Y. Sun, O. Gurewitz, and D. B. Johnson, “RI-MAC: a receiver-initiated asynchronous duty cycle MAC protocol for dynamic traffic loads in wireless sensor networks,” *Proceedings of the 6th ACM conference on Embedded network sensor systems*, pp. 1–14, 2008.
- [43] Y. Liu, K. Ota, K. Zhang et al., “QTSAC: an energy-efficient MAC protocol for delay minimization in wireless sensor networks,” *IEEE Access*, vol. 6, pp. 8273–8291, 2018.
- [44] M. A. Yigitel, O. D. Incel, and C. Ersoy, “QoS-aware MAC protocols for wireless sensor networks: a survey,” *Computer Networks*, vol. 55, no. 8, pp. 1982–2004, 2011.
- [45] H. Kdouh, G. Zaharia, C. Brousseau, H. Farhat, G. Grunfelder, and G. El Zein, “Application of wireless sensor network for the monitoring systems of vessels,” in *Wireless Sensor Networks—Technology and Applications*, pp. 285–308, In Tech, Rijeka, Croatia, 2012.
- [46] J.-F. Martinez, A.-B. Garcia, I. Corredor, L. López, V. Hernández, and A. Dasilva, “Modelling QoS for wireless sensor networks,” in *IFIP Conference on Wireless Sensor and Actor Networks*, pp. 143–154, 2007.
- [47] O. Chughtai, N. Badruddin, A. Awang, and M. Rehan, “A novel route discovery procedure for congestion avoidance in multi-hop WSNs,” *International Journal of Sensor Networks*, vol. 25, no. 4, pp. 229–243, 2017.
- [48] S. Sarang, M. Driberg, and A. Awang, “Multi-priority based QoS MAC protocol for wireless sensor networks,” in *2017 7th IEEE International Conference on System Engineering and Technology (ICSET)*, pp. 54–58, Shah Alam, Malaysia, October 2017.
- [49] F. Z. Djiroun and D. Djenouri, “MAC protocols with wake-up radio for wireless sensor networks: a review,” *IEEE Communications surveys & tutorials*, vol. 19, no. 1, pp. 587–618, 2016.
- [50] L. Guntupalli, *Energy efficiency in wireless sensor networks: transmission protocols and performance evaluation*, Ph. D. Dissertation, University of Agder, Norway, 2016.
- [51] M. Ghribi and A. Meddeb, “Survey and taxonomy of MAC, routing and cross layer protocols using wake-up radio,” *Journal of Network and Computer Applications*, vol. 149, article 102465, 2019.
- [52] A. K. Azad, M. S. Alam, and S. A. Shawkat, “DCDS-MAC: a dual-channel dual-slot MAC protocol for delay sensitive wireless sensor network applications,” *The Journal of Communication*, vol. 14, pp. 1–10, 2019.
- [53] T. Kaur and D. Kumar, “ETPS-MAC: energy traffic priority scheduling-based QoS-aware MAC protocol for hierarchical WSNs,” *International Journal of Electronics*, vol. 106, no. 9, pp. 1344–1359, 2019.
- [54] J. Varghese and S. V. Rao, “Performance analysis of synchronous and receiver initiated MAC protocols under varying traffic density over Wireless Sensor Networks,” in *2014 International Conference on Control, Instrumentation, Communication and Computational Technologies (ICCICCT)*, pp. 1228–1232, Kanyakumari, India, July 2014.
- [55] W. Ye, J. Heidemann, and D. Estrin, “An energy-efficient MAC protocol for wireless sensor networks,” in *Proceedings. Twenty-First Annual Joint Conference of the IEEE Computer and Communications Societies*, New York, NY, USA, USA, June 2002.
- [56] W. Ye, J. Heidemann, and D. Estrin, “Medium access control with coordinated adaptive sleeping for wireless sensor networks,” *IEEE/ACM Transactions on networking*, vol. 12, no. 3, pp. 493–506, 2004.
- [57] Y. Sun, S. Du, O. Gurewitz, and D. B. Johnson, “DW-MAC: a low latency, energy efficient demand-wakeup MAC protocol for wireless sensor networks,” *Proceedings of the 9th ACM international symposium on Mobile ad hoc networking and computing*, pp. 53–62, 2008.
- [58] P. Lin, C. Qiao, and X. Wang, “Medium access control with a dynamic duty cycle for sensor networks,” in *2004 IEEE Wireless Communications and Networking Conference (IEEE Cat. No.04TH8733)*, pp. 1534–1539, Atlanta, GA, USA, USA, March 2004.
- [59] K. Sohrabi, J. Gao, V. Ailawadhi, and G. J. Pottie, “Protocols for self-organization of a wireless sensor network,” *IEEE Personal Communications*, vol. 7, no. 5, pp. 16–27, 2000.
- [60] H. Kim and S.-G. Min, “Priority-based QoS MAC protocol for wireless sensor networks,” in *2009 IEEE International Symposium on Parallel & Distributed Processing*, pp. 1–8, Rome, Italy, March 2009.

- [61] B. A. Muzakkari, M. A. Mohamed, M. F. Kadir, and M. Mamat, "Queue and priority-aware adaptive duty cycle scheme for energy efficient wireless sensor networks," *IEEE Access*, vol. 8, pp. 17231–17242, 2020.
- [62] K. Venugopal and M. Kumaraswamy, "DQTSM: distributed QoS in time synchronized MAC protocol for WSNs," in *QoS Routing Algorithms for Wireless Sensor Networks*, pp. 71–81, Springer, 2020.
- [63] J. Polastre, J. Hill, and D. Culler, "Versatile low power media access for wireless sensor networks," *2nd International Conference on Embedded Networked Sensor Systems (SenSys)*, pp. 95–107, 2004.
- [64] G. P. Halkes, T. Van Dam, and K. Langendoen, "Comparing energy-saving MAC protocols for wireless sensor networks," *Mobile Networks and Applications*, vol. 10, no. 5, pp. 783–791, 2005.
- [65] J. Lee and S. Kim, "EnRI-MAC: an enhanced receiver-initiated MAC protocol for various traffic types in wireless sensor networks," *Wireless Networks*, vol. 26, no. 2, pp. 1193–1202, 2020.
- [66] M. Buettner, G. V. Yee, E. Anderson, and R. Han, "X-MAC: a short preamble MAC protocol for duty-cycled wireless sensor networks," *Proceedings of the 4th international conference on Embedded networked sensor systems*, pp. 307–320, 2006.
- [67] E.-Y. Lin, J. M. Rabaey, and A. Wolisz, "Power-efficient rendez-vous schemes for dense wireless sensor networks," in *2004 IEEE International Conference on Communications (IEEE Cat. No.04CH37577)*, pp. 3769–3776, Paris, France, France, July 2004.
- [68] M. S. Adam, L. Yee, M. R. Hussain et al., "An adaptive wake-up-interval to enhance receiver-based Ps-Mac protocol for wireless sensor networks," *Sensors*, vol. 19, no. 17, p. 3732, 2019.
- [69] X. Fafoutis, A. Di Mauro, and N. Dragoni, "Sustainable medium access control: implementation and evaluation of ODMAC," in *2013 IEEE International Conference on Communications Workshops (ICC)*, pp. 407–412, Budapest, Hungary, June 2013.
- [70] S. C. Kim, J. H. Jeon, and H. J. Park, "QoS aware energy-efficient (QAEE) MAC protocol for energy harvesting wireless sensor networks," *International Conference on Hybrid Information Technology*, pp. 41–48, 2012.
- [71] N. T. Thu-Hang, N. C. Trinh, and N. T. Ban, "Delay and reliability analysis of p-persistent carrier sense multiple access for multievent wireless sensor network," in *IEEE International Conference on Telecommunications (ICT)*, pp. 427–431, Hanoi, Vietnam, Vietnam, April 2019.
- [72] S. Argoubi, K. Maalaoui, M. H. Elhdhili, and L. A. Saidane, "Priority-MAC: a priority based medium access control solution with QoS for WSN," in *IEEE/ACS 13th International Conference of Computer Systems and Applications (AICCSA)*, pp. 1–6, Agadir, Morocco, December 2016.
- [73] B. Yahya and J. Ben-Othman, "Energy efficient and QoS aware medium access control for wireless sensor networks," *Concurrency and Computation: Practice and Experience*, vol. 22, no. 10, pp. 1252–1266, 2010.
- [74] A. Boulis, *Castalia: a simulator for wireless sensor networks and body area networks*, NICTA: National ICT Australia, 2011.
- [75] Crossbow Technology, "TelosB mote platform datasheet," 2020, https://www.willow.co.uk/TelosB_Datasheet.pdf.
- [76] R. Han, W. Yang, Y. Wang, and K. You, "DCE: a distributed energy-efficient clustering protocol for wireless sensor network based on double-phase cluster-head election," *Sensors*, vol. 17, no. 5, p. 998, 2017.
- [77] S. Shen, L. Huang, J. Liu, A. C. Champion, S. Yu, and Q. Cao, "Reliability evaluation for clustered WSNs under malware propagation," *Sensors*, vol. 16, no. 6, p. 855, 2016.
- [78] H. Zhou, Y. Wu, L. Feng, and D. Liu, "A security mechanism for cluster-based WSN against selective forwarding," *Sensors*, vol. 16, no. 9, p. 1537, 2016.

Research Article

Truthful Mechanism Design for Multiregion Mobile Crowdsensing

Yu Qiao ¹, Jun Wu,² Hao Cheng,¹ Zilan Huang,¹ Qiangqiang He,¹ and Chongjun Wang ¹

¹National Key Laboratory for Novel Software Technology, Nanjing University, China

²Jiangsu Provincial Key Laboratory of E-Business, Nanjing University of Finance and Economics, China

Correspondence should be addressed to Chongjun Wang; chjwang@nju.edu.cn

Received 11 March 2020; Revised 18 June 2020; Accepted 24 July 2020; Published 19 August 2020

Academic Editor: Wei Yu

Copyright © 2020 Yu Qiao et al. This is an open access article distributed under the Creative Commons Attribution License, which permits unrestricted use, distribution, and reproduction in any medium, provided the original work is properly cited.

In the age of the development of artificial intelligence, we face the challenge on how to obtain high-quality data set for learning systems effectively and efficiently. Crowdsensing is a new powerful tool which will divide tasks between the data contributors to achieve an outcome cumulatively. However, it arouses several new challenges, such as incentivization. Incentive mechanisms are significant to the crowdsensing applications, since a good incentive mechanism will attract more workers to participate. However, existing mechanisms failed to consider situations where the crowdsourcer has to hire capacitated workers or workers from multiregions. We design two objectives for the proposed multiregion scenario, namely, weighted mean and maximin. The proposed mechanisms maximize the utility of services provided by a selected data contributor under both constraints approximately. Also, extensive simulations are conducted to verify the effectiveness of our proposed methods.

1. Introduction

With the rapid development of the hand-held mobile devices, mobile crowdsensing [1] has become a new tool for problem-solving, and there has been lots of applications in real life, such as healthcare [2], smart city [3], and localization [4]. Due to the fact that workers' participation will depreciate their devices, such as consumption of CPU and battery, they may take a toll on their participation. Incentive mechanisms are significant to the crowdsensing applications, since a good incentive mechanism will attract more workers to participate. Estimating workers' personal cost is a hurdle. Workers' private cost is subjective, which is associated with various factors. These factors are hard to observe, such as difficulties of tasks and abilities of workers. A reasonable method is to offer an estimated optimal bonus to compensate costs of workers.

With the limited budget, workers may be reluctant to participate, if the offered price is too low. Offering a high price to workers may result in lower outcome. We will use a powerful tool from the algorithmic game to ensure both the efficiency and workers' incentivization.

The mechanism design is a tricky issue for the crowdsourcer with budget constraint, since designing a budget constraint allocating scheme needs understanding its payoff to workers, which is also related to the allocating scheme itself. Most existing works aim at maximizing the efficiency of crowdsensing by hiring workers in a single region. Nevertheless, with some geographical limitations, the crowdsourcer is necessary to procure service from workers in multiple regions to perform tasks and consider the interactions of different regions. Consider a crowdsourcer with a hard budget who wants to estimate the residential information in Eastern Asia which consisted of five countries, China, Japan, South Korea, North Korea, and Mongolia. Due to the geographical limitation, the crowdsourcer has to hire workers in each country to perform tasks separately. Furthermore, the populations or the area of the territories of five countries are different. Thus, the crowdsourcer has to design mechanisms to allocate proper budgets to each region and considers the incentives for workers from different regions.

In this paper, we introduce and study a new scenario, where the crowdsourcer or buyer wants to buy service in a macroregion which is composed of several nonoverlapped

microregions. The crowdsourcer will get a utility for each microregion, respectively, and aggregate results in each microregion to get a final result. We introduce and study two optimization goals when combining results of each microregion, namely, weighted mean and maximin. Under the first model, we define the crowdsourcer's utility as the weighted mean of utility obtained in each microregion. Under the second model, the crowdsourcer's utility is defined as the minimum utility obtained in all microregions. Compared with single region settings, our multiple region setting leads to more useful solutions in practice. By this work, we proposed an incentive mechanism for the weighted mean model firstly, which consists of a task allocation algorithm and a worker compensation algorithm. Then, we extend the proposed mechanism to the maximin model.

The main of our paper can be summarized as follows:

- (i) A major contribution of this work is introducing a new problem, multiregion crowdsensing. Two objectives are introduced to measure the utility of multiregion crowdsensing. Although we study our problem in the context of crowdsensing, the framework and solution proposed in this paper can be applied to a broad range of domains, such as procurement and resource allocation
- (ii) For a multiunit budget-feasible mechanism, we propose a novel method via a proportional share allocation rule instead of the random sampling method applied in [5]. Also, our proposed mechanism can handle the multiregion procurement settings

2. Related Work

In recent years, the mobile crowdsensing system has a wide range of application in our daily life [1–3, 6–10]. At the same time, game theoretic models become an effective tool for incentive mechanism in mobile crowdsensing systems because of the strategic behavior of workers [11, 12]. Jin et al. considered integrating information quality into the design of the incentive mechanism for mobile systems [13]. Zhang et al. designed an incentive mechanism by which crowd workers were encouraged to label a set of binary tasks within strict budget constraints [14]. Another Zhang et al. studied three models of cooperation and competition among service providers [15]. Gao et al. devoted to providing a sufficient long-term participation incentive for crowd workers [16]. Feng et al. studied the key dimension of location information in smartphones which are assigned sensing tasks [17]. Qiao et al. studied the task crowdsensing under the background of the cross market [18]. Zhao et al. designed online incentive mechanisms for crowdsensing systems [19]. Liu et al. studied a two-phase group buying based on the auction mechanism for mobile crowdsensing [20]. Xu et al. improved online crowdsourcing auctions via a two-tiered framework [21]. Xu et al. [22] also proposed a mechanism with a strategy-proof discovery phase and a budget-constrained purchasing stage.

Budget-feasible incentive mechanism design, which was initially studied by Singer [23] when he found a novel class of mechanism design problems where the outcomes are limited by payments, becomes a newly emerging branch of mechanism design. Chen et al. designed a stochastic budget-feasible mechanism with a polynomial time approximate ratio and a deterministic budget-feasible mechanism with an exponential time approximate ratio [24]. Bei et al. studied the budget-feasible mechanism through random sampling and designed a constant approximation mechanism for all subadditive functions in Bayesian environment [25]. Anari et al. investigated a model to solve the mechanism design problem in the context of large-scale crowdsensing markets such as Amazon's Mechanical Turk [26]. Then, Singer applied this model to influence maximization in social networks [27] while Horel et al. applied this model to an experiment design problem [28]. Chan and Chen came up with multiunit budget-feasible mechanism design which has been a new setting in budget-feasible incentive mechanism design [5].

In our setting, a crowdsourcer or buyer wants to procure service in a macroregion, which is composed of $[r] = \{1, \dots, r\}$ nonoverlapping microregions. A set of sellers or workers $N = \{1, \dots, n\}$ is scattered in each microregion.

Let $r(\cdot)$ be a function to specify the region. Let c_i index the private cost of the worker i . Each worker i could provide m_i units of homogeneous service, which is common knowledge. We use s_i to denote the set of service which could be provided by worker i . Let $M = \cup_{i \in N} s_i$ denote the total service that can be provided by all workers in the macroregion, thus the number of total service in the macroregion $|\mathcal{M}| = \sum_{i \in N} m_i$.

This paper studies the service procurement with strategic players, and each worker will report his cost strategically in order to maximize his benefit. Let $\mathbf{b} = (b_1, b_2, \dots, b_n)$ index bids of all workers. In our mechanism, there are two functions, a payment function and an allocation function. The payment scheme will decide the payoff p_i to the worker i , and the quota of service x_i procured from worker i is the outcome of the allocating scheme. The output of the designed mechanism is two vectors, payment vector $\vec{\mathbf{p}} = \{p_1, p_2, \dots, p_n\}$ and allocating vector $\vec{\mathbf{x}} = \{x_1, x_2, \dots, x_n\}$. The benefit $u_i(\vec{\mathbf{b}})$ of service provider i is quasilinear. Formally, we have

$$u_i(\vec{\mathbf{b}}) = \begin{cases} p_i(\vec{\mathbf{b}}) - c_i \cdot x_i(\vec{\mathbf{b}}), & \text{if } x_i(\vec{\mathbf{b}}) \leq m_i, \\ -\infty, & \text{otherwise.} \end{cases} \quad (1)$$

2.1. Problem Formulation

2.1.1. Single-Region Utility Measurement. Since the utility in each microregion is calculated, respectively, we need to know the quota of procured service in each microregion. We use $k_j = \sum_{i \in N, r(i)=j} x_i$ to present the quota of procured services in microregion j . Then, the utility obtained in microregion j is measured by a symmetrical submodular function $\mathcal{A}(k_j) = \sum_{i=1}^{k_j} v_i$, where v_i is the marginal incremental value by

procuring the i -th unit service from the workers when the crowdsourcer has brought $i-1$ service. The symmetrical submodularity means v_i will decrease as i grows, and $v_1 \geq v_2 \geq \dots \geq v_n \geq 0$.

2.1.2. Multiregion Utility Measurement. The crowdsourcer will get a final result by combining the outcomes in each microregion. Two optimization objectives are introduced, namely, *maximin* and *weighted mean*. In the weighted mean scheme, each microregion i is related with a region weight w_i ($0 \leq w_i \leq 1$, $\sum_{i \in [r]} w_i = 1$), which measures the relative significance of every microregion. The global utility is calculated by the weighted mean of utility obtained in each microregion. Formally, the weighted mean maximization model can be summarized as follows.

Problem: weighted mean maximization.
Objective: maximize $\mathcal{A}_{wm} = \sum_{j=1}^r w_j \mathcal{A}(k_j)$,
Subject to:

$$\sum_{j=1}^r w_j = 1, \quad 0 \leq w_j \leq 1, \quad (2)$$

$$\sum_{i \in N} p_i \cdot x_i \leq B. \quad (3)$$

In the maximin model, the global benefit of the crowdsourcer is calculated by the minimum of the accuracy rate achieved in all microregions.

Problem: minimum maximization.
Objective: maximize $\mathcal{A}_{mm} = \min_{j \in \{1, \dots, r\}} \mathcal{A}(k_j)$,
Subject to:

$$\sum_{i \in N} p_i \cdot x_i \leq B. \quad (4)$$

We use $\text{OPT}_{wm}(B, M)$ and $\text{OPT}_{mm}(B, M)$ to index the optimal results for weighted mean and maximin, respectively.

Due to the fact that the worker i 's cost c_i is private information, the problem in our paper belongs to the single parameter mechanism design problem. According to the well-known Myerson's lemma [29], any truthful auctions must have a monotone allocating scheme and a payment scheme with a threshold payment. For the more complex multiunit setting in our paper, we have the following lemma.

Lemma 1. *A single-parameter multiunit domain, a normalized auction $\mathcal{H} = (\mathbf{x}, \mathbf{p})$ is truthful, if and only if,*

- (1) *Monotone allocation:* $x_i(c_i, c_{-i}) > 0, \forall i \in N$, implied $x_i(c_i', c_{-i}) > 0$, if $c_i' < c_i$
- (2) *Threshold payment to the selected workers:* $p_i(c_i) = \sum_{j=1}^{x_i(c_i)} q_j$, where $q_j = \inf \{c_i : x_i(b_i) < j\}$

Proof. The first condition is trivial and could be obtained via Myerson's lemma [29]. For the second condition, we use w to index $x_i(b_i)$. Then, we obtain

$$\begin{aligned} p_i(b_i) &= w b_i + \int_{b_i}^{qw} w dz + \int_{qw}^{qw-1} w - 1 dz + \dots + \int_{q_2}^{q_1} 1 dz \\ &= q_w + q_{w-1} + \dots + q_1. \end{aligned} \quad (5)$$

Thus, the lemma holds.

We expect our designed auctions are

- (i) *Truthful:* for any worker i , his benefit is maximized by reporting his true cost, regardless of the bidding of others: $\forall b_i, \vec{\mathbf{b}}_{-i} : u_i(b_i, \vec{\mathbf{b}}_{-i}) \geq u_i(b_i', \vec{\mathbf{b}}_{-i})$
- (ii) *Individually rational:* workers are not worse off by participating in the campaign. Formally, it requires $\forall \vec{\mathbf{b}}_{-i} : u_i(b_i, \vec{\mathbf{b}}_{-i}) \geq 0$
- (iii) *Budget-feasible:* the total payment to workers does not exceed the buyer's budget
- (iv) *Computationally efficient and performance guaranteed:* the results of function x and p could be found out in polynomial time, and constant approximations are expected for our proposed mechanisms

3. Weighted Mean Maximization

Based on Myerson's well-known lemma [29], strategy-proof auctions must have a monotone allocating scheme and a payment scheme with a threshold payment. For the mechanism design under budget constraint, selecting items for the candidate set according to the benefit-to-cost ratio is a natural fit. The basic idea of our proposed mechanism is to select workers greedily based the marginal of each worker and terminate with an appropriate threshold payment.

First, we would like to introduce a greedy but nonmonotone selecting rule. Then, we modify this rule to make it monotone. Given a set of procured service M , we define the marginal value of a unit service $s^i \in \mathcal{M} \setminus M$ for the weighted mean model as

$$\mathcal{U}_{i|M} = \mathcal{A}_{wm}(M \cup s^i) - \mathcal{A}_{wm}(M). \quad (6)$$

Our greedy algorithm selects a group of services one by one. In each stage i , it adds a service s^i that maximizes the benefit-to-cost ratio $\mathcal{U}_{i|M_{i-1}}/c_i$, in which we use M_{i-1} to denote first $i-1$ services selected by our algorithm; without loss of generality, we assume $M_0 = \emptyset$. Since the utility is computed separately, the contribution of service s^i to the global utility equals the incremental value of s^i in its own microregion. We use $u_{\{i|M_{i-1}\}}$ to denote the utility increment in

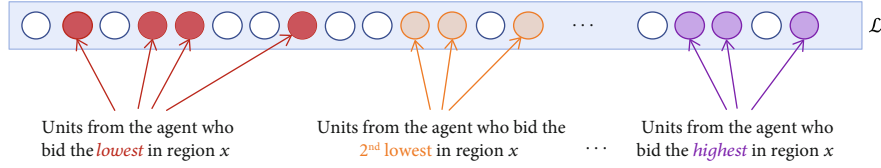


FIGURE 1: For each microregion, each worker's units are placed in \mathbb{L} as nonoverlapping clusters and ordered according to increasing bid. Total payments do not exceed the budget.

region $r(s^i)$ with service s^i and the given set M_{i-1} . Formally, we have

$$s^i = \arg \max_{s^i \in \mathcal{M} \setminus M_{i-1}} \frac{u_{i|M_{i-1}}}{c_i} = \arg \max_{s^i \in \mathcal{M} \setminus M_{i-1}} \frac{u\{i | M_{i-1}\} \cdot w_{r(i)}}{c_i}. \quad (7)$$

If there are multiple candidate workers, we sort them lexicographically. For each s^i , selected in stage i , we use u_i^* , w_i^* , and c_i^* as abbreviations for $u_{\{i|M_{i-1}\}}$, $w_{r(i)^*}$, and c_i^* , respectively. Through the greedy selecting principle, we have a sorted list \mathbb{L} :

$$\mathbb{L} : \frac{u_1^* w_1^*}{c_1^*} \geq \frac{u_2^* w_2^*}{c_2^*} \geq \dots \geq \frac{u_M^* w_M^*}{c_M^*}. \quad (8)$$

We choose workers as candidates iteratively until the budget constraint is exceeded. Formally, we have

$$c_i^* \leq \frac{B}{(1 + n \cdot \mathcal{M})} \cdot \frac{w_i^* u_i^*}{\mathcal{A}_{wm}(M_i)}. \quad (9)$$

This allocation rule is a variation of the proportional share rule which is the basis for mechanisms under a budget. Observing that if k services are selected according to this rule and each selected worker is paid according to their proportional contribution, the one nice feature about this allocation rule is that for any submodular function, it can be proven that the incentive compatible payments do not exceed the workers' proportional contributions. We will further discuss payments after describing the entire mechanism below. Importantly, this allocation rule achieves a bounded approximation ratio.

$$\begin{aligned} & \sum_{i=1}^k B \cdot \left(\frac{\mathcal{A}_{wm}(M_i) - \mathcal{A}_{wm}(M_{i-1})}{\mathcal{A}_{wm}(M_k)} \right) \\ & \leq \frac{B}{\mathcal{A}_{wm}(M_k)} \sum_{i=1}^k (\mathcal{A}_{wm}(M_i) - \mathcal{A}_{wm}(M_{i-1})) \\ & = \frac{B}{\mathcal{A}_{wm}(M_k)} \cdot \mathcal{A}_{wm}(M_k) = B. \end{aligned} \quad (10)$$

Lemma 2. Given a sorted list \mathbb{L} and a service $s^i \in \mathbb{L}$, we use $\mathbb{L}(s^i)$ to denote the position of s^i in \mathbb{L} . For any two services from the same region,

- (i) if $c_i < c_j$, then $\mathbb{L}(s^i) < \mathbb{L}(s^j)$
- (ii) if $c_i = c_j$, then $\mathbb{L}(s^i) < \mathbb{L}(s^j)$, iff $i < j$

Proof.

- (1) With $c_i < c_j$, we assume $\mathbb{L}(s^j) < \mathbb{L}(s^i)$. Thus, we have

$$\frac{u\{j | M_{j-1}\} \cdot w_{r(j)}}{c_j} \geq \frac{u\{i | M_{i-1}\} \cdot w_{r(i)}}{c_i}. \quad (11)$$

Since $r(j) = r(i)$, we have $u_{\{j|M_{j-1}\}} = u_{\{i|M_{i-1}\}}$, then $c_i \geq c_j$. Thus, we have a contradiction!

- (2) With $c_i = c_j$, service s^i and s^j are sorted according to the lexicographical order

No two services from the same region intersect with each other in \mathbb{L} if they are provided by two different workers. For each region, each agent's units are placed in \mathbb{L} as nonoverlapping clusters and ordered according to increasing bid. An illustration of the services' position is in Figure 1.

Lemma 3. The greedy selection principle is monotone.

Proof. For each service s^l chosen as the candidate, the rest of the service in M can be classified into 4 classes:

- (i) T^+ : all services ranked higher than s^l in region $r(l)$
- (ii) T^- : all services ranked lower than s^l in region $r(l)$
- (iii) F^+ : all services not in region $r(l)$ whose rank is higher than s^l
- (iv) F^- : all services not in region $r(l)$ whose rank is lower than s^l

Assume that worker l declares a cost $c^l \leq c_l$ and achieves a utility u^l . Let \hat{T}^+ , \hat{T}^- , \hat{F}^+ , and \hat{F}^- denote the four updated classes. We can easily obtain that no service s^d can be moved forward to the front of s^l . If $l = d$, they are owned by the same worker, and we still have $\mathbb{L}(s^l) < \mathbb{L}(s^d)$. If $l \neq d$, we have $c_d \geq c_l > c^l$, and we obtain $\mathbb{L}(s^l) < \mathbb{L}(s^d)$. Thus, we obtain $\hat{T}^+ \subset T^+$ and $u^l \leq u^*$. Services in $F^+ \cup F^-$ are unchanged. No service s^d in F^- could be moved before s^l ; this is because the cost-to-benefit ratio of s^d is unchanged, and

$$\frac{w_d^* u_d^*}{c_d^*} \leq \frac{w_l^* u_l^*}{c_l^*} \leq \frac{w_l^* u^l}{c^l}. \quad (12)$$

Therefore, we obtain $\widehat{F}^+ \subset F^+$. Furthermore,

$$\begin{aligned}
\frac{c'}{w_i^* u_i^*} &< \frac{c_s^*}{w_i^* u_i^*} \\
&\leq \frac{B}{(1 + \ln|\mathcal{M}|) \sum_{i < l} w_i^* u_i^*} \\
&= \frac{B}{(1 + \ln|\mathcal{M}|) \sum_{(s' \in (T^+ \cup F^+ \cup S^+))} w_i^* u_i^*} \\
&= \frac{B}{(1 + \ln|\mathcal{M}|) (w_i^* \mathcal{A}_{wm}(|F^+| + 1) + \sum_{s' \in F^+} w_i^* u_i^*)} \\
&\leq \frac{B}{(1 + \ln|\mathcal{M}|) (w_i^* \mathcal{A}_{wm}(|\widehat{F}^+| + 1) + \sum_{s' \in \widehat{F}^+} w_i^* u_i^*)}. \tag{13}
\end{aligned}$$

Thus, each service will be allocated with a lower cost declaration, and the monotonicity achieved.

Through the greedy selecting principle, we get a candidate set, denoted by M_k . Unfortunately, M_k could not provide any lower bound guarantee, if we regard M_k as the winners. We consider another feasible candidate solution, s^* which is the single service with the highest marginal utility, i.e., $s^* = \arg \max_{s' \in \mathcal{M}} (w_i u_i / c_i) \cdot \{s^*\}$, is a possible solution. In order to get a bounded approximation ratio, we will compare these two sets, M_k and $\{s^*\}$, and select the one with higher utility. We have the following theorem.

Theorem 4. Let $\text{OPT}_{wm}(B, M)$ denote the optimal solution for the weighted mean model, i.e., $\text{OPT}_{wm}(B, \mathcal{M}) \leq (3 + 21\ln|\mathcal{M}|) \times \max \{\mathcal{A}_{wm}(\{s^*\}), \mathcal{A}_{wm}(M_k)\}$.

Sort workers like \mathbb{L} . We use l to present the largest index such that $\sum_{i=1}^l c_i < B$. For analysis convenience, we add a new virtual worker v with a single service s^v , who reports his cost $c_v = B - \sum_{i=1}^l c_i$ and his utility is $u^v = \mathcal{A}_{wm}(s^v) = ((B - \sum_{i=1}^l c_i) / (c_l + 1)) (\mathcal{A}_{wm}(M_{l+1}) - \mathcal{A}_{wm}(M_l))$. Obviously, the optimal result over all workers in $\mathcal{M}^+ = \mathcal{M} \cup s^v$ is higher than the optimal result from all workers in \mathcal{M} . Through greedy selection principle, the first l workers will be chosen in both \mathcal{M}^+ and \mathcal{M} . In the rest of the proof, we will index service s^v as s_{l+1} .

Due to the optimality, we have

$$\mathcal{A}_{wm}(M_{l+1}) = \sum_{i=1}^l w_i^* u_i^* + w_{l+1}^* u^v \geq \text{OPT}_{wm}(B, M). \tag{14}$$

Next, $\mathcal{A}_{wm}(M_{l+1})$ will be regarded as the benchmark for analysis. Since all workers are sorted in decreasing order of their benefit-to-cost ratio, for each $i \in [k+1, \dots, l+1]$, we get

$$\frac{w_i^* u_i^*}{c_i^*} \leq \frac{w_{k+1}^* u_{k+1}^*}{c_{k+1}^*}. \tag{15}$$

Combining the above inequalities, which imply

$$\begin{aligned}
\frac{c_{k+1}^*}{w_{k+1}^* u_{k+1}^*} \sum_{i=k+1}^{l+1} w_i^* u_i^* &= \frac{c_{k+1}^*}{w_{k+1}^* u_{k+1}^*} (\mathcal{A}_{wm}(M_{l+1}) - \mathcal{A}_{wm}(M_k)) \\
&\leq \sum_{i=k+1}^{l+1} c_i^* \leq B. \tag{16}
\end{aligned}$$

Then, we obtain

$$c_{k+1}^* \leq B \cdot \frac{w_{k+1}^* u_{k+1}^*}{\mathcal{A}_{wm}(M_{l+1}) - \mathcal{A}_{wm}(M_k)}. \tag{17}$$

Based on the concept of notation k , we obtain

$$c_{k+1}^* > \frac{B}{(1 + \ln|\mathcal{M}|)} \cdot \frac{w_{k+1}^* u_{k+1}^*}{\mathcal{A}_{wm}(M_{k+1})}. \tag{18}$$

From inequalities (17) and (18), we know

$$\mathcal{A}_{wm}(M_{l+1}) - \mathcal{A}_{wm}(M_k) < (1 + \ln|\mathcal{M}|) \mathcal{A}_{wm}(M_{k+1}). \tag{19}$$

Thus, we have

$$\begin{aligned}
\mathcal{A}_{wm}(M_{l+1}) &= \mathcal{A}_{wm}(M_{l+1}) - \mathcal{A}_{wm}(M_k) + \mathcal{A}_{wm}(M_k) \\
&< (1 + \ln|\mathcal{M}|) \mathcal{A}_{wm}(M_{k+1}) + \mathcal{A}_{wm}(M_k) \\
&\leq (1 + \ln|\mathcal{M}|) \mathcal{A}_{wm}(s^*) + (2 + \ln|\mathcal{M}|) \mathcal{A}_{wm}(M_k). \tag{20}
\end{aligned}$$

Finally, we get

$$\begin{aligned}
\text{OPT}_{wm}(B, \mathcal{M}) &\leq \text{OPT}_{wm}(B, \mathcal{M}^+) \\
&\leq \mathcal{A}_{wm}(M_{l+1}) \\
&\leq (3 + 21\ln|\mathcal{M}|) \max \{\mathcal{A}_{wm}(s^*), \mathcal{A}_{wm}(M_k)\}. \tag{21}
\end{aligned}$$

However, one can show that simply selecting $\max \{\mathcal{A}_{wm}(\{s^*\}), \mathcal{A}_{wm}(M_k)\}$ would violate incentive compatibility. To address this issue, we further design Algorithm 1 to ensure the monotonicity, in which the total cost is bounded by $B/(1 + \ln|\mathcal{M}|)$. Therefore, we remove the services with costs larger than $B/(1 + \ln|\mathcal{M}|)$, indexed by $M(B/(1 + \ln|\mathcal{M}|))$. Different from the previous greedy algorithm, we compare $\mathcal{A}_{wm}(s^*)$ with the optimal solution for the set M_- with budget $B/(1 + \ln|\mathcal{M}|)$, where $M_- = \mathcal{M} \setminus (\{s^*\} \cup M_{B/(1 + \ln|\mathcal{M}|)})$. Algorithm 1 will compare $\text{OPT}(B/(1 + \ln|\mathcal{M}|), M_-)$ with $3 \mathcal{A}_{wm}(s^*)$ to determine the final outcome.

Lemma 5. Algorithm 1 is monotone.

Proof. We prove this lemma through contradiction. With a cost vector \vec{c} , we assume there exists a winner $i \in \mathcal{M}$ with a single service such that he is not allocated when

```

1: Input: a set of workers  $N$  from  $r$  microregions with total  $\mathcal{M}$  service available, a budget  $B$  and a bidding profile  $\mathbf{b}$ ;
2: Output: a set of winning worker  $M^*$ 
3:  $M_k \leftarrow 0$ ;
4:  $s^* \leftarrow \arg \max_{s^i \in M} (w_i u_i / c_i)$ ;
5: while  $\mathcal{M} \setminus M_k$  and  $c_{i^*} \leq (B/(1 + \ln |\mathcal{M}|)) \times (w_{i^*}^* u_{i^*}^* / \mathcal{A}_{wm}(s^{i^*} \cup M_k))$  do
6:    $M_k \leftarrow M_k \cup s^{i^*}$ ;
7:    $s^{i^*} \leftarrow \arg \max_{\mathcal{M} \setminus (M_k^*)} (w_i^* u_i^* / c_i^*)$ 
8: end while
9:  $M^- \leftarrow \mathcal{M} \setminus (\{s^*\} \cup M_{B/(1 + \ln |\mathcal{M}|)})$ ;
10:  $\text{OPT}(B/(1 + \ln |\mathcal{M}|), M_-) \leftarrow$  optimal solution for the set  $M_-$  with budget  $B/(1 + \ln |\mathcal{M}|)$ ;
11: if  $\text{OPT}(B/(1 + \ln |\mathcal{M}|), M_-) \geq 3\mathcal{A}_{wm}(s^{i^*})$  then
12:    $M^* \leftarrow M_k$ 
13: else
14:    $M^* \leftarrow s^*$ 
15: end if

```

ALGORITHM 1: Task allocation algorithm ($\mathcal{TA}(B, M)$).

declaring $c_i' \leq c_i$. The lemma will be analyzed from two conditions:

- (1) If $M^* = s^*$, then we have $\text{OPT}(B/(1 + \ln |\mathcal{M}|), M_-) \leq 3\mathcal{A}_{wm}(s^*)$. Due to the fact that the cost of the owner of s^* will not change $\text{OPT}(B/(1 + \ln |\mathcal{M}|), M_-)$ and $\mathcal{A}_{wm}(s^*)$, s^* will still be allocated if s^* 's owners reported cost changes
- (2) If $M^* = M_k$, then it implies that $\text{OPT}(B/(1 + \ln |\mathcal{M}|), M_-) > 3\mathcal{A}_{wm}(s^{i^*})$. $\text{OPT}(B/(1 + \ln |\mathcal{M}|), M_-)$ increases as i 's reported cost decreases. Furthermore, i ranks higher in \mathbb{L} , since $c_i' < c_i$. Assume the update index in new \mathbb{L} , $j \leq i$. According to the symmetrical submodularity of $\mathcal{A}_{wm}(\cdot)$, the incremental value of service at i is lower than that at j , i.e., $w_j^* u_j^* \geq w_i^* u_i^*$. We obtain $\mathcal{A}_{wm}(M_{i-1} \cup \{i\}) \geq \mathcal{A}_{wm}(M_{j-1} \cup \{j\})$. Then, we have

$$\begin{aligned}
c_i' < c_i &\leq \frac{B}{(1 + \ln |\mathcal{M}|)} \times \frac{w_i^* u_i^*}{\mathcal{A}_{wm}(M_{i-1} \cup \{i\})} \\
&\leq \frac{B}{(1 + \ln |\mathcal{M}|)} \times \frac{w_j^* u_j^*}{\mathcal{A}_{wm}(M_{i-1} \cup \{i\})}.
\end{aligned} \tag{22}$$

Thus, it does not violate the budget constraint, and the worker i will still be in the solution set. The above conclusion implies that the worker i will still be selected as a winner when he decreases his bid. Thus, the allocating scheme is monotone.

Now, we move to our payment scheme which is presented in Algorithm 2. The basic idea of the payment scheme can be summarized as follows. If $M^* = s^*$, we pay s^* 's owner B . If $M^* = M_k$, we sort workers in region $r(i)$ in nondecreasing order of their bids. Let y denote the position of worker i . Then, remove all service from worker i and sort the remain-

ing units to the sequence \mathbb{L}' according to the benefit-to-cost ratio. Then, for each worker j in the region $r(i)$, we index the first and the last of its service in \mathbb{L}' as f_j and l_j . According to Lemma 2, we obtain

$$\begin{aligned}
L' = f_1 < l_1 < f_2 < l_2 < \dots < f_{y-1} < l_{y-1} \\
< f_{y+1} < l_{y+1} < \dots < f_{|h|} < l_{|h|},
\end{aligned} \tag{23}$$

where $|h|$ denotes the number of workers in region h . Thus, the threshold could be found between these intervals

$$\left(f_{y-1}, \dots, l_{y+1}\right], \left(f_{y+1}, \dots, l_{y+2}\right], \left(f_{y+2}, \dots, l_{y+3}\right], \dots, \tag{24}$$

and the search for the largest value worker i could be reported, which could make s^i be positioned next to one of the unit intervals and be selected. Based on worker i 's current reported cost information, we will insert unit s^i to the interval $(f_{y-1}, \dots, l_{y+1}]$ and be selected. Worker i must report the cost lower in order to move s^i to some earlier intervals. So the search could begin at the interval $(f_{y-1}, \dots, l_{y+1}]$.

We can show that the payment for the selected workers can be bounded.

Lemma 6. *If s^i is selected, $c_i \leq B/(1 + \ln |\mathcal{M}|)\mathbb{L}(s^i)$.*

Proof. We assume that the mechanism will select first k services, i.e., $\{s^1, \dots, s^k\}$, in \mathbb{L} . We then resort these k services in nonincreasing order of their benefit-to-cost ratio, as $\{s_1^+, \dots, s_k^+\}$. Let s^{j^+} 's incremental contribution as u_j^+ . We use $c_{s_j^+}$ and $w_{r(s_j^+)}$, as c_j^+ and w_j^+ for short.


```

1: Input: a set of workers  $N$  from  $r$  microregions with total  $M$  service available, a budget  $B$  and a bidding profile  $b$ , and a set of winning worker  $M^*$ ;
2: Output: a payment profile of workers  $\vec{p}$ ;
3:  $\vec{p} \leftarrow 0$ ;
4: if  $M^* = \{s^*\}$  then
5:    $p^* \leftarrow B$ 
6:   return  $\vec{p}$ ;
7: else
8:   while  $i \in M^*$  do
9:     1. Order the workers in region  $h$  as  $\{n_1, n_2, \dots, n_{|h|}\}$  according to increasing cost bid, let  $y$  satisfy  $n_y = i$ ;
10:    2. Order all services except from worker  $i$ , according to decreasing benefit-to-cost ratio, as  $\mathbb{L}' = \{s^1, \dots, s^{|\mathcal{M} \setminus \Phi_i|}\}$ ;
11:    3. For each  $j \in [|\mathcal{M}'|] \setminus \{y\}$ , get the first unit  $f_j$  and last unit  $l_j$ ;
12:    4. Get the last position  $k'$  s.t.  $(c'_k/w'_k, u'_k) \leq B/(1 + \ln |\mathcal{M}'|) \sum_{y \leq k'} w'_y u'_y$ ;
13:     $l_0 = 0$ ;  $k = l_{y-1} + 1$ ;  $z = 1$ ;  $S = \emptyset$ ;
14:    while  $k \leq k' + 1$  do
15:      if  $k = f_{y+z} + 1$  then
16:         $k = l_{y+z}$ ;  $z++$ ;
17:      else
18:         $\Gamma = \sum_{j=1}^{y-1} |s^j| + \sum_{j=2}^z |s^{y+j-1}| + j$ ;
19:         $\delta = \mathcal{A}_{wm}(\Gamma) - \mathcal{A}_{wm}(\Gamma - 1)$ 
20:         $t = \min \{\delta(c'_k/w'_k, u'_k), (B\delta/(1 + \ln |\mathcal{M}'|))(1/\sum_{i \leq k-1} u'_i + l_{\Gamma-j+1} + \dots + l_\Gamma)\}$ 
21:         $S = S \cup \{t\}$ ;  $k++$ ;
22:      end if
23:    end while
24:    5.  $p_i \leftarrow$  the max value in  $S$ 
25:  end while
26:  return  $\vec{p}$ ;
27: end if

```

ALGORITHM 2: Payment algorithm ($\mathcal{P}(B, M)$).

We assume that $\exists 1 \leq e \leq k$ satisfying $c_e^+ > B/(1 + \ln |\mathcal{M}'|)e$, then

$$\begin{aligned}
\frac{c_k^*}{w_k^* u_k^*} &\leq \frac{B}{(1 + \ln |\mathcal{M}'|) \sum_{j \leq k} w_j^* u_j^*} \\
&= \frac{B}{(1 + \ln |\mathcal{M}'|) \sum_{j \leq k} w_j^+ u_j^+} \\
&\leq \frac{B}{(1 + \ln |\mathcal{M}'|) \sum_{i \leq e} w_i^+ u_i^+} \\
&\leq \frac{B}{(1 + \ln |\mathcal{M}'|) e \cdot w_e^+ u_e^+}.
\end{aligned} \tag{25}$$

Furthermore, we have $B < (1 + \ln |\mathcal{M}'|)e \cdot c_e^+$ and so

$$\frac{B}{(1 + \ln |\mathcal{M}'|) e \cdot w_e^+ u_e^+} < \frac{c_e^+}{w_e^+ u_e^+}. \tag{26}$$

Combining these two inequalities, we have

$$\frac{c_k^*}{w_k^* u_k^*} < \frac{c_e^+}{w_e^+ u_e^+}. \tag{27}$$

It is a contradiction, because $\mathbb{L}(s^k) < \mathbb{L}(s^e)$ in \mathbb{L} , and therefore, s^k cannot be selected.

With the previous lemma, we still do not know whether worker i could report $c' > B/(1 + \ln |\mathcal{M}'|)\mathbb{L}(s^i)$ and get a new position index $\mathbb{L}'(s^i)$, and make s^i win.

Lemma 7. *The threshold reported cost ϵ_i for a single service s^i is bounded by $B/(1 + \ln |\mathcal{M}'|)\mathbb{L}(s^i)$.*

Proof. Suppose $\exists s^{e+}$, $e \leq k$, and $\epsilon_e > B/(1 + \ln |\mathcal{M}'|)e$. So, worker i_e^+ could report a higher cost c' to satisfy $(B/(1 + \ln |\mathcal{M}'|)e) < c' < \epsilon_e$ and make s^{e+} be selected. Now, assume worker i_e^+ bid c' and let u' be the incremental value of unit s^{e+} in such a case. Obviously, we have $u' \leq u_e^+$, and

$$\frac{c'}{w_e^+ u'} \geq \frac{c'}{w_e^+ u_e^+} > \frac{B}{(1 + \ln |\mathcal{M}'|) e \cdot w_e^+ u_e^+} \geq \frac{c_k^*}{w_k^* u_k^*}. \tag{28}$$

For any s^{j+} where $j < e$ (the unit used to rank ahead unit s^{e+} in the greedily sorted list), Let u'_j index its new incremental contribution as u'_j and new reported cost as c'_j . There could be

1: **for** each microregion j **do**
 2: Run task allocation $\mathcal{TA}(B/r, M_j)$ under budget B/s and M_j ;
 3: Run worker compensation $\mathcal{P}(B/r, M_j)$ under budget B/s .
 4: **end for**
 5: Aggregate the outcome from each microregion.

ALGORITHM 3: Maximin mechanism.

3 cases for the relations of the items of s^{j+} and s^{e+} , which are as follows:

Case 1 (belong to the same worker). By the lexicographical rule, $\mathbb{L}(s^{j+}) < \mathbb{L}(s^{e+})$ still holds in \mathbb{L} , and thus, $u'_j > u'$.

Case 2 (belong to different workers in the same region). Since $u_j^+ \geq u_e^+$, $c_j^+ \leq c_e^+$, and therefore,

$$c'_j = c_j^+ \leq c_e^+ \leq c'. \quad (29)$$

Case 3 (belong to different regions). It is trivial to have $u'_j = u_j^+$ and $c'_j = c_j^+$, and thus,

$$\frac{c'_j}{u'_j w_j^+} = \frac{c_j^+}{u_j^+ w_j^+} \leq \frac{c_k^*}{u_k^* w_k^*} < \frac{c'}{u' w_e^+}. \quad (30)$$

Moreover, we have $u'_j = u_j^+ \geq u_e^+ \geq u'$.

It is obvious to know in all 3 cases, service s^{j+} will be selected and be ranked before s^{e+} in \mathbb{L} . We denote e' as the unit s^{e+} 's new position index. We have $e' \geq e$, and thus,

$$c' > \frac{B}{(1 + \ln |\mathcal{M}|)e} \geq \frac{B}{(1 + \ln |\mathcal{M}|)e'}. \quad (31)$$

According to Lemma 6, s^{e+} could not be selected, and we have a contradiction. Based on the previous lemma, we can get the upper bound for total threshold payment of all the selected units directly.

Lemma 8. *The payment to all workers in worker compensation algorithm is upper bounded by B .*

Proof. By Lemma 7, the threshold payment is

$$\begin{aligned} \sum_{e=1}^k e_i &\leq \sum_{e=1}^k \frac{B}{(1 + \ln |\mathcal{M}|)e} \leq \sum_{e=1}^{|\mathcal{M}|} \frac{1}{e} \frac{B}{(1 + \ln |\mathcal{M}|)} \\ &\leq (1 + \ln |\mathcal{M}|) \frac{1}{(1 + \ln |\mathcal{M}|)} B. \end{aligned} \quad (32)$$

That is, it is upper bounded by B .

Now, we have the following theorem.

Theorem 9. *The weighted mean mechanism is truthful, budget feasible, individual rational and tractable.*

Proof. Truthful: based on Lemma 1, 5, and 6, we conclude that reporting truthful cost is a dominant strategy for each worker.

Individual rational: the worker whose cost is larger than B will be removed directly. Therefore, if $M^* = s^*$, the individual rational is obvious. For the case of $M^* = M_k$, the payment to each worker is the sum of the threshold bid of his procured services, which is larger than his bid unit cost. *Budget feasible:* from Lemma 8, we can assure the property of being budget feasible. *Computationally efficient:* it is obvious that the task allocation algorithm and payment algorithm can be computed in a polynomial time.

Theorem 10. *Weighted mean multiunit multiregion budget-feasible mechanism achieves a constant ratio approximation: $(4 + 3 \ln |M|)$.*

Proof. Drawing from the proof of Theorem 4, we obtain $\text{OPT}(B/(1 + \ln |\mathcal{M}|), M_-) \leq 3 \times \max \{\mathcal{A}_{wm}(\{s^*\}), \mathcal{A}_{wm}(M_k)\}$. There are two cases. If $\text{OPT}(B/(1 + \ln |\mathcal{M}|), M_-) \geq 3 \times \mathcal{A}_{wm}(s^*)$, from above inequality, we have $\mathcal{A}_{wm}(M_k) \geq \mathcal{A}_{wm}(\{s^*\})$. Based on Theorem 4, we have $\text{OPT}_{wm}(B, M) \leq (3 + 2 \ln |M|) \times \mathcal{A}_{wm}(M_k)$. Then, we have the expected approximation ratio. Otherwise, if $\text{OPT}(B/(1 + \ln |\mathcal{M}|), M_-) < 3 \times \max \mathcal{A}_{wm}(\{s^*\})$; in this case, we get

$$\begin{aligned} \text{OPT}_{wm}(B, \mathcal{M}) &= \text{OPT}_{wm}(B, \mathcal{M}^-) + \mathcal{A}_{wm}(\{s^*\}) \\ &\leq (1 + \ln |\mathcal{M}|) \times \text{OPT}_{wm}\left(\frac{B}{(1 + \ln |\mathcal{M}|)}, M^-\right) \\ &\quad + \mathcal{A}_{wm}(\{s^*\}) \\ &\leq 3(1 + \ln |\mathcal{M}|) \mathcal{A}_{wm}(\{s^*\}) + \mathcal{A}_{wm}(\{s^*\}) \\ &= (4 + 3 \ln |\mathcal{M}|) \times \mathcal{A}_{wm}(\{s^*\}). \end{aligned} \quad (33)$$

4. Minimum Maximization

In the weighted mean model, the buyer will perform a single auction to allocate tasks and compensate workers from all micro-regions. However, in the maximin, the buyer will allocate budget B/r to each microregion and perform mechanism in each microregion in parallel. Let $M_j = \cup_{i \in N, r(i)=j} \Phi_i$ index services could be provided in microregion j . The maximin mechanism is referred to Algorithm 3.

Theorem 11. *Maximin mechanism is truthful, budget feasible, individual rational, and computationally efficient.*

Since mechanisms performed in each microregion are truthful, budget feasible, individual rational, computationally efficient, and independent from each other, multiregion maximin mechanism is also truthful, budget feasible, individual rational, and computationally efficient.

Corollary 12. *With payment algorithm $\mathcal{P}(B/r, M_j)$ and task allocation algorithm $\mathcal{T}\mathcal{A}(B/r, M_j)$, the mechanism will achieve a constant approximation ratio $4 + 3\ln M_j$, in a single microregion j .*

Proof. Trivial: the setting in a microregion j can be regarded as a special case of weighted multiregion setting with $r = 1$ and $w_j = 1, j \in [r]$.

Use $\text{OPT}_j(B, M_j)$ to index the optimal result for the M_j with budget B in a single microregion j . Let us make these following observations on the optimal solutions in microregion j .

Lemma 13. *$\text{OPT}_j(B, M_j)$ is nondecreasing with B .*

Lemma 14. *$\text{OPT}_j(B, M_j)/B$ is nonincreasing with B between $(0, +\infty]$.*

Lemma 15. *For any $B, M_j, \epsilon \in [0, 1]$, $\text{OPT}_j(\epsilon B, M_j) \geq \epsilon \text{OPT}_j(B, M_j)$.*

Proof. For the set M_j , if B increases, more service will be procured. However, the incremental value is nonincreasing under B . So the payment for unit service will be higher, as B increases. It implies that $\text{OPT}_j(B, M_j)/B$ is nonincreasing with B , and we get

$$\frac{\text{OPT}_j(B, M_j)}{B} \leq \frac{\text{OPT}_j(\epsilon B, M_j)}{\epsilon B} \Rightarrow \epsilon \text{OPT}_j(B, M_j) \leq \text{OPT}_j(\epsilon B, M_j). \quad (34)$$

Let B_{\max} be the largest amount of the budget that the buyer used in a microregion in $\text{OPT}_{mm}(B, M)$. Let β index the B/B_{\max} . The $1/\beta$ denotes the largest fraction of total budget allocated for a microregion in $\text{OPT}_{mm}(B, M)$, intuitively. We use k_j^* to denote the total service procured in microregion j in the optimal result $\text{OPT}_{mm}(B, \mathcal{M})$.

Theorem 16. *In the maximin model, the mechanism achieves a constant approximation ratio: $r(4 + 3 \ln |\mathcal{M}|)/\beta$*

Proof. Based on the definition of the maximin problem, we get

$$\mathcal{A}_{mm}(B, \mathcal{M}) = \min([\mathcal{A}(k_1), \dots, \mathcal{A}(k_r)], \quad (35)$$

$$\text{OPT}_{mm}(B, \mathcal{M}) = \min(\mathcal{A}(k_1^*), \dots, \mathcal{A}(k_r^*)). \quad (36)$$

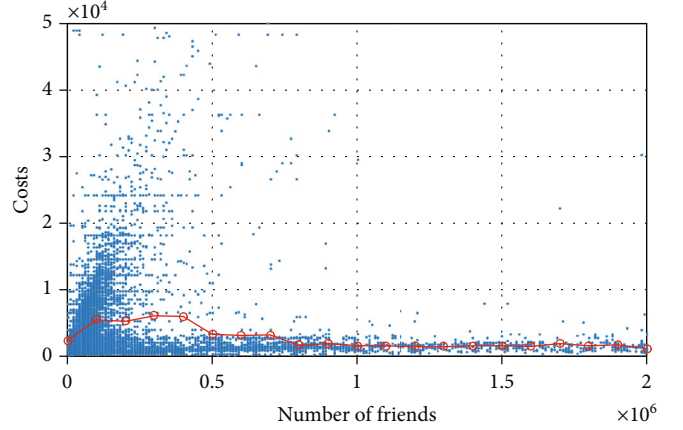


FIGURE 2: Cost information with numbers of friends.

Since the single-region performance is guaranteed in Corollary 12, we obtain

$$\begin{aligned} \mathcal{A}(k_j) &\geq \frac{1}{4 + 3 \ln M_j} \text{OPT}_j\left(\frac{B}{r}, M_j\right) \\ &\geq \frac{1}{4 + 3 \ln |\mathcal{M}|} \text{OPT}_j\left(\frac{B}{r}, M_j\right). \end{aligned} \quad (37)$$

Since we have known

$$B_j \leq \frac{B}{\beta}, \quad (38)$$

and the conclusions of Lemma 13, 14, and 15, we obtain

$$\text{OPT}_j\left(\frac{B}{r}, M_j\right) \geq \beta \text{OPT}_j\left(\frac{B/\beta}{r}, M_j\right) \geq \beta \text{OPT}_j\left(\frac{B_j}{r}, M_j\right). \quad (39)$$

Thus, we have

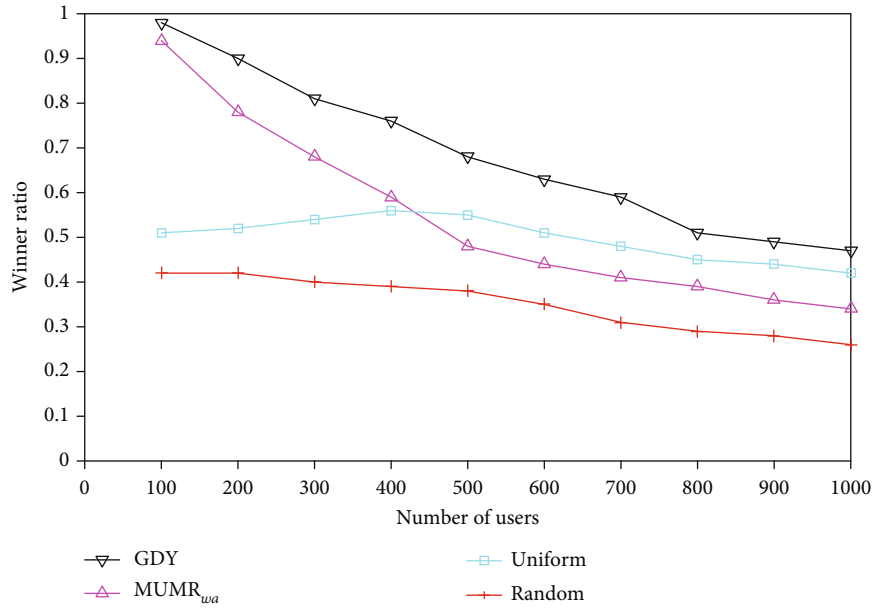
$$\mathbb{E}[\mathcal{A}(k_j)] \geq \frac{1}{4 + 3 \ln |\mathcal{M}|} \beta \text{OPT}_j\left(\frac{B_j, M_j}{r}\right). \quad (40)$$

Then, we have

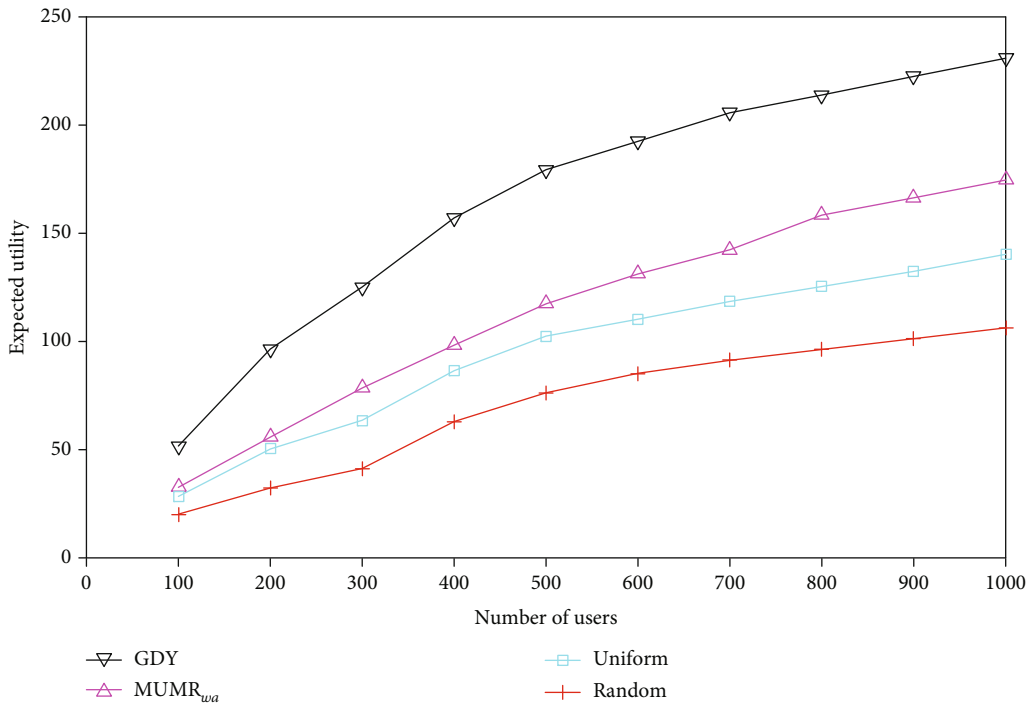
$$\begin{aligned} \mathcal{A}_{mm}(B, \mathcal{M}) &\geq \min_j \left(\frac{1}{4 + 3 \ln |\mathcal{M}|} \beta \text{OPT}_j\left(\frac{B_j, M_j}{r}\right) \right) \\ &\geq \frac{\beta}{(4 + 3 \ln |\mathcal{M}|)r} \min_j (\text{OPT}_j(B_j, M_j)) \\ &\geq \frac{\beta}{(4 + 3 \ln |\mathcal{M}|)r} \text{OPT}_{mm}(B, \mathcal{M}). \end{aligned} \quad (41)$$

5. Simulations

5.1. Simulation Setup. It is hard to get the bidding data of workers directly; thus, it is necessary for us to infer the cost profile via historical cost information. Drawing from [30],

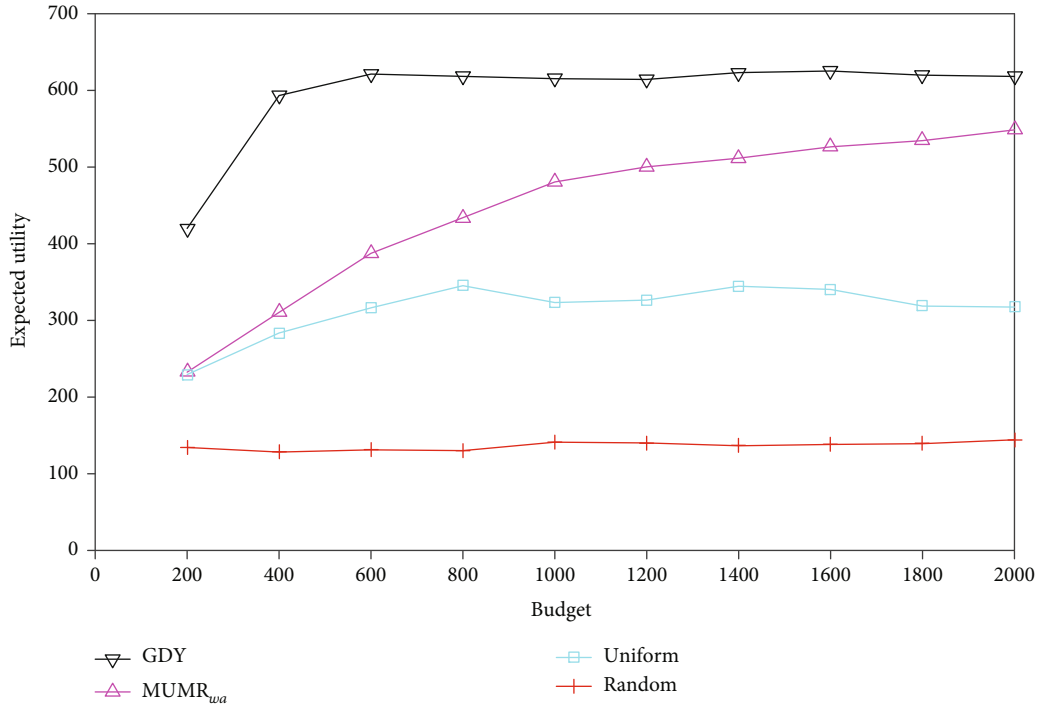


(a) Winner ratio



(b) Utility

FIGURE 3: Continued.



(c) Utility

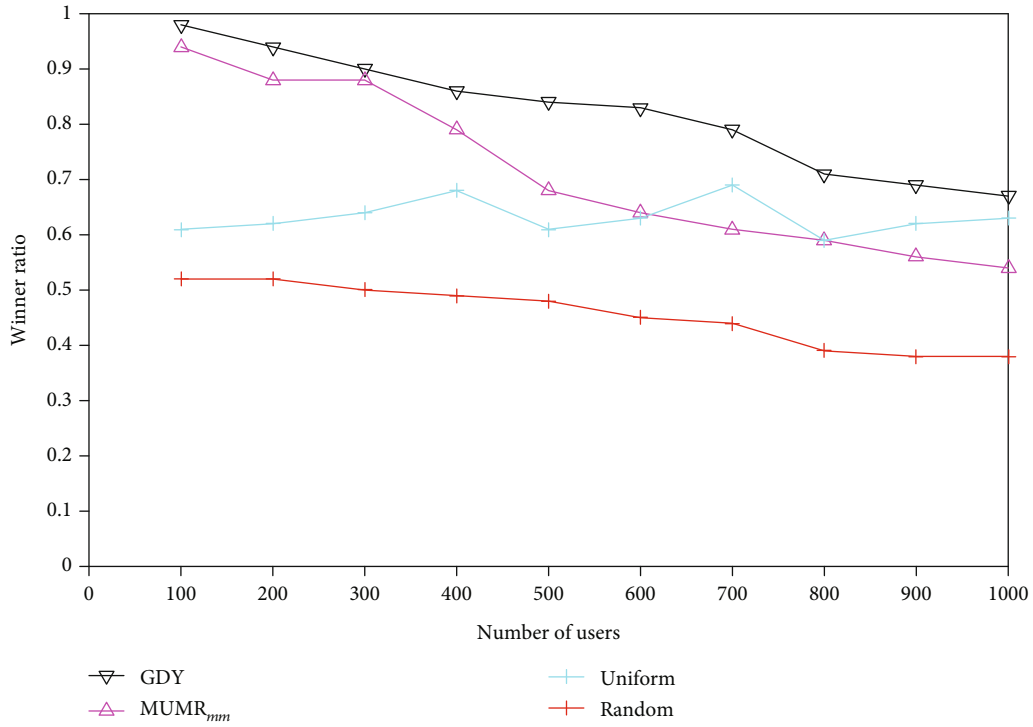
FIGURE 3: Results on weighted mean model.

we will estimate workers' cost information on a website, called weiboyi (<http://www.weiboyi.com>), which is for social advertising. In the website, advertisers are required to post their desired compensation to advertise to fans in the Weibo. From Figure 2, we show the cost information of 15012 advertisers. The range of their reported cost is from 0 to $5 * 10^4$, and the range of the number of their friends is from 0 to $2 * 10^6$. We use advertisers' number of friends to simulate workers' capacity. The cost information of advertisers will be normalized to (0,5) and the number of friends to [0,2]. The data set generation process is to select an instance in weiboyi data set and use the c_a/m_f for the worker's cost and the normalized number of friends for workers' capacity iteratively, in which c_a denotes the advertiser's normalized cost and m_f indexes the advertiser's normalized number of friends. We set crowdsourcer's utility $\mathcal{A}(k)$ (in a single region) with three symmetrical submodular functions, where $\mathcal{A}(k) = k^{0.9}$, $\mathcal{A}(k) = k$, and $\mathcal{A}(k) = \sum_{i=1}^k 100/(100+k)$. We consider the a service subscriber wants to hire workers from 6 microregions. To obtain statistically 330 sound results, we run the simulation 1000 rounds for each parameter setting, and the microregion weight will be randomized in each round of experiments.

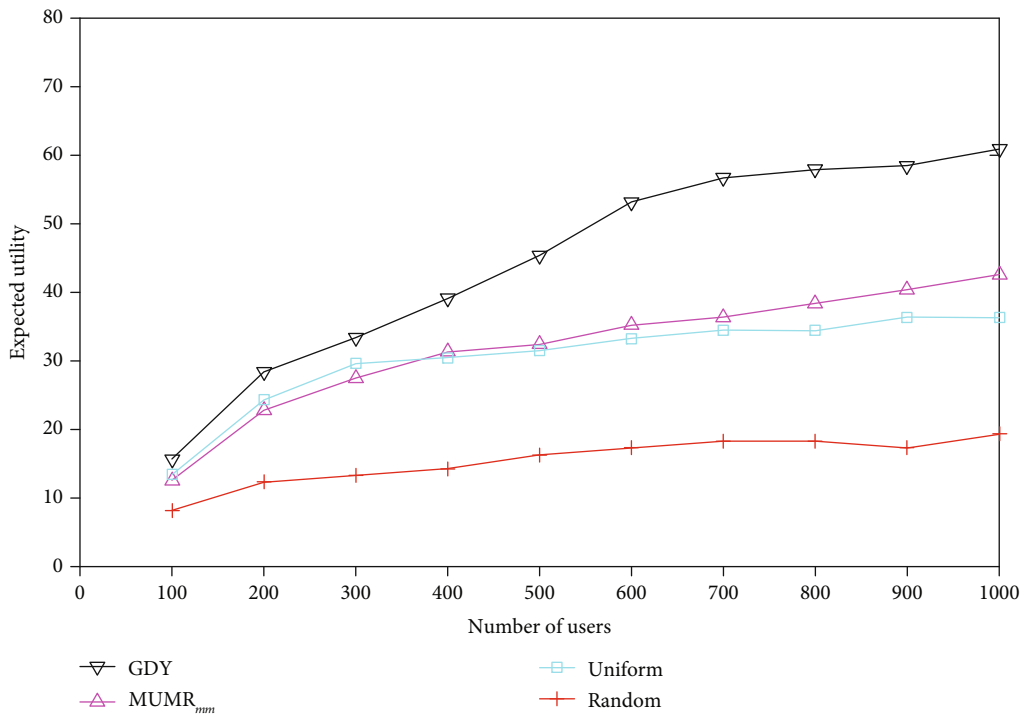
5.2. Benchmarks. We compare our designed auctions (MUMR_{wm} and MUMR_{mm} for two models) with 3 baselines. The first benchmark is the greedy algorithm, which will return the optimal solution. The greedy algorithm is not truthful and has full information of workers' costs. The sec-

ond benchmark is a uniform-price mechanism which is near-optimal, which is introduced in [31]. The last one is a random selecting algorithm. The mechanism chooses workers randomly and payoffs to workers are their declared cost, which are the lower bound performance of our designed problem. For maximin, the above three algorithms will be performed in each microregion in parallel with the same budget. We evaluate two performances of our proposed mechanism, crowdsourcer's valuation and winner ratio. The first one means the utility achieved in the entire region. The second one represents the percentage of selected workers over all workers.

5.3. Results. We will present the results of the winner ratio, firstly. Since the simulation results of the three crowdsourcer's valuations are similar, we just present the results of $\mathcal{A}(k) = k^{0.9}$ here. We set the budget at 1000 and the number of workers from 100 to 1000. The results are shown in Figures 3(a) and 4(a) for both two models. We observe that the winner ratio decreases as the number of workers increases. The reason is that the auctions are more competitive with more workers. For the uniform pricing mechanism, the ratio will be stable, since the uniform pricing mechanism will choose a set of workers as the candidates when the scale of workers is relatively small. According Figures 3(b) and 4(b), we can know that the valuation of the buyer when the budget is 500 and the scale of workers is from 100 to 1000. The buyer's utility grows with the increase of workers in all algorithms in both models. With a larger scale of workers, the buyer will utilize the budget



(a) Winner ratio



(b) Utility

FIGURE 4: Continued.

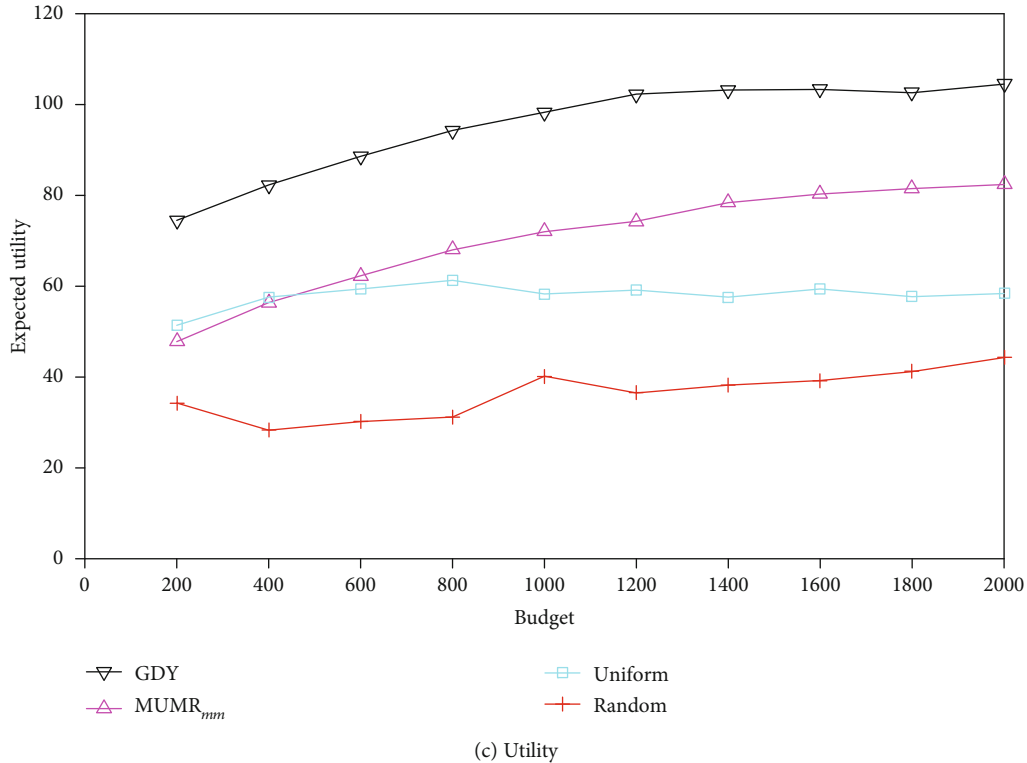


FIGURE 4: Results on maximin model.

more effectively. Our proposed mechanism outperforms random and uniform pricing mechanisms in the weighted mean model. MUMR's performance approaches the performance of the greedy algorithm and uniform pricing mechanism in the maximin model. Figures 3(c) and 4(c) show the service subscriber's valuation when the number of workers is 500 with the budget from 200 to 2000. From the figure, we know that the utility of the buyer increases simultaneously in algorithms MUMR_{wm} and MUMR_{mmm} and greedy algorithm as the budget increases. The reason is that when the budget becomes larger, more workers can be hired. The greedy-based method performs well in the simulation; however, it is not strategy-proof. The performance of the uniform price mechanism approaches the one of MUMR_{wm} and MUMR_{mmm} with the small budget. For the uniform price mechanism, the buyer's valuation decreases as the budget increases. Since the mechanism will infer a threshold payoff based on the workers' cost information, the one selected by the mechanism with larger budget may not be the optimal one.

6. Conclusion

In this work, we introduce and study the multiregion crowdsensing problem and design two models for the multiregion crowdsensing. We propose a novel multiunit budget-feasible mechanism to solve problems. Our designed mechanisms are budget feasible, truthful, and individual rational and have a constant approximation ratio. Extensive simulations demonstrate the effectiveness of our solution.

Data Availability

The data adopted to support the findings of this manuscript are available from all authors upon request.

Conflicts of Interest

The authors declare that there is no conflict of interest regarding the publication of this paper.

Authors' Contributions

Yu Qiao: the contribution of Yu Qiao is to provide the idea of the paper. Also, he finished the proof and wrote the paper. Jun Wu: the contribution of Jun Wu is to improve the idea and help the first author to finish the proof. Hao Cheng: the contribution of Hao Cheng is to conduct the experiments of the paper. Zilan Huang: the contribution of Zihan Huang is to conduct the experiments of the paper. Qiangqiang He: the contribution of Qiangqiang He is to depict the figures in the editable format in the paper after acceptance. Chongjun Wang: the contribution of Chongjun Wang is to improve the idea and help the first author to finish the proof.

Acknowledgments

This paper is supported by the National Key Research and Development Program of China (Grant No. 2016YF-B1001102), the National Natural Science Foundation of China (Grant Nos. 61502227 and 61876080), the Fundamental Research Funds for the Central Universities

(No. 020214380040), and the Collaborative Innovation Center of Novel Software Technology and Industrialization at Nanjing University.

References

- [1] R. K. Ganti, F. Ye, and H. Lei, "Mobile crowdsensing: current state and future challenges," *IEEE Communications Magazine*, vol. 49, no. 11, pp. 32–39, 2011.
- [2] D. Hasenfratz, O. Saukh, S. Sturzenegger, and L. Thiele, "Participatory air pollution monitoring using smartphones," *Mobile Sensing*, vol. 1, pp. 1–5, 2012.
- [3] S. Hu, L. Su, H. Liu, H. Wang, and T. F. Abdelzaher, "SmartRoad," *ACM Transactions on Sensor Networks*, vol. 11, no. 4, pp. 1–27, 2015.
- [4] R. Gao, M. Zhao, T. Ye et al., "Jig410 saw: indoor floor plan reconstruction via mobile crowdsensing," in *Proceedings of the 20th annual international conference on Mobile computing and networking - MobiCom '14*, pp. 249–260, 2014.
- [5] H. Chan and J. Chen, "Truthful multi-unit procurements with budgets," in *International Conference on Web and Internet Economics*, pp. 89–105, Springer, 2014.
- [6] Y. Zhang, Y. He, J. Wang et al., "Share brings benefits: towards maximizing revenue for crowdsourced mobile network access," in *2017 14th Annual IEEE International Conference on Sensing, Communication, and Networking (SECON)*, pp. 1–9, San Diego, CA, USA, June 2017.
- [7] J. Xu, Z. Rao, L. Xu, D. Yang, and T. Li, "Mobile crowd sensing via online communities: incentive mechanisms for multiple cooperative tasks," in *14th IEEE International Conference on Mobile Ad Hoc and Sensor Systems, MASS 2017*, pp. 171–179, Orlando, FL, USA, October 2017.
- [8] J. Xu, J. Xiang, and Y. Li, "Incentivize maximum continuous time interval coverage under budget constraint in mobile crowd sensing," *Wireless Networks*, vol. 23, no. 5, pp. 1549–1562, 2017.
- [9] X. Yang, T. Wang, X. Ren, and W. Yu, "Copula-based multi-dimensional crowd428 sourced data synthesis and release with local privacy," in *2017 IEEE Global Communications Conference, GLOBECOM 2017*, pp. 1–6, Singapore, December 2017.
- [10] X. Yang, C. Zhao, W. Yu, X. Yao, and X. Fu, "A user incentive-based scheme against dishonest reporting in privacy-preserving mobile crowdsensing systems," in *Wireless Algorithms, Systems, and Applications - 12th International Conference, WASA 2017*, pp. 755–767, Guilin, China, June 2017.
- [11] C. Li, S. Chang, H. Zhu, H. Chen, and T. Lu, "Lotus: evolutionary blind regression over noisy crowdsourced data," in *2018 15th Annual IEEE International Conference on Sensing, Communication, and Networking (SECON)*, pp. 1–9, 2018.
- [12] X. Zhang, Z. Yang, Y. Liu, and S. Tang, "On reliable task assignment for spatial crowdsourcing," *IEEE Transactions on Emerging Topics in Computing*, vol. 7, no. 1, pp. 174–186, 2019.
- [13] H. Jin, L. Su, D. Chen, K. Nahrstedt, and J. Xu, "Quality of information aware incentive mechanisms for mobile crowd sensing systems," in *Proceedings of the 16th ACM International Symposium on Mobile Ad Hoc Networking and Computing*, pp. 167–176, 2015.
- [14] Q. Zhang, Y. Wen, X. Tian, X. Gan, and X. Wang, "Incentivize crowd labeling under budget constraint," in *2015 IEEE Conference on Computer Communications (INFOCOM)*, pp. 2812–2820, 2015.
- [15] X. Zhang, G. Xue, R. Yu, D. Yang, and J. Tang, "Truthful incentive mechanisms for crowdsourcing," in *2015 IEEE Conference on Computer Communications (INFOCOM)*, pp. 2830–2838, 2015.
- [16] L. Gao, F. Hou, and J. Huang, "Providing long-term participation incentive in participatory sensing," in *2015 IEEE Conference on Computer Communications (INFOCOM)*, pp. 2803–2811, 2015.
- [17] Z. Feng, Y. Zhu, Q. Zhang, L. M. Ni, and A. V. Vasilakos, "Trac: truthful auction for location-aware collaborative sensing in mobile crowdsourcing," in *IEEE INFOCOM 2014 - IEEE Conference on Computer Communications*, pp. 1231–1239, Toronto, ON, Canada, April 2014.
- [18] Y. Qiao, J. Wu, L. Zhang, and C. Wang, "Mechanism design for cross-market task crowdsourcing," in *Proceedings of the International Symposium on Quality of Service*, pp. 1–10, June 2019.
- [19] D. Zhao, X.-Y. Li, and H. Ma, "How to crowdsource tasks truthfully without sacrificing utility: online incentive mechanisms with budget constraint," in *IEEE INFOCOM 2014 - IEEE Conference on Computer Communications*, pp. 1213–1221, Toronto, ON, Canada, April 2014.
- [20] T. Liu, Y. Zhu, and L. Huang, "Tgba: a two-phase group buying based auction mechanism for recruiting workers in mobile crowd sensing," *Computer Networks*, vol. 149, pp. 56–75, 2019.
- [21] J. Xu, C. Guan, H. Wu, D. Yang, L. Xu, and T. Li, "Online incentive mechanism for mobile crowdsourcing based on two-tiered social crowdsourcing architecture," in *2018 15th Annual IEEE International Conference on Sensing, Communication, and Networking (SECON)*, pp. 55–63, Hong Kong, China, June 2018.
- [22] J. Xu, S. Yang, W. Lu, L. Xu, and D. Yang, "Incentivizing for truth discovery in edge-assisted large-scale mobile crowdsensing," *Sensors*, vol. 20, no. 3, p. 805, 2020.
- [23] Y. Singer, "Budget feasible mechanisms," in *2010 IEEE 51st Annual Symposium on Foundations of Computer Science*, pp. 765–774, Las Vegas, NV, USA, October 2010.
- [24] N. Chen, N. Gravin, and P. Lu, "On the approximability of budget feasible mechanisms," in *Proceedings of the Twenty-Second Annual ACM-SIAM Symposium on Discrete Algorithms*, pp. 685–699, San Francisco, California USA, January 2011.
- [25] X. Bei, N. Chen, N. Gravin, and P. Lu, "Budget feasible mechanism design: from prior-free to Bayesian," in *Proceedings of the 44th symposium on Theory of Computing - STOC '12*, pp. 449–458, 2012.
- [26] N. Anari, G. Goel, and A. Nikzad, "Mechanism design for crowdsourcing: an optimal 1-1/e competitive budget-feasible mechanism for large markets," in *2014 IEEE 55th Annual Symposium on Foundations of Computer Science*, pp. 266–275, Philadelphia, PA, USA, October 2014.
- [27] Y. Singer, "How to win friends and influence people, truthfully: influence maximization mechanisms for social networks," in *Proceedings of the fifth ACM international conference on Web search and data mining - WSDM '12*, pp. 733–742, 2012.
- [28] T. Horel, S. Ioannidis, and S. Muthukrishnan, "Budget feasible mechanisms for experimental design," in *LATIN 2014: Theoretical Informatics*, pp. 719–730, Springer, 2014.

- [29] R. B. Myerson, "Optimal auction design," *Mathematics of Operations Research*, vol. 6, no. 1, pp. 58–73, 1981.
- [30] L. Zhang, H. Chen, J. Wu, C.-J. Wang, and J. Xie, "False-name-proof mechanisms for path auctions in social networks," in *Proceedings of the Twenty-second European Conference on Artificial Intelligence*, pp. 1485–1492, 2016, IOS Press.
- [31] R. Engelbrecht-Wiggans and C. M. Kahn, "Multi-unit auctions with uniform prices," *Economic Theory*, vol. 12, no. 2, pp. 227–258, 1998.

Research Article

LoRa-Based Smart IoT Application for Smart City: An Example of Human Posture Detection

Jinkun Han ^{1,2}, Wei Song ^{1,3}, Amanda Gozho,¹ Yunsick Sung,⁴ Sumi Ji,⁴ Liangliang Song,⁵ Long Wen,⁶ and Qi Zhang⁷

¹School of Information Science and Technology, North China University of Technology, Beijing 100144, China

²Department of Computer Science, Georgia State University, Atlanta, 30303 GA, USA

³Brunel London School, North China University of Technology, Beijing 100144, China

⁴Department of Multimedia Engineering, Dongguk University-Seoul, Seoul 04620, Republic of Korea

⁵Roadway Smart (Beijing) Technology Co., Ltd., Beijing, China

⁶Beijing Municipal Engineering Research Institute, Beijing, China

⁷Beijing Capital Road Development Group Co., Ltd., Beijing, China

Correspondence should be addressed to Wei Song; sw@ncut.edu.cn

Received 18 May 2020; Revised 13 June 2020; Accepted 15 July 2020; Published 4 August 2020

Academic Editor: Wei Yu

Copyright © 2020 Jinkun Han et al. This is an open access article distributed under the Creative Commons Attribution License, which permits unrestricted use, distribution, and reproduction in any medium, provided the original work is properly cited.

Scientists have explored the human body for hundreds of years, and yet more relationships between the behaviors and health are still to be discovered. With the development of data mining, artificial intelligence technology, and human posture detection, it is much more possible to figure out how behaviors and movements influence people's health and life and how to adjust the relationship between work and rest, which is needed urgently for modern people against this high-speed lifestyle. Using smart technology and daily behaviors to supervise or predict people's health is a key part of a smart city. In a smart city, these applications involve large groups and high-frequency use, so the system must have low energy consumption, a portable system, and a low cost for long-term detection. To meet these requirements, this paper proposes a posture recognition method based on multisensor and using LoRa technology to build a long-term posture detection system. LoRa WAN technology has the advantages of low cost and long transmission distances. Combining the LoRa transmitting module and sensors, this paper designs wearable clothing to make people comfortable in any given posture. Aiming at LoRa's low transmitting frequency and small size of data transmission, this paper proposes a multiprocessing method, including data denoising, data enlarging based on sliding windows, feature extraction, and feature selection using Random Forest, to make 4 values retain the most information about 125 data from 9 axes of sensors. The result shows an accuracy of 99.38% of extracted features and 95.06% of selected features with the training of 3239 groups of datasets. To verify the performance of the proposed algorithm, three testers created 500 groups of datasets and the results showed good performance. Hence, due to the energy sustainability of LoRa and the accuracy of recognition, this proposed posture recognition using multisensor and LoRa can work well when facing long-term detection and LoRa fits smart city well when facing long-distance transmission.

1. Introduction

Modern medical science proves human behaviors influence human health. In this day, people continue in a posture for a long time when working until they get a warning from the body that is tired, which means their bodies already hurt but they are not aware of it. Therefore, people need a reminder to let them know when to change a posture or rest.

On the other hand, for some special groups of people like children or the elderly, supervising their daily activities guarantees basic exercise in a day. To build a smart city, people not only focus on making living and transportation smarter but also wish their health is smartly supervised. With the development of big data [1] and artificial intelligence technology on health [2–4], scientists research more relationships between human daily activities, or postures, and health, to

strengthen people's bodies or prevent diseases. Human posture recognition is also widely used in sports games, health monitoring, sports rehabilitation, sports competitions, and so on [5].

With the rise of hardware, human posture recognition is not only applicable to short-term, fast, real-time recognition based on videos or pictures but is also applicable to long-term posture recognition for specific groups based on IoT (Internet of Things) devices, such as LoRa, ZigBee, and Wi-Fi devices. Considering mobile object, long-distance, and low power requirements, LoRa performs better. At present, there are needs for human posture recognition in the market, but different solutions have some different defects [6], such as high energy consumption, limited space, and network requirements. The long-term posture recognition monitoring needs a large number of transmission nodes, complex transmission network, and high-frequency usage. At the same time, long-term recognition requires that the posture information acquisition module of the system should have the characteristics of low energy consumption, easy to carry, low cost, long transmission distance, and so on, to meet all possible specific needs. Posture recognition based on computer vision can easily obtain the trajectory, contour, and other information of human motion, but the existence of some blind angles and people walking out of the observation range will cause the recognition based on cameras to be less effective. Therefore, the long-term monitoring of the human posture recognition system should also be flexible, not limited to space.

To meet these requirements, this paper proposes a multisensor-based posture recognition system using LoRa (Long Range) [7, 8]. LoRa is a low-power wide-area network (LPWAN) technology, which has the advantages of low power consumption and extra long-range signal transmission [9]. The theoretical coverage of LoRa is 15 km for suburban and 5 km for urban areas [10], in which case, one LoRa gateway is adequate for an organization, like a school or scientific research institution, to deploy a LoRa system.

In this system, wearable multisensor clothing is designed as a LoRa node to make people comfortably wear it without posture limitations while doing any daily activities. The clothing is equipped with a nine-axis IMU (Inertial Measurement Unit) sensor, an Arduino Mega board, and a LoRa shield. The nine-axis IMU sensor consists of an accelerometer [11], an angular speedometer, and a magnetometer. People's daily activities are calculated and recognized by analyzing one group of data obtained by the nine-axis sensor. The LoRa shield transmits datasets to the LoRa gateway and server while the Arduino board connects and controls the LoRa shield and sensors.

The system consists of three parts, the terminal part (LoRa nodes), gateway and server part, and application part. The wearable clothing with a multisensor integrated is regarded as the terminal part to collect daily activity datasets, which include walking, running, going upstairs or downstairs, and standing activities. The gateway and server part is used to transmit and save the datasets in the server. The application is utilized to analyze and show the data to users or managers.

In the terminal part, due to the limited transmission limitation in LoRa technology, this paper proposes a serial method to compress datasets, such as extracting real human activity datasets to form new features like max-min values and the mean and standard deviation to conclude the information of posture data waves to achieve the dimension reduction, using Random Forest algorithm to calculate the importance of features and select the first few important features LoRa nodes required. Then, the LoRa nodes are reset to collect selected features. In the experiment, six machine learning algorithms are utilized to extract the best posture recognition method. Finally, after training 3239 groups of datasets, the result proves that Random Forest performs best with an accuracy of 95.06%. Different users tested the system, and it functioned efficiently. Hence, this paper proves that multisensor posture recognition using IoT and LoRa is available and works well for long-term detection.

The remainder of this paper is organized as follows. Section 2 provides an overview of related work. Section 3 introduces the proposed LoRa posture recognition system based on multisensor. Section 4 evaluates the performance of the proposed system, and Section 5 concludes the paper.

2. Related Work

Wearable sensor design for the healthcare problem should be preventive, predictive, preemptive, and personalized. Advanced smart clothing not only promotes a healthy lifestyle but also allows the detection of any potential health risks and facilitates the implementation of preventive measures at an earlier stage [12]. Aging people who wear such clothes are effectively protected. In the proposed system, the IMU sensor is used in smart clothing. The IMU sensor provides the acceleration, angular velocity, and magnetometer values, which are analyzed to recognize human activities like walking, running, and even falling down [13]. Prathivadi et al.'s team did the research and proved that IMU has good performance on activity recognition [14].

In the healthcare system, the traditional data acquisition methods are Bluetooth, Wi-Fi, and the Internet. Bluetooth has a short distance disadvantage and a low power advantage [15]. Using Wi-Fi or the Internet on a smartphone to get datasets lifts the limit of distances [16], however, requiring high spending and high power. A smartphone is integrated with many devices and functions, which are the main source of power consumption [17], while not detecting the state of health. Besides, the user does not always move about with their smartphone. When using an application on a smartphone, people may experience some serious privacy issues [18].

Nowadays, more medical devices use IoT technology to collect data [19]. Presently, the main IoT technologies utilized in the market are NB-IoT (Narrow Band Internet of Things), ZigBee, Sigfox, and LoRa. NB-IoT communication is authorized to use the frequency band below 1 GHz, which charges companies' money. NB-IoT [20, 21] cannot provide the same battery life as LoRa due to the consideration of service quality. If an organization needs good service, NB-IoT is a good choice while the features of low cost and a large

number of connections are perfect for LoRa service. ZigBee [22, 23] has advanced features of low complexity, low power, and low price but is limited by its transmission range, which is only 10-75 meters. Sigfox [24] has an ultralong transmission distance of 50 km, but to ensure the energy-saving characteristics, the number of daily transmissions will be limited. In comparison with the IoT method, using Kinect [25] or camera [26] is preferred to identify the postures. With this kind of detection based on the image, a blind angle of vision appears, resulting in poor user experience. Using posture detection based on continuous signal data avoids space limitation and visual blind area. Compared to picture or video information, pure digital signal data is easier to encrypt and its representation harder to understand [27, 28]. On the other hand, signal data describes important information in its wave changes [29], which explains why a person stands up after a long time of sitting without the detector's warning. Because there is an average supervision time in the detector, this person feels tired even after sitting for a while. Then, the application adjusts to fit personal habits.

Considering the limitation of LoRa transmission, extracting significant information from multisensor data with a reasonable communication cost becomes a crucial problem. In the study of He et al. [30], their team proposed approximate aggregation to extract significant information. Peng proposed using Random Forest to optimize the characteristic high voltage signal of a PD cable to improve the accuracy and efficiency of PD pattern recognition and visualization of PD parameters [31]. The results show that the calculation of the importance of Random Forest to features is reliable. Hence, this system tries to use Random Forest to select the key features LoRa nodes require. SVM, KNN, and Random Forest have outstanding performance in the classification of human posture [32–34]. For the continuous signal data collected by LoRa nodes, a classifier with the highest accuracy is required to highly improve the accuracy of posture recognition. Due to the limitation of LoRa transmission and too much data compression, the optimal classifier is necessary. Facing current smart cyberphysical systems, the data compression should not only save uploading energy but guarantee privacy [35].

3. Posture Recognition System

3.1. System Framework. The LoRa-based human posture recognition system consists of four modules, posture information sensor module, wireless transmission module, human posture recognition module, and user interface module as color-coded in Figure 1. The terminal device, including the posture information sensor module and LoRa shield, collects the posture datasets and transmits them to the nearest LoRa gateway. After receiving a complete dataset package, the LoRa gateway delivers the datasets to the net server, which saves it. The Random Forest (RF) algorithm then analyzes the datasets and recognizes the postures. Then, the output results are as required by the users' operations.

The posture sensor module consists of an accelerometer, gyroscope, and magnetometer, which are utilized to periodically collect the posture datasets like running, walking, stand-

ing, jumping, and going upstairs or downstairs. The integrated posture information sensor module performs data denoising, data segmentation, and feature extraction automatically. In practice, it is equipped within the clothes as a wearable smart sensor as is shown in Figure 2.

The wireless transmission module is composed of a LoRa shield, gateway, and server. The terminal device combines multisensors and LoRa shield as a mobile detector to collect datasets and transmit the datasets to the LoRa gateway, which is a transfer station and delivers the datasets to the net server. This LoRa-based module can wirelessly transmit data from the terminal node to the server with high quality, low power consumption, and over a long distance. The transmitting process is based on a broadcast protocol, which ensures that users connect to the gateway wherever they are and the devices can upload the datasets automatically.

Before using the human posture recognition module shown in Figure 1, the red rectangle, the server, needs to set up the local recognition application. Because the magnetometer used in the terminal device is influenced by the local buildings and the location of the city, a trained module from other places will not work as efficiently as one from the local environment. Setting a local recognition application needs five steps: collecting local datasets, data preprocessing like denoising and smoothing, feature extraction, training new modules, and resetting the terminal device with the new feature extracted data format. After setting a local module, then when a group of new datasets comes in, users can get local results.

3.2. Posture Information Sensor Module. After analyzing some of the most popular human posture recognition products, the accelerometer, gyroscope, and magnetometer are selected to collect the human activity information. These sensors collect three-axis signal data of the x -, y -, and z -axes. In total, nine types of original signals were collected. The CPU is the Arduino Mega board.

These three sensors detect the values in real-time with a frequency of 25 Hz and have their monitoring value ranges. Every sensor has three axes, x -, y -, and z -axes. In total, the three sensors have nine axes and collect 25 groups of datasets, where every single dataset includes nine digital values, in one second. The Arduino Mega board calculates the max and min values, mean, and standard deviation of 25×5 groups of datasets every 5 seconds. Limited by the signal bandwidth of LoRa, every transmitting interval is approximately 10 seconds. Therefore, every transmission includes two groups of max and min values, the mean, and standard deviation to represent what postures the user is in within these 10 seconds. The terminal node with sensors and Arduino Mega board should be fixed on the user's back or chest to collect points, which are more globally characterized than other limb placements.

3.3. Wireless Transmission Module. LoRa uses linear spread spectrum modulation technology, and its link budget allows the communication distance to be 15 km or higher. However, its signal is blocked by the buildings in cities so its distance usually is 1~2 km in cities. The LoRa network works in

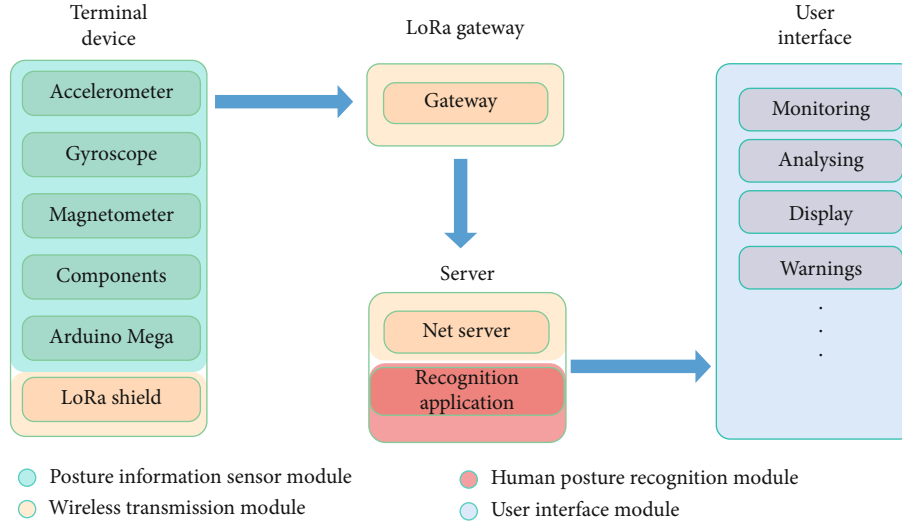


FIGURE 1: Four modules in LoRa posture recognition system.



FIGURE 2: LoRa wearable integrated sensors: (a) the position of a LoRa node on clothing; (b) person wearing the clothing; (c) the clothing inside view.

unlicensed bands such as 433 Hz, 868 Hz, and 915 Hz, and the infrastructure and operating costs of the LoRa WAN are thus low.

The wireless transmission module mainly consists of a LoRa node, LoRa gateway, and network server. The LoRa node, the terminal device, is mainly responsible for the transmission of electrical signals from the microcontroller. The LoRa gateway, as a transfer station, temporarily stores data and checks data integrity, then sends datasets to the network server. The LoRa WAN adopts a star network topology; that is, each node and gateway can communicate with each other in two directions. Broadcasting is utilized to achieve this requirement. Whatever the user's destination, the LoRa node always connects to the current nearest gateway instead of an exact gateway. This structure realizes the requirements of long-distance transmission and reduces the complexity of the network structure to reduce energy consumption and extend the internal battery life of nodes.

To ensure the feasibility of the star network, the LoRa gateway has the ability to deal with a large amount of information from each node. LoRa's high network capacity is achieved by using adaptive data rates and transceivers with multichannel and multiple modems in the gateway. Figure 3 illustrates the process of uploading datasets. Due to each group of data uploaded by broadcast protocol, a gate-

way may receive datasets from different nodes, which cause LoRa gateway itself to use different data receiving rates although the transmitting rate in each node is fixed. Because LoRa is modulation based on the spread spectrum, each signal is orthogonal. When the expansion factor changes, the effective data rate also changes. With this performance, the gateway can accept different data rates on the same channel simultaneously.

The most important factors to ensure that the gateway receives data at the maximum rate are the number of concurrent channels, data rate, load length, and the frequency of data transmission between nodes. Therefore, LoRa cannot transmit long data between nodes and gateway.

$$f(PL) = \max \left(\text{ceil} \left(\frac{PL + \text{Header} + \text{CRC} - 4SF - 20H}{4(SF - 2DE)} \right) \times CR, 0 \right). \quad (1)$$

PL represents the number of payload bytes, which is the posture dataset the system needs. Header is composed of preloaded information. CRC is used to check for cyclic redundancy. SF represents the spread-spectrum factor. When using the data header, H equals 0, otherwise, H equals 1. If the data transmission mode is set to low data rate

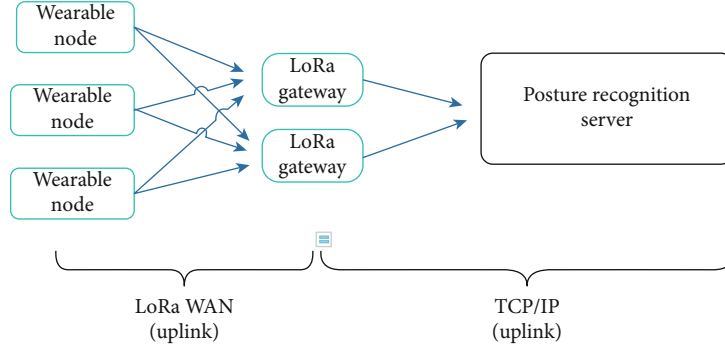


FIGURE 3: Structure of the LoRa wireless transmission module.

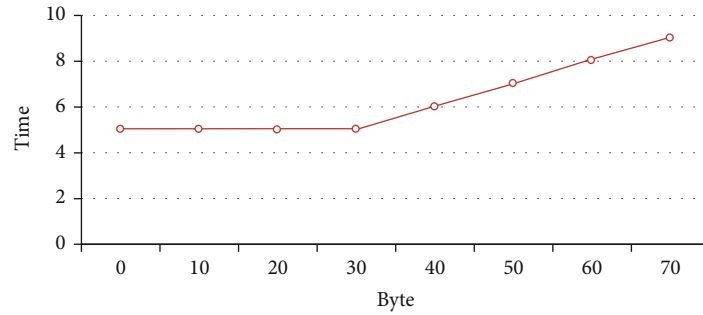


FIGURE 4: The change of time influenced by bytes in LoRa transmission.

optimization, $DE = 1$, otherwise, $DE = 0$. CR stands for coding rate, value is 1 to 4. The function $\text{ceil}()$ returns a value that is bigger than the calculated result in parentheses or equals. Then, the max function is used to get the biggest value between 0 and $\text{ceil}() \times CR$. When other coefficients are fixed, PL becomes larger and then, the result, $f(PL)$, becomes larger, which means LoRa delivers more information in this transmission.

$$f(f(PL)) = T_{pre} + f(PL) \times T_{pay}, \quad (2)$$

T_{pre} represents the time required for preamble transmission while T_{pay} is the selected transmitting mode. When $f(PL)$ becomes larger and LoRa bandwidth is fixed, the overall transmitting time becomes larger. As posture datasets required, 25 groups of datasets are needed to be transmitted every second. LoRa also has itself min transmitting time, five seconds in Figure 4. What the system requires is that the whole posture datasets, 9-axis data times 25 frames each second and 5 seconds in total, should be compressed from 0 to 30 bytes. In the recognition module, a method using the Random Forest algorithm to catch key features of datasets will be explained.

Another way to compress information is to transfer the original data type into bytes. The received datasets are in the form of float type data, which takes up 4 bytes in Arduino Mega's memory. When transmitting to the LoRa gateway, the data type is transferred from float to string, which nearly doubles the size of the float.

TABLE 1: A comparison among the types of int, float, string, and char in Arduino Mega.

Data type	Int	Float	String	Char[2]
Size	4	4	8	2

As shown in Table 1, the char type takes the least memory when transmitting. Thus, Arduino Mega transfers float type data into $\text{char}[2]$, where $\text{char}[0]$ represents the integer part while $\text{char}[1]$ is the decimal part. In Table 2, an example is listed. At the beginning of a dataset package, a symbol position is added because char type only contains the values without positive or negative. Then, posture values are filled in after completing the dataset feature extraction. As for Arduino Mega board settings, every char type data consists of 8 bits. Symbol position is one char data and is composed of 8 bits representing positive or negative values of the sensors in Table 3.

In this module, the web server is responsible for managing all data originating from the gateway. All gateways communicate with the web server via a standard IP connection. If there are multiple gateways in one area, the network server automatically filters duplicate packets from different gateways to select the best quality packets. Besides, the web server verifies data security and sends confirmation characters to the gateway. Another core aspect of the web server is to periodically send data to the application server.

3.4. Posture Recognition Module. The posture recognition module is the core of this system and decides whether the

TABLE 2: Posture data format in Arduino Mega.

Symbol		Accelerometer—X					Gyroscope—mean			Magnetometer—Y			
F	E	0	0	1	2	0	0	D	1	0	0	f	2

TABLE 3: The format of positive and negative values.

1	0	0	1	1	1	0	0
+	—	—	+	+	+	Null	Null

system effectively recognizes postures. In Figure 5, what is required in this module is to do the data preprocessing, feature extraction, and feature selection; to train the module; and to improve the accuracy as much as possible.

3.4.1. Data Preprocessing. From the commercial posture detection products based on Bluetooth, we can see that the posture data is cyclical and smooth in Figure 6. In this system, the posture information sensor module is self-made so there are some errors in the measurement of the sensors. The errors are usually internal errors of the sensor and the jitter errors caused by wearing them on the human body, resulting in burrs, noises, etc. This kind of noise signal, which affects the amplitude of data fluctuation, will directly affect the subsequent feature extraction, classification, and recognition effect. At this time, the module needs to calibrate the sensor data in advance and denoise the collected original data.

The recursive average filtering method has a simple working mechanism and low computational complexity. The principle of the recursive average filtering method is to slide the sampling value step by step and then filter with the way of averaging the previous multiple samples. The effective sampling value is put into use and is obtained by the formula

$$y(i) = \sum_{n=0}^{m-1} \frac{x(i-n)}{m}, (i \geq n), \quad (3)$$

where $x(i)$ is the real-time sensor signal data, $y(i)$ is the recursive average value calculated at this time, and m is the number of sample values, which are randomly selected. It is found that when $m = 5$, the original fluctuation state of data is preserved, and the errors caused by burr and jitter are removed. Compared with when $m = 3$, the denoising effect is not obvious, and when $m = 10$, excessive denoising results in the elimination of some fluctuation features. The final value is 5.

Posture data is based on time serial and frames, and the transmission interval of LoRa technology is fixed. The datasets collected exclude the middle state values resulting in the above two factors. Thus, aiming at adding lost information, a mining value method, named sliding windows illustrated in Figure 7, is utilized for data preprocessing. The length and coverage of the sliding windows are two impor-

tant parameters. If the window is too small, a complete human posture is not captured. If the window is too large and contains many human body postures, the characteristics of a posture are weakened. Our experiment concluded that 3 frames and 5 frames are the two most suitable interval values as shown in Table 4. Utilizing varieties of recognition algorithms does not alter the results as the three-frame interval always provides the best accuracy. Due to the small amount of data in this experiment, the 3-frame value is used as the interval value for the experiment.

3.4.2. Feature Extraction and Selection. To further improve the frequency of human posture recognition and meet the conditions of the LoRa terminal node transmission, this study uses the feature selection algorithm of Random Forest to select a few samples of the most representative features out of 45 features extracted by the scientific analysis method for posture recognition training.

(1) Feature Extraction. In Figure 6, the features of various postures have certain differences, like the values of the peaks and troughs, dispersion degrees, max-min ranges, and means. In acceleration wave Figure 6, peaks and troughs of the waves represent the vigorous exercise, like jumping or running. In this case, only using this feature, the posture of stand and others can be easily distinguished.

$$\begin{aligned} x_{sa_{\max}} &= \max(x_{sa0}, x_{sa1} \cdots x_{sa125}), \\ x_{sa_{\min}} &= \min(x_{sa0}, x_{sa1} \cdots x_{sa125}). \end{aligned} \quad (4)$$

In this formula, x_{sa} represents sensor s and axis a . The data of every single axis has 25 values hence, in 5 seconds, 125 values. Therefore, the result is the max values of the 125 values from a single axis.

$$y = x_{sa_{\max}} - x_{sa_{\min}}, \quad (5)$$

where y represents the max range values minus min range values in a signal wave. In statistics, the range is often used to describe the dispersion degree of a group of data, as well as the variation range and dispersion range of variable distribution. The greater the range, the greater the degree of dispersion, while the smaller the range, the smaller the degree of dispersion.

$$\text{Mean}(x_{sa}) = \frac{\sum_{i=1}^n x_{sai}}{n}. \quad (6)$$

Mean describes the average values of the waveform. x_{sai} represents the data in a sliding window in formula (6). Then, these values in the same sliding window are summed and the summed value is divided by the total amount to get the mean. In Figure 6, the means of different features reach different

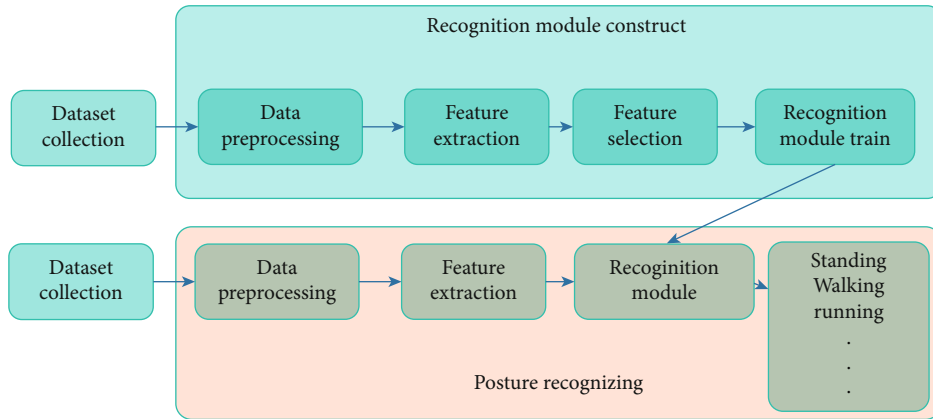


FIGURE 5: The processing of module construct and recognition in LoRa posture recognition module.

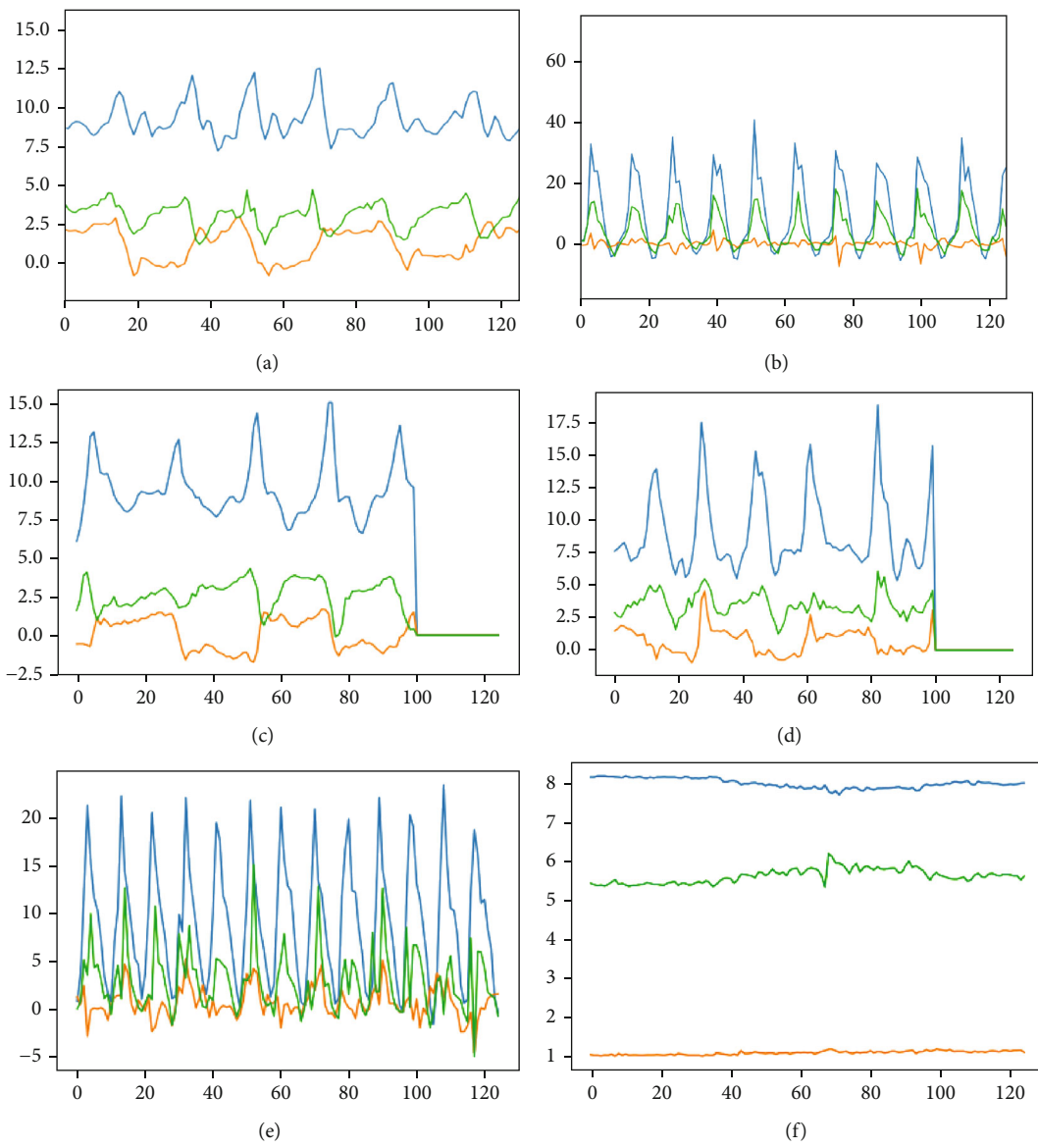


FIGURE 6: Acceleration triaxial signal graph of six postures: (a) walking; (b) jumping; (c) going upstairs; (d) going downstairs; (e) running; (f) standing.

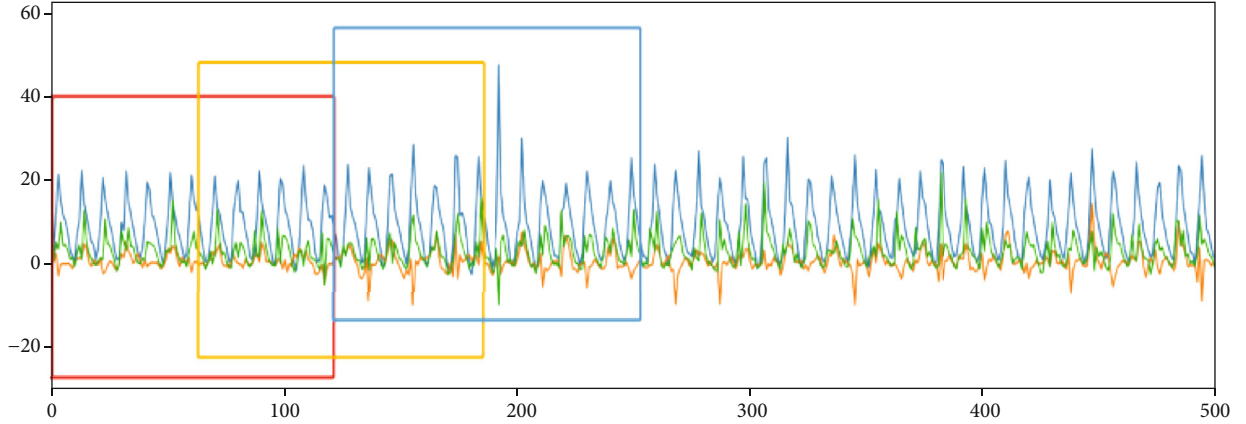


FIGURE 7: Posture data segmentation based on sliding windows.

TABLE 4: Comparison of accuracy with different interval time for sliding windows.

Interval	KNN	SVM	RF	NN	LR	Bayes
25 frames	0.66	0.83	0.85	0.82	0.49	0.75
15 frames	0.77	0.83	0.87	0.83	0.67	0.72
5 frames	0.88	0.94	0.92	0.82	0.64	0.82
3 frames	0.91	0.97	0.96	0.88	0.63	0.83

levels because these waves of postures are all nearly symmetrical and have their unique peak, with two features; a unique mean is generated and used as a significant feature in recognition.

$$\sigma = \sqrt{\sigma^2} = \sqrt{\frac{\sum_{i=1}^n (x_{sai} - \text{mean}(x_{sa}))^2}{n}}, \quad (7)$$

where σ^2 represents variance while σ represents the standard deviation. The standard deviation reflects the discrete degree of a data set. The standard deviation may not be the same for two groups of data with the same mean. Thus, to some extent, the standard deviation solves the problem, the same mean but different postures. Also, the standard deviation effectively calculates the degree of data dispersion. The standard deviation of a posture with a large range in the wave will be larger than that of a posture with a small range in the wave such as standing and speaking. Therefore, the standard deviation is used as one of the effective recognition features.

Every single axis of a sensor has 5 extracted features, maximum and minimum value, max-min range, mean, and the standard deviation. Therefore, one group dataset in five minutes has 45 features in total. Due to the limitation of LoRa transmission, what this system requires is to select the four most important features in these extracted features. In this study, four features are selected as the most important; however, in different areas and spaces, the importance may be altered by the environment and irresistible factors. Therefore, they are also useful even though not selected in this particular study.

(2) *Feature Selection.* Random Forest uses random resampling technology and node random splitting technology to generate multiple decision trees, and the final result is given by voting. The Random Forest calculates the importance of each variable in the training classification process, and this excellent property is open to development in many projects.

Every decision tree in the Random Forest algorithm uses the out-of-bag data method (an error estimation method that replaces the test set) to calculate the corresponding out-of-bag data error, which is recorded as erroob1. Random Forest randomly adds a noise interference to the features of all samples of out-of-bag data, which is used to randomly change the value of samples at feature x , and then calculates the error of out-of-bag data, which is recorded as erroob2. Supposing that there are n decision trees in a Random Forest algorithm, the importance of feature x is expressed as follows:

$$f(X) = \frac{1}{N} \sum (\text{erroob2} - \text{erroob1}). \quad (8)$$

This formula is used as a measure of the importance of variables. When random noise is added to a variable, the accuracy outside the bag decreases obviously; this shows that this feature has a great influence on the result of sample classification. In other words, its importance accounts for a relatively high proportion.

The feature selection is based on the importance of variables in the Random Forest data, and the dimension reduction is completed by selecting a series of data with high importance manually. When selecting features, we should pay attention to the selection of data groups with high correlation and importance, the selection of features with fewer data, and the selection of features that can maximize the reflection of prediction results. To generate the features, firstly, the characteristic variables in the Random Forest are sorted in a descending order or ascending order. Secondly, identify unnecessary features, remove data with particularly low correlation, and get new data groups. Then, establish a new Random Forest model with a new set of eigenvectors and calculate the importance of the features. Finally, repeat steps 1-3 until m features are left.

TABLE 5: Posture accuracy of different algorithms.

Algorithms	KNN	SVM	RandomForest	Neural network	Logistic regression	Bayes GaussianNB
Accuracy (%)	91.26	91.05	95.06	89.81	87.96	86.01

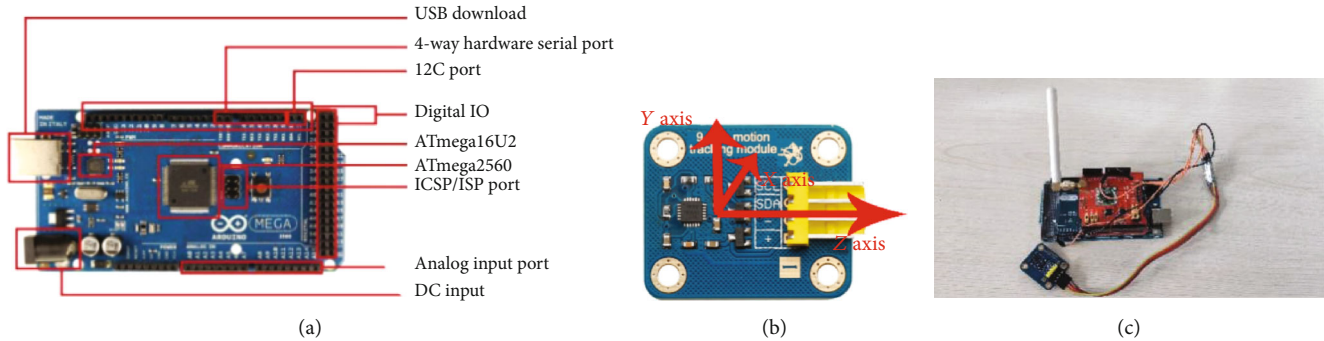


FIGURE 8: LoRa sensor and posture sensor introduction: (a) Arduino Mega 2560; (b) integrated sensors; (c) terminal equipment assembly.

After the above steps, the most important four features selected in this experiment are the max-min range of accelerometer z -axis, magnetometer y -axis, the standard deviation of the gyroscope x -axis, and the max-min range of magnetometer x -axis.

3.4.3. Posture Recognition. In the posture recognition module, multisource sensor information was used to recognize human postures. To guarantee a high level of accuracy as possible, the best classifier is required. In the study, 6 machine learning methods are utilized to train the four selected features and the accuracy is shown in Table 5. Hence, the Random Forest algorithm is selected as the classifier.

Random Forest is a supervised learning algorithm. From the name of Random Forest, one knows that it is a classifier composed of multiple decision trees. The essence of this classifier is based on the idea of ensemble learning in machine learning, which combines several small classifier models to form a larger classifier to make prediction and recognition. Each small classifier is independent of the other and studies and tests the samples independently. Finally, the classification results of multiple small classifiers are combined to form a large single classification prediction output. From the principle algorithm, the final result is better than each small individual classifier.

(1) Generation of the Training Set. The algorithms to realize the decision tree include ID3, C4.5, and CART algorithms. Among them, ID3 chooses information gain value as the evaluation standard of the split attribute, because information gain tends to rely on multivalued characteristic attributes in the calculation process, which makes the result biased and easy to fall into local optimum. Based on this problem, C4.5 improves. It changes the evaluation standard of attribute splitting to information gain rate and eliminates the resulting bias caused by quantity. In the CART [36] algorithm, the Gini index is used as the evaluation standard of attribute splitting, and the attribute with the least impurity is selected.

Besides, another feature of CART is to use dichotomy to form a binary tree for tree structure, and there are only two values of yes or no for feature division. This design discretizes the continuous attributes, making it possible to deal with the continuous attributes and achieve data regression prediction. Wholly, in addition to the evaluation criteria and tree structure mentioned above, the framework and mode of cart decision tree and common decision tree are consistent, that is, the three processes of attribute selection based on the evaluation, top-down recursive spanning tree structure, and decision tree pruning.

In general, the same sample can only build a decision tree. If we want to use the same batch of data samples to build multiple decision trees, we need to select multiple samples by way of resampling data and replacing them. Each selected sample can build a cart decision tree, and resample can build a cart decision tree classifier. The set of these classifiers constitutes a Random Forest. If the sampling method without replacement is adopted, the training samples used by each tree will be completely different, which will lead to a certain degree of deviation for each decision tree, and the voting mechanism of the subsequent Random Forest is the process of seeking the same, which will not be conducive for the construction of the model.

The randomness of Random Forest is reflected not only in the randomness of sample selection but also in the randomness of feature selection. Randomly selected features from all attributes of samples are used for the construction of the classifier. The purpose of this operation is to reduce the correlation between the decision trees. The lower the correlation, the lower the error rate.

(2) Generation of Decision Tree. The sampling method in the first step is used to generate training set samples and train each decision tree model. Decision trees in Random Forest do not particularly need to be pruned. The training samples of the decision tree are filtered by random samples and random features, which makes the decision tree unlikely to overfit in the construction process.

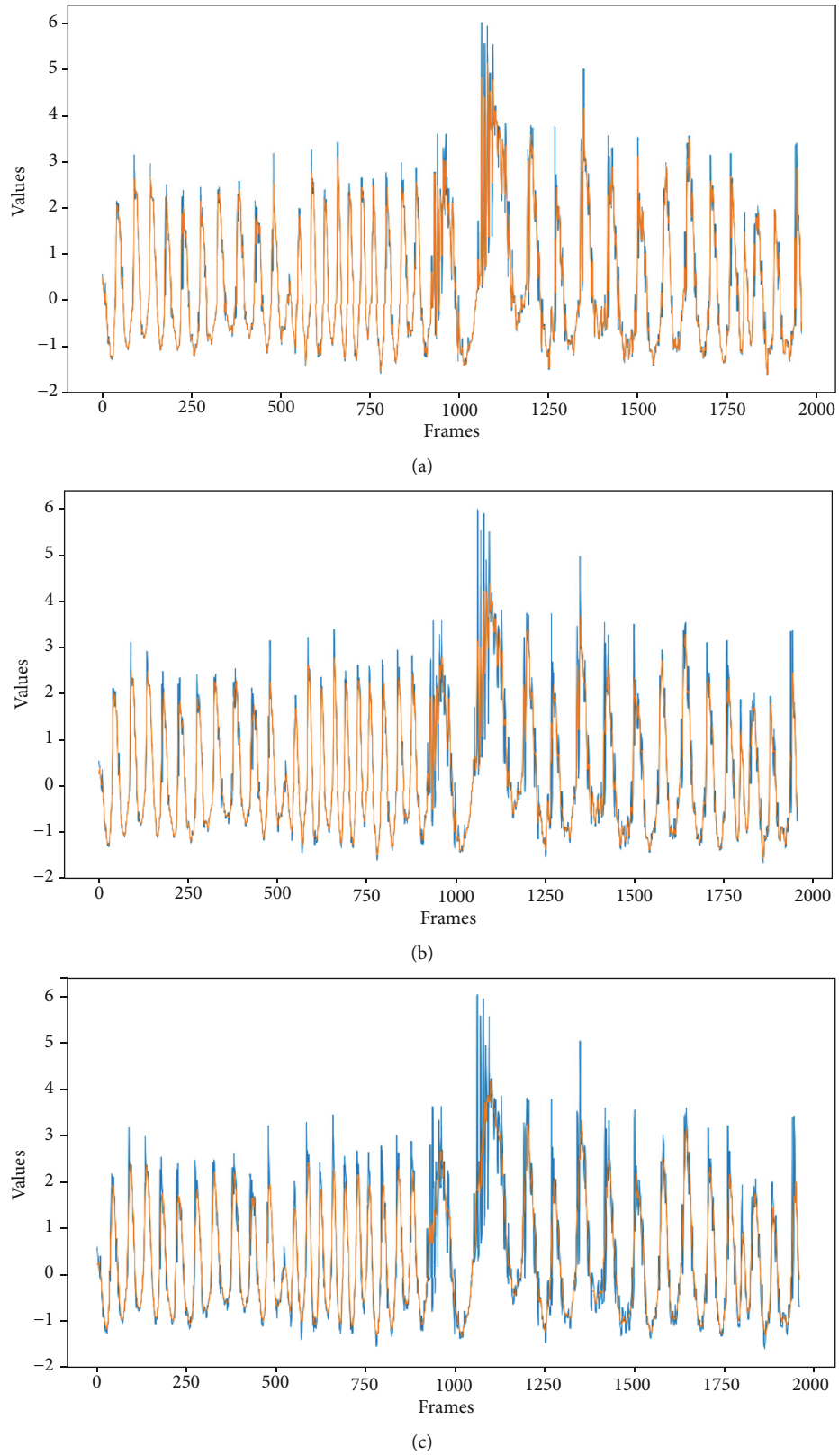


FIGURE 9: Different effects of the recursive average filtering when $m = 3, 5, 10$: (a) $m = 3$; (b) $m = 5$; (c) $m = 10$.

(3) *Formation of RF.* After training multiple decision trees, the classification results of the decision trees are summarized and the prediction results of the final model are selected by

voting rules. Common voting rules include a one-vote veto system, a minority subject to the majority, and a weighted majority. Here, minority subject to the majority is used.

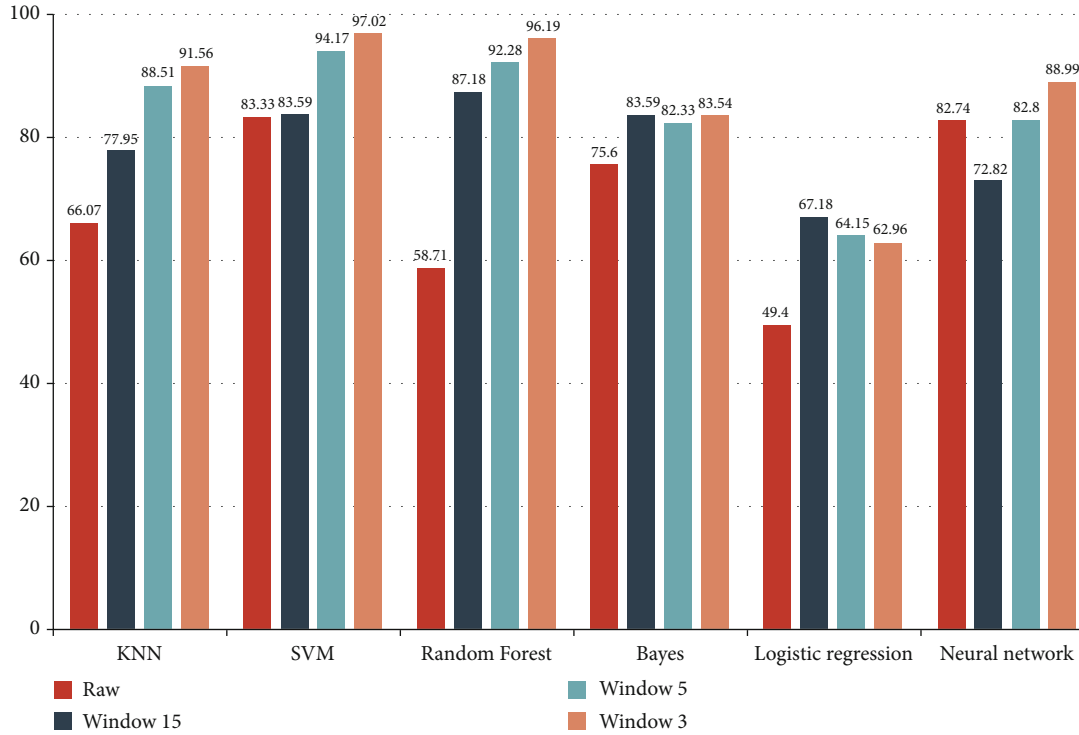


FIGURE 10: Accuracy of different cases: raw data, sliding window $m = 15, 5$, and 3 , respectively.

4. Experiments and Analysis Conclusions

In the experimental part, the parameters of the LoRa nodes and gateway are given in detail. The key results of data denoising, feature extraction, and feature selection are displayed in the figures with different parameters. After a comparative analysis, the best classification algorithm is selected as the main recognition method in this system.

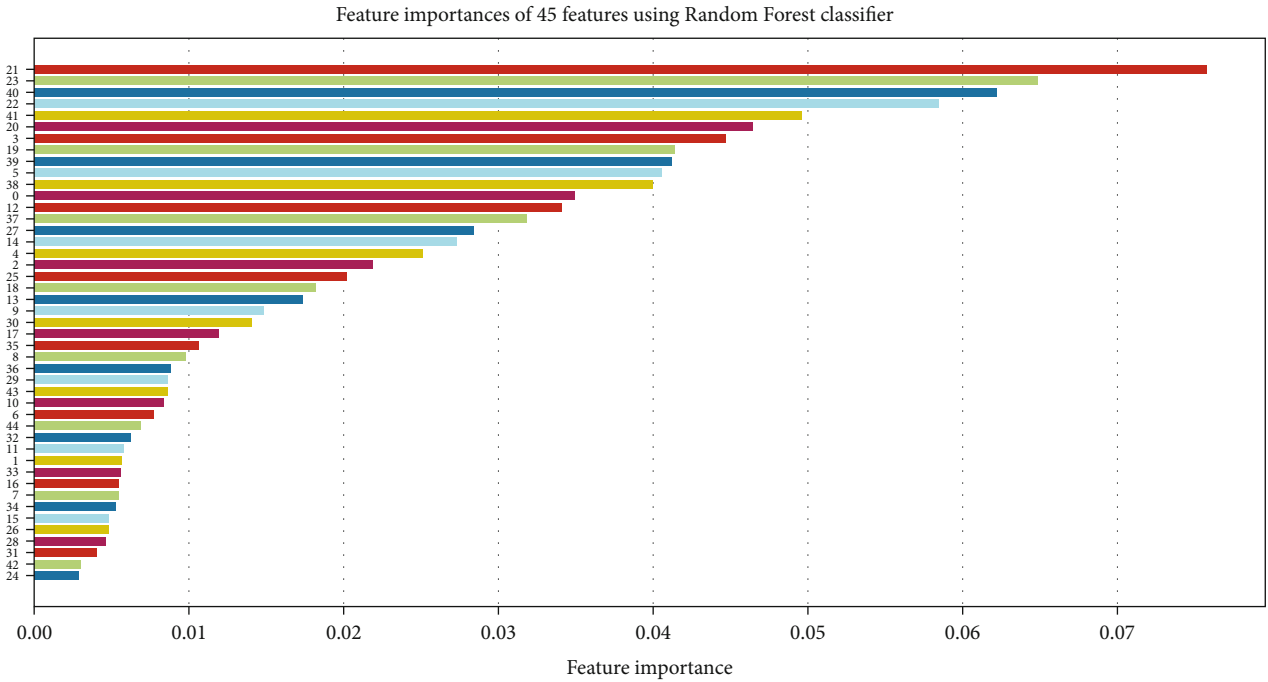
Figure 8(a) shows the integrated sensors with the accelerometer, gyroscopes, and magnetometers, which detect three-axis data, respectively. Their detecting frequency is 25 Hz. Figure 8(b) shows the Arduino Mega. In the sensor data acquisition module, Arduino Mega 2560 is selected as the microprocessor, which has high performance and low power consumption characteristics. Arduino Mega 2560 is a master development board based on ATmega2560. In addition to providing serial port data transmission, this processor supports Wi-Fi, Lora, and other wireless transmission modules, and users can select the appropriate transmission mode with the use of scenarios. In Figure 8(c), the red board is the LoRa shield, which is utilized for gateway connection and transmission. The LoRa shield chip parameters are as follows: equipment size $62 \times 43 \times 23$ mm, equipment weight 22 g, package size $11 \times 70 \times 36$ mm, and package weight 53 g. Lora shield is compatible with 3.3 V or 5 V I/O performance. Its frequency band is 915 MHz/868MHz/433 MHz three different optional intervals. This frequency band is factory configured. LoRa shield boards are compatible with Arduino Leonardo or Uno or Mega or due. LoRa shield's signal transmission is through I-Pex external connector antenna for data

exchange and has the characteristics of low power consumption. Three parts are assembled to form the terminal equipment as a LoRa node.

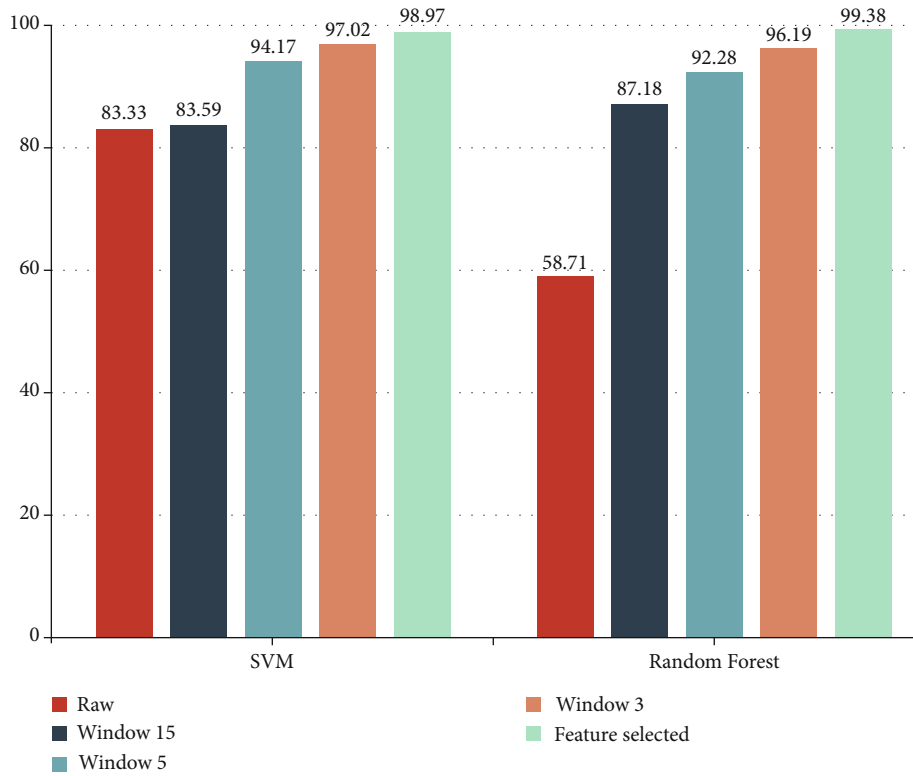
Due to the limitation of LoRa transmission, the posture datasets cannot be wirelessly transmitted directly. The terminal device is connected by PC to collect the raw datasets to go on the next analysis. In the part of collecting raw datasets, the sample rate is 25 frames per second. These raw datasets are saved in different CSV files according to the different types of postures.

Raw datasets have some certain noises, which are caused by the sensor itself or the environment. To guarantee the accuracy of the trained module, data denoising is required. The recursive average filtering method is utilized to smooth the waves. Figure 9 shows the effects of the recursive average filtering when $m = 3$, $m = 5$, and $m = 10$, respectively. It is clear that when $m = 3$, there are still some sharp changes and noise remaining. When $m = 10$, it is too smooth that it loses some key information like real peak values. When $m = 5$, it neither devalues the peaks nor retains noise. Therefore, all posture datasets are processed with $m = 5$ and resaved in CSV files.

The raw datasets are based on frame sampling with a sampling frequency of 25 frames per second. This operation will cause some information between two consecutive samples to be lost. Hence, using the sliding window method enlarges datasets and fills in the lost posture information. Initially, raw datasets are 500 groups of posture datasets. After using the sliding window where the sliding step is 15, there are 647 groups of datasets. When the sliding window is 5,



(a)



(b)

FIGURE 11: (a) Importance of 45 features. (b) Accuracy including the selected feature.

there are 1942 groups of datasets, while when the sliding window is 3, there are 80975 lines of datasets, which are 3239 groups of datasets.

Figure 10 shows the accuracy of raw data and window = 15, 5, and 3, respectively. There are six learning algorithms,

KNN, SVM, Random Forest, Bayes, logistic regression, and neural network. Every algorithm has four histograms representing the accuracy of raw data and window = 15, 5, and 3. As shown, when the sliding window step gradually decreases and the amount of samples increases, the accuracy of most

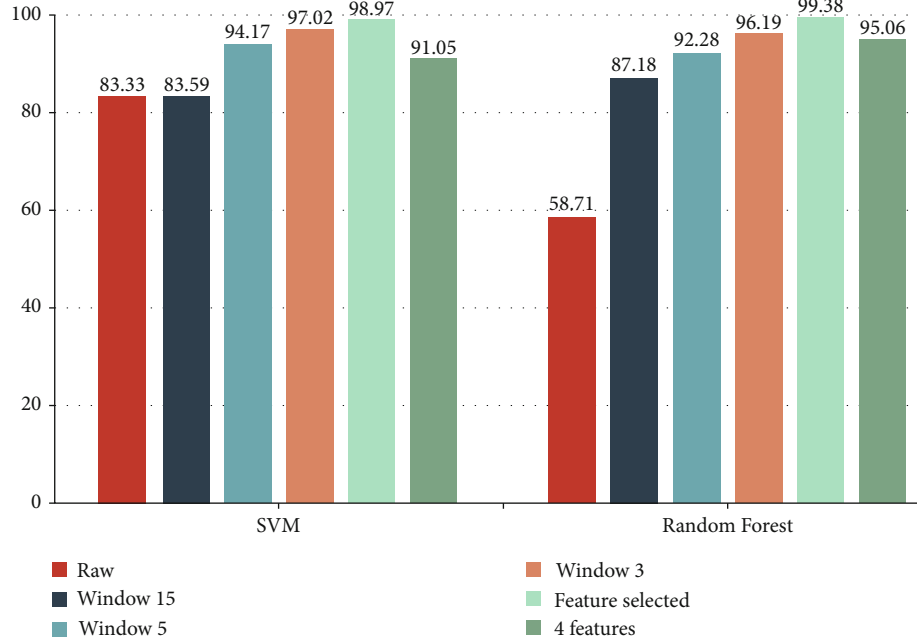


FIGURE 12: A comparison of the recognition accuracy among using 4 extracted features and the others.

algorithms greatly improves, even when the sliding window = 3, and the accuracy of SVM and Random Forest can reach 97.02% and 96.19%, respectively, which is approximately a 15% and 38% increase in comparison with the accuracy of raw data.

Up to now, the accuracy is improved and the sliding window is proved successful. However, LoRa transmission still requires a small data size. Hence, feature extraction and selection should be implemented.

All axes, the 5 features included, max values, min values, max-min range, mean, and standard deviation, are extracted as new input datasets. In total, features have 45 types generated from 9 axes. According to the equipment in this experiment, we used Random Forest to calculate the importance and selected the most important 4 features to meet the LoRa basic requirement. Figure 11(a) shows the descending order of 45 features. As seen, the 21st, 23rd, 40th, and 22nd features get the highest scores. These 4 features represent the max-min range of the accelerometer, z -axis; magnetometer, y -axis; the standard deviation of the gyroscope, x -axis; and the max-min range of the magnetometer, x -axis.

Figure 11(b) shows the best two learning algorithms with 5 processed datasets, where the last green histogram is selected feature datasets. This figure shows feature extraction and selection which more effectively conclude the information of datasets, and when these are applied in learning, the accuracy is directly improved. The raw data only tells what sample, pattern, or wave the data is, while extracted features tell what is behind the data, like whether it is symmetrical movement or violent movement.

When put into the learning module, the datasets of 4 selected features show slightly lowered accuracy in Figure 12. Due to the information lost when giving up the other 41 features, this case is understood and accepted. The

accuracy, 91.05% and 95.06% in SVM and Random Forest, also represents high correctness, and they prove that we selected the right features. Finally, due to the better performance of the Random Forest algorithm, it is selected as the final recognition module for the overall system structure.

According to previous experiments, the key features are found. Then, the terminal device, the LoRa node, is required to reset the transmission format and data values to meet the transmission basis. Now, the process of setting up the human posture module is finished.

To determine the accuracy and strength of the system, we tested the different human postures as follows. We collected 500 hundred groups of datasets, 100 datasets per posture, from 3 different people as shown in Table 6. The posture stand has perfect accuracy of 100% recognition. Going upstairs and downstairs is likely to be mistaken as walking while walking and running are likely to be mistaken as going upstairs and downstairs. Although there are some small errors, the recognition module works well when experiencing other posture datasets.

5. Conclusion

This paper presents a LoRa posture recognition system based on multisensor fusion. This paper describes how and why human posture recognition is important for a smart city. Human posture recognition helps people monitor their health and collect information for scientists to develop healthy exercise method and find the secret between health and daily postures. The system includes sensor modules based on accelerometer, gyroscope, and magnetometer to collect posture information. It uses LoRa wireless network technology to transmit sensor data to the network server. After receiving the data from the cloud server, the application

TABLE 6: Confusion matrix of the Random Forest model.

	Stand	Upstairs	Down-stairs	Walk	Run	Jump
Stand	100	0	0	0	0	0
Upstairs	0	86	6	8	0	0
Downstairs	0	4	92	4	0	0
Walk	0	1	2	96	1	0
Run	0	3	2	0	95	0

server recognizes and classifies the human posture. This paper proposes how to preprocess the frame-based posture data, extract features, and select features. It includes data denoising based on recursive average filtering and data stream segmentation based on the sliding window. In 5 seconds, 45 key features are extracted and the first 4 key features are selected to reset the terminal equipment. The experimental results show that the recognition rate of the four features is 95.06%. This achieves the goal of using a small number of features to maintain high classification accuracy. In future work, we will collect additional postures as a training set for further postural recognition. But the extra postures may need more features because it will not get high accuracy with only four features. Hence, we are actively looking for a stronger LoRa gateway.

Data Availability

The data can be available upon request to the corresponding author.

Conflicts of Interest

The authors declare no conflict of interest.

Acknowledgments

This research was funded by the MSIT (Ministry of Science, ICT), Korea, under the High-Potential Individuals Global Training Program (2019-0-01585) supervised by the IITP (Institute for Information & Communications Technology Planning & Evaluation), National Nature Science Foundation of China (No. 61503005), the Great Wall Scholar Program (CIT&TCD20190304, CIT&TCD20190305), and "Yuyou" Project of North China University of Technology.

References

- [1] J. Wang, Y. Yang, T. Wang, R. S. Sherratt, and J. Zhang, "Big data service architecture: a survey," *Journal of Internet Technology*, vol. 21, no. 2, pp. 393–405, 2020.
- [2] S. Kumar and M. Singh, "Big data analytics for healthcare industry: impact, applications, and tools," *Big Data Mining and Analytics*, vol. 2, no. 1, pp. 48–57, 2019.
- [3] B. Alkouz, Z. A. Aghbari, and J. H. Abawajy, "Tweetluenza: predicting flu trends from twitter data," *Big Data Mining and Analytics*, vol. 2, no. 4, pp. 273–287, 2019.
- [4] Y. Yu, M. Li, L. Liu, Y. Li, and J. Wang, "Clinical big data and deep learning: applications, challenges, and future outlooks," *Big Data Mining and Analytics*, vol. 2, no. 4, pp. 288–305, 2019.
- [5] S. Z. Reza, M. T. Hamidreza, and R. Rouhollah, "Smart-phone-centric human posture monitoring system," in *2014 IEEE Canada International Humanitarian Technology Conference - (IHTC)*, pp. 1–4, Montreal, QC, Canada, 2014.
- [6] Q. Dang, J. Yin, B. Wang, and W. Zheng, "Deep learning based 2D human pose estimation: a survey," *Tsinghua Science and Technology*, vol. 24, no. 6, pp. 663–676, 2019.
- [7] A. Zourmand, A. L. K. Hing, C. W. Hung, and M. AbdulRehman, "Internet of Things (IoT) using LoRa technology," in *2019 IEEE International Conference on Automatic Control and Intelligent Systems (I2CACIS)*, pp. 324–330, Selangor, Malaysia, 2019.
- [8] A. Lavric and V. Popa, "Internet of Things and LoRa™ low-power wide-area networks challenges," in *2017 9th International Conference on Electronics, Computers and Artificial Intelligence (ECAI)*, pp. 1–4, Targoviste, Romania, 2017.
- [9] Y. Tian, T. Li, W. Song, S. Fong, L. Song, and J. Han, "Smart power management Internet of Things system with 5G and LoRa hybrid wireless network," in *5G-Enabled Internet of Things*, p. 13, Taylor & Francis Group, 2019.
- [10] V. A. Dambal, S. Mohadikar, A. Kumbhar, and I. Guvenc, "Improving LoRa signal coverage in urban and sub-urban environments with UAVs," in *2019 International Workshop on Antenna Technology (iWAT)*, pp. 210–213, Miami, FL, USA, 2019.
- [11] M. Sun, Y. Jiang, Q. Liu, and X. Liu, "An auto-calibration approach to robust and secure usage of accelerometers for human motion analysis in FES therapies," *Computers, Materials & Continua*, vol. 60, no. 1, pp. 67–83, 2019.
- [12] Y.-L. Zheng, X. R. Ding, C. C. Y. Poon et al., "Unobtrusive sensing and wearable devices for health informatics," *IEEE Transactions on Biomedical Engineering*, vol. 61, no. 5, pp. 1538–1554, 2014.
- [13] Y. Yan and Y. Ou, "Accurate fall detection by nine-axis IMU sensor," in *2017 IEEE International Conference on Robotics and Biomimetics (ROBIO)*, pp. 854–859, Macau, China, 2017.
- [14] Y. Prathivadi, J. Wu, T. R. Bennett, and R. Jafari, "Robust activity recognition using wearable IMU sensors," in *IEEE SEN-SORS 2014 Proceedings*, pp. 486–489, Valencia, Spain, 2014.
- [15] X. Shen, W. Cheng, and M. Lu, "Wireless sensor networks for resources tracking at building construction sites," *Tsinghua Science and Technology*, vol. 13, no. S1, pp. 78–83, 2008.
- [16] X. Su, H. Tong, and P. Ji, "Activity recognition with smart-phone sensors," *Tsinghua Science and Technology*, vol. 19, no. 3, pp. 235–249, 2014.
- [17] E. Ahmadoh and L. A. Tawalbeh, "Power consumption experimental analysis in smart phones," in *2018 Third International Conference on Fog and Mobile Edge Computing (FMEC)*, pp. 295–299, Barcelona, Spain, 2018.
- [18] Y. Liang, Z. Cai, J. Yu, Q. Han, and Y. Li, "Deep learning based inference of private information using embedded sensors in smart devices," *IEEE Network Magazine*, vol. 32, no. 4, pp. 8–14, 2018.
- [19] Z. U. Ahmed, M. G. Mortuza, M. J. Uddin, M. H. Kabir, M. Mahiuddin, and J. Hoque, "Internet of Things based patient health monitoring system using wearable biomedical device," in *2018 International Conference on Innovation in Engineering and Technology (ICIET)*, pp. 1–5, Dhaka, Bangladesh, 2018.

- [20] Y. Lin, H. Tseng, Y. Lin, and L. J. Chen, "NB-IoTtalk: a service platform for fast development of NB-IoT applications," *IEEE Internet of Things Journal*, vol. 6, no. 1, pp. 928–939, 2019.
- [21] N. Mangalvedhe, R. Ratasuk, and A. Ghosh, "NB-IoT deployment study for low power wide area cellular IoT," in *2016 IEEE 27th Annual International Symposium on Personal, Indoor, and Mobile Radio Communications (PIMRC)*, pp. 1–6, Valencia, Spain, 2016.
- [22] T. Elarabi, V. Deep, and C. K. Rai, "Design and simulation of state-of-art ZigBee transmitter for IoT wireless devices," in *2015 IEEE International Symposium on Signal Processing and Information Technology (ISSPIT)*, pp. 297–300, Abu Dhabi, UAE, 2015.
- [23] M. Zhang and Q. Hu, "A hybrid network smart home based on Zigbee and smart plugs," in *2017 7th International Conference on Communication Systems and Network Technologies (CSNT)*, pp. 389–392, Nagpur, India, 2017.
- [24] N. I. Osman and E. B. Abbas, "Simulation and modelling of LoRa and Sigfox low power wide area network technologies," in *2018 International Conference on Computer, Control, Electrical, and Electronics Engineering (ICCCEEE)*, pp. 1–5, Khartoum, Sudan, 2018.
- [25] H. P. H. Shum, E. S. L. Ho, Y. Jiang, and S. Takagi, "Real-time posture reconstruction for Microsoft Kinect," *IEEE Transactions on Cybernetics*, vol. 43, no. 5, pp. 1357–1369, 2013.
- [26] D. Brulin, Y. Benezeth, and E. Courtial, "Posture recognition based on fuzzy logic for home monitoring of the elderly," *IEEE Transactions on Information Technology in Biomedicine*, vol. 16, no. 5, pp. 974–982, 2012.
- [27] X. Zheng, Z. Cai, and Y. Li, "Data linkage in smart internet of things systems: a consideration from a privacy perspective," *IEEE Communications Magazine*, vol. 56, no. 9, pp. 55–61, 2018.
- [28] X. Zheng and Z. Cai, "Privacy-preserved data sharing towards multiple parties in industrial IoTs," *IEEE Journal on Selected Areas in Communications*, vol. 38, no. 5, pp. 968–979, 2020.
- [29] S. Cheng, Z. Cai, and J. Li, "Curve query processing in wireless sensor networks," *IEEE Transactions on Vehicular Technology*, vol. 64, no. 11, pp. 5198–5209, 2015.
- [30] Z. He, Z. Cai, S. Cheng, and X. Wang, "Approximate aggregation for tracking quantiles and range countings in wireless sensor networks," *Theoretical Computer Science*, vol. 607, pp. 381–390, 2015.
- [31] X. Peng, J. Li, G. Wang et al., "Random forest based optimal feature selection for partial discharge pattern recognition in HV cables," *IEEE Transactions on Power Delivery*, vol. 34, no. 4, pp. 1715–1724, 2019.
- [32] H. J. Lee, S. H. Hwang, S. M. Lee, Y. G. Lim, and K. S. Park, "Estimation of body postures on bed using unconstrained ECG measurements," *IEEE Journal of Biomedical and Health Informatics*, vol. 17, no. 6, pp. 985–993, 2013.
- [33] J. E. Estrada and L. A. Vea, "Real-time human sitting posture detection using mobile devices," in *2016 IEEE Region 10 Symposium (TENSymp)*, pp. 140–144, Bali, Indonesia, 2016.
- [34] C. H. Zhao, B. L. Zhang, J. He, and J. Lian, "Recognition of driving postures by contourlet transform and random forests," *IET Intelligent Transport Systems*, vol. 6, no. 2, pp. 161–168, 2012.
- [35] Z. Cai and X. Zheng, "A private and efficient mechanism for data uploading in smart cyber-physical systems," *IEEE Transactions on Network Science and Engineering*, vol. 7, no. 2, pp. 766–775, 2020.
- [36] H. Peng, F. Long, and C. Ding, "Feature selection based on mutual information criteria of max-dependency, max-relevance, and min-redundancy," *IEEE Transactions on Pattern Analysis and Machine Intelligence*, vol. 27, no. 8, pp. 1226–1238, 2005.